Extracellular vesicle-mediated bidirectional communication between macrophages and lesions in the peritoneal microenvironment of endometriosis

Yifan Wang

St Cross College, University of Oxford

Michaelmas Term, 2024

Supervisors: Prof Christian Becker[1]
Dr Rebecca Dragovic[1]
Dr Jen Southcombe[1]
Prof Erin Greaves[2]

1 Oxford Endometriosis CaRe Centre,
Nuffield Department of Women's & Reproductive Health,
University of Oxford, Oxford, United Kingdom
2 Division of Biomedical Sciences,
Warwick Medical School, University of Warwick,
Coventry, United Kingdom

Extracellular vesicle-mediated bidirectional communication between macrophages and lesions in the peritoneal microenvironment of endometriosis

Yifan Wang

Michaelmas Term 2024, St Cross College

A thesis submitted in partial fulfilment of the requirements for the degree of Doctor of Philosophy at the University of Oxford

Abstract

Endometriosis is characterised by the growth of endometrium like tissue outside the uterus (lesions). Small extracellular vesicles (sEV) in the peritoneal microenvironment of endometriosis modulate intracellular communication and disease progression. This study aimed to characterize the cellular origins of sEV, examine their potential as biomarkers, and investigate their functional role in disease progression by affecting macrophage phagocytic activity.

Using MACSPlex EV flow cytometry and Nanoparticle Tracking Analysis (NTA), the size, concentration, and surface epitopes of sEV from peritoneal fluid (PF), in vitro cultured peritoneal macrophages (pMΦ), and endometrial/lesion derived epithelial organoids (EEO) were characterised.

Flow cytometry revealed distinct sEV profiles from different cellular origins: CD14 and HLA-DR on pMΦ -sEV, and EpCAM and CD133/1 on EEO-sEV. EEO-sEV from lesions expressed higher levels of CD44 and CD29 compared to EEO-sEV from eutopic endometrium. High expression of HLA-DR, EpCAM, and CD133/1 in PF-sEV indicated a predominance of epithelial derived and pMΦ -sEV. Hormonal treatment (HT) was associated with lower EpCAM and higher CD24 expression on PF-sEV. However, no differences were found between endometriosis and control patients. NTA showed lower PF-sEV concentration in HT compared to non-HT. EEO polarity also affected EV size and concentration. Functional

analysis revealed impairment of macrophage phagocytic activity (assays using pH-sensitive pHrodo E.coli bioparticles) by PF-sEV and lesion EEO-sEV, mediated through the CD47/SIRP-alpha.

This study revealed the complexity of sEV profiles predominantly from antigen-presenting cells and endometrial epithelial cells. While sEV profiles were distinct from different sources and reflected environmental changes like HT, their use as biomarkers requires further investigation. The functional roles of EV in disease progression potentially extend beyond impairing macrophage phagocytosis as demonstrated in this study, as these sEV expressed various functionally important markers.

Acknowledgement

I must first offer my thanks to my supervisor, Prof Christian Becker, for making this journey possible. Your inspiring lectures on endometriosis during my study in MSc Clinical Embryology course ignited my passion for this field and encouraged me to pursue a PhD in the department. Your continuous support over the past four years has been instrumental, and I am deeply grateful for your guidance and belief in my work.

To Dr Rebecca Dragovic and Dr Jen Southcombe, thank you for being the strongest safety nets and anchors in the lab. This journey began with a rough start during the pandemic, but you always had my back. And let's not forget the late-night emergency calls to troubleshoot flow cytometry and NanoSight—you handled them like true experts. Your optimism, advice, and support turned what could have been a tough journey into one that was both rewarding and enjoyable.

I would also like to thank Prof Erin Greaves for providing additional support for my DPhil project, particularly in macrophage research.

Next, I am grateful for Zhixing for everything. From long days in tissue culture room to countless nights in the flow cytometry room—your enthusiasm and curiosity have been infectious. I will always remember the excitement of discovering new results together. Without your collaboration, I could not have explored so deeply into organoid experiments or completed the final experimental chapter within such a short timeframe. Thank you, not only as a collaborator but also as a friend, for sharing both laughter and tears.

To the incredible lab team—Adriana, Ana, Fitnat, Magda, Abbe, Tatjana, and Gavin—thank you for always thinking of my work and for your generosity in sharing patient samples. Your willingness to take on tedious tasks while I was away made me feel like we are part of a big, supportive team that always has each other's backs. I also want to thank Prof Krina

Zondervan and the entire Endometriosis Care Group, especially Becca and Kurtis for making the Endometriosis Care Group feel like a family.
My gratitude also extends to Kelly, Lisa, Shanice, Sarah, Ka Yee and Sandra for their tireless efforts in recruiting patients and collecting samples for the FENOX/ENDOX studies. To all the patients who participated, I am deeply appreciative of your generosity.

I want to thank my dearest friends, especially Shitong and Xinyu, for your support and encouragement. Your friendship has been my greatest source of strength and comfort throughout this journey. Yinan, thank you for being patient every time I pulled you away from your own research to help me untangle my statistical and programming messes. Your support during the toughest times kept me going, and your calm presence always made everything feel so much easier to handle. Thank you.

Finally, I want to express my deepest gratitude to my parents, 汪金良 and 李毅, for your selfless love and support. 感谢你们无私的支持和爱，让我相信自己。

Table of Contents

Abbreviations

AI	Aromatase Inhibitors
ANOVA	Analysis of Variance
APC	Allophycocyanin
BCA	Bicinchoninic Acid
BMI	Body Mass Index
BSA	Bovine Serum Albumin
cAMP	Adenosine 3',5'-Cyclic Monophosphate
CCR2	C-C Chemokine Receptor Type 2 (CCR2)
CD	Cluster of Differentiation
CM	Conditioned Media
CON	Control
COCP	Combined Contraceptive Pills
CSF-1	Colony-Stimulating Factor-1
CRIg	Complement Receptor of the Immunoglobulin superfamily
CyTOF	Cytometry by time of flight
DE	Deep Infiltrating Endometriosis
DMS0	Dimethyl sulfoxide
EEO	Endometrial Epithelial Organoid
EFI	Endometriosis Fertility Index
EGF	Epidermal Growth Factor
ELISA	Enzyme-Linked Immunosorbent Assay
EM	Endometriosis
ESCRT	Endosomal Sorting Complex Required for Transport
ExM	Expansion Media
FBS	Fetal Bovine Serum
FCS	Forward Scatter
FITC	Fluorescein isothiocyanate
fPBS	0.1 um Membrane Filtered PBS
FSH	Follicle-Stimulating Hormone
GnRH	Gonadotropin-Releasing Hormone
GnRHa	Gonadotropin-Releasing Hormone Agonists
HA	Hyaluronic Acid

HT	Hormonal Treatment
IFN- γ	Interferon-Gamma
IL	Interleukin
lncRNA	Long Non-Coding RNA
IOF	Inner Organoid Fluid
IUD	Intrauterine Devices
ITIM	Immunoreceptor Tyrosine-Based Inhibitory Motif
LH	Luteinizing Hormone
LpM	Large Peritoneal Macrophages
LPS	lipopolysaccharide
MHC II	Major Histocompatibility Complex Class II
miRNA	Micro RNA
MMP	Matrix Metalloproteinases
MRI	Magnetic Resonance Imaging
MVE	Multivesicular Endosomes
nMFI	Normalised Median Fluorescent Intensity
NTA	Nanoparticle Tracking Analysis
OE	Ovarian Endometrioma
PAEP	Progestogen-Associated Endometrial Protein
PE	Phycoerythrin
PD-1	Programmed Cell Death Protein 1
PD-L1	Programmed Cell Death Ligand 1
PF	Peritoneal Fluid
pMΦ	Peritoneal Macrophages
PMA	Phorbol 12-Myristate 13-Acetate
POP	Progestin-Only Pills
PS	Penicillin-Streptomycin
rASRM	revised American Society for Reproductive Medicine (score)
REA	Recombinant Engineered Antibody
SD	Standard Deviation
SE	Standard Error
SE	Superficial Endometriosis
SEC	Size Exclusion Chromatography
SHP	Src Homology 2 Domain Containing Protein Tyrosine Phosphatase

Siglec-10	Sialic Acid-Binding Ig-Like Lectin-10
Sirp- α	Sialic Acid-Binding Ig-Like Lectin-10
sEV	Small Extracellular Vesicles
SOP	Standard Operating Procedure
SpM	Small Peritoneal Macrophages
SPP-1	Secreted Phosphoprotein One
SSC	Side Scatter
TAM	Tumour Associated Macrophages
Tregs	Regulatory T cells
TNF-α	Tumour Necrosis Factor-α
TGF- β1	Transforming Growth Factor Beta-1
TEM	Transmission Electron Microscopy
VEGF	Vascular Epithelial Growth Factor
WGA	Wheat Germ Agglutinin

Chapter 1 Introduction

1.1 Endometriosis

Endometriosis is a chronic inflammatory disease affecting approximately 10% of women of reproductive age (1). This condition not only impacts individual health but also imposes a substantial economic burden on society, with annual costs exceeding £8.2 billion in the UK alone (1, 2). It is characterised as the aberrant growth of endometrium-like tissue (lesions) outside the uterus. These lesions can manifest in various forms and locations, most commonly along the mesothelial cell-lined peritoneal cavity (referred to as superficial endometriosis or SE), as ovarian endometriosis cysts (ovarian endometriomas or OE), or as deep nodules beneath the peritoneal surface (deep endometriosis or DE) (2)

The clinical presentation of endometriosis is diverse and often debilitating. Patients typically experience a combination of symptoms, including cyclical and non-cyclical pelvic pain, dysmenorrhea, fatigue and pain during and after sexual intercourse(2). Many women also report discomfort during defecation and urination (2). The impact of endometriosis extends beyond pain, as approximately 30% to 50% of patients with this condition struggle with subfertility (3).

To categorise the severity and extent of endometriosis, medical professionals employ various classification systems. The revised American Society for Reproductive Medicine (rASRM) classification system divides the condition into stages I-IV based on the location, depth, and size of lesions and adhesions (4). For cases of DE, the Enzian classification (5) provide a more detailed characterisation. Furthermore, the Endometriosis Fertility Index (EFI) serves as a valuable tool for predicting pregnancy outcomes in affected individuals (6).

Recent advancements in medical imaging technologies have improved the diagnostic capabilities for certain forms of endometriosis. Magnetic Resonance Imaging (MRI) and ultrasound techniques have demonstrated reasonable specificity and sensitivity in detecting OE and DE which are similar to laparoscopic visualisation in women presenting with similar pelvic pain symptoms or fertility problem (7, 8). However, the definitive

diagnosis of endometriosis, particularly peritoneal SE, still relies on laparoscopic examination and histological verification (1). One of the most perplexing aspects of endometriosis is the often poor correlation between the extent of the disease (as determined by clinical staging) and the severity of pain experienced by patients (9).

As an oestrogen-driven disease, endometriosis primarily affects women during their reproductive years. Clinically, it often manifests as early as adolescence (1). Inadequate imaging, non-specific symptoms, stigmatisation, and lack of awareness result in diagnostic delay of 8 years on average and frequently require laparoscopic investigation (10). Current treatment approaches for endometriosis, including both medical and surgical interventions, are often associated with high recurrence rates and significant side effects and risks (11, 12). This reality means that for many patients, endometriosis becomes a long-term condition that substantially impairs their quality of life (1, 2).

The complex nature of endometriosis, from its varied clinical presentations to its profound impact on women's health and fertility, underscores the urgent need for continued research and improved diagnostic and treatment strategies. Understanding mechanism involved in disease development and progression is crucial.

The architecture of endometriosis lesions is variable but typically comprises endometrial stromal and epithelial cells with immune cell infiltration, fibrogenesis, neovascularization and innervation (1, 2, 13). Endometrial stromal cells represent the most predominant cell population in ectopic lesions and are thought to be primarily responsible for the attachment of lesions to the peritoneum (14). Recent research has shed new light on the role of endometrial epithelial cells in the pathogenesis of endometriosis. These cells have been found to carry most of the genetic mutations associated with the condition (15).

The most widely accepted theory of endometriosis pathogenesis is that of retrograde menstruation, proposed by Sampson in 1927 (16). This theory suggests that endometriosis lesions develop from endometrial cells and tissue that flow backward from the uterine cavity during menstruation, through the fallopian tubes, and into the peritoneal cavity.

However, this theory alone cannot fully explain the development of endometriosis, as retrograde menstruation occurs in up to 90% of females, yet only a fraction develops the disease (17). This discrepancy indicates that additional mechanisms, likely involving the regulation of cell adhesion, proliferation and invasion, must play a role in the pathogenesis of endometriosis.

Recent genome-wide association studies have identified 42 genomic regions associated with endometriosis; however, none reached genome-wide significance for stage I/II disease, suggesting limited genetic contribution in early-stage cases (18). Even in stage III/IV, genetic variants explain only around 5% of cases, predominantly linked to ovarian endometriomas. Key genetic associations in endometriosis implicate pathways involved in cell adhesion, angiogenesis, and hormone metabolism and inflammation include Wingless/Integrated (WNT) **and** Mitogen-Activated Protein Kinase (MAPK) signalling pathways (1)**.** Significant genetic correlations have been found between endometriosis and pain conditions, including neurological conditions like migraine (18).

Immune dysregulation and cellular communication within the peritoneal microenvironment have been found to be linked with disease progression and pain. This is supported by the genetic correlation of endometriosis with inflammatory conditions like asthma and osteoarthritis (18)

1.2 Immune dysregulation in peritoneal microenvironment of endometriosis

Endometriotic lesions and the mesothelial cell layer are exposed to immune cells in the peritoneal fluid (PF). The PF of women with endometriosis exhibits a complex milieu of immune cells that have been described to create a permissive environment for the survival and proliferation of ectopic endometrial tissue (19).

Recent studies using advanced techniques such as mass cytometry and single-cell RNA sequencing have revealed distinct immune cell profiles in the PF of endometriosis patients compared to healthy controls (20, 21). Over 40 types of immune cells have been identified in the PF, including components of both the innate and adaptive immune systems (20). This diverse array of immune cells undergoes significant alterations in endometriosis, contributing to the complex immunological landscape of the disease.

Immune cells originate from hematopoietic stem cells in the bone marrow, which differentiate into two main lineages: myeloid and lymphoid progenitors (22). The myeloid lineage gives rise to cells such as monocyte derived macrophages, neutrophils, and dendritic cells, while the lymphoid lineage primarily produces T cells, B cells, and natural killer (NK) cells (22). In endometriosis, several key immune cell populations show alterations in the PF, potentially contributing to disease development and progression:

1. Macrophages: Often the most abundant immune cells in the PF, macrophages from endometriosis patients have been shown to have impaired phagocytotic abilities (23, 24). These may contribute to the survival and attachment of refluxed endometrial cells and tissue. Furthermore, increased macrophage abundance is positively correlated with pelvic pain scores in endometriosis patients (25).
2. NK cells: Women with endometriosis often display reduced NK cell cytotoxicity in their PF (19).
3. T cells: The second largest immune cell population (20%) in PF (26) and favouring T killer cells (CD8+) (20). The T helper (CD4+) immune pattern in the PF of endometriosis patients is typically shifted toward a Th2 anti-inflammatory response, which may favour lesion growth (27, 28). Additionally, regulatory T cells (Tregs) have been implicated in disease development through interactions with endometrial stromal cells and macrophages (29-31).
4. B cells: While less studied, alterations in B cell populations and autoantibody production have been observed in endometriosis (32).

Furthermore, cellular communication between immune cells, ectopic endometrial cells, nerves and the peritoneal mesothelium plays a crucial role in disease progression (33, 34).

This communication occurs through various mechanisms, including secretion of soluble factors (cytokines, growth factors, and hormones) (33-35) and release of small extracellular vesicles (sEV) containing proteins, lipids, and nucleic acids (36, 37).

Among the various immune cell populations affected in endometriosis, peritoneal macrophages (pMΦ) stand out as particularly significant contributors to disease pathophysiology. Given their abundance and crucial role in the peritoneal immune landscape, I elaborate on phenotypes and functional roles of pMΦ in endometriosis.

1.2.1 The phenotypes of peritoneal macrophages (pMΦ) in endometriosis

Macrophages represent a significant component of the peritoneal immune landscape in endometriosis, accounting for almost 50% of immune cells in the PF (20). These pMΦ comprise a heterogeneous population originating from embryonic precursors and bone marrow which give rise to tissue-resident macrophages and monocyte-derived macrophages recruited to the peritoneal cavity during local inflammation (38). Increased numbers of pMΦ have been found in endometriosis patients (20).

The recruitment and activation of pMΦ in endometriosis are influenced by various factors, including macrophage growth factors and chemokines such as colony-stimulating factor-1 (CSF-1) and monocyte chemoattractant protein-1 (MCP-1/CCL2) (39, 40). The mesothelium, endometriotic stromal cells, and nerve fibres all participate in the chemotactic recruitment of macrophages to the pelvic cavity, a process that is notably oestrogen-dependent (33, 41) Oestrogen exerts its effects on pMΦ and endometriotic lesions through the oestrogen receptors alpha (ERα) and beta (ERβ) (42, 43), highlighting the hormonal influence on the immune environment in endometriosis.

Flow cytometry studies have revealed the heterogeneity within human pMΦ populations, identifying various subsets based on the expression of canonical markers such as CD14, CD16, and HLA-DR (44), as well as the expression of Complement Receptor of the Immunoglobulin subfamily (CRIg) and C-C chemokine receptor type 2 (CCR2) (45). pMΦ are capable of differentiating into specific subtypes in response to local stimuli. This high

plasticity results in a diverse array of macrophage phenotypes within the peritoneal cavity (46). Unique subpopulation presentations have been related to endometriosis. One study has found an increased pro-repair response in $CD14^{+low}$ and $CD68^{+low}$ pMΦ populations in endometriosis (47) while another study revealed an increase of the $CD14^{high}$ subpopulation in endometriosis patients (25). Recent advancements in single-cell RNA-Seq analysis have further expanded our understanding of pMΦ heterogeneity, identifying seven distinct subtypes of macrophages in the PF from an endometriosis patients (21) and reporting five subpopulations of tissue-resident and blood-derived macrophages in ectopic lesions (48). These findings underscore the complexity of the macrophage landscape in endometriosis and highlight the need for further validation and functional studies to determine if these newly identified pMΦ subtypes have distinct roles in disease progression.

Mouse models of experimental endometriosis have provided valuable insights into the origins and phenotypes of pMΦ. In mice, pMΦ are characterised into large peritoneal macrophages (LpM; F4/80hi MHC IIlo) and monocyte-derived small peritoneal macrophages (SpM; F4/80lo MHC IIhi) (38). LpM, which are dominant in the peritoneal cavity, consist primarily of self-renewing embryonic-derived cells that perform immunosurveillance (49) (50). Under inflammatory conditions like endometriosis, monocytes infiltrate the pelvic cavity and transform into pro-inflammatory SpM, which eventually differentiate into LpM (51).

Notably, studies in mouse models have revealed that tissue-resident, embryonic-derived LpM promote lesion growth, while monocyte-derived LpM appear to limit the growth of lesions (52). However, it is important to note that these findings on the origins of pMΦ and SpM/LpM functions in mouse models cannot be directly translated to the human macrophage system, which displays a higher level of complexity and heterogeneity. This discrepancy underscores the critical need for further research on the origins, phenotypes, and functions of human pMΦ in both homeostasis and disease states.

pMΦ in endometriosis present both pro-inflammatory and pro-repair phenotypes (20). Lesions and T cells have been found to influence pMΦ polarisation and activation. Regulatory T cells (Tregs) can promote macrophage polarisation towards pro-repair

phenotypes through the secretion of soluble fibrinogen-like protein 2 (31). Several studies have revealed the modulation of ectopic endometrial stromal cells on macrophage polarisation (35, 53).

1.2.2 Functional roles of pMΦ in endometriosis pathogenesis

The activated pMΦ in endometriosis produce numerous cytokines and growth factors in the peritoneal microenvironment, including interleukin-1 beta (IL-1β), interleukin-6 (IL-6), interleukin-8 (IL-8), interleukin-12 (IL-12), tumour necrosis factor-alpha (TNF-α), vascular epithelial growth factor (VEGF), and transforming growth factor-beta 1 (TGF-β1). This diverse array of factors contributes to various aspects of endometriosis progression, including lesion implantation, growth, and angiogenesis (2).

One of the key characteristics of pMΦ in endometriosis patients is their impaired phagocytotic abilities, which is attributed to the downregulation of CD36 (23, 24). This functional deficit may contribute significantly to the survival and attachment of refluxed endometrial cells and tissue, facilitating the establishment and persistence of ectopic lesions. Co-culture experiments of ectopic endometrial stromal cells and macrophages showed reduced phagocytosis of macrophages while increasing survival and growth of stromal cells compared to eutopic endometrial stromal cells (54).

The role of pMΦ in endometriosis extends beyond their direct effects on lesion development and growth. The inflammatory responses mediated by pMΦ in endometriosis contribute to pain through various mechanisms. Macrophages are attracted to nerve fibres under the influence of CSF-1 and CCL2 (35, 51), and the recruited macrophages secrete nerve growth factors such as insulin growth factor 1 and VEGF. These factors promote neurogenesis and nerve sensitisation, processes that are mediated by oestrogen (2, 33).
These actions may activate and sensitise peripheral nerve fibres, potentially leading to central sensitization through long-term peripheral nociceptive input (49, 50).

Persistent cytokine-driven inflammation within the peritoneal cavity can continue to activate peripheral nociceptors, maintaining pain signalling even in the absence of lesions. This prolonged peripheral input can lead to the activation of spinal microglia and contribute to central sensitisation. This is marked by structural and functional changes in both ascending and descending neural pathways (1). As a result, the nervous system becomes hypersensitive to pain stimuli, and patients may experience chronic pain that does not correlate with lesion number or severity, and which can persist even after surgical removal of lesions.

Moreover, increased pMΦ abundance has been correlated with higher pelvic pain scores in endometriosis patients (25). Interestingly, the severity of pain symptoms does not always correlate with the rASRM stages (55). These findings suggest the involvement of complex mechanisms in pain generation, likely involving macrophages, that extend beyond lesion growth.

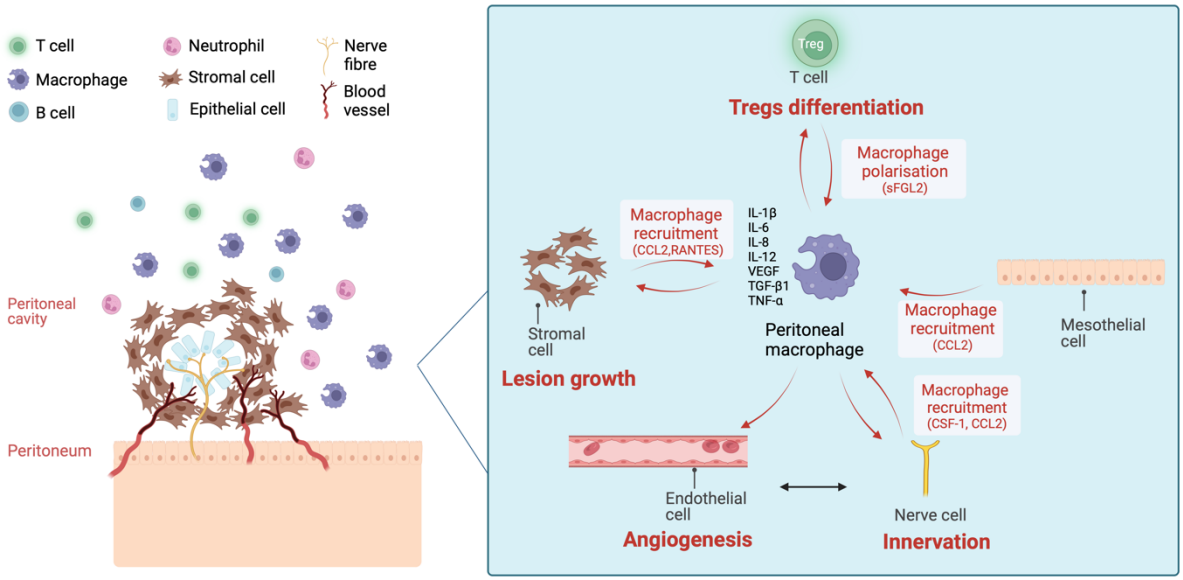

Figure 1.1. Macrophage - centred intercellular communication network in the peritoneal microenvironment of endometriosis. Ectopic endometriotic lesions in the peritoneal cavity consist of stromal and epithelial cells, infiltrated by blood vessels and nerve fibres. The surrounding peritoneal fluid (PF) contains various immune cells, including an increased number of total peritoneal macrophages (pMΦ) and CD206+/CD163+ macrophages in endometriosis patients. Stromal cells from endometriotic lesions, peritoneal mesothelial cells, and nerve fibers attract macrophages via MCP-1/CCL2, CSF-1, and RANTES (CCL5). Existing pMΦ further recruit macrophages by secreting MCP-1. Treg cells induce macrophage polarisation into pro-repair subtypes through sFGL2 secretion, promoting lesion growth. pMΦ contribute to lesion growth, angiogenesis, neurogenesis, and Treg differentiation by secreting cytokines and growth factors including IL-1β, IL-6, IL-8, IL-12, TNF-α, VEGF, and TGF-β1. Figure from Wang et al 2023 (56).

These studies demonstrate that pMΦ are intricately associated with endometriosis progression through complex intercellular communication with other immune components and the endometriotic lesions in the peritoneal microenvironment (Figure 1). The multifaceted roles of pMΦ in lesion development, angiogenesis, and pain generation underscore their importance as key players in the pathophysiology of endometriosis. The remarkable plasticity of pMΦ in response to diverse stimuli presents both opportunities and challenges. This adaptability makes pMΦ attractive targets for potential therapeutic interventions. However, their heterogeneity and dynamic nature also create hurdles in characterisation and targeted treatment development. Understanding the complex roles and behaviours of pMΦ is crucial for advancing our knowledge of endometriosis.

1.3 Small extracellular vesicle (sEV)-mediated cellular communication

It is important to note that intercellular crosstalk in the peritoneal microenvironment is not limited to soluble factors. Small extracellular vesicles (sEV) have emerged as important mediators of cell communication in various disease contexts. According to MISEV 2024 guidelines, sEV, previously referred to as exosomes, are defined as particles that are released from cells (30nm to 150nm), are delimited by a lipid bilayer, and cannot replicate on their own (57). sEV are present in almost all biological fluids, including PF (58). They are formed by the inward budding of multivesicular endosomes (MVE) and secreted after the fusion of MVE with the cell surface (59).

This process is regulated by several molecular sorting mechanisms. The main pathway involves the ESCRT (Endosomal Sorting Complex Required for Transport) machinery, which requires recruitment of multiple components (ESCRT-0, I, II, III,) working together to sort and package cellular materials into EVs (60). A simpler alternative pathway, known as the syndecan-syntenin-ALIX pathway, involves two adaptor proteins (syntenin and ALIX) and only requires ESCRT-III for vesicle formation through syndecan clustering (61). Besides these ESCRT-dependent pathways, cells can also form sEV through ESCRT-independent mechanisms, such as ceramide-mediated budding, which creates vesicles by changing membrane shape and organization (62).

sEV carry specific cargoes (proteins, lipids, nucleic acids, and metabolites) that reflect their cell of origin. These vesicles can deliver their contents to recipient cells, modulating their activities and contributing to intercellular communication (63). Notably, sEV are elevated in several diseases where they display altered phenotypes (59). Studies characterizing the role of sEV have advanced our knowledge of the pathology of various diseases, including cardiovascular diseases (64), neurological diseases (65), autoimmune disorders (66), and cancer (67).

The emerging importance of sEV in disease processes has led to their recognition as valuable biomarkers and potential therapeutic targets (68, 69). In the context of endometriosis, the role of sEV in mediating communication between pMΦ, ectopic endometrial cells, and other components of the peritoneal microenvironment represents an exciting area for further research.

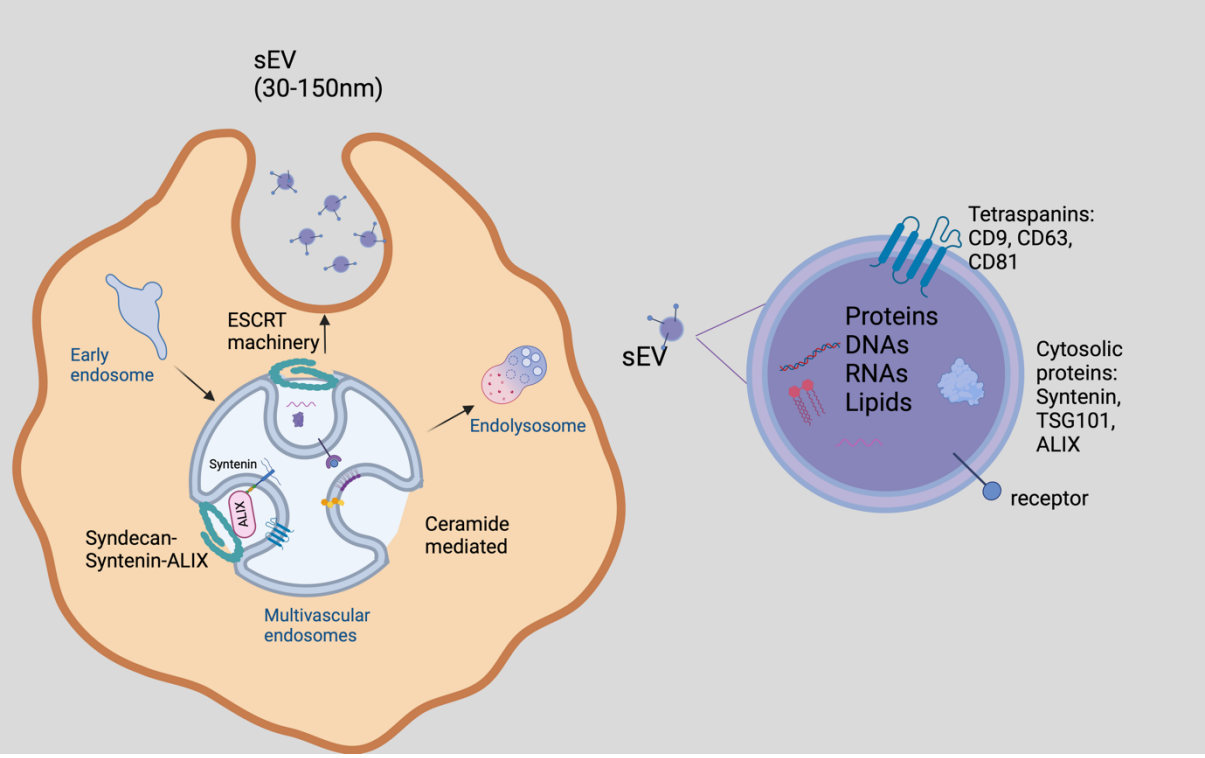

Figure 1.2. Biogenesis and composition of small extracellular vesicles (sEV). There are three major sEV formation pathways. The classical ESCRT-dependent pathway requires sequential recruitment of ESCRT complexes (ESCRT-0, -I, -II, and -III) for cargo sorting and vesicle formation. The syndecan-syntenin-ALIX pathway represents a simpler alternative that begins in multivesicular endosomes (MVE) where syndecan clusters with its cargo. This pathway involves two key adaptor proteins (syntenin and ALIX) that connect directly to ESCRT-III, bypassing the need for early ESCRT complexes. The ceramide-mediated pathway represents an ESCRT-independent mechanism shown occurring in the MVE. sEV are released into the extracellular space when MVE fuse with the plasma membrane. A typical sEV compose of tetraspanins (CD9, CD63, CD81) as membrane proteins, cytosolic proteins (Syntenin, TSG101, ALIX), various cargo molecules including proteins, DNAs, RNAs, and lipids, as well as surface receptors. Figure adapted from Lee et al 2024 (70).

The following subchapters will discuss sEV-mediated intracellular crosstalk in several different tissue microenvironments and consider how these mechanisms may contribute to endometriosis development.

1.3.1 The biogenesis and uptake of sEV

sEV facilitate the transfer of functional proteins, lipids, and nucleic acids to recipient cells, playing a significant role in intercellular signalling (59). The cargo of sEV generally reflects that of their parent cells, with a particular enrichment in small non-coding RNAs, such as microRNAs (miRNAs) and RNA fragments (71, 72).

In the context of endometriosis, altered miRNA expression profiles have been observed in patients, suggesting a potential role for sEV-mediated miRNA transfer in the disease process. Given that miRNAs also function as epigenetic regulators, sEV could contribute to the epigenetic alterations associated with endometriosis (73).

The uptake of sEV can occur both locally at the site of release and distantly as they circulate in biological fluids (74). Interestingly, some sEV demonstrate cell-type specificity in their uptake, as exemplified in cases of sEV-mediated organ-specific metastasis in cancer (75). The cellular uptake of sEV is largely determined by their surface composition (76).

Once sEV reach the recipient cells, they can exert their effects through various mechanisms. They may trigger signalling pathways by directly interacting with surface receptors, fuse with the plasma membrane, or be internalised by the cell (74). For the functional utilization of sEV-encapsulated miRNAs and RNAs, internalisation is necessary. Following internalisation, sEV must bypass degradation pathways and release their cargos in a manner that allows targeting to the endoplasmic reticulum for translation (77).

When sEV come into contact with biological fluids, a shell of proteins (protein corona) forms outside sEV, potentially influencing their biodistribution, cellular uptake, and biological effects (78). Albumin, a common protein found in biological fluids (79), has been currently viewed as a potential co-isolate in sEV preparations (57). However, latest research suggests that albumin is detected as the most abundant corona protein by several studies (78, 80, 81). Albumin in the corona could protect sEV from degradation, alter their cellular uptake, or even contribute to their targeting capabilities (78).

1.3.2 sEV-mediated crosstalk in healthy and diseased microenvironments

Endometriotic lesions share several clinical similarities with cancer, including a metastatic phenotype characterised by adhesion, invasion, and neuroangiogenesis. However, it is important to note that the lack of driver mutations limits the malignant potential of most forms of endometriosis (2). Given these similarities, insights from cancer research on sEV-mediated communication can provide valuable perspectives for understanding endometriosis.

Tumour-associated macrophages (TAMs) and their derived sEV (TAM-sEV) have been extensively studied in the context of cancer. TAM-sEV have been found to regulate various aspects of tumour progression, including tumorigenesis (82), metastasis (83, 84), and drug resistance (85). These effects are mediated through the transfer of miRNAs and proteins to other cells within the tumour microenvironment. The specific regulatory effects appear to be dynamic and dependent on the cancer type. For example, in gastric cancer, TAMs promote the migration of cancer cells by transferring functional Apolipoprotein E via sEV, thereby activating the PI3K-Akt signalling pathway (83). TAM-sEV can also indirectly regulate tumour progression by targeting other cell types in the microenvironment. In pancreatic ductal adenocarcinoma, TAM-sEV carrying miR-155-5p and miR-211-5p promote angiogenesis and tumour growth by suppressing E2F2 expression in endothelial cells (86). In epithelial ovarian cancer, TAM-sEV induce an imbalance between regulatory T cells and T helper 17 cells, contributing to tumour progression and metastasis (87).

Importantly, the sEV-mediated communication within the tumour microenvironment is bidirectional. For instance, in colorectal cancer, tumour-derived sEV miR-934 has been shown to induce macrophage polarization towards an anti-inflammatory phenotype, promoting liver metastasis (88). However, the sEV-mediated regulation of TAMs is not limited to inducing anti-inflammatory polarisation. In oral squamous cell carcinoma, tumour-derived sEV can activate pro-inflammatory TAMs, promoting tumour migration (89).

Beyond cancer, sEV also play crucial roles in other reproductive pathologies and in normal endometrial function. For example, in adenomyosis, a condition often associated with endometriosis (90), sEV secreted by endometrial organoids contain miRNAs associated with pregnancy complications and disease progression (91). In embryo implantation, protein cargos of sEV derived from endometrial epithelial cells have been shown to enhance the adhesive capacity of trophoblasts, potentially facilitating successful implantation (92). (90, 91).

1.3.3 The sEV-mediated crosstalk in the peritoneal microenvironment of endometriosis

The study of sEV in endometriosis is an emerging field with significant potential. Despite the limited number of studies (less than 100 in PubMed as of this writing), the results have shown promising insights into the complex network of sEV-mediated communication within the peritoneal microenvironment of endometriosis.

Macrophage derived-sEV have been shown to exert significant influence on endometrial stromal cells through various mechanisms. pMΦ-sEV can transfer miR-22-3p to endometrial stromal cells, enhancing cell proliferation, migration, and invasion through the regulation of the SIRT1/NF-κB signalling pathway (93). Another study revealed that pMΦ-sEV induce proliferation and migration of ectopic stromal cells *in vitro* and promote lesion growth in an endometriosis mouse model via the transfer of the long non-coding RNA (lncRNA) CHL1-AS1 (94). This lncRNA is the antisense of the *CHL1* gene, which can either suppress or promote cancer development at different stages (95). Overexpression of both the *CHL1* gene and lncRNA CHL1-AS1 has been found in the ectopic endometrium from ovarian endometriosis patients (96).

Interestingly, the effects of macrophage-derived sEV on endometriosis progression appear to depend on the phenotype of the source macrophages. This phenotype-dependent effect adds another layer of complexity to the role of sEV in endometriosis. For instance, sEV from LPS-induced macrophages can reduce endometriosis lesion growth by repolarising anti-inflammatory macrophages into pro-inflammatory subtypes in mice (97). These

macrophage-derived sEV also repress stromal cell migration and angiogenesis *in vitro* (97). These studies collectively suggest that macrophage-derived sEV could target various cells and pathways in endometriosis. The ultimate effect of these sEV - whether they promote or suppress endometriosis progression - appears to be determined by the phenotypes of the macrophages from which they are derived.

Conversely, sEV derived from stromal cells induced macrophage polarisation into an anti-inflammatory subtype with decreased phagocytotic abilities, leading to increased lesion size (98). A recent study found that ectopic stromal cells collected from patients with recurrent ovarian endometriosis induced anti-inflammatory polarisation of macrophages via the secretion of sEV (99).

Apart from regulating pMΦ, sEV derived from endometrial stromal cells have been found to induce neuroangiogenesis (100). Additionally, sEV from endometrial stromal cells of endometriosis patients exhibit differential profiles of miR-21 and lncRNA antisense hypoxia inducible factor 1 alpha (HIF-1α), promoting proangiogenic properties in endothelial cells (101, 102). The lncRNA HIF-1α derived from endometrial stromal cells targets VEGF, a potent pro-angiogenic molecule highly expressed in endometriosis lesions and PF of endometriosis patients (102).

Interestingly, some stromal cell-derived sEV contents may have protective effects. For example, miR-214 and miR-214-3p secreted in stromal cell-derived sEV have been found to suppress fibrosis of endometriosis lesions in murine models (103, 104). Notably, miR-214-3p was significantly downregulated, and its target, connective tissue growth factor, was upregulated in ectopic lesions from endometriosis patients (104).

While research on endometrial stromal cells is extensive, studies on sEV from endometrial epithelial cells in endometriosis remain limited. Recent findings have highlighted the significance of epithelial cell-derived sEV. For instance, miR-30c encapsulated in sEV from endometriotic epithelial cells was found to suppress epithelial cell invasion and migration, attenuating endometriosis progression in a mouse model (105). EV characterisation is hindered by difficulties of maintaining polarity and functions of primary endometrial

epithelial cell in 2D culture. 3D models, such as endometrial epithelial organoids (EEOs), which maintain cell polarity and preserve clinical characteristics of endometriosis lesions *in vitro*, offer promising tools for future EV investigations (106, 107). EEO models, successfully applied in an EV study of eutopic endometrium tissue in adenomyosis (91), could potentially be expanded to study eutopic and ectopic endometrium tissue in endometriosis.

These *in vitro* and *in vivo* studies indicate that the peritoneal microenvironment likely contains a variety of sEV carrying key factors instrumental in the pathogenesis of endometriosis. In addition to the known miRNA and lncRNA profiles, a distinct sEV protein profile has been identified in a mass spectroscopy proteomic study of PF-derived sEV from endometriosis patients compared to controls (39). Investigating the cell origins and functional roles of these PF-sEV are important in identifying therapeutic and diagnostic targets.

Despite expanding research on sEV in the peritoneal microenvironment, there remain gaps in understanding sEV-mediated communication between immune cells, nerves, and endometrial epithelial cells. I propose that sEV-mediated communication in the peritoneal microenvironment of endometriosis involves multiple cell types and carries diverse molecular cargos. These sEV likely modulate various aspects of the disease, from lesion attachment to local inflammation (Figure 2.)

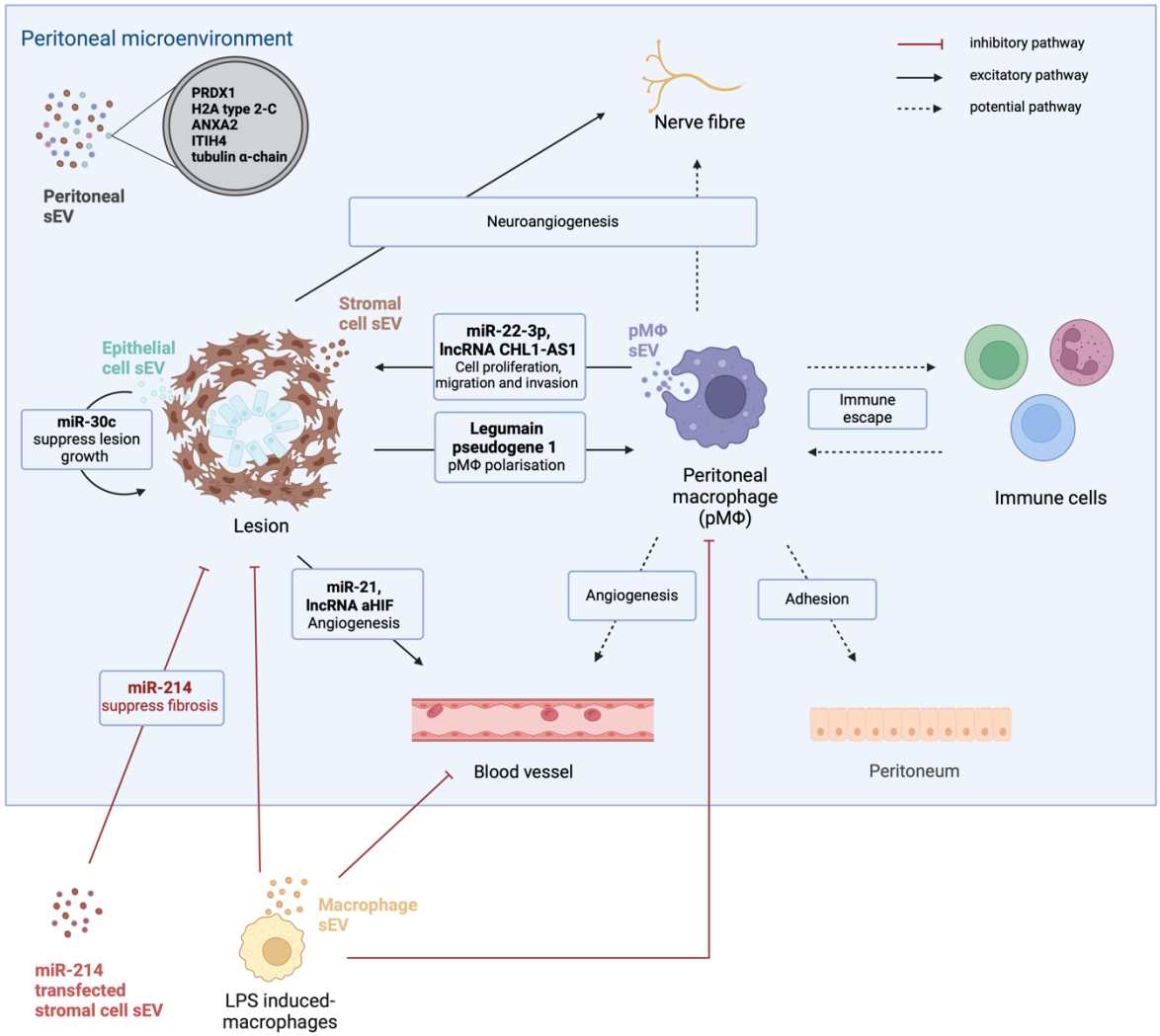

Figure 1.3. Small extracellular vesicle-mediated intercellular communication in endometriosis. Small extracellular vesicles (sEV) in peritoneal fluid (PF) exhibit distinct protein profiles in endometriosis patients compared to controls. Five proteins (PRDX1, H2A type-2-C, ANXA2, ITIH4, and tubulin alpha-chain) are uniquely present in PF-sEV from endometriosis patients. sEV facilitate intercellular communication within the peritoneal microenvironment of endometriosis. Stromal cell-derived sEV regulate macrophage polarisation via legumain pseudogene 1 and promote angiogenesis through miR-21 and lncRNA aHIF, while also enhancing neuro-angiogenesis. Endometrial epithelial cell sEV inhibit lesion growth by transferring miR-30c. Peritoneal macrophage (pMΦ)-sEV promote lesion growth by delivering miR-22-3p and lncRNA CHL1-AS1 to stromal cells, and potentially regulate angiogenesis, neuroangiogenesis, and immune escape. Therapeutic approaches include miR-24 transfected sEV from stromal cells suppressing fibrosis in mouse models, and LPS-induced macrophage-derived sEV attenuating endometriosis progression through pMΦ repolarization, angiogenesis inhibition, and stromal cell proliferation reduction. Figure from Wang et al 2023 (56).

1.4 Hypothesis & Aims

The preceding chapters have highlighted the complex nature of endometriosis as a hormone-dependent disorder, the significance of macrophages in the peritoneal microenvironment in disease progression, and the emerging role of sEV in mediating intercellular communication and potentially influencing disease pathogenesis. Drawing from these foundations, I propose the following hypotheses for this DPhil study:

i. PF-sEV originate from diverse cell types, including pMΦ and endometriosis lesions.
ii. PF-sEV could serve as indicators for environmental changes in the peritoneal microenvironment, such as disease progression or hormonal status.
iii. PF-sEV, especially those derived from endometrial epithelial cells, have distinct effects on macrophage differentiation and function, contributing to the pathogenesis of endometriosis.

To test these hypotheses, the following aims were addressed in subsequent chapters:

Chapter 2: Characterisation of pMΦ and pMΦ derived sEV (pMΦ-sEV). This chapter focused on:

a) Isolating and phenotyping pMΦ from endometriosis patients and controls.
b) Characterising the surface protein expression of pMΦ-sEV.
c) Comparing EV profiles and phenotypic profiles of these macrophages.

Chapter 3: Characterisation of Peritoneal Fluid-derived Small Extracellular Vesicles (PF-sEV). This chapter focused on:

a) Isolating sEV from PF of endometriosis patients and controls.
d) Characterizing the surface protein expression of PF-sEV.
b) Identifying disease-specific sEV signatures.
c) Identifying hormone treatment-specific sEV signatures.

Chapter 4: Investigation of the effect of PF-sEV on Macrophage Differentiation and Functions. This chapter focused on:

a) Establishing an *in vitro* macrophage model
b) Investigating the changes in macrophage functions (e.g., phagocytosis, cytokine production) induced by PF-sEV.
c) Exploring potential mechanisms by which PF-sEV modulate macrophage behaviour.

Chapter 5: Characterisation and Functional Analysis of Endometrial Epithelial Organoid-derived sEV. This chapter focused on:

a) Establishing and characterising endometrial epithelial organoids (EEOs) from eutopic endometrium from endometriosis patients and controls, and from endometriosis lesions.
b) Isolating and characterising sEV derived from EEOs from eutopic endometrium from endometriosis patients and controls, and from endometriosis lesions.
c) Assessing the impact of EEO-sEV on macrophage differentiation and functions.
d) Conducting an integrated analysis comparing sEV profiles of PF, pMΦ and EEOs.

Chapter 2 Characterisation of peritoneal macrophages (pMΦ) and pMΦ-derived small extracellular vesicles (sEV)

2.1 Introduction

pMΦ are the largest resident immune cell population that typically freely float in fluid in the peritoneal cavity. They conduct both immune surveillance and maintain tissue homeostasis by engaging in phagocytosis of apoptotic cells and tissue repair, presenting antigens to activate T cells and producing cytokines (108-110). In endometriosis, pMΦ undergo substantial alteration in both numbers and functions which will be discussed below. Blood derived monocytes will be attracted to site of inflammation like endometriosis lesions, emerging evidence suggests that pMΦ can migrate directly across the mesothelial lining of visceral organs to reach sites of injury (111). They have emerged as key mediators in the pathogenesis of endometriosis, promoting inflammation, lesion growth, angiogenesis and neurogenesis (112). Depletion of pMΦ in an endometriosis mouse model has shown they are essential in lesion growth and vascularisation (113).

The plasticity of macrophages allows them to adopt different phenotypes in response to environmental cues, ranging from pro-inflammatory (M1) to pro-repair (M2) states (114). In endometriosis, there is growing evidence of a skew towards the M2 phenotype, which is associated with tissue remodelling, angiogenesis, fibrosis and immunosuppression – all processes that facilitate the progression of the disease (53, 115, 116). However, it is important to note that the traditional M1/M2 classification, largely based on *in vitro* studies, fails to capture the full complexity of macrophage phenotypes observed *in vivo*.

Recent investigations have revealed a more complex picture, with studies reporting increased macrophage infiltration of both pro-inflammatory and pro-repair subtypes in endometriosis (20, 26, 117). Furthermore, macrophage status appears to differ between

disease stages (I/II vs. III/IV), with different studies drawing varied conclusions. A single cell protein phenotyping study using Cytometry by Time of Flight (CyTOF) demonstrated significantly increased frequencies of both M2 (CD163+/CD206+) and M1 (CD40+/CD16+) macrophage signatures in PF of stage I/II endometriosis patients. Interestingly, these populations were reduced in more severe disease stages (118). In contrast, another study examining peritoneal lavage samples found a decrease in M1 (CD86+) macrophages and an increase in M2 (CD163+) macrophages in stage III/IV compared to stages I/II (119). Single-cell RNA sequencing of PF revealed seven distinct subtypes of pMΦ and individual macrophages could express both pro-inflammatory and pro-repair markers simultaneously, with no significant shift towards either phenotype (26). These discrepancies may be attributed to several factors, including limited sample sizes, restricted and potentially biased marker selection, and patient-specific immunophenotypes.

Additionally, the dynamic nature of macrophage populations throughout the progression of endometriosis further complicates the characterization of these cells in different disease stages. Most pMΦ phenotyping studies have been conducted using mouse models (52, 116). In mice, two main pMΦ subsets have been identified based on F4/80 and MHC II expression. Tissue-resident "large" peritoneal macrophages (LpM) are characterized as F4/80^{high}, MHC II^{low}, while monocyte-derived "small" peritoneal macrophages (SpM) are F4/80^{low}, MHC II^{high} (120). Lesion-resident monocyte-derived macrophages have been found to be promote lesion growth while monocyte derived LpM were protective (52). In human studies, CD14^{high} CD16^{high} macrophages have been characterised as resident pMΦ (121), but their status in endometriosis remains unclear. Other investigations have revealed an increase in CD14^{high} subpopulations in endometriosis patients (122). Importantly, a recent single-cell cross-species analysis of mouse and human pMΦ revealed concordance in pro-disease and pro-resolving populations (123). This finding bridges the gap between mouse models and human studies, potentially allowing for more translatable research outcomes.

Recent advances in cellular biology, especially in cancer studies, have highlighted another crucial aspect of macrophage function: their ability to secrete sEV. These nano-sized membrane-bound structures serve as important intercellular communicators, carrying a diverse cargo of proteins, lipids, and nucleic acids (124). In endometriosis, pMΦ-sEV have

been implicated in various pathological processes, including the promotion of stromal cell growth and angiogenesis in the peritoneal microenvironment (56).

Despite the growing recognition of the importance of pMΦ-sEV in disease processes, their characterisation remains limited. While some studies have explored RNA signatures of these vesicles (37, 125), an analysis of their protein composition, particularly their surface marker expression, is lacking. Such characterisation could provide valuable insights into the functional properties of these vesicles and their potential roles in disease establishment and progression.

This chapter aims to provide a comprehensive characterisation of both pMΦ and their derived sEV in endometriosis. I will begin by exploring the phenotypic and functional alterations of pMΦ in endometriosis patients compared to healthy controls. This will include an in-depth analysis of their activation states and polarisation profiles, by flow cytometry. Following this cellular characterisation, I will focus on pMΦ-sEV. I will first optimise protocols for the *in vitro* EV isolation and characterise isolated EV following MISEV guidelines (57), a critical step in ensuring the purity and integrity of the samples. Subsequently, I will conduct detailed phenotypic characterisation of their surface marker expression.

Currently, there is no universal EV isolation method, meaning that various methodologies (detailed in Figure 2.1) are used. As a result, isolated EV populations can substantially vary between different research studies or groups. To address this variability, the MISEV guidelines require that the general characterisation of EV must reflect at least two EV markers: a transmembrane protein (such as tetraspanins CD9, CD63, or CD81) and a cytosolic protein (like ESCRT and accessory proteins syntenin, ALIX, or TSG101). Additionally, at least one negative protein marker (e.g., apolipoproteins A1/2 or B, or albumin) is necessary to assess the purity of EV preparations (57).

For protein composition analysis, methods such as Western blotting, single EV flow cytometry (126, 127), and bead-based flow cytometry assays (128, 129) are commonly used. Additional techniques offer further insights into EV characteristics. Nanoparticle Tracking

Analysis (NTA) provides measurements of EV size distribution and concentration by tracking the Brownian motion of individual particle in suspension, while also allowing examination of protein expression through fluorescence-based detection. Electron microscopy (EM) complements these methods by providing high-resolution images of EV morphology, size, and sample purity.

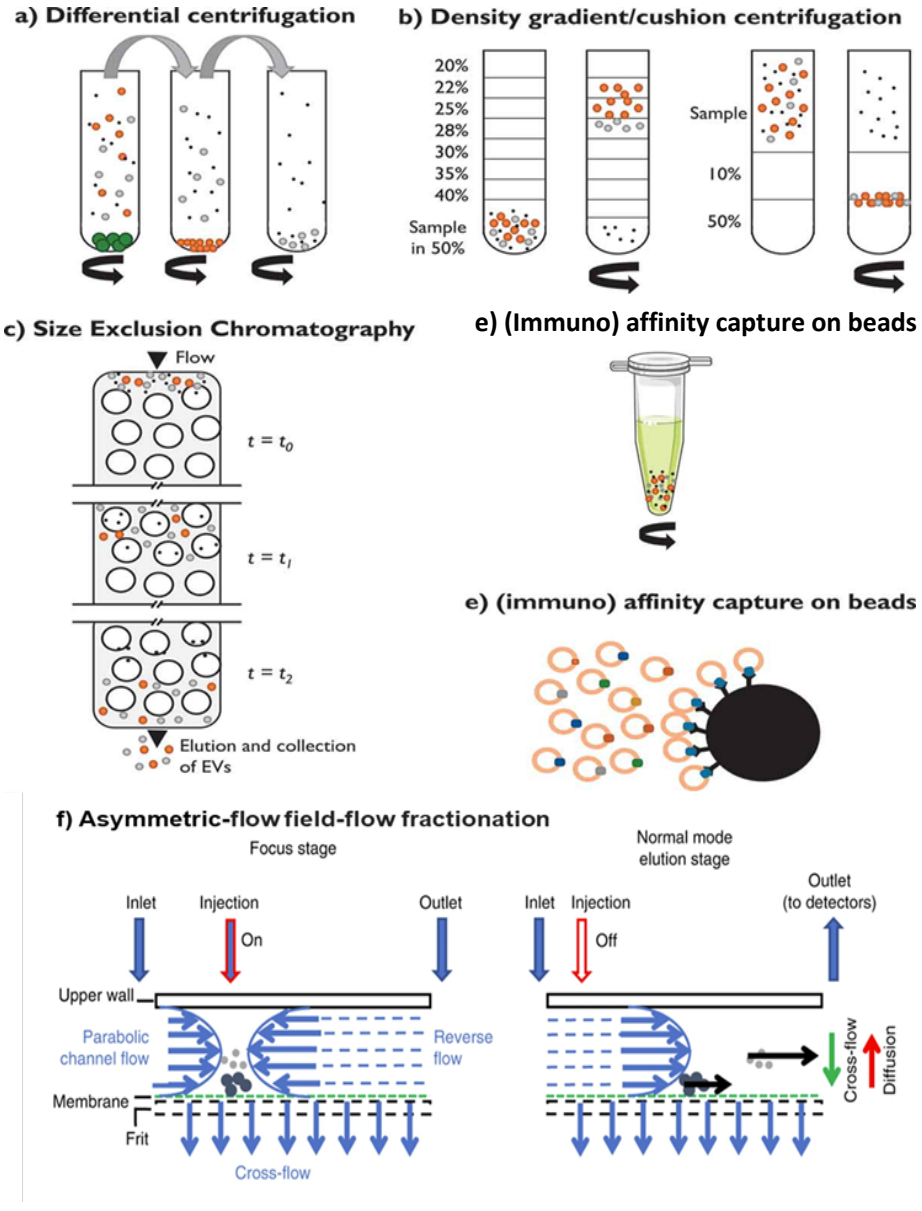

Figure 2.1. Different techniques used for extracellular vesicle isolation. a) Differential (ultra) centrifugation: sequential isolation of EV based on sedimentation rate. Final pelleting typically requires ultracentrifugation (>100,000 x g). **b)** Density gradient centrifugation: separation of particles with different compositions (proteins/lipids) based on their densities. **c)** Size exclusion chromatography (SEC): separation based on size, larger EV elute first, followed by smaller EV, while smaller molecules (i.e. soluble proteins) are delayed by entering pores in the matrix. **d)** Precipitation kits: utilize aggregating agents like

polyethylene glycol to precipitate EV and proteins based on their solubility. **e)** Immunoaffinity techniques: capture EV by binding specific EV transmembrane proteins using antibodies. **f)** Symmetric flow field-flow fractionation: a two-stage process - opposing flows concentrate the sample then single-direction flow elutes particles, with smaller ones emerging first, in addition a semi-permeable lower wall removes unwanted particles. Images modified from Zhang et al. 2019 (130) and Mateescu et al. 2017 (131).

I used a bead-based MACSPlex EV kit IO (for immuno-oncology) to characterise pMΦ-EV protein composition (Figure 2.2). It allows quick and sensitive measurement of 37 surface epitopes, including sEV enriched tetraspanins (CD9, CD63 and CD81) and immune signalling molecules including HLA-DR, and CD24. This technique has been applied in biomarker detection in various diseases (132, 133).

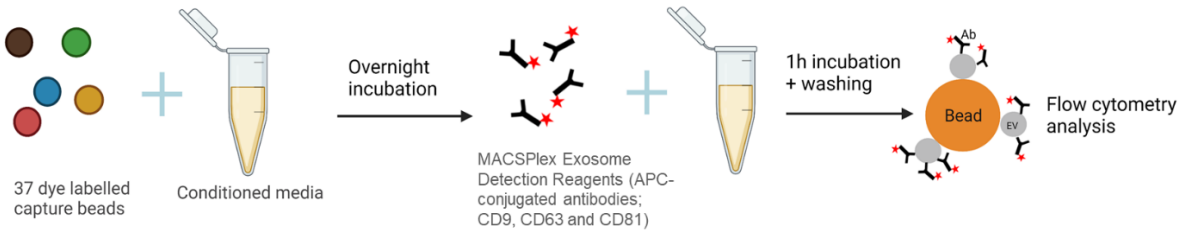

Figure 2.2. Principle of multiplex bead-based assay using MACSPlex EV kit IO (for immuno-oncology). The assay uses a set of 37 differently fluorescently labelled capture beads. Each bead population is designed to bind to a specific EV surface protein. When mixed with a sample containing EV overnight, these capture beads bind to their corresponding antigens on the EV surface. After the EV are captured, a cocktail of detection antibodies is added. These antibodies are typically against common EV markers (CD9, CD63, and CD81) and are conjugated with the fluorophore Allophycocyanin (APC). This allows for identification of different bead populations based on their unique fluorescence and quantification of bound EV based on the intensity of the detection antibody fluorescence by flow cytometry.

It is well established that the content of EV, including their protein and surface marker composition, is highly dependent on the source cells (134). This relationship between cellular state and EV characteristics presents an intriguing opportunity to use EV signatures as potential indicators of cellular origins and changes in the peritoneal microenvironment. Notably, the MACSPlex EV kit IO has been successfully employed to analyse EV surface markers in serum samples and establish their correlation with cellular marker expressions of various immune cells (135). Building on these advances, I aim to extend this methodology to the context of pMΦ in endometriosis. By comparing the MACSPlex EV kit IO analysis of

pMΦ-EV with flow cytometry measurements of pMΦ cell surface expression, I seek to determine the extent to which EV surface markers mirror those of their parent cells in endometriosis.

By establishing the relationship between cellular and EV phenotypes in a controlled *in vitro* setting, I will be better equipped to interpret the more complex EV populations found in PF and their potential cellular origins in the subsequent chapter.

2.2 Methods

2.2.1 Peritoneal fluid (PF) collection

The biological samples and clinical data were collected as part of the prospective FENOX study (17/SC/0664) of endometriosis and uterine fibroids at the Oxford Endometriosis CaRe Centre. These samples and data were collected, processed, and stored according to World Endometriosis Research Foundation Endometriosis Phenome and Biobanking Harmonisation Project (WERF EPHect) protocols (136-139). The exclusion criteria were malignancy, pregnancy, breastfeeding, and an inability to understand the study or the consent form. PF samples were obtained from women of reproductive age (18-49 years old) undergoing laparoscopy for suspected endometriosis. PF samples were kept on ice to minimise cell adherence and processed within 1 h for pMΦ isolation. PF samples collected had minimal blood contamination from surgery. Lavage samples were excluded. A total of 28 PF samples (age: 28.4 ± 6.2 years; BMI: 26.6 ± 5.9 kg/m^2; mean ± SD) were used in the studies presented in this chapter with patient information listed in Table 2.1.

Table 2.1. Clinical Characteristics of recruited FENOX patients. Patient numbers (1-28) are listed with corresponding endometriosis stage (0-4, as rASRM classification), menstrual cycle phase (proliferative/secretory), exogenous hormone use (Yes or No, Y/N), age and BMI. N/A indicates that information was not available.

Patient Number	Endometriosis staging (0-4)	Cycle	Hormone use	Age	BMI
1	0	Secretory	Y	22	22.9
2	0	N/A	Y	27	21.7
3	0	Proliferative	N	22	23.4
4	0	N/A	Y	48	N/A
5	0	N/A	Y	21	23.3
6	0	N/A	Y	24	26.6
7	0	Secretory	Y	22	31.2
8	1	Proliferative	N	24	18.7
9	1	N/A	Y	25	36.7
10	1	Secretory	N	34	25.3
11	1	N/A	Y	25	22.5

12	1	N/A	Y	29	31
13	1	N/A	Y	26	28.5
14	1	N/A	Y	24	22
15	1	Secretory	N	34	29
16	1	Secretory	N	30	34.9
17	1	N/A	Y	28	33.3
18	1	Proliferative	N	30	32.4
19	1	Secretory	N	28	22.4
20	2	N/A	Y	30	35.2
21	2	Secretory	Y	38	20.4
22	2	N/A	Y	20	20.7
23	2	Proliferative	Y	25	19.9
24	2	N/A	N	34	20.2
25	2	Secretory	N	34	N/A
26	2	N/A	N	38	37.9
27	3	Secretory	N	26	29.6
28	4	Proliferative	N	28	21.6

2.2.2 Peritoneal macrophage (pMΦ) isolation and culture

pMΦ were isolated by a previously described method (140). In brief, fresh PF (3-5 mL) was overlaid onto Ficoll-Paque Plus (Cytiva, USA) and centrifuged (800 × g, 20 min). The mononuclear cell layer was collected and washed with 12 mL RPMI 1640 media (Thermo Fisher Scientific, USA) at 300 × g for 10 min. The cell pellet was resuspended in 1 mL RPMI 1640 media. The cells were counted, and cell viability was assessed by trypan blue staining. Cells were seeded at a density of 2×10^6 cells/well in 24-well plates for 30 min for adherence. The adherent cells were cultured in complete media composed of RPMI 1640 media with 100 U/mL Penicillin/Streptomycin (P/S) (Sigma Aldrich, USA) and 10% (v/v) Fetal Calf Serum (FCS) (Sigma Aldrich, USA). Cells were incubated at 37°C with 5% CO_2. Culture media was changed every 2-3 days to maintain optimal growth conditions. On day 4, 2 wells of pMΦ were detached from plates after incubation with Accutase cell detachment solution (Sigma Aldrich, USA) for flow cytometry analysis, and the remaining wells (2-4 wells) had their growth media changed to EV-depleted media for EV collection. After EV collection on day 6, pMΦ were resuspended in 100 µL 1× Pierce™ RIPA lysis buffer (Thermo Fisher Scientific, USA) with

protease inhibitor (PI) (cOmplete™, Mini, EDTA-free Protease Inhibitor Cocktail, Roche, Switzerland) and stored at -20°C for western blotting.

2.2.3 pMΦ-sEV isolation

FCS was ultracentrifuged at 150,000 x g for 16 h at 4°C to deplete the FCS of EV. RPMI 1640 media containing 10% (v/v) EV-depleted FCS and P/S (EV-depleted media) was prepared. pMΦ were washed with phosphate buffered saline (PBS, Sigma Aldrich, USA) three times and cultured in EV-depleted media.

For initial time point optimisation, supernatants from 4 pMΦ samples were collected at both 24h and 48h of incubation (2-4 mL per sample) to compare EV characteristics measured by Nanoparticle Tracking Analysis (NTA). For all other experiments, supernatants were collected after 48h incubation. The collected supernatant was centrifuged twice at 1500 x g for 10 min to remove cell debris. The supernatant was then further centrifuged at 16,000 x g for 30 min to remove large vesicles. The supernatant was transferred into Ultra Clear ultracentrifuge tubes (5 mL; Beckman coulter, USA) and topped up with 0.1 µm PVDF membrane (Sarstedt, Germany) filtered PBS (fPBS). Samples were then ultracentrifuged using an Optima XE-90 ultracentrifuge (Beckman coulter, USA) with SW55-Ti swinging bucket rotor (Beckman coulter, USA) at 150,000 x g for 2 h. The supernatant was discarded, and pMΦ-sEV pellets were resuspended in fPBS.

2.2.4 Nanoparticle Tracking Analysis (NTA)

The isolated pMΦ-sEV were measured using a NanoSight NS500 instrument (405 nm laser) with NTA software, version 3.4 (Malvern Panalytical, UK). Samples were diluted with fPBS to achieve a concentration between $2x10^8$ and $1x10^9$ particles/ml for analysis. Diluted samples were loaded into a 1 mL syringe and infused into the sample chamber using a syringe pump set at a flow rate of 15 arbitrary units. For each sample, five 60-second videos were recorded with camera brightness levels of 12 or 13. In each video, >5,000 valid tracks were recorded. The EV concentration and EV mode/mean size was determined for all samples.

2.2.5 Transmission Electron Microscopy (TEM)

For EV visualization, TEM was performed by Errin Johnson at the Sir William Dunn School of Pathology. In brief, a carbon-coated 300 mesh copper grid was glow discharged and then incubated on a 10 µL droplet of the sample for 2 min, blotted with filter paper, negatively stained with 2% uranyl acetate for 10 seconds, blotted, and air dried. Grids were imaged at an accelerating voltage of 120 kV in a FEI T12 TEM using a Gatan OneView digital camera.

2.2.6 Bicinchoninic Acid (BCA) Assay

Protein concentration of pMΦ-sEV and pMΦ cell lysates used for Western blot was determined by the Pierce™ BCA protein assay kit (Thermo Fisher Scientific, USA) with a working range of 0.125-2 mg/mL. Absorbance was measured at 280nm using a FLUOstar Optima microplate reader (BMG LabTech, Germany). The resulting data were processed and analysed with Optima Data Analysis 3.01 R2 software (BMG LabTech, Germany).

2.2.7 Western Blotting

The sEV-associated protein Syntenin and the negative marker albumin were examined using a modified MACSPlex EV kit IO, capture bead protocol (132). Briefly, pMΦ-sEV were isolated from pooled samples collected from three endometriosis patients as described in section 2.2.3. and were resuspended in 120 µL MACSplex buffer and incubated overnight with 15 µL of MACSplex EV kit IO capture beads. After centrifugation (3000 x g, 5min), the supernatant was removed and sEV bound to the capture beads were resuspended in 20 µL 1 x Pierce™ RIPA lysis buffer (Thermo Fisher Scientific, USA) with PI (cOmplete™, Mini, EDTA-free Protease Inhibitor Cocktail, Roche, Switzerland) and samples stored at -20°C. Protein concentration was determined by BCA assay. For each analysis, 5-20 µg of sEV were used with an equal amount of pMΦ cell lysates as controls. Samples were prepared by adding NuPAGE™ LDS Sample Buffer (4×) and NuPAGE™ Sample Reducing Agent (10×) (both from Thermo Fisher Scientific, USA) to the sEV or cell lysate samples. Proteins were denatured at

100°C for 5 min, and debris was removed by centrifugation at 13,000 × g for 1 min at room temperature. Samples were then loaded onto a NuPAGE Novex 4-12% Bis-Tris Gel (Thermo Fisher Scientific, USA).

Protein separation was performed using NuPAGE MOPS SDS Running Buffer (Thermo Fisher Scientific, USA) at 150 V for 1 h. Proteins were then transferred to a methanol activated PVDF membrane via electroblotting at 25 V for 1 h. Successful protein transfer was verified using Ponceau S staining (Thermo Fisher Scientific, USA). Membranes were blocked using 5% Blotto (Alpha Diagnostic International, USA) and incubated with specific primary antibodies in blocking solution overnight at 4°C. Primary antibodies used were anti-Syntenin (1:1000, Monoclonal rabbit, EPR8102, Abcam, UK) and anti-albumin (1:1000, polyclonal rabbit, Cell Signalling Technology, USA). Next, membranes were washed three times with 0.05% Tween 20 in PBS, then probed with HRP-conjugated Goat-Anti-Rabbit or Goat-Anti-Mouse secondary antibody (1:2000 dilution, Dako, USA) at room temperature for 1 h. Following additional washes, protein bands were visualized using an EZ-ECL kit (Biological Industries, Israel) and imaged with a Gel-Box imaging system (Syngene, India).

2.2.8 Flow Cytometry

Flow cytometry was conducted using an LSRII flow cytometer (BD Biosciences, USA) equipped with 405nm, 488nm and 633nm lasers (BD Biosciences, USA). Data analysis was performed using FlowJo 10 software.

2.2.8.1 pMΦ characterisation

The macrophage purity panel included CD14, CD3, CD10, CD45 and EpCAM (Table 2.2).

Table 2.2. pMΦ purity flow panel. Fluorescein Isothiocyanate: FITC; PE: Phycoerythrin; APC: Allophycocyanin.

Antibodies	Clone	Fluorophore	Final concentration	Cell type
CD14	61D3	PE/Cy5	12.5 µg/mL	Monocyte/macrophage
CD3	SK7	Brilliant Violet 510™	2 µg/mL	T cell
CD10	HI10a	FITC	5 µg/mL	Stromal cell
CD45	HI30	Brilliant Violet 650™	2.5 µg/mL	Pan immune cell
EpCam	9C4	PE	6.25 µg/mL	Epithelial cell
Zombie NIR™ viability dye		APC/Cy7	1:1000	

CD14, CD206, CD163, HLA-DR and CD86 were selected for the macrophage characterisation panel (Table 2.3). All antibodies were purchased from BioLegend (USA). Cultured macrophages were first detached from plates by incubation with Accutase® (Sigma Aldrich, USA) for 30 min at 37°C. Cells were washed with PBS at 300 x g for 5 min and stained for viability. The Zombie NIR™ viability dye was reconstituted according to the manufacturer's protocol. DMSO (100 µL) was added to one vial of lyophilised Zombie NIR™ dye and mixed until fully dissolved. The reconstituted dye was aliquoted into 1 µL portions and stored at -20°C. For use, one 1 µL aliquot was thawed and diluted in 1 mL of PBS (1:1000 dilution). For each pMΦ sample, 100 µL of this working solution was added to the cells. Samples were then incubated for 15-30 min at room temperature in the dark. Cells were further washed with 1 mL PBS at 300 x g for 5 min and incubated with antibodies in 2% v/v FCS in PBS (PBS/FCS) at 4°C for 30 min in the dark. Cells were washed with PBS/FCS three times at 300 x g for 5 min to remove unbound antibodies and resuspended in 350 µl of PBS/FCS and analysed using flow cytometry. A minimum of 5000 events were collected for each sample. Unstained cells were run as a control.

ArC™ Amine Reactive Compensation Bead Kit (Thermo Fisher Scientific, USA) and Anti-Mouse Ig,κ/Negative Control Compensation Particles Set (BD Biosciences, USA) were used for compensating fluorophore spectral overlap for the viability dye or antibodies respectively.

Table 2.3. pMΦ characterisation flow panel

Antibodies	Clone	Fluorophore	Final concentration
CD14	63D3	APC/Cy7	10 µg/mL
HLA-DR	L243	Alexa flour 700	5 µg/mL
CD16	3G8	Brilliant Violet 785™	2.5 µg/mL
CD206	15-2	APC	5 µg/mL
CD163	GHI/61	Brilliant Violet 711™	5 µg/mL
LIVE/DEAD Fixable Blue		Brilliant Violet 421™	

pMΦ were split into two aliquots: one was heat-killed at 70°C for 15 minutes to generate non-viable cells, and the other was left untreated. Equal proportions of live and dead cells were mixed, stained with viability to confirm gating of dead and live population. For marker validation, unstained and fully stained pMΦ (with applied compensation) were used. Gates were set based on the clear separation between negative and positive populations for each marker. Representative gating plots for controls are shown in Appendix Figure 1.

2.2.8.2 pMΦ-sEV characterization

sEV surface proteins were characterised using the MACSPlex EV kit IO (Miltenyi Biotec, Germany) following the manufacturer's instructions (Figure 2.2). The kit is a microbead based technique, allowing the detection of 37 sEV surface epitopes as well as two isotype controls (Table 2.4).

In brief, pMΦ-sEV in fPBS (prepared in section 2.2.3) were first toped up with MACSPlex buffer to 120 µl and incubated with 15µl capture beads overnight at room temperature with rotation. After washing in MACSPlex buffer (3000 x g, 5 min), the captured pMΦ-sEV were incubated with 15 µl of APC-conjugated antibody cocktail (5 µl each of anti-CD9, CD63, and CD81) for 1 h at room temperature with rotation. The samples were washed at 3000 x g for 5 min and incubated in 1 mL of MACSPlex buffer for a further 15 min at room temperature under rotation. Finally, the samples were centrifuged (3000 x g, 5 min) and resuspended in 350 µL of MACSPLEX buffer for flow cytometry analysis.

To optimize EV input for MACSPlex analysis, a titration experiment was performed using pMΦ-sEV concentrations ranging from $5x10^7$ to $5x10^9$ EV/mL. Two pooled samples were quantified by NTA to determine initial EV numbers. Each concentration was incubated with capture beads and antibodies as described above and assessed by flow cytometry. The singlet bead population was gated using forward scatter (FSC) and side scatter (SSC) characteristics. Individual bead populations were then detected and distinguished using a FITC versus PE dot plot, based on their unique fluorescence intensities. The median APC signal intensity of each bead population correlates with the amount of bound sEV, indicating the relative abundance of specific surface epitopes in the sample.

Table 2.4. 37 surface epitopes detected by MACSPlex EV kit IO. The MACSPlex assay is designed to identify 37 distinct surface markers. Each of these markers is associated with one of two isotypes: either mouse-derived immunoglobulin G1 (mIgG1) or recombinant engineering antibodies developed by Miltenyi (REA, marked with an asterisk *).

Target Protein	Antibody isotype	Antibody	Isotype	Antibody	Isotype
HLA-DR*	Recombinant human IgG1	CD3	Mouse IgG2a	CD63	Mouse IgG1
CD56*	Recombinant human IgG1	CD4	Mouse IgG2a	CD40	Mouse IgG1k
CD105*	Recombinant human IgG1	CD19	Mouse IgG1	CD11C	Mouse IgG2b
CD49E*	Recombinant human IgG1	CD8	Mouse IgG2a	MCSP	Mouse IgG1
SSEA-4*	Recombinant human IgG1	CD2	Mouse IgG2b	CD146	Mouse IgG1
HLA-ABC*	Recombinant human IgG1	CD1c	Mouse IgG2a	CD24	Mouse IgG1
CD62P*	Recombinant human IgG1	CD25	Mouse IgG1	CD86	Mouse IgG1

CD81*	Recombinant human IgG1	CD29	Mouse IgG1k	CD326	Mouse IgG1
CD41B*	Recombinant human IgG1	CD69	Mouse IgG1k	CD133/1	Mouse IgG1k
CD42A*	Recombinant human IgG1	CD142	Mouse IgG1k	CD44	Mouse IgG1
ROR1	Mouse IgG1k	CD45	Mouse IgG2a	CD14	Mouse IgG2a
CD209	Mouse IgG1	CD31	Mouse IgG1	REA control	Recombinant human IgG1
CD9	Mouse IgG1	CD20	Mouse IgG1	mIgG1 control	Mouse IgG1

2.2.9 Statistical Analysis

Unpaired two-tailed Student's t-tests were used to compare the means of two groups. For multiple group comparisons, a one-way ANOVA with a Tukey's post-hoc test was applied. Pearson's correlation coefficient (r) was used to assess relationships between marker expression on pMΦ-sEV and pMΦ cell surface. Correlation strengths were interpreted as: 0.00-0.19 "very weak", 0.20-0.39 "weak", 0.40-0.59 "moderate", 0.60-0.79 "strong", and 0.80-1.0 "very strong". $P < 0.05$ was considered significant for correlations. Normality was assessed using the Shapiro-Wilk test, with non-parametric alternatives used for non-normal data. Throughout all analyses, $p < 0.05$ was considered statistically significant. Statistical analyses were performed using GraphPad Prism 9.0 and R.

2.3 Results

2.3.1 Establishment of a Standard Operating Procedure (SOP) for pMΦ Isolation and Characterisation

There was considerable variation in PF volume between patients (n=19), ranging from 0.5 mL to 20 mL, with an average volume of 5.2 mL ± 5.3mL. Peritoneal cells were collected by ficoll centrifugation. The total number of cells collected from PF samples prior to adherence also showed significant variability, ranging from 3 x 10^5 to 1 x 10^7 cells. Interestingly, there was a moderate correlation (r = 0.44) between PF volume and peritoneal cell number (Figure 2.3), however this did not reach significance. I also investigated potential correlations with menstrual cycle phase and the use of hormonal treatments. However, no associations were found between these factors and either PF volume or peritoneal cell number.

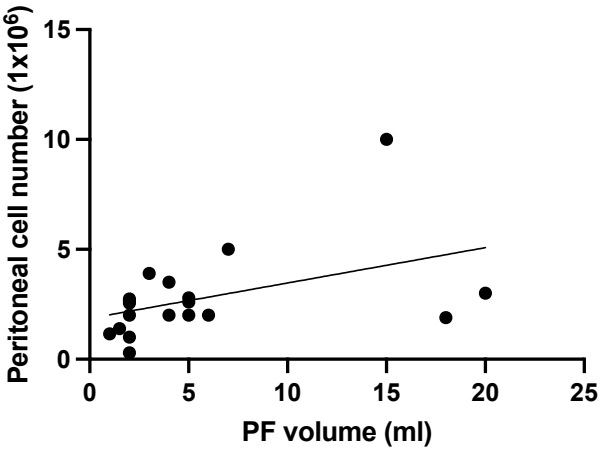

Figure 2.3. Correlation of PF volume and peritoneal cells. Scatter plot showing correlation (r = 0.44, P = 0.057 between PF volume and total peritoneal cell count in patient samples (n=19). Each point represents an individual patient sample.

Adherent cells were considered to be pMΦ (140). Isolated pMΦ were closely examined for their morphological characteristics under the light microscope. As expected, they exhibited features typical of macrophages after 4 days in culture (Figure 2.4). To assess their longevity and behaviour in culture, cells were monitored over an extended period. The cells remained viable in culture media for up to 10 days, with distinct phases observed throughout this period. In Days 0-2, a large number of cells were observed floating in the culture media. In

Days 3-6, the cells remained healthy and exhibited optimal morphology. They were well-spread on the culture surface and displayed numerous delicate protrusions extending from the cytoplasm, indicative of active and healthy macrophages. After day 10, cells began to detach from the culture surface and showed signs of decreased viability.

Based on these observations, I determined that the optimal window for phenotypic characterisation and sEV collection was between days 4-6, when cell viability consistently exceeded 80%.

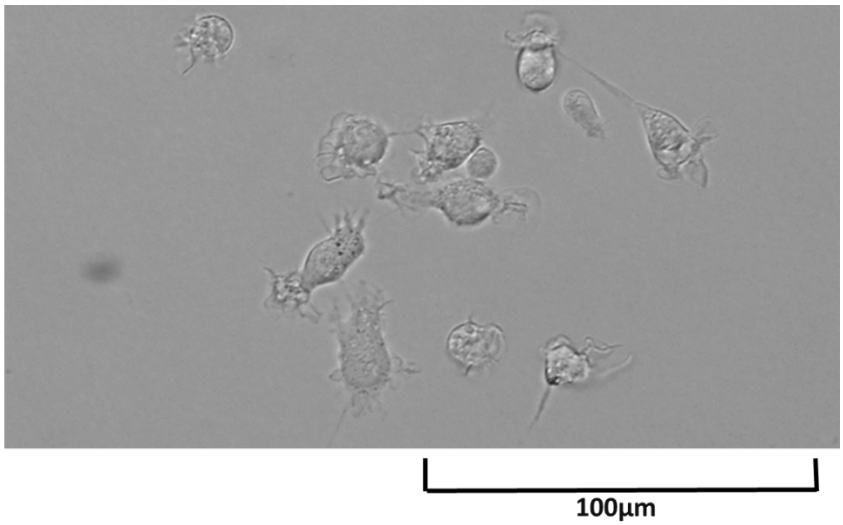

Figure 2.4. Morphology of pMΦ after 4 days of *in vitro* culture. Cells were imaged at X40 magnification with a phase contrast inverted microscope.

To assess the purity of the isolated cells, multi-colour flow cytometry analysis was performed using a panel of markers including CD14 (macrophage), CD10 (stromal cell), EpCAM (epithelial cell), and CD3 (T cell). The gating strategy is illustrated in Figure 2.5. Initially, cells were gated based on their size and granularity using a forward scatter-area (FSC-A) versus side scatter-area (SSC-A) plot (Figure 2.5a). This step allowed for the selection of cells with characteristics typical of macrophages. Next, to exclude doublets and cell aggregates, single cells were gated using a FSC-Height (FSC-H) versus FSC-A plot (Figure 2.5b). Single cells were then displayed on a SSC-A vs. APC/Cy7 Zombie NIR plot to identify and gate live cells (Figure 2.5c).

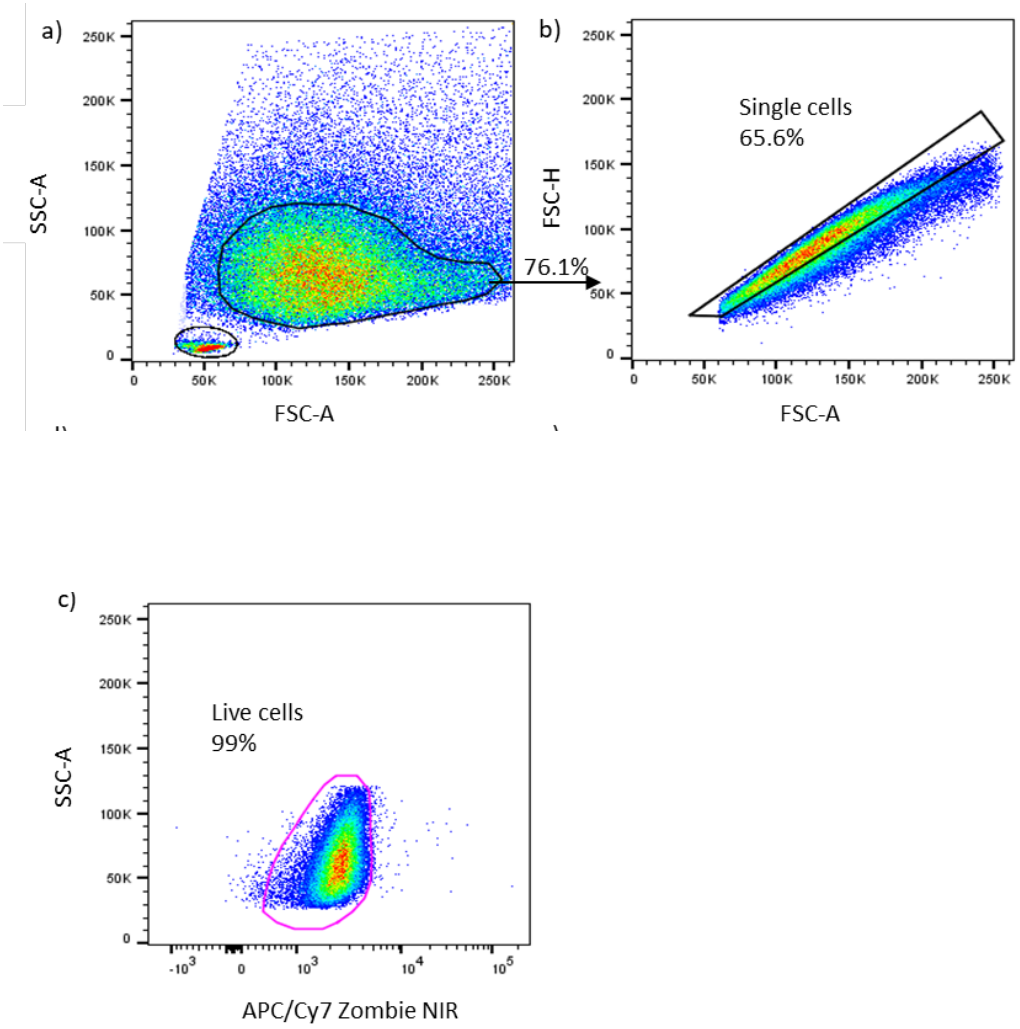

Figure 2.5. The flow cytometry gating strategy for pMΦ. a) Initial gating based on cell size and granularity using forward vs. side scatter (FSC-A versus SSC-A; b) Selection of single cells using FSC-H vs. FSC-A to exclude doublets and cell aggregates; c) Live cells were gated based on APC/Cy7 Zombie NIR signal.

The protein marker expression analysis is presented in Figure 2.6, with unstained cells serving as controls. The isolated cells were 86.2% CD14+ (Figure 2.6a) and 94.2% CD45+ (Figure 2.6b), while negative for CD10, EpCAM, and CD3 (Figure 2.6c, d, e).

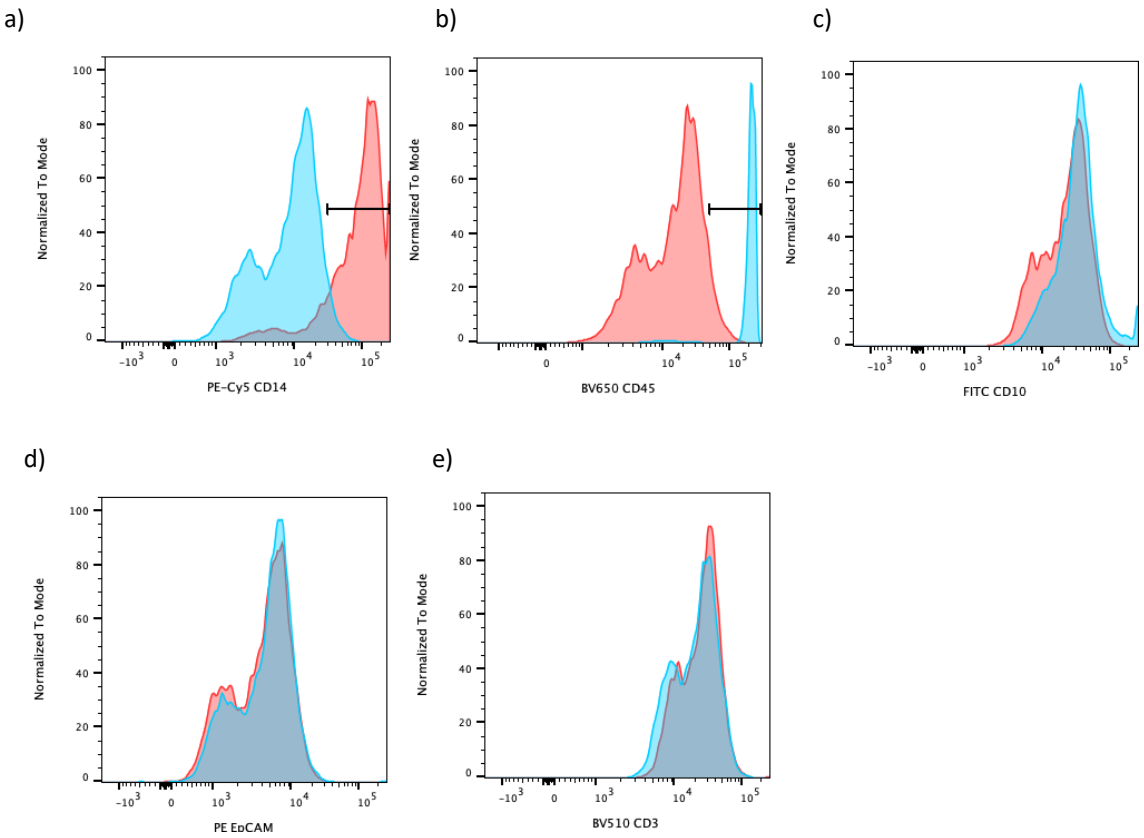

Figure 2.6. Flow cytometry analysis of isolated pMΦ to assess purity. Red histogram = a) CD14 expression, b) CD45 expression, c) CD10 expression, d) EpCAM expression, e) CD3 expression. Unstained cells were used as controls (blue histograms).

Interestingly, a small population (3.3%) of cells distinct in size and granularity was also detected in the pMΦ sample (Figure 2.7a). Further analysis of this subpopulation showed that they were CD14- and 54.1% were CD3+ (Figure 2.7d).

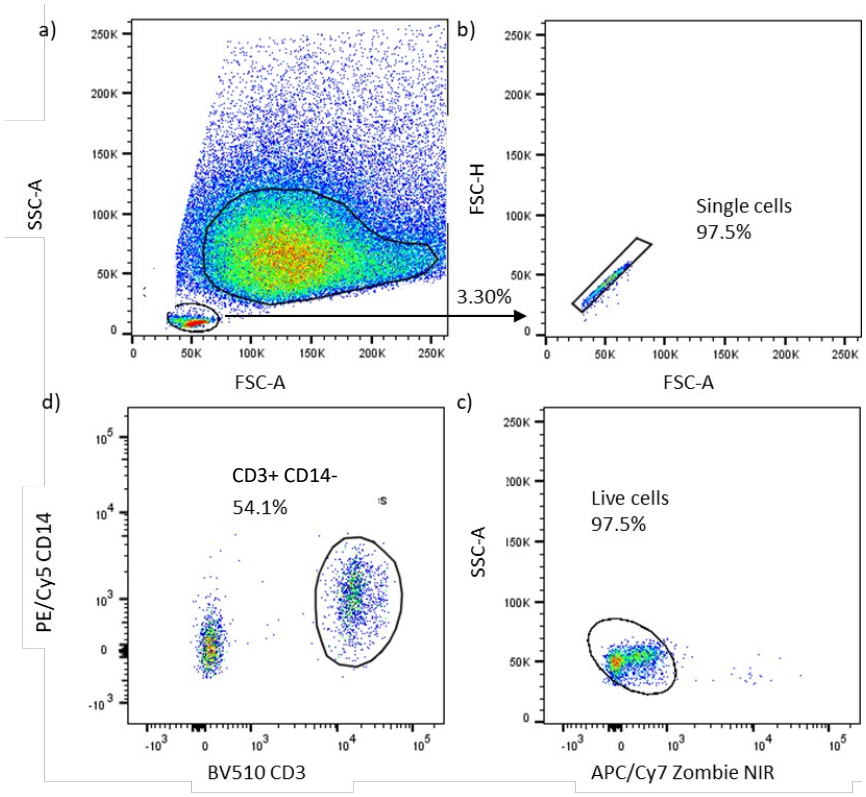

Figure 2.7. Characterization of a distinct cell subpopulation in the pMΦ sample. a) Cells were firstly selected based on scatter (FSC-A vs SSC-A), b) Single cells selected (FSC-A vs FSC-H), c) live cells gate (APC/Cy7 Zombie NIR negative), d) 54% of this cell population were CD3+ and CD14.

During flow cytometry analysis, I observed that pMΦ emitted strong autofluorescence, particularly at high energy wavelengths ranging from 450 to 600 nm. This observation aligns with previous literature identifying macrophages, especially pMΦ, as the most autofluorescent human cells (141, 142). Unstained pMΦ exhibited pronounced autofluorescence in the PE (Figure 2.8a) and FITC (Figure 2.8b) channels (488nm blue excitation) and in the BV421 (Figure 2.8c) channel (405nm violet excitation). In comparison, when excited by the red 633nm laser, unstained pMΦ displayed a lower level of autofluorescence in the APC/Fire 750 (Figure 2.8d) channel.

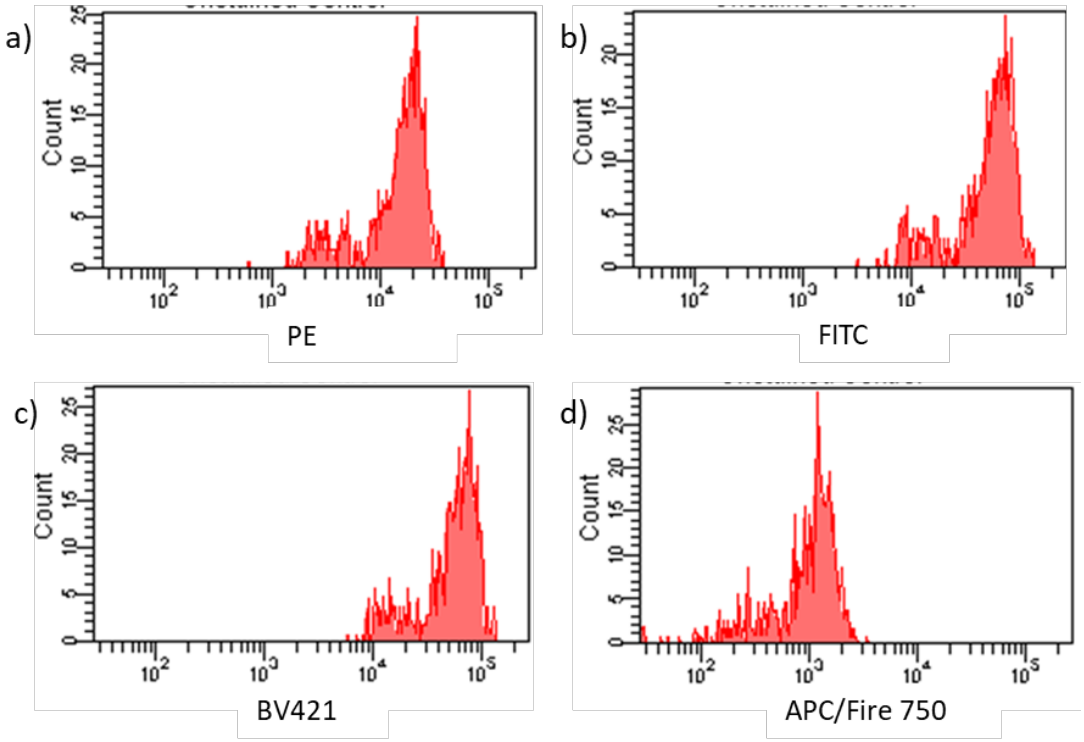

Figure 2.8. Flow cytometry analysis examining autofluorescence of pMΦ in different channels. The autofluorescence of unstained pMΦ were examined in different detection channels. a) PE, b) FITC, c) BV421, d) APC/Fire 750 .

This high level of autofluorescence presents challenge in flow cytometry analysis of pMΦ. It can potentially mask the detection of positive signals from fluorophores, especially those with emission spectra overlapping with the autofluorescence range, leading to false-negative or false-positive results. The problem is particularly acute for detecting markers with low expression levels, as their fluorescence signals may be overwhelmed by the strong autofluorescence.

To mitigate this issue, where possible, fluorophores excited by the red 633nm laser were used in subsequent experiments.

2.3.2 Characterisation of pMΦ

Two distinct subpopulations of pMΦ were identified based on their marker expression profile of CD14 and CD16, $CD14^{high}CD16^{high}$ and $CD14^{low}CD16^{low}$ (Figure 2.9a). The proportion of these two subpopulations varied between samples. No significant differences

were observed in the distribution of these subpopulations when comparing endometriosis patients to control groups.

However, when the analysis was focused specifically on the CD14^{high} CD16^{high} subgroup, a significant difference related to disease progression was observed (Figure 2.9b). Specifically, the proportion of CD163 and CD206 positive cells was significantly higher in patients with endometriosis I/II (57 ± 12%, mean ± SD) than that in patients without the disease (24± 11%, mean ± SD) %) (Figure 2.9c).

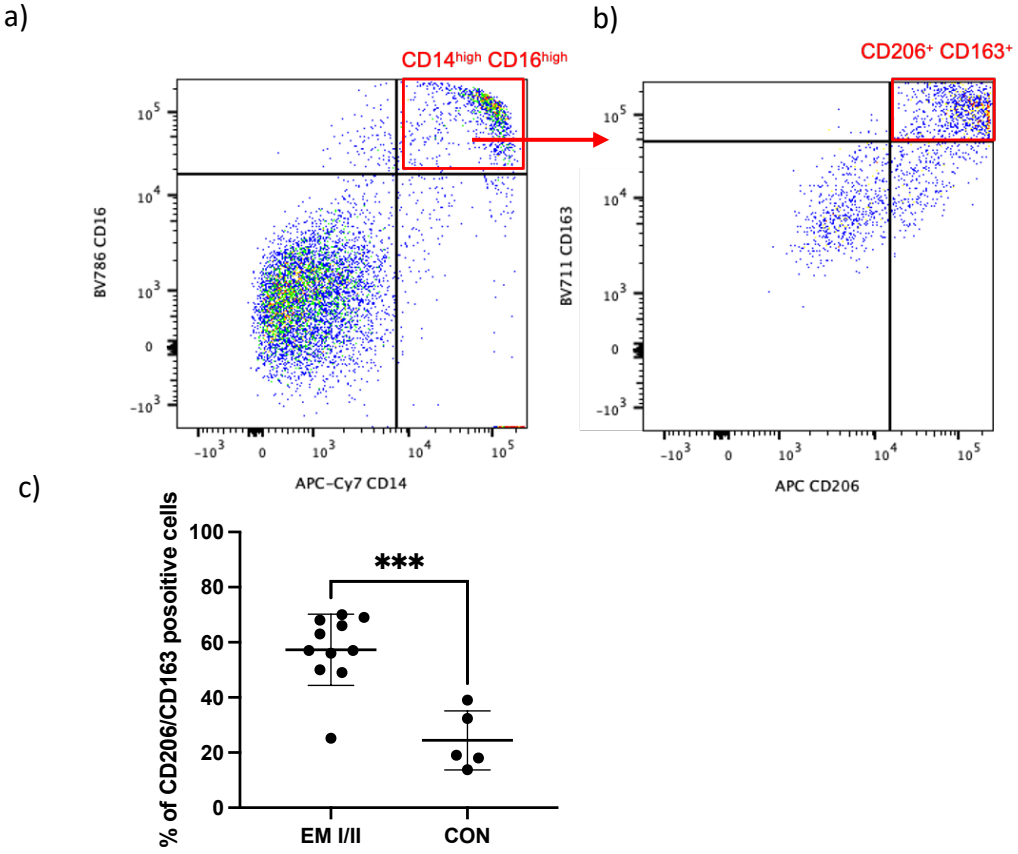

Figure 2.9. Flow cytometry analysis of pMΦ subpopulations in endometriosis. a) CD14/CD16-based pMΦ subpopulations. b) CD206$^{+/}$CD163^{+} in CD14^{high} CD16^{high} pMΦ . c) Increased CD206^{+} /CD163^{+} cells within CD14^{high} CD16^{high} pMΦ in endometriosis stage I/II patients (EM I/II) vs. controls (CON). Bars = Mean ± SD. Unpaired t-test ,***P<0.001

2.3.3 Establishment of SOP for pMΦ-sEV Isolation and Characterisation

Having established a method for isolating pMΦ, I next aimed to develop a standardised protocol for the isolation and characterization of sEV from pMΦ.

Cell supernatants were collected after 24h and 48h incubations, and sEV were isolated by ultracentrifugation. The isolated EV were examined using NTA.

NTA showed no significant difference in the mode or mean size of sEV collected at 24h or 48h time points (Figure 2.10a). The 24h collection produced EV with a mode size of 137 ± 9 nm and a mean size of 154 ± 21 nm, while the 48h collection resulted in EV with a mode size of 133 ± 8 nm and a mean size of 156 ± 11 nm. EV concentration was marginally increased after 48h of culture compared to 24h, but this difference was not statistically significant (Figure 2.10b). To obtain a maximal number of EV for future experiments, I opted to isolate EV after 48h of culture. In these experiments, 'EV depleted media' was used as a negative control, this contained fewer than $4x10^7$ vesicles/mL, which falls below the NTA detection limit.

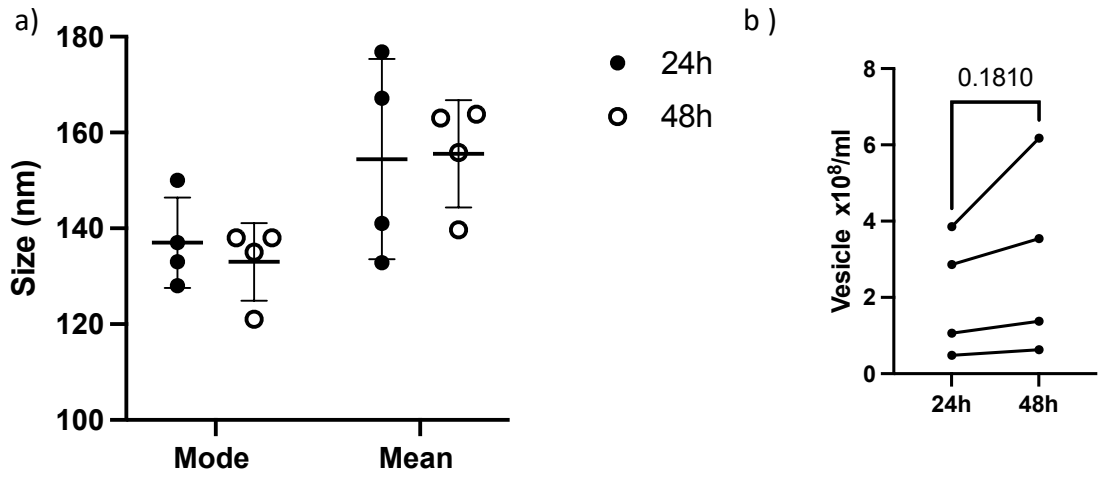

Figure 2.10. NTA size and concentration measurements of pMΦ-sEV isolated from 24hr and 48hr culture (n=4). a) pMΦ-sEV mode and mean size (nm) after 24h and 48h incubation, statistical comparison by unpaired t-test (Shapiro-Wilk test: $p > 0.05$). b) pMΦ-sEV concentration comparison between 24h and 48h timepoints, statistical comparison by paired t-test (Shapiro-Wilk test: $p > 0.05$).

To characterize surface epitopes, I employed the MACSPlex EV kit IO and conducted a titration experiment to optimize EV input concentration. This optimisation was necessary as previous studies demonstrated that EV input quantity affects detection and characterisation using the MACSPlex EV kit IO (143). pMΦ-sEV from two pooled samples were quantified by NTA and prepared as a concentration series ranging from $5x10^7$ to $5x10^9$ EV/mL for titration analysis. The nMFI of each marker at each concentration is presented in Figure 11.

sEV-enriched tetraspanins CD81, CD9, and CD63 were detectable even at the lowest input of $5x10^7$ vesicles/mL. Raw MFI data changed with EV input, with higher EV concentrations yielding higher raw MFI values. To account for this variation, MFI values were normalized by using the average MFI of three tetraspanins (CD81, CD9, and CD63) according to the manufacturers' instructions. Most nMFI values remained stable at different EV inputs, but some markers like HLA-DR and CD24 showed variable nMFI (Figure 2.11), emphasizing the need for consistent EV input. The REA isotype control nMFI is higher with lower EV input, which results in the CD49E expression to fall beneath isotype levels at $1x10^8$ and $5x10^7$ vesicles/mL. Stable positive marker expression was observed at $2x10^8$ and $5x10^8$ vesicles/mL. However, when EV input was too high ($5x10^9$ EV/mL for HLA-DR, CD9, and CD81; $1x10^9$ EV/mL for HLA-DR), raw MFI values of highly expressed markers exceeded the detection limit (Figure 2.10). As a result, it was not possible to determine an accurate nMFI for all markers when EV input was above $1x10^9$ EV/mL.

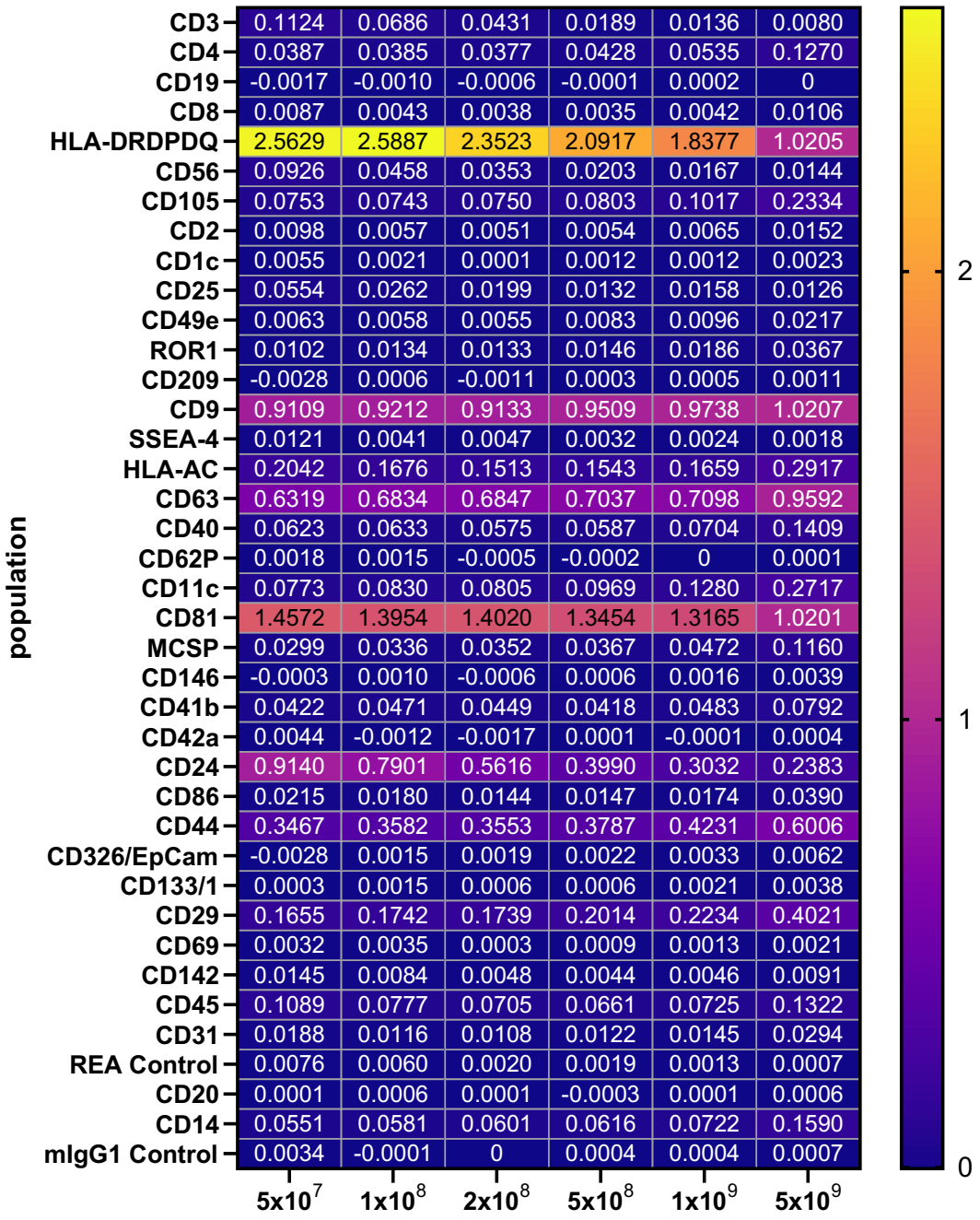

Figure 2.11. Influence of EV input into the MACSPlex EV kit IO on surface marker expression of pMΦ-sEV. Heatmap showing normalized median fluorescence intensity (nMFI) for 37 surface markers on pMΦ-sEV at EV concentrations ranging from $5x10^7$ to $5x10^9$ vesicles/mL. nMFI values were calculated by subtracting background from raw MFI and then normalizing to the mean of CD81, CD9, and CD63 expression (n=1).

Based on these findings, $2x10^8$ and $5x10^8$ EV/mL were determined to be the optimal EV input. However, given the limited volume of PF and pMΦ isolated per sample, I chose to use an input of 2 x 10^8 EV/mL in future experiments, given it may not always be plausible to obtain the higher concentration of $5x10^8$ EV/mL. Furthermore, by using $2x10^8$ EV/mL this would maximize the number of samples that could be analysed.

2.3.4 Characterisation of pMΦ-sEV

EV characterisation using a combination of NTA, TEM and the MACSPlex EV kit IO confirmed that the isolated vesicles secreted by pMΦ were sEV, following the latest MISEV guidelines (57).

pMΦ-sEV (n=21) had an average modal size of 128nm ± 20nm and over 95% were smaller than 200nm (Figure 2.12a). Western Blot analysis demonstrated positive expression of the sEV marker Syntenin in pMΦ-sEV (Figure 2.12b). Although the expression of the negative marker albumin was detected in pMΦ-sEV, its expression level was notably lower compared to the pMΦ lysate control (Figure 2.12b). TEM analysis confirmed the presence of biconcave double membrane vesicles characteristic of sEV, although particles were observed in the background (Figure 2.11c). These non-EV particles, smaller than 50nm, were present in the media control as well, suggesting they may be residual components from the EV-depleted culture media.

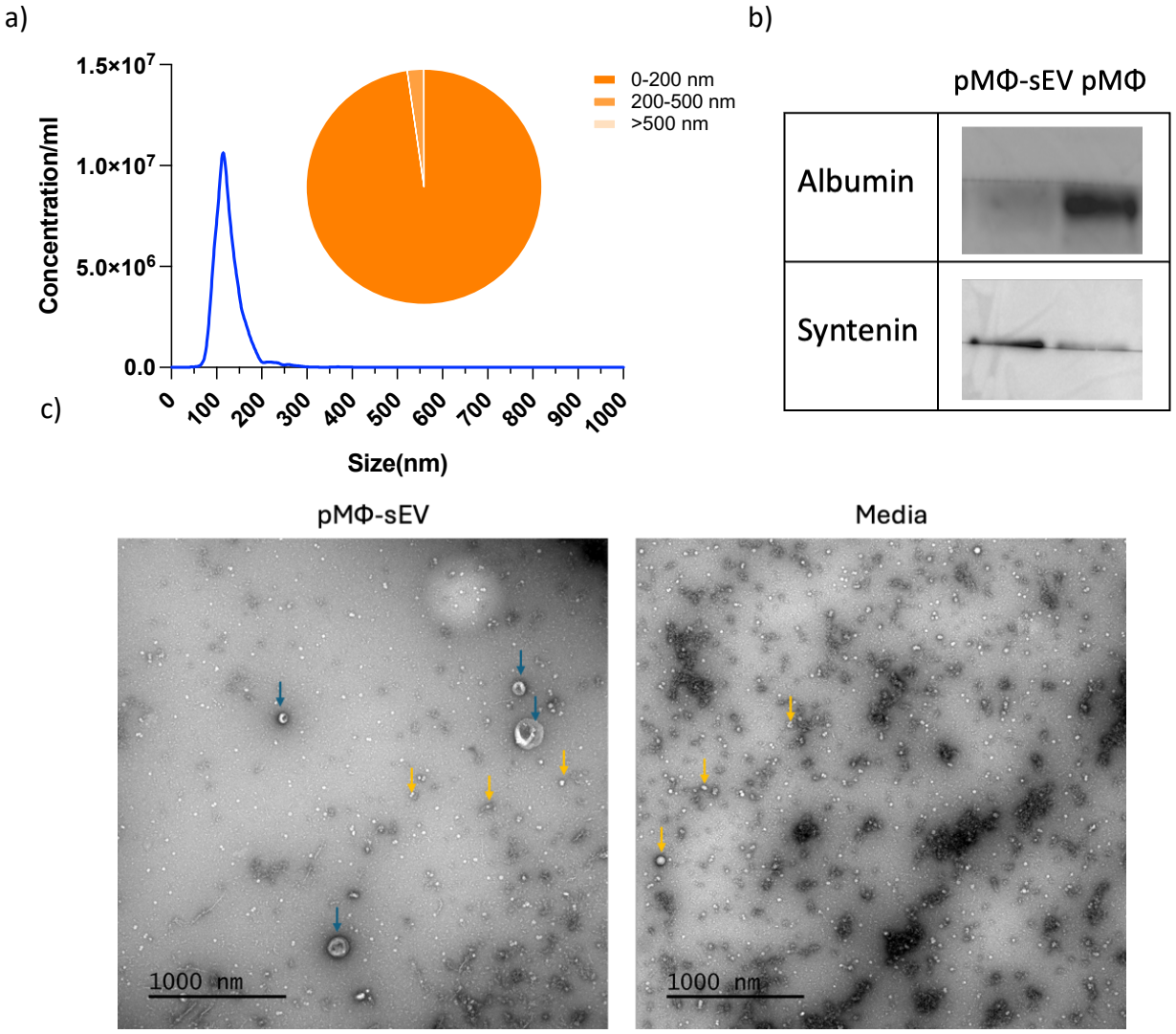

Figure 2.12. Characterization of pMΦ-sEV. a) NTA size distribution profile of EV, composite image of 21 pMΦ-sEV samples. b) Western Blot analysis of Syntenin-1 and Albumin protein expression of pMΦ-sEV and pMΦ cell lysates, 5 ng protein loaded per well. c) Representative morphology of isolated vesicles visualised by TEM, from pMO-sEV (left) and EV-depleted media (right). Blue arrows indicate sEV and yellow arrows indicate non-EV co-isolates. Scale bar=1000nm.

EV surface proteins were characterised using the MACSPlex EV kit IO . In the analysis, only raw MFI values above the respective isotype controls were analysed. A total of 27 surface markers are present in all collected sEV from 19 samples including three sEV enriched markers, CD9, CD63 and CD81 (Figure 2.16). No difference of expression pattern was detected between endometriosis and control patients.

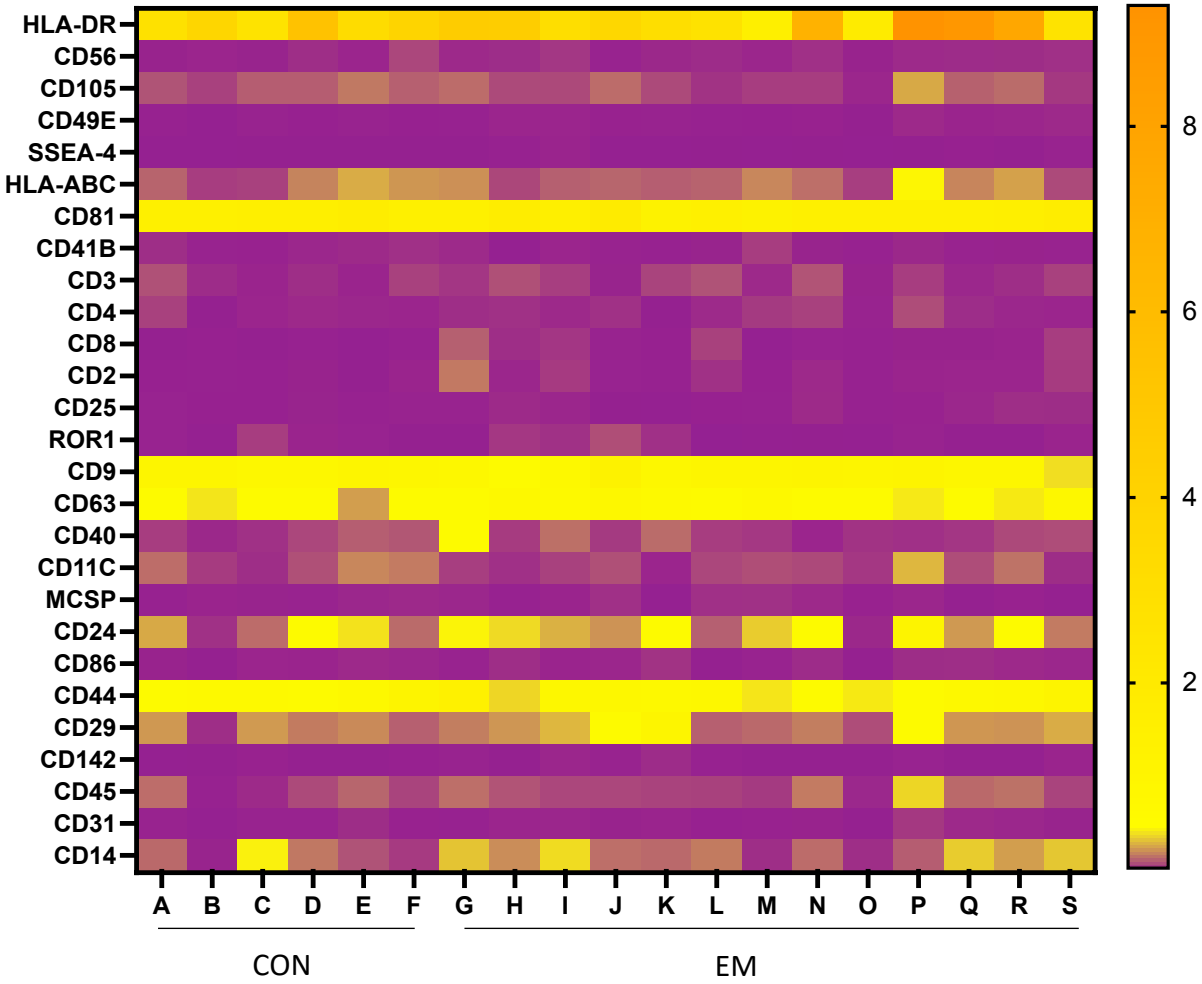

Figure 2.13. Surface marker profiles of pMΦ-sEV between endometriosis patients and controls. CON=control (n=6), EM=endometriosis (n=13). Normalised MFI = MFI/average MFI of CD81, CD9 and CD63.

Analysis of the nMFI ±SD values presented in Table 2.5 revealed a distinct profile of surface markers on pMΦ-sEV. A total of 27 markers were consistently detected across all pMΦ samples. The presence of sEV in the samples was confirmed by the high expression of three sEV-enriched markers: CD9, CD81, and CD63. Notably, HLA-DR was the highest expressed marker, with an average nMFI of 4.3 ± 2.31, surpassing even the sEV-enriched markers CD9, CD63, and CD81. The other top 5 highly expressed markers were CD44 (0.74 ± 0.26), CD24 (0.37 ± 0.25), CD29 (0.29 ± 0.21), and CD14 (0.21 ± 0.14). This profile not only confirms the macrophage origin of these sEV but also suggests their potential role in immunomodulation.

Table 2.5. Surface marker profile of pMΦ- sEV. Data are presented as mean ± SD. n=19

Antibody	Number of positive samples	Mean nMFI ± SD	Antibody	Number of positive samples	Mean nMFI ± SD
REA control	19/19	0.003 ± 0.004	CD24	19/19	0.370 ± 0.248
HLA-DR	19/19	4.306 ± 2.297	CD86	19/19	0.028 ± 0.013
CD56	19/19	0.039 ± 0.017	CD44	19/19	0.743 ± 0.257
CD105	19/19	0.127 ± 0.061	CD29	19/19	0.286 ± 0.209
CD49E	19/19	0.017 ± 0.009	CD142	19/19	0.013 ± 0.009
SSEA-4	19/19	0.008 ± 0.004	CD45	19/19	0.126 ± 0.087
HLA-ABC	19/19	0.191 ± 0.100	CD31	19/19	0.022 ± 0.013
CD81	19/19	1.530 ± 0.144	CD14	19/19	0.214 ± 0.135
CD41B	19/19	0.026 ± 0.017	CD62P	04/19	0.005 ± 0.002
mIgG1 control	19/19	0.004 ± 0.004	CD42A	04/19	0.008 ± 0.008
CD3	19/19	0.065 ± 0.035	CD19	02/19	0.004 ± 0.001
CD4	19/19	0.043 ± 0.026	CD1C	14/19	0.006 ± 0.004
CD8	19/19	0.031 ± 0.035	CD209	3/19	0.005 ± 0.003
CD2	19/19	0.035 ± 0.044	CD146	9/19	0.009 ± 0.006
CD25	19/19	0.020 ± 0.013	EpCAM	13/19	0.060 ± 0.123
ROR1	19/19	0.026 ± 0.031	CD133/1	13/19	0.072 ± 0.151
CD9	19/19	0.930 ± 0.179	CD69	10/19	0.006 ± 0.003
CD63	19/19	0.581 ± 0.144	CD20	7/19	0.006 ± 0.005
CD40	19/19	0.109 ± 0.105			
CD11C	19/19	0.118 ± 0.078			
MCSP	19/19	0.024 ± 0.013			

The assay detected 10 additional markers in some of the pMΦ-sEV samples. However, most of these had very low nMFI values (below 0.01), while all consistently expressed markers had nMFI values above 0.01. These low-level signals may represent false positives arising from background media. Interestingly, EpCAM and CD133/1, which were detected in 13 out of 19 samples, showed notable expression levels with average nMFI values of 0.60 ± 0.12 and 0.72 ± 0.15, respectively. The presence of these epithelial cell markers on macrophage-derived sEV could be attributed to the phenomenon where macrophages acquire epithelial cell markers upon phagocytosis of apoptotic cancer cells, as reported in previous studies (144).

2.3.5 Comparison of EV and phenotypic profiles of pMΦ

To assess whether the sEV signatures measured by the MACSPlex EV kit IO can reflect cellular profiles, I examined the relationship between HLA-DR and CD14 expression on pMΦ and their secreted sEV.

The analysis revealed a strong positive correlation between the nMFI of HLA-DR on EV and the HLA-DR expression on pMΦ (r=0.703, p = 0.007) (Figure 2.14a). In contrast, no significant correlation for CD14 expression between sEV and pMΦ was observed (r= 0.219, p=0.495) (Figure 2.14b).

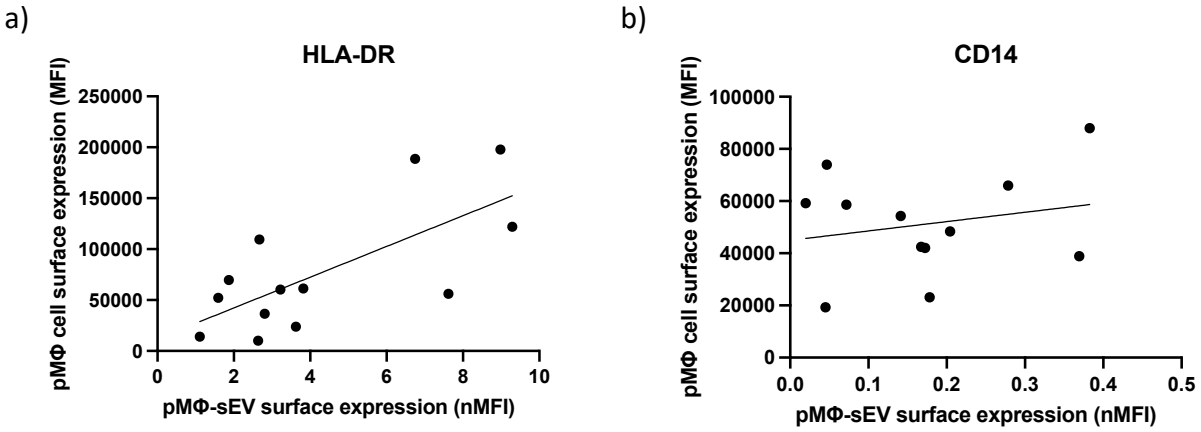

Figure 2.14. **Correlation analysis of protein expression between pMΦ and their secreted sEV.** Scatter plots comparing the expression of a) HLA-DR and b) CD14 expression on pMΦ-sEV (nMFI, x-axis) with expression on pMΦ cell surface (MFI, y-axis). The best-fit line is shown for each plot.

2.4 Discussion

2.4.1 pMΦ characterisation

In this chapter, I successfully isolated pMΦ from fresh PF utilising the adherent characteristics of macrophages. While pMΦ demonstrated longevity in culture for up to 10 days, I found that a 4-day culture period was optimal for experiments. This provides a valuable window for studying these cells and collecting their secreted vesicles. The use of primary cells allowed physiologically relevant observations in the study. However, it's important to acknowledge the limitations of this model. PF volume is highly variable, and the collection is totally dependent on surgical schedule, and there is potential blood contamination during collection. In this study, minimal blood contaminated samples were utilised. This variability, combined with the finite lifespan of primary cells, make this model suboptimal for long-term characterisation. Future studies might benefit from the generation of an immortalised cell line to overcome these limitations and enable more extensive, standardised experiments.

The flow cytometry analysis confirmed that over 97% of the isolated cells were indeed macrophages, as assessed by size, forward scatter properties, and expression of CD14. Importantly, these cells were negative for CD10, EpCAM, and CD3 expression, confirming they were pMΦ cells. The remaining 3% of the population with distinct SSC and FSC were CD14-. Interestingly, a proportion of these cells were CD3+. These observations were consistent in all 8 samples tested for purity. Further investigation is needed to determine the sources of this non-pMΦ population.

Additionally, I observed significant autofluorescence in pMΦ. Unstained pMΦ exhibited pronounced autofluorescence across multiple channels, including PE and FITC (excited by 488nm blue laser) and BV421 (excited by 405nm violet laser). In contrast, lower autofluorescence levels were observed in the APC/Fire 750 channel when excited by the red 633nm laser, suggesting potential benefits in utilizing longer wavelength fluorochromes for analysing these cells.

This observation is consistent with previous studies that have identified macrophages, especially pMΦ, as highly autofluorescent human cells (141, 142). The autofluorescence is likely derived from cellular components such as flavins and lipids (145). This high level of autofluorescence presents challenges in distinguishing positive populations from background noise and limits the design of multicolour panels. Full spectral cytometry has been reported to improve the resolution of autofluorescent populations (146, 147).

Literature has reported $CD14^{high}$ $CD16^{high}$ populations as resident pMΦ (121), I was also able to characterise pMΦ using CD14 and CD16 into $CD14^{high}CD16^{high}$ and $CD14^{low}CD16^{low}$, but there were no overall differences in the proportion of these subpopulations between endometriosis patients and controls.

However, I noted a higher population of activated pMΦ (CD163+ and CD206+) in $CD14^{high}$ and $CD16^{high}$ subgroups in endometriosis stage I/II patients compared to endometriosis-free controls. This finding suggests a potential activation of resident pMΦ toward an M2-like phenotype in endometriosis patients. This activation could be influenced by factors produced by endometriotic lesions, such as cytokines like IL-6 (148) and EV (36, 149, 150), which have been reported to modulate macrophage phenotypes in endometriosis. Due to sample limitations, all endometriosis cases in the study were stage I/II. It therefore remains unknown about the pattern change in stage III/IV disease, which have been shown to display distinct immune profiles in the literature (118) .

2.4.2 pMΦ-sEV characterisation

The pMΦ-sEV were isolated using ultracentrifugation, a method commonly employed for isolating EV from culture supernatants (151, 152). FCS has been reported to be a source of additional EV and non-EV co-isolates like lipoproteins (153, 154). These components can interfere with the isolation and characterisation of sEV derived from cultured cells. I therefore used an overnight ultracentrifugation protocol (152, 154) to prepare EV-depleted FCS for the culture media. TEM analysis of the samples revealed the presence of additional

structures alongside the isolated EV. These structures appeared different from typical EV morphology and the size range was smaller than 50nm. These non-EV particles were also present in media controls, indicating their origin from the culture media rather than cellular production. Their size and morphology resembled lipoproteins, which are known to be present in FCS and can persist even after depletion protocols (155). Despite 16h of ultracentrifugation to remove vesicles in FCS, studies have reported significant amounts of vesicles with similar size to sEV remain (156) and this method is less effective in removing particles smaller than 250nm than a precipitation method (157). The presence of these non-EV particles should not affect the surface marker analysis in this study as the MACSPlex EV kit IO selects vesicles based on the expression of the sEV enriched markers CD9, CD81 and CD63.

Future functional studies investigating the effects of pMΦ-sEV on cells may require additional purification steps. Density gradient centrifugation can separate EV from soluble proteins and protein complexes (158, 159), but inefficiently from lipoproteins (160). For improved separation of lipoproteins and EV, Size Exclusion Chromatography (SEC) is considered more effective (161). Additionally, sequential application of different isolation protocols has been reported to produce purer samples than single isolation methods alone (162, 163).

The characterisation of pMΦ-sEV using the MACSPlex EV kit IO provides the first insights into surface epitope expression of these vesicles in endometriosis. The initial titration experiments demonstrated the critical importance of determining appropriate EV input and maintaining consistent EV concentrations across samples. Notably, such titration experiments have not been consistently reported in studies using multiplex bead assays, despite their significance. Welsh et al. reported that the binding affinity of EV to capture beads is affected by differences in surface area and epitope abundance, as well as the expression of multiple proteins (164). Although the relative abundance of epitopes might remain consistent within a specific range of EV input, it's not possible to accurately predict how signal intensity will vary across different markers without first conducting a titration experiment. For pMΦ, I observed constant readings in the range of $2x10^8$ to $5x10^8$ particles/mL, while low EV input results in elimination of some markers and high EV input results in out-of-scale readings for some markers. Titration should always be included when

first using multiplex bead assays for different sample types to establish the appropriate working range.

Normalisation is also crucial for maintaining comparability. The normalisation method employed in this study follows the manufacturer's manual recommendations, which involved subtracting the background noise (from EV-free media) from the raw MFI and then dividing the difference by the mean of CD81, CD9, and CD63 signals. It's important to note that other normalisation methods and platforms exist, and the choice of normalisation technique can significantly influence data interpretation and final findings (164).

The MACSPlex EV kit IO demonstrated high throughput of sEV-enriched markers CD81, CD9, and CD63 with just $6x10^6$ EV. Typically, for western blot, around $1x10^9$ sEV (equivalent to 5µg) are required to obtain a positive signal for the sEV enriched marker syntenin while CD9 failed to be detected. This approach is particularly helpful in EV protein composition characterisation required by MISEV guidelines when EV numbers are limited.

Apart from the expression of the macrophage marker CD14, the MACSPlex EV kit IO revealed the expression of immunoregulatory markers like CD24, CD29, CD44 and HLA-DR on pMΦ-sEV. CD44, a cell-surface glycoprotein that interacts with hyaluronic acid (165), shows high expression on mouse pMΦ and plays a role in regulating phagocytosis (164) and supressing inflammatory responses (166). It also mediates trafficking of pMΦ following visceral tissue injury (167) which may be important in endometriosis progression. It is also involved in T cell activation (168), and epithelial-mesenchymal transition to promote cancer invasion and metastasis (169). HLA-DR, is an MHC class II, important in antigen presentation and CD4+ T cells (170). CD29 (integrin β1) has been found to promote cancer cell migration (171) and T cell cytotoxicity (172).

The expression of these markers on pMΦ-sEV could either reflect the cellular expression of these markers on the parent pMΦ or indicate specific functional roles of the vesicles themselves. If the marker profile mirrors that of the parent cells, it may serve as an indicator of pMΦ phenotype and activation state in endometriosis. Alternatively, if these markers confer specific functions to the pMΦ-sEV, they could directly modulate the peritoneal

microenvironment through signalling pathway activation (173) or marker transfer to other cells (174). Further research is needed to differentiate between these possibilities and understand the implications of this marker profile on pMΦ-sEV in endometriosis pathogenesis.

Interestingly, the detection of other cell markers on pMΦ-sEV, such as CD3, CD56, CD105, and even EpCAM in some samples, raises intriguing questions about their origin and function. pMΦ have been shown to have the ability to acquire markers from epithelial cells and stem cells through phagocytosis (144). This could also result in expressing their markers on EV. This phenomenon could explain the presence of unexpected markers on pMΦ-sEV and suggests a complex interplay between pMΦ and other cell types in the peritoneal microenvironment.

Although no significant differences in sEV characteristics between endometriosis patients and controls were observed, this finding is likely hindered by the small sample size and the heterogeneity of pMΦ. pMΦ are diverse cells originating from different sources (embryo-derived or monocyte derived) and present with different subsets (112). Mouse studies have revealed opposing roles of macrophages from different origins in endometriosis progression, underlining the complexity of these cells in the disease context (52). Investigating sEV derived from a specific subgroup of pMΦ, such as $CD14^{high}CD16^{high}$ may result in more targeted findings. Additionally, *in vitro* culture may have altered pMΦ phenotypes and secretion profiles, potentially masking important *in vivo* characteristics.

MACSPlex analyses in this study were conducted with a mixture of CD9, CD81, and CD63 capture beads; analysing EV captured by single capture bead subpopulations may reveal different signatures (175) and uncover differences between endometriosis and controls.

The final part of the study revealed EV surface epitopes showed correlation with cell marker expression, with HLA-DR demonstrating a stronger correlation. This suggests that HLA-DR surface proteins may originate from simple loading processes such as plasma membrane budding. Interestingly, CD14 expression on sEV did not directly reflect the expression levels on the originating pMΦ. This discrepancy between cellular and EV marker expression

highlights the selective nature of EV cargo loading. Several studies have shown that EV cargo selection is a highly regulated process involving various molecular mechanisms (134, 176). For instance, specific sorting machineries such as the ESCRT (Endosomal Sorting Complex Required for Transport) pathway have been implicated in the selective incorporation of proteins into EV (177). Moreover, post-translational modifications like ubiquitination and SUMOylation can influence protein sorting into EV (178).

2.4.3 Future Directions

Future studies should aim to expand the sample size and diversity of the patient cohort, including more samples from patients with advanced-stage endometriosis (stages III/IV). A power calculation conducted using G*Power 3 estimated that a total of 330 participants (110 per group: CON, EM I/II and EM III/IV) are required to detect a medium effect size (Cohen's f = 0.40) with 80% power (1-β = 0.8) and statistical significance using one-way ANOVA (179). An even larger sample size is required to enable assessment of pain symptoms and further subcharacterisation.

As endometriosis stage does not necessarily correlate with symptoms (180), it would be valuable to characterise pMΦ not only by disease stage but also by clinical symptoms, such as pain. This expanded approach would enhance the ability to detect subtle differences between groups and allow for a more comprehensive analysis of how various factors influence pMΦ characteristics and their derived sEV, potentially revealing disease-specific signatures not apparent in the current study.

Advanced flow cytometry techniques, such as full spectrum flow cytometry, should be employed to overcome the limitations of conventional methods on cells with high autofluorescence like pMΦ (146, 147). This would allow for expanded characterisation panels, including markers like CRIg and CCR2 (extra resident pMΦ markers) (45), and markers associated with phagocytosis evasion (don't eat me signals) such as SIRP-alpha, Siglec-10, and PD-L1 (181). The autofluorescence observed in pMΦ could be utilised as a

marker for phagocytic ability (182), providing insights into the functional capacity of these cells without additional staining.

Future studies using single EV flow cytometry to analyse EV populations would be beneficial. Implementing single EV flow cytometry offers several advantages over the MACSPlex EV kit IO. It allows quantification of the absolute number of EV positive for specific markers, potential for multiparameter analysis of individual EV, and the possibility to sort and collect specific EV subpopulations for further analysis. These improvements would allow for a more detailed and quantitative characterization of pMΦ-derived EV, potentially revealing subtle differences between endometriosis and control samples that were not detectable with the current method.

Investigating the functional impacts of pMΦ-sEV on various cellular components of the endometriotic microenvironment is crucial. This includes examining their effects on lesion cells and immune cells like T cells, given the presence of immunoregulatory molecules such as HLA-DR, CD44, CD24 and CD29 on these EV.

In summary, this chapter has analysed pMΦ phenotypes and for the first time characterised their derived sEV in endometriosis. pMΦ revealed heterogeneity and two subsets of CD14 and CD16 expression ($CD14^{high}$ $CD16^{high}$ and $CD14^{low}$ $CD16^{low}$) and higher CD163+/CD206+ in the $CD14^{high}$ $CD16^{high}$ subpopulation. The study of pMΦ-sEV using the MACSPlex EV kit IO unveiled a total of 27 surface markers, with high expression of immunoregulatory molecules like CD44, HLA-DR, CD24, and CD29. Importantly, HLA-DR expression correlated with surface marker expression, indicating that the MACSPlex EV kit IO identified sEV surface epitopes with the ability to present cellular antigens. CD14 revealed a more complex sorting mechanism in sEV. The titration and optimisation of EV characterisation using the MACSPlex EV kit IO performed in this study provide valuable insights for the EV analysis of more complicated biological fluid samples, for example PF which will be explored in the next chapter. While no significant differences were observed between endometriosis stage I/II and control samples, this study has laid important groundwork for future investigations into the role of pMΦ and their sEV in endometriosis pathophysiology.

Chapter 3 Characterisation of PF- sEV

3.1 Introduction

The establishment, growth and maintenance of endometriotic lesions involves complex interactions between cell types including immune cells and mesothelial cells in the peritoneal microenvironment. Investigating PF, which surrounds these lesions and cells, provides a unique window into the local microenvironment. Studies have identified over 47 distinct immune cell populations in PF, with specific immune profiles associated with endometriosis (20). Additionally, elevated levels of cytokines such as IL-8 and TGF-beta have been observed in the PF of endometriosis patients (183, 184). Immune dysregulation has been closely linked to disease progression (19). The secretion profiles of each cell type and how they change with disease progression still requires further investigation. Apart from soluble factors, such as cytokines and chemokines, sEV have emerged as key components of cellular secretion profiles.

Recent studies have revealed the presence of sEV in PF and these PF-sEV exhibit distinct protein and RNA profiles in endometriosis patients compared to controls and carry disease specific cargo that are potentially involved in the pathogenesis of endometriosis (58, 185). While these proteomic and transcriptomic studies have provided valuable insights into the overall composition of PF-sEV, they have limitations in representing the full picture of EV characteristics, particularly in terms of surface marker expression.

3.1.1 EV interactions with recipient cells

EV communicate with recipient cells through various mechanisms. Numerous cellular EV uptake routes are evident, including clathrin-dependent/lipid raft mediated/receptor mediated endocytosis, phagocytosis, micropinocytosis, and direct membrane fusion (Figure 3.1) (186, 187). The uptake of EV can be specific to certain cell types, as demonstrated by tumour-derived exosomes creating tissue-specific pro-metastasis microenvironments

through unique integrin presentation (188). Additionally, some EV can regulate recipient cell activities through antigen presentation while remaining on the cell surface (189).

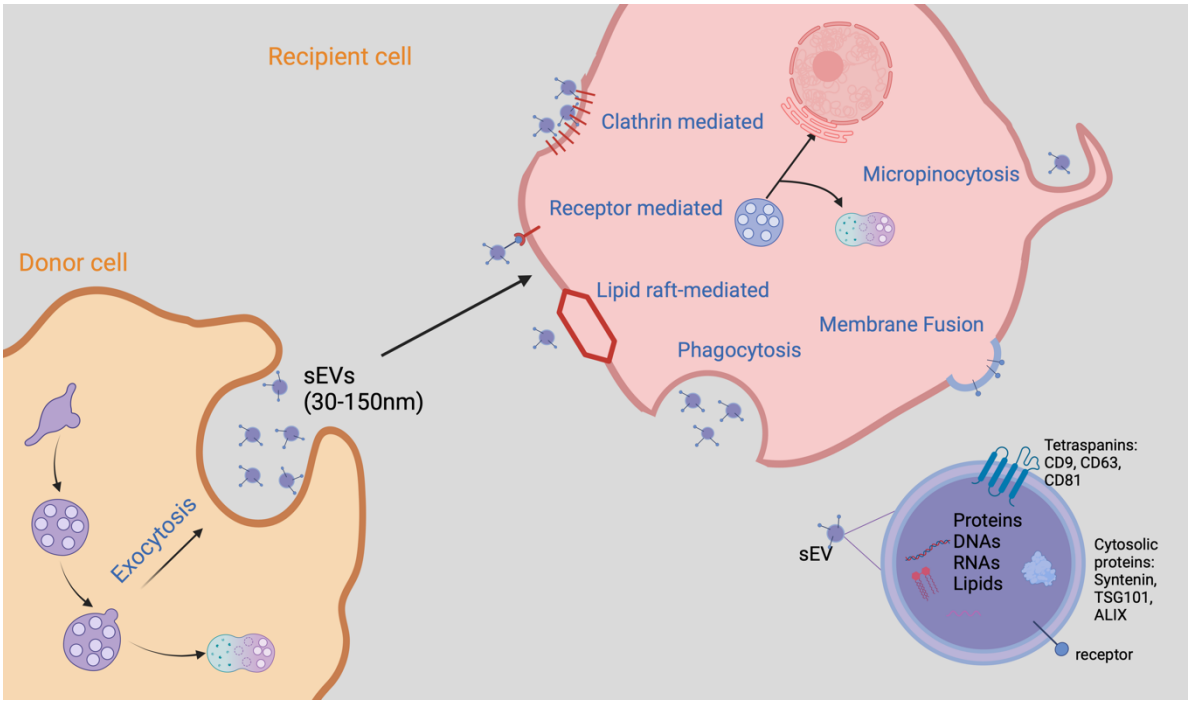

Figure 3.1. The interaction of sEV with a recipient cell. sEV may enter recipient cells via direct fusion with the cell surface. EV may also be up taken through various endocytic pathways, including clathrin mediated/lipid raft-mediated/receptor mediated endocytosis, macropinocytosis and phagocytosis. Afterwards, EV are enclosed in endocytic vesicles which transiently contact the endoplasmic reticulum (ER) and are destinated to lysosomal degradation. Modified from Wiklander et al 2019 (187).

Importantly, sEV uptake does not necessarily lead to a biological function (190), for this to happen sEV must bypass degradation pathways. Therefore, surface markers are particularly significant in EV biology. These surface proteins can act as ligands for cell-surface receptors (191), facilitate EV docking and internalization (192), and potentially determine the specificity of EV-cell interactions (193). Moreover, surface markers are likely to represent the cellular origins of sEV (134), thus, EV are essentially a 'fingerprint' of their parent cell and the complex microenvironments in cancer and potentially in endometriosis.

To comprehensively analyse surface markers of PF-sEV, we employed the MACSPlex EV kit IO, which allows for the simultaneous detection of 37 surface epitopes. This approach has proven valuable in reflecting cellular origins and mirroring cellular expression of these markers as highlighted in Chapter 2.

The characterisation provides insights into the intercellular communication networks operating within the peritoneal cavity. Secondly, it may help identify specific EV populations that are altered in disease states, potentially leading to the development of novel diagnostic or prognostic biomarkers. In endometriosis, biomarkers may aid in diagnosis, particularly for superficial lesions that are difficult to detect through imaging, and inform treatment stratification, such as guiding the choice between hormonal therapy and surgery. Lastly, elucidating the cellular sources of PF-sEV could pave the way for targeted therapeutic interventions that modulate EV production or uptake.

In Chapter 2, TEM revealed the presence of non-EV co-isolates following ultracentrifugation. While these non-EV co-isolates do not affect PF-sEV surface marker characterisation using bead-based assays, they may confound downstream functional analyses of PF-sEVs in Chapter 4. To ensure isolation of a consistent and purer sEV population, a refined protocol combining ultracentrifugation with SEC and filtration will be tested. This optimised method will be used for both MACSPlex surface marker profiling of PF-sEVs in this chapter and functional studies in Chapter 4.

Apart from comparing PF-sEV profiles between endometriosis patients and controls, I am also interested to investigate the change of EV signatures in women on hormonal treatments.

3.1.2 Hormonal treatments in endometriosis-associated pain

Endometriosis is an oestrogen-dependent disease, and hormone treatments (HT) are one of the treatment pillars for endometriosis-associated pain (EAP) for women not trying to conceive according to the latest European Society of Human Reproduction and Embryology (ESHRE) guidelines (194). EAP includes dysmenorrhea, non-cyclical pelvic pain and pain during/after sex, urination, and defecation (195). 82% of endometriosis patients experience at least one type of EAP (196) and more than 60% report chronic pelvic pain (197). Patients

experience EAP with varied severity which is often quantified using the Visual Analogue Scale (VAS), scoring from 0 to 10 (198).

The main aims of HT in endometriosis are to achieve a stable low steroid hormone environment by inhibiting ovulation, halting menstruation or mitigating oestrogen action. Active chemicals in hormonal therapies include progestins, combined contraceptives, gonadotropin-releasing hormone (GnRH) agonists/antagonists, and aromatase inhibitors (AI), each with distinct mechanisms of action (Figure 3.2).

Progestins, considered as first-line treatment, can be administered in various forms such as pills (with or without oestrogen), implants, intrauterine devices and injections (199). Progestin is a synthetic form of progesterone that blocks gonadotrophin secretion via actions on both pituitary and hypothalamus centre, leading to anovulation (200). Progestin also suppresses endometrial cell proliferation and retards lesion growth and exerts anti-inflammatory effects (201). Common types of progestins used in endometriosis treatment include dienogest, norethindrone acetate, medroxyprogesterone acetate, a levonorgestrel implant and the levonorgestrel intrauterine system (202).

Another key target is the hypothalamic-pituitary-gonadal (HPG) axis. The HPG axis plays a crucial role in regulating oestrogen secretion through a complex system of hormonal interactions and feedback mechanisms. The hypothalamus initiates this process by secreting GnRH in a pulsatile manner, stimulating the anterior pituitary gland to produce and release follicle-stimulating hormone (FSH) and luteinizing hormone (LH). These gonadotropins act on the ovaries, promoting follicular development and stimulating oestrogen production.

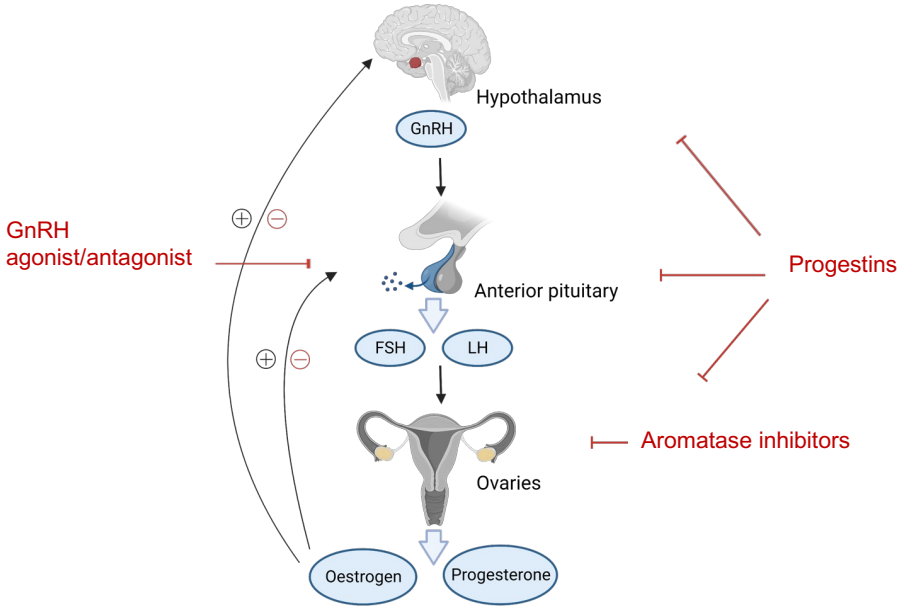

Figure 3.2. Targets of common hormonal treatments in endometriosis. The effects of various hormonal treatments on the hypothalamic-pituitary-gonadal (HPG) axis in endometriosis management. 1) Progestins: Suppression of gonadotropin secretion via hypothalamus and pituitary with additional direct endometrial effects. 2) GnRH Agonists: Downregulation of GnRH receptors. 3) GnRH Antagonists: Competitive binding to GnRH receptors. 4) Aromatase Inhibitors: Blockade of oestrogen biosynthesis in endometrium.
GnRH agonist/antagonist treatments on their own are typically limited to 6-month courses due to concerns about hypoestrogenic side effects such as vasomotor symptoms and reduced bone density, often necessitating hormone replacement therapy (HRT) as an add-back treatment (203, 204). Continuous administration of GnRH agonists downregulates GnRH receptors and the secretion of gonadotrophin (205) while GnRH antagonists block gonadotrophin secretion by competing with endogenous GnRH (206).

Aromatase inhibitors, recommended as second/third-line treatments in ESHRE guidelines, block the enzyme aromatase, which is responsible for the final step in oestrogen biosynthesis and its level is abnormally high in endometriosis (207). Efficacy has been shown in treating postmenopausal endometriosis when combined with other treatments (208) (194). Table 3.1 provides a comprehensive overview of common HT used in endometriosis treatment, including their formulations and typical usage.

Table 3.1. Common hormonal treatments used in endometriosis management.

Active ingredients	Routes of administration
Oestradiol + progestin	Oral, vaginal, transdermal (Combined contraceptive pills (COCPs), contraceptive ring, contraceptive patch)
Progestin	Oral (Progestin-only pills)
	Intrauterine (IUD, Mirena)
	Subcutaneous
	Intramuscular
GnRH agonists/antagonists	Subcutaneous Intramuscular
Aromatase inhibitors	Oral

Despite the widespread use of the first-line treatments using progestin or COCPs, significant variability in patient response and conflicting findings regarding their efficacy in treating endometriosis have been reported (199, 201). One fourth to one third of women receiving these treatments are not responsive to resolve EAP (209). The underlying cause, potentially related to progesterone resistance, require further investigation (210). Similarly, there is still a lack of evidence surrounding the efficacy of GnRH agonists/antagonists (194).

EV profiles are closely linked to cellular profiles and specific subpopulations can change in response to physiological factors, including diet (211), exercise (212) and sex (213-215). Hormones play a crucial role in shaping EV profiles, with their influence extending beyond basic sex differences. In females, the hormonal fluctuation during the menstrual cycle (215) and menopause (216) induce change in EV profiles. For exogeneous hormones, studies have revealed an increased number of microparticles (large EV) derived from platelets after exposure to COCP in healthy women (216) and women with polycystic ovary syndrome (217).

In deep infiltrating endometriosis, one study has revealed that plasma-derived large EV decrease women using COCP (218). However, there is limited evidence how sEV profiles, particularly their surface marker expression, are affected by HT. This knowledge gap is particularly relevant given that most studies on endometriosis exclude patients on HT due to the unknown effects of these treatments. When analysing patient demographics of those recruited in Oxford to the ENDOX/FENOX studies, I found approximately half of the patients were on hormones. This exclusion potentially limits our understanding of the disease in a significant proportion of patients.

Importantly, if HT does alter EV surface marker profiles, this could have important implications for using PF-sEV as biomarkers and might necessitate consideration of a patient's treatment history when interpreting EV-based diagnostic or prognostic tests.

To address these knowledge gaps, this chapter aims to:

3.2.1. Optimise protocols for isolating sEV from PF with reduced protein contamination. The use of IZON SEC columns and filtration will be assessed. These SOPs will serve as the foundation for the functional analysis of these sEV in Chapter 4.

3.2.1. To investigate PF-sEV size, concentration, and marker expression analysed by the MACSPlex EV kit IO in relation to disease status.

3.2.1. To investigate PF-sEV size, concentration, and marker expression analysed by the MACSPlex EV kit IO in relation to HT status.

3.2.1. To investigate whether progestin and GnRH agonists effect PF-sEV profiles, and if the administration route of progestin results in alternate profiles.

3.2.1. To investigate the potential predictive value of PF-sEV for pain severity or treatment response.

3.2 Methods

3.2.1 Sample Collection

PF samples were collected as part of the FENOX (17/SC/0664) and ENDOX (09/H0604/58) studies. These samples and data were collected, processed, and stored according to World Endometriosis Research Foundation Endometriosis Phenome and Biobanking Harmonisation Project (WERF EPHect) protocols (136-139). PF without visible blood contamination was collected from participants and centrifuged at 900 x g for 5 minutes to remove cellular debris. Processed samples were then stored at -80°C for later use. A total of 50 PF samples were used in this study. The age and BMI (mean ± SD) of participants are 31.6 ± 7.0 years and 22.9 ± 3.2 kg/m², respectively (Table 3.2). For the analysis of PF from women with differing HT, only samples from patients using single HT were selected. The hormone use was self-reported by the participants in EPHect patient questionnaires. Information from the short form McGill Pain Questionnaire v1 in EPHect patient questionnaires (139) were used to analyse pain severity. The pain score (0-10) of patients' worst acyclic pelvic pain in the last three months' were analysed in the 15 patients using the complete pain questionnare in the ENDOX study.

Table 3.2 Clinical characteristics of PF samples. Clinical data for 50 PF samples collected from patients. Patient number (1-50), endometriosis stage (0-4, according to rASRM classification), age (years), BMI, exogenous hormone use (N: none, POP: progestogen-only pill, Zoladex: GnRH agonist without add-back hormone replacement therapy (HRT), COCP: combined oral contraceptive pill, Mirena: levonorgestrel-releasing intrauterine system), and menstrual cycle phase (proliferative/secretory) are presented. N/A indicates unavailable information.

Patient number	Endometriosis staging (0-4)	Menstrual cycle	Hormone use	Age	BMI
1	0	Secretory	N	32	23
2	0	Secretory	N	38	21
3	0	Secretory	N	23	19
4	0	Proliferative	N	40	25
5	0	Proliferative	N	40	24

6	4	Proliferative	N	33	25
7	2	Proliferative	N	38	33
8	2	Proliferative	N	27	18
9	3	Proliferative	N	31	22
10	4	proliferative	N	28	22
11	2	Secretory	N	30	22
12	3	Secretory	N	29	24
13	4	Secretory	N	43	22
14	1	Secretory	N	25	24
15	2	Secretory	N	40	24
16	4	Secretory	N	29	20
17	0	Secretory	POP	26	26
18	0	N/A	POP	20	25
19	0	N/A	POP	27	22
20	1	N/A	POP	24	23
21	1	N/A	POP	24	18
22	1	Proliferative	POP	34	23
23	1	Secretory	POP	24	20
24	1	N/A	POP	N/A	21
25	4	N/A	POP	39	29
26	4	N/A	POP	30	28
27	0	N/A	Mirena	23	23
28	0	N/A	Mirena	28	N/A
29	0	N/A	Mirena	36	26
30	2	Proliferative	Mirena	33	18
31	1	N/A	Mirena	34	23
32	1	N/A	Mirena	21	23
33	1	N/A	Mirena	23	21
34	1	N/A	Mirena	36	23
35	3	N/A	Mirena	43	26
36	3	N/A	Mirena	38	21

37	4	N/A	Mirena	36	24
38	4	N/A	Mirena	31	22
39	1	N/A	COCP	36	18
40	2	Proliferative	COCP	23	27
41	1	Proliferative	COCP	23	22
42	4	Proliferative	COCP	30	21
43	3	N/A	COCP	33	22
44	3	Secretory	COCP	24	19
45	0	Proliferative	Zoladex	23	N/A
46	0	N/A	Zoladex	48	N/A
47	2	N/A	Zoladex	33	23
48	1	N/A	Zoladex	41	21
49	4	Secretory	Zoladex	45	30
50	4	N/A	Zoladex	32	19

3.2.2 PF-sEV isolation

Frozen PF samples were thawed at 37 °C and centrifuged at 16,000 x g for 30 mins. PF samples (0.5-1 mL) were run through SEC columns (qEV original 35nm columns Legacy & Gen 2; IZON Science, New Zealand), according to the manufacturer's instructions. Briefly, columns were equilibrated to room temperature and washed with 30 mL of fPBS. Once washed, 500 µL of PF was added to the top of the column and allowed to enter completely. fPBS was then added to the column, and fractions (500 µL each) were collected. The void volume was discarded, and the subsequent sEV-enriched fractions (fraction 6-9) were pooled and filtered through a 0.22 µm PVDF membrane (Sarstedt, Germany) twice. In 2024, IZON updated their protocol for the use of Gen 2 columns. PF-sEV isolated using the Gen 2 updated protocol, were collected as 400 µL fractions. Fractions containing the sEV (1.6 mL to 2 mL) were transferred into Ultra Clear ultracentrifuge tubes (5 mL; Beckman coulter, USA) and topped up with fPBS. Samples were then ultracentrifuged in an Optima XE-90 ultracentrifuge (Beckman coulter, USA) with SW55-Ti swinging bucket rotor (Beckman coulter, USA) at

150,000 x g for 2h. The supernatant was removed and the pellet containing the sEV was resuspended in 300-400 µL fPBS or RIPA lysis buffer for WB.

3.2.3 Nanoparticle Tracking Analysis (NTA)

NTA was performed as described in Chapter 2 Section 2.2.4.

3.2.3.1 SEC Column Optimization

EV concentration and size distribution in eluted fractions were analysed by NTA during the optimization of the SEC column. For legacy and Gen 2 protocols, 25 fractions were analysed (n=3), while for the updated Gen 2 protocol, fractions 1 to 10 were examined (n=2).

3.2.3.2 Membrane Filtration Evaluation

To evaluate additional filtration effects, pooled fractions 6-9 were analysed with and without 0.22 µm PVDF filtration. Filtered and unfiltered samples (n=3 each) were compared using NTA.

3.2.3.3 PF-sEV Characterisation

The size and concentration profile of isolated PF-sEV from all samples were analysed by NTA to compare among disease status and HT status. This analysis encompassed 11 samples processed by an MSc student (Banayot Hosh) under my supervision and 39 samples analysed directly by me.

3.2.4 Transmission Electron Microscopy (TEM)

TEM analysis was conducted on one representative PF-sEV sample isolated from an endometriosis patient following the protocol outlined in Chapter 2 Section 2.2.5 to visualize the morphology and confirm the presence of sEV in the isolated samples.

The size of PF-sEV isolated from one endometriosis patient was analysed. 5 random TEM images were taken and sizes were measured by Image J software with a total of 50 EV. The sizing data was compared to NTA.

3.2.5 Western Blot

The Jess Automated Western Blot System (Bio-Techne, USA) was used following the manufacturer's instructions. In brief, 4µL of EV samples (0.1 to 2 mg/mL) were prepared with 1 µL of fluorescent 5X Master Mix and denatured at 95°C for 5 minutes. Primary antibodies (Table 3.3) were diluted 1:2 to 1:50. The 12-230 kDa Separation Module was used. The microplate was loaded with samples, ladder, primary antibodies, and secondary antibodies with pre-optimised concentration (Anti-rabbit or anti-mouse detection modules; Bio-Techne, USA) and chemiluminescent reagents as per manufacturer's instructions. The Jess instrument automatically performed protein separation, immunoprobing, and detection. Data analysis was conducted using Compass for SW software, which identified and quantified protein bands based on chemiluminescent signals.

Table 3.3. Antibodies used in JESS Automated Western Blot System for EV.

Antibody	Molecular weight	Host species	Supplier
Syntenin	32KDa	Monoclonal rabbit, EPR8102	Abcam, UK
CD81	30KDa	Polyclonal rabbit, ab93485	Abcam, UK
ALIX	95KDa	Polyclonal rabbit, NBP1-49701	Novus Biologicals, USA
CD9	20KDa	Monoclonal mouse, C-4	Santa Cruz Biotechnology, USA

Conventional Western blots were performed to visualize PF-sEV markers syntenin and TSG101, as well as albumin (purity marker). Following ultracentrifugation, PF-sEV samples were resuspended in 1 x RIPA lysis buffer containing protease inhibitors (Roche, Switzerland) and stored at -20°C. Protein concentration was determined using the BCA assay. For each

sample, 7 µg of protein was loaded onto the gel. The gel loading, protein transfer, and exposure protocols were conducted as previously described in Chapter 2 Section 2.2.7. Primary antibodies for syntenin (detail in above table) and TSG101 (polyclonal rabbit, Abcam, UK) were used at a 1:1000 dilution, while the albumin antibody (polyclonal rabbit, Cell Signalling Technology, USA) was used at a 1:1000 dilution.

3.2.6 Flow cytometry

Surface marker expression of PF-sEV was measured by LSRII flow cytometry (BD Biosciences, USA) using the MACSPlex EV kit IO, following the same protocol described in Chapter 2 Section 2.2.8.2.

3.2.6.1 Titration experiment

A titration experiment was conducted by an MSc student (Banayot Hosh) under my daily supervision. PF-sEV input concentrations ranging from $3.75x10^7$ to $1.5x10^9$ particles were tested (n=3).

3.2.6.2 PF-sEV surface marker characterisation

A total of 50 PF-sEV samples were characterized. Results from 11 patient samples analysed by Banyot Hosh are presented in section 3.3.2.3. Results from 39 samples analysed by myslef are combined with Hosh's data and presented in section 3.3.3.1 for impact of hormonal treatment.

3.2.7 BCA Assay

BCA assays were performed as described in Chapter 2 Section 2.2.6. BCA assays were used to assess the protein level of the eluted SEC column fractions in optimisation experiments and was also used for quantification of protein for WB.

3.2.8 Statistical analysis

One-way ANOVA was used to compare EV characteristics between eluted SEC fractions and MACSPlex results. Unpaired student's t-tests were employed to assess differences before and after membrane filtration. One-way ANOVA or unpaired t-tests were used to analyse marker expression of PF-sEV between groups. Two-way ANOVA was utilized to analyse PF-sEV size and concentration profiles across menstrual cycle stages and disease conditions, or disease stage and HT status. Tukey's HSD (Honestly Significant Difference) post-hoc test was conducted following significant ANOVA results to identify specific group differences. Correlation of acyclic pelvic pain severity with EV concentration and marker expression was assessed using Pearson correlation coefficients. For all tests, $p < 0.05$ was considered statistically significant. Data analysis and visualization were performed using GraphPad Prism 9 software.

3.3 Results

3.3.1 SOP of PF-sEV isolation

This subchapter aimed to establish an SOP for isolating and characterizing PF-sEV. It focused on evaluating SEC columns (IZON, New Zealand) to determine the most appropriate fractions for sEV collection and assess membrane filtration in further purifying EV. Additionally, titration experiments of PF-sEV using the MACSPlex EV kit IO were performed to determine optimal EV input for subsequent experiments.

3.3.1.1 Isolation of PF-sEV using IZON qEV Original 35nm columns and membrane filtration

The use of IZON qEV Original 35nm columns have proven to generate purer PF-sEV populations than ultracentrifugation. I applied the recommended standardised protocol which it was based on plasma samples. It's important to note that biological fluids can exhibit significant variations, and modifications of protocols for other fluids are recommended. Throughout this study (conducted from 2021 to 2024), IZON updated columns from Legacy and Gen 2 and updated protocols for Gen 2 in 2024. In response to these changes, I consistently adapted the recommended protocols to suit sEV isolation from PF samples. To determine optimal fractions for sEV enrichment, each 500µL fraction was characterized using NTA for EV quantification and size distribution, and BCA assay for protein content.

For Legacy columns, the NTA and BCA results are presented in Figure 3.3. NTA results revealed that EV were first detectable (>$2x10^8$ EV/mL) in fraction 6, with a concentration of $8.1x10^8 \pm 9.7x10^8$ vesicles/mL (mean ± SD). The EV concentration increased progressively, reaching a peak in fraction 8 ($1.7x10^{10} \pm 9.7x10^9$ EV/mL), before declining in subsequent fractions. Fraction 11 ($3.5x10^8 \pm 3.5x10^8$ EV/mL) represented the last fraction with detectable EV by NTA.

Protein analysis revealed that fractions 6, 7, and 8 had protein levels below the BCA kit's detection limit (<25µg/mL). Fraction 9 was the first to show detectable protein (68.9 ± 38.5 µg/mL, mean ± SD), with concentrations steadily increasing to a peak in fraction 16 (8383.1 ± 2715.9 µg/mL, mean ± SD) before declining.

A clear trend of decreasing EV size across fractions was observed (Figure 3.4). The mode size (mean ± SD) of fraction 6 (434.5 ± 182.0 nm) was significantly larger than subsequent fractions: fraction 7 (144.3 ± 30.7 nm), fraction 8 (106.1 ± 14.2 nm), fraction 9 (109.3 ± 11.3 nm) and fraction 10 (93.3 ± 105.7 nm).

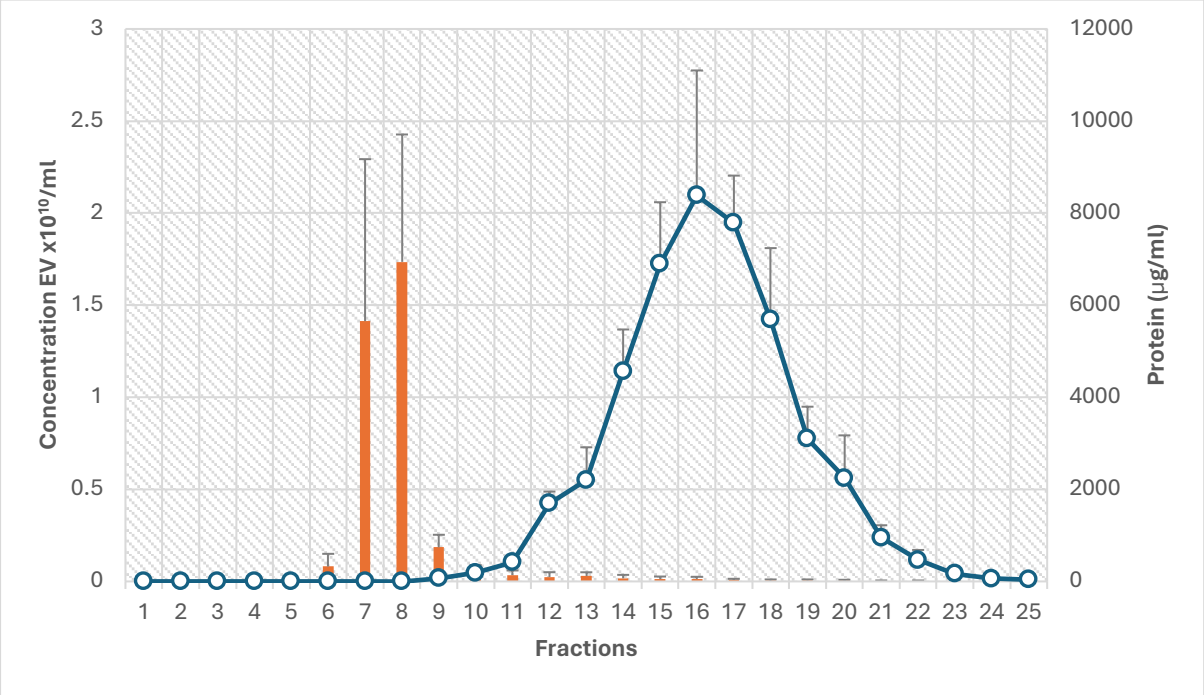

Figure 3.3. Characterisation of PF-sEV isolation using Legacy columns in first 25 fractions (n=3). Distribution of EV and protein concentrations across eluted fractions. PF samples were fractionated into 25 sequential 0.5mL fractions. EV concentration (orange bars) was quantified by NTA, while protein concentration (blue line) was determined using the BCA. Bars= mean ± SD.

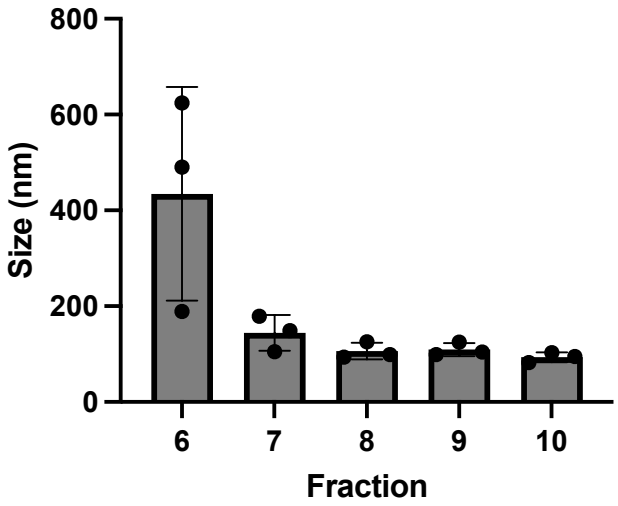

Figure 3.4. The NTA mode Size of PF-sEV in SEC fractions using Legacy columns. EV were isolated from PF (n=3) samples using SEC Legacy columns. Eluted fractions (500 µL each, fractions 6-10) were collected and analysed for EV mode size by NTA. Bars represent mean ± SD.

These data confirm the IZON column's efficacy in separating PF-sEV from soluble proteins based on size. To optimize EV yield while minimizing protein contamination, fractions 6 to 9 were collected for downstream experiments, as recommended in the manual. Although fraction 6 contained larger EV, these were considered a minority due to the low overall EV concentration. Additionally, although fraction 10 still contained a small amount of EV, it was excluded due to relatively high soluble protein levels.

sEV-enriched fractions were pooled and subjected to additional membrane filtration prior to ultracentrifugation. The efficacy of this step was assessed by NTA. Size distribution profiles showed a more homogeneous EV population after membrane filtration (Figure 18a, blue line) compared to before membrane filtration (Figure 3.5a, orange line). The percentage of EV larger than 200nm was significantly lower after membrane filtration (4.7 ± 5.2%, mean ± SD) compared to before membrane filtration (16.6 ± 2.1%, mean ± SD) (Figure 3.5b). Subgroup analysis examining EV size distribution (≤10% or ≤ 50%) showed no significant difference between pre and post filtration. These results indicate that the additional membrane filtration step effectively removed larger EV while preserving the sEV population.

a)

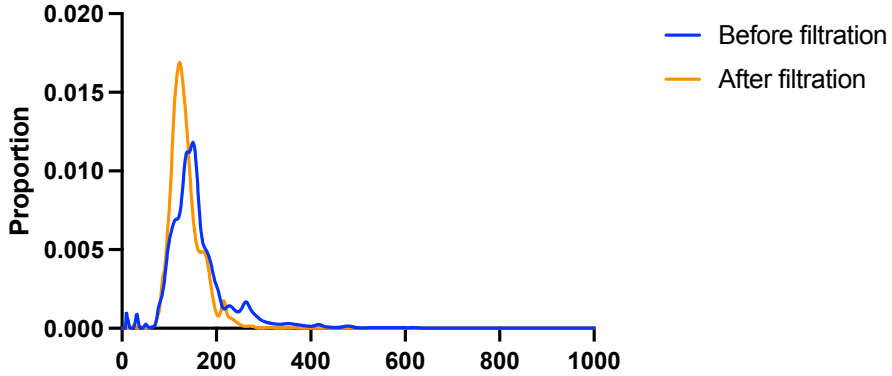

b)

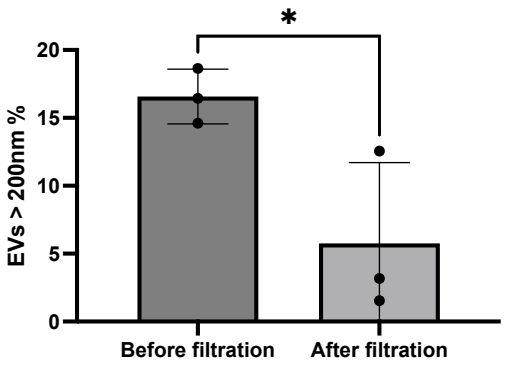

Figure 3.5. NTA evaluation of membrane filtration on EV size. sEV-enriched fractions collected from SEC columns were pooled and subjected to 0.22 µm filtration. NTA was performed on samples before and after membrane filtration to assess the impact on EV size distribution. a) Representative size distribution profiles of EV before (n=3, blue line) and after (n=3, orange line) filtration. b) Comparison of the percentage of EV larger than 200 nm in filtered and unfiltered samples. Data are presented as mean ± SD (n=3 before filtration; n=3 after filtration). Unpaired two-tailed *t*-test (Shapiro-Wilk test: $p > 0.05$), *$p<0.05$.

For Gen 2 IZON qEV columns, the recommended protocol initially remained unchanged but claimed to offer improved separation of proteins and EV (219). Using these columns, I confirmed that sEV-enriched fractions still corresponded to fractions 6, 7, 8, and 9 (Figure 3.6).

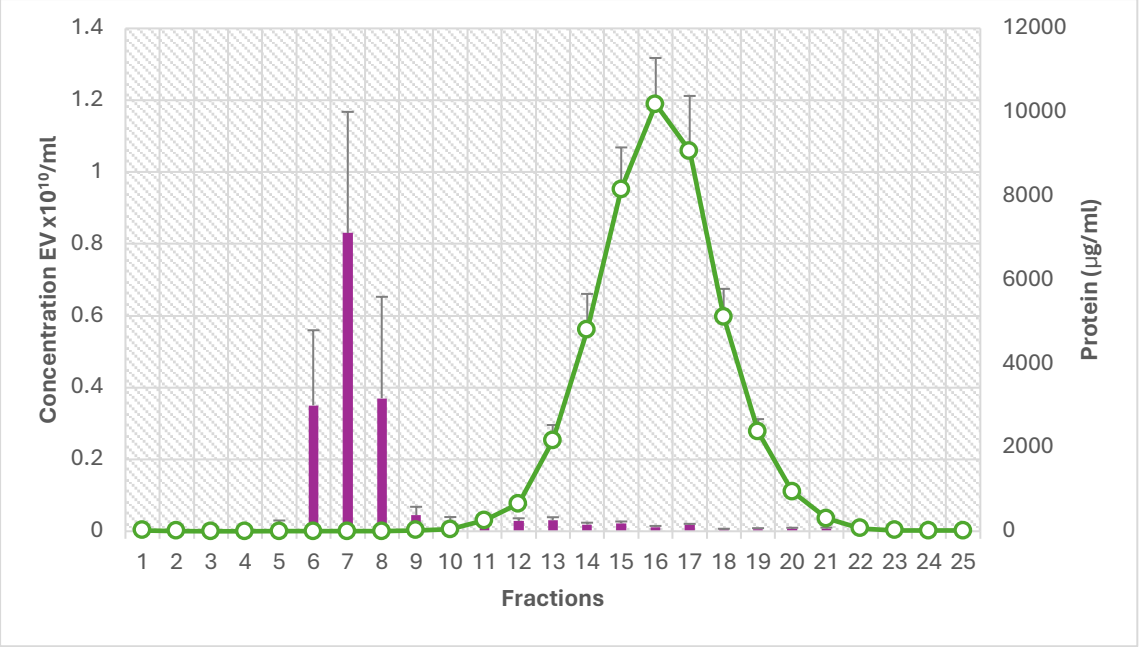

Figure 3.6. Characterisation of PF-sEV isolated using Gen 2 columns (n=3). Distribution of EV and protein concentrations across eluted fractions. PF samples were fractionated into 25 sequential 0.5mL fractions. EV concentration (purple bars) was quantified by NTA, while protein concentration (green line) was determined using the BCA assay. Bars= mean ± SD.

Similarities with Legacy columns included the initial detection of EV in fraction 6, as well as a comparable trend of decreasing mode size (mean ± SD) across fractions 6-10 (6: 291.5±86.3nm; 7: 159.1±15.2nm; 8: 118.0±28.2nm; 9: 95.1±20.4nm; 10: 102.7±26.5nm) (Figure 3.7a).

Several key differences were observed between Legacy and Gen 2 columns. Gen 2 columns showed lower soluble protein levels in sEV-enriched fractions. Notably, fraction 9 exhibited a 70% reduction in protein content (21.2 ± 32.4µg/mL), with protein levels below accurate BCA detection in two out of three samples. This contrasts with consistently detectable protein levels in fraction 9 of Legacy columns (Figure 3.7b). Additionally, fraction 10 in Gen 2 columns showed significantly lower protein levels (42.3 ± 7.67 µg/mL) compared to Legacy. Gen 2 columns also demonstrated a shift in EV distribution across fractions 6-10 (Figure 3.7c). A significantly higher percentage of EV was collected in fraction 6 (Legacy: 3.1 ± 3.29%; Gen 2: 25.3 ± 15.42%; $P<0.05$). Moreover, the EV concentration peaked in fraction 7 for Gen

2, compared to fraction 8 for Legacy. Significantly less EV were collected in fraction 8 of Gen 2 compared to Legacy (P<0.01).

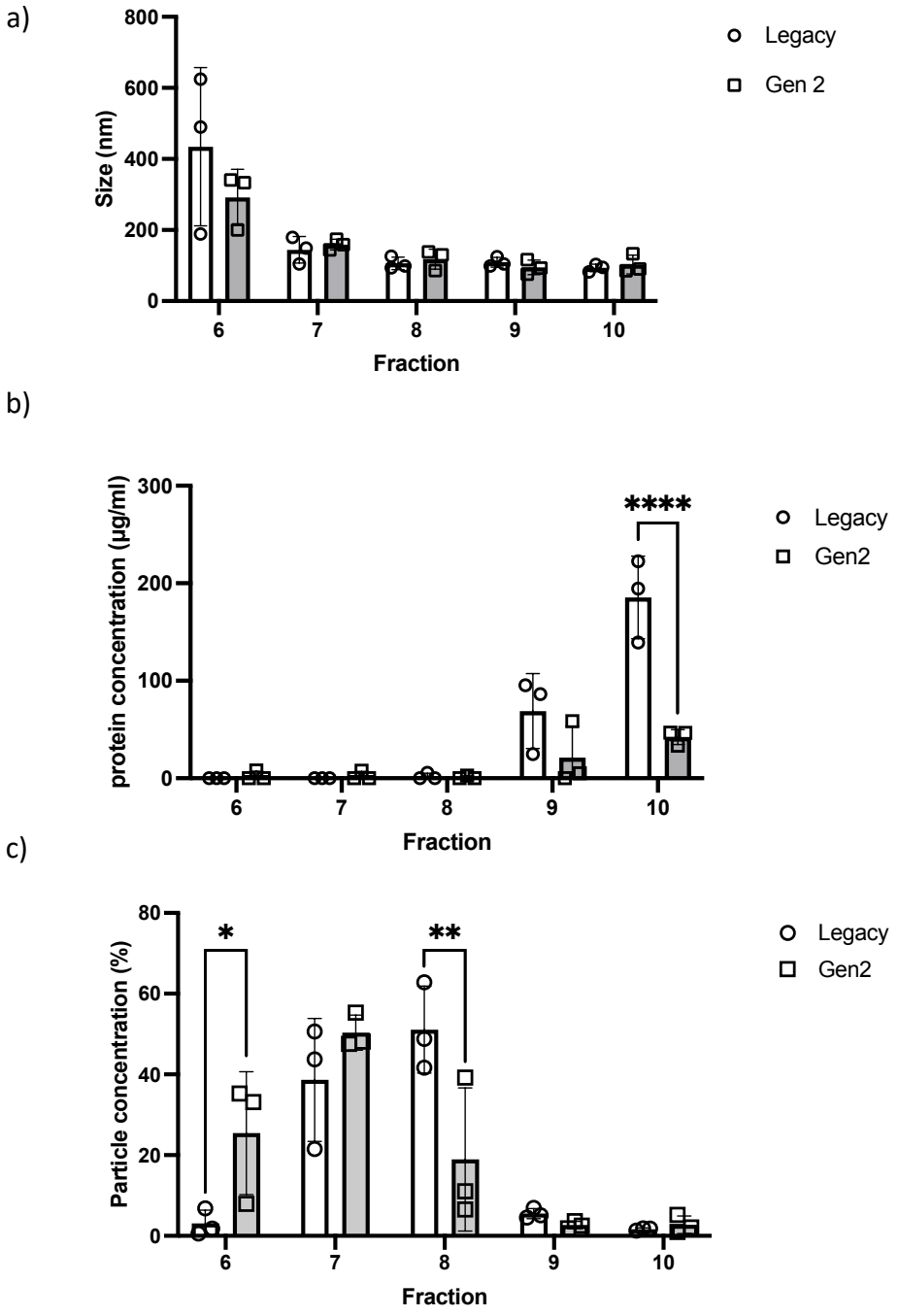

Figure 3.7. Comparison of protein concentration and particle mode size between Legacy and Gen 2 columns (n=3). a) NTA mode size of particle, b) protein concentration and c) NTA particle concentration in fractions 6-10 for Legacy and Gen 2 columns. Bars= mean ± SD. Two-way ANOVA with multiple comparisons (Shapiro-Wilk test: p > 0.05),*p<0.05, **p<0.01, ****p<0.0001.

These findings support the manufacturer's claim of wider separation between proteins and EV in Gen 2 columns. The shift towards earlier elution of EV, coupled with later elution of soluble proteins, indicates an enhanced separation efficiency.

In 2024, IZON introduced new protocols for Gen 2 columns, revising the collection volume per fraction from 500 µL to 400 µL for undisclosed reasons. The Gen 2 updated (2024) protocol defines the first 5-6 fractions as void, with sEV-enriched fractions corresponding to the subsequent 4 fractions (either 6-9 or 7-10; totalling 1.6 mL).

To evaluate EV characteristics in this modified protocol, EV from two PF samples from endometriosis patients were collected and fractions (1-10) analysed by NTA.

EV were again first detected in fraction 6, but with a notably large average mode size of 896.0 nm (Figure 3.8). Fractions 7, 8, 9, and 10 exhibited progressively smaller average mode sizes of 205.0 nm, 172.5 nm, 101.5 nm, and 90.5 nm, respectively.

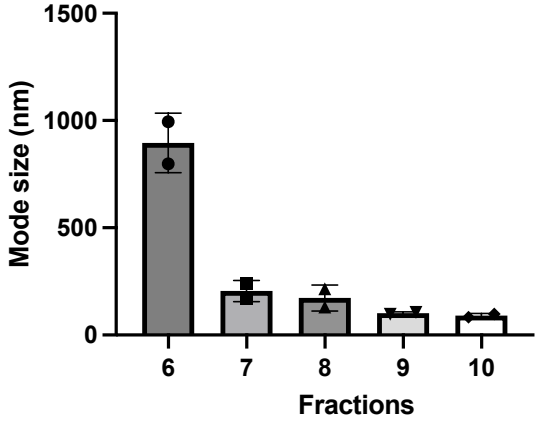

Figure 3.8. NTA mode size of PF-EV in SEC fractions using the Gen 2 (2024) updated protocol. SEC was performed to separate EV based on size. Eluted fractions (400 µL each) were collected and analysed for EV mode size NTA (n=2). Bars= mean ± SD.

Based on these findings, the protocol was adjusted to collect fractions 7 to 10, excluding fraction 6 which predominantly contained larger EV. Following membrane filtration and ultracentrifugation of fractions 7-10, NTA (n=3) revealed modal sizes (mean ± SD) of 214.2 ± 63.2 nm for the pooled sEV enriched fractions. Importantly, no significant difference was

observed between these results and those obtained from the same three samples isolated using previous protocols before 2024 (Figure 3.9).

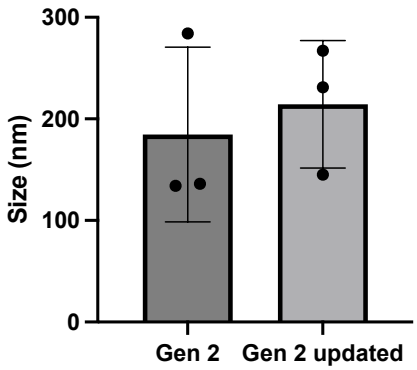

Figure 3.9. NTA comparison of PF-sEV mode size using Gen2 (pre-2024) and Gen 2 updated (2024) protocols (n=3). Mode size of PF-sEV using the pre-2024 protocol and the updated 2024 protocol for Gen 2 columns. Bars= mean ± SD. Paired two-tailed *t*-test (Shapiro-Wilk test: $p > 0.05$).

3.3.1.2 MACSPlex EV Kit IO Optimisation for PF-sEV Analysis

Building upon the findings from Chapter 2, which emphasized the importance of standardised EV input for the MACSPlex EV kit IO, optimisation experiments for PF-sEV were conducted. This experimental work was performed by a MSc project student who I supervised. Two titration experiments (n=3) ranging from $3.75x10^7$-$1.5x10^9$ EV count (Figure 3.10) were performed to determine the optimal EV concentration for the assay. The analysis revealed consistent expression of three sEV enriched markers (CD9, CD63 and CD81) across all examined EV counts. In contrast, CD24 and CD133/1 displayed significant expression variability, with nMFIs ranging from 0.34 to 1.94 and 0.93 to 3.04 respectively, decreasing as EV count increased.

Several markers like SSEA-4, CD146, and CD86 were undetectable at the lowest EV count ($3.75x10^7$) but were expressed at higher counts. These results suggest that higher EV counts may enable the detection of less abundant markers.

Considering that a single run of the IZON column (500 µL PF) typically yields $1x10^9$ EV and balancing the need to include as many PF samples as possible, I selected $7.5x10^8$ EV as the standardised PF-sEV input for subsequent experiments.

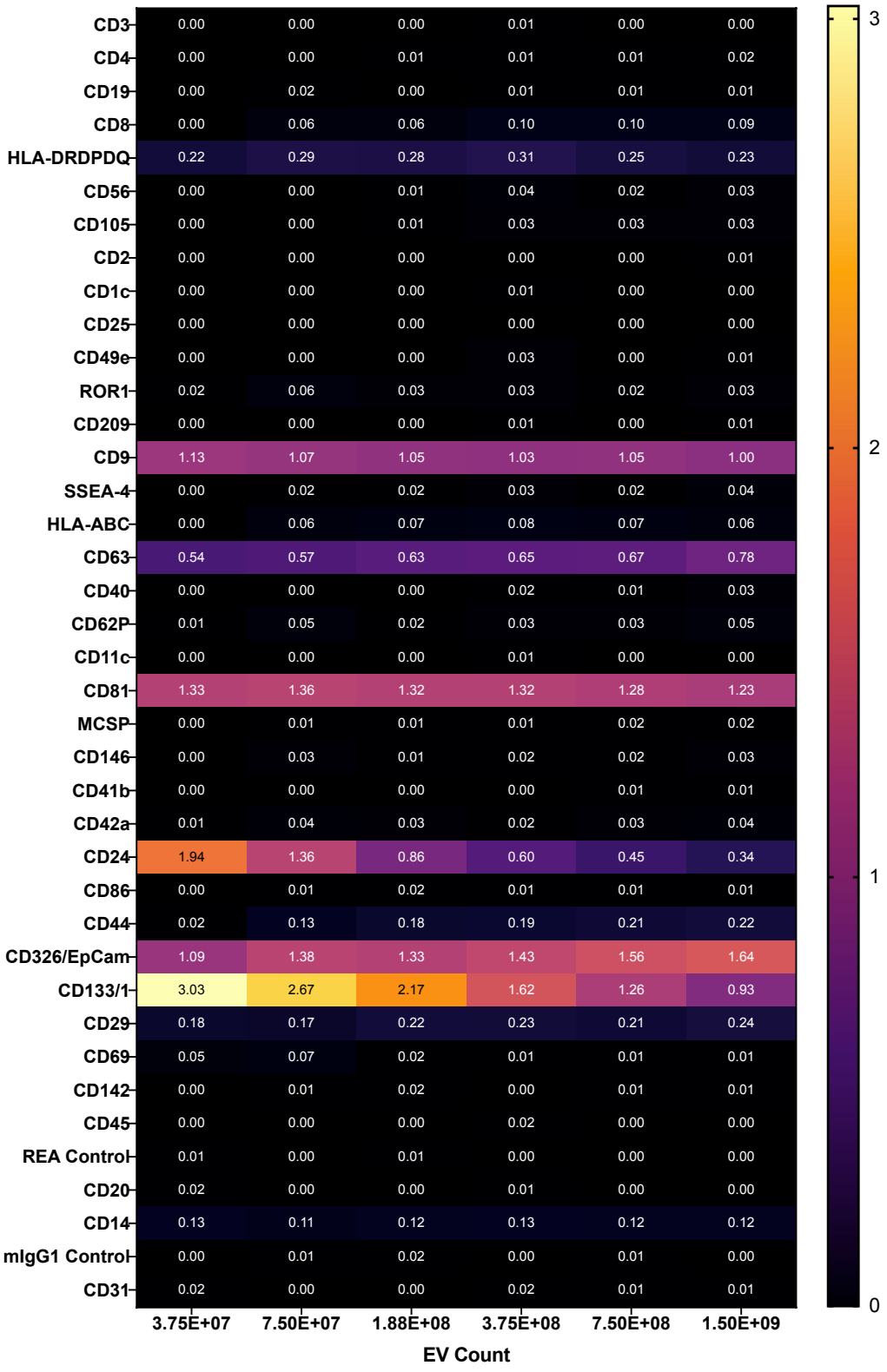

Figure 3.10. Titration experiment of EV input into MACSPlex EV kit IO using PF-sEV (n=3) Heatmap showing nMFI for 37 surface markers on pMΦ-sEV at EV concentrations ranging from $3.75x10^7$ to $1.5x10^9$ EV. nMFI values were calculated by subtracting background from raw MFI and then normalizing to the mean of CD9, CD63 and CD81 expression.

3.3.2 PF-sEV Characterisation

This chapter aimed to characterize the quantity and quality of PF-sEV preparations following the MISEV guidelines (57). Physical properties were examined using NTA for size distribution and concentration, supported by TEM analysis. Protein composition was analysed by western blot for cytosolic and negative markers, and the MACSPlex EV kit IO for 3 sEV enriched transmembrane markers (CD81, CD63 and CD9) as well as the expression of 34 additional markers. The MACSPlex data was analysed for cellular origins of PF-sEV. Comparative analyses between endometriosis patients and controls, as well as across menstrual cycle phases, were conducted.

3.3.2.1 PF-sEV size and concentration analysis by NTA and TEM

Sixteen PF-sEV samples from women with no hormonal treatments (NHT) were isolated by SEC, filtration and ultracentrifugation. The average age was 32.9 ± 6.2 (mean ± SD), with an average BMI of 23.0 ± 3.3 (mean ± SD). NTA revealed a concentration range from $2.7x10^9$/mL to 2.0 $x10^{10}$/mL, with an average of $8.6x10^9$ ± $5.8x10^9$/mL (mean ± SD) (Figure 3.11). Statistical analysis revealed no significant influence of either disease status or menstrual cycle phase on the concentration of PF-sEV (P>0.05).

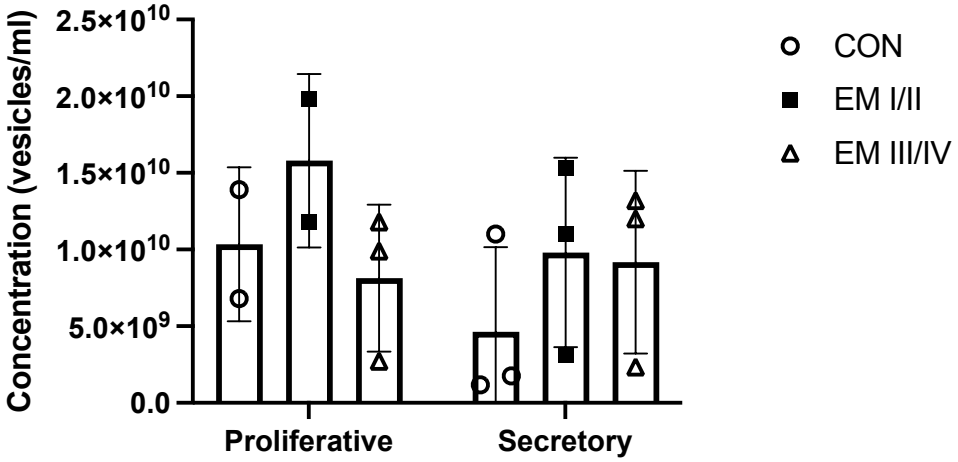

Figure 3.11. Concentration of PF-sEV analysed by NTA. Samples were categorised based on disease status (endometriosis stage I/II: n=5, endometriosis stage III/IV: n=6, control: n=5) and menstrual cycle phase (proliferative: n=7, secretory: n=9). Bars=mean±SD. Two-way ANOVA with Turkey's multiple comparisons.

The mode size (mean ± SD) of PF-sEV was also analysed across different groups (Figure 3.12). For endometriosis patients, the mode size was 220.9 ± 52.7 nm, while for controls it was 202.6 ± 47.4 nm. When comparing menstrual cycle phases, the mode size was 234.3 ± 37.6 nm for the proliferative phase and 200.3 ± 55.8 nm for the secretory phase. No significant differences were found between any groups (P>0.05).

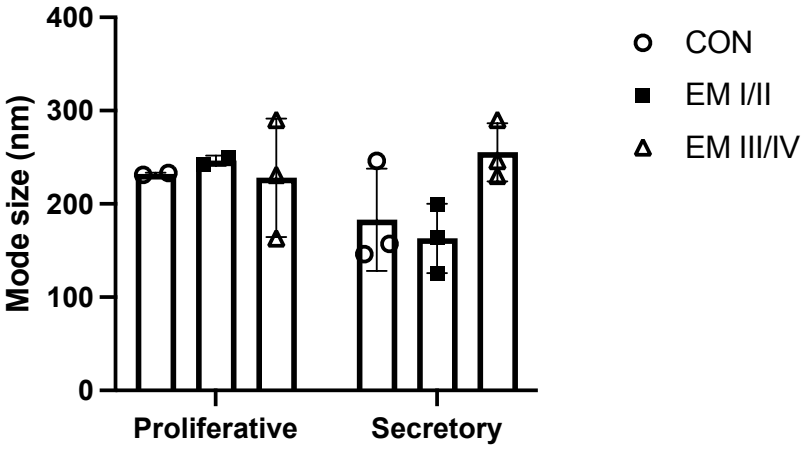

Figure 3.12. Size of PF-sEV analysed by NTA. Samples were categorised based on disease status (endometriosis stage I/II: n=5, endometriosis stage III/IV: n=6, control: n=5) and menstrual cycle phase (proliferative: n=7, secretory: n=9). Bars=mean±SD. Two-way ANOVA with Turkey's multiple comparisons.

The similarity in PF-sEV size between groups was further confirmed by their size distribution patterns. Both endometriosis patients and controls exhibited similar distributions (Figure 3.13), characterized by two distinct peaks: one at approximately 120 nm and another at 220 nm.

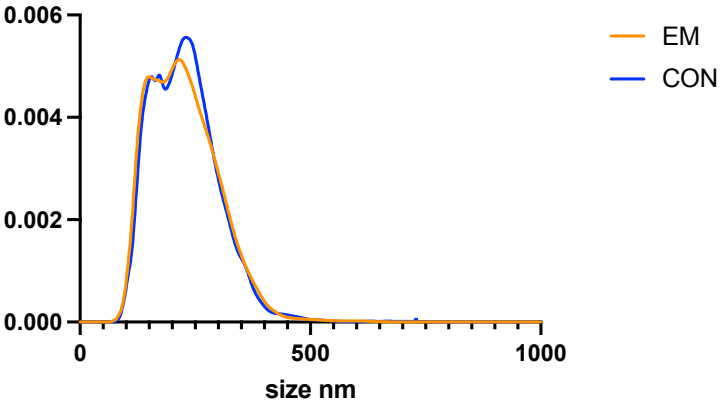

Figure 3.13. NTA Size distribution of PF-sEV. Comparison of average size distribution patterns between endometriosis (orange line, n=10) and control (blue line, n=6) groups.

The size distribution of PF-EV was also measured using TEM (Figure 3.12a) and directly compared to the NTA measurement (n=1). Five random TEM images from one PF-sEV sample were selected (Figure 3.14a), and EV size was measured by ImageJ computer software. The comparison revealed notable differences between the two techniques. The size of PF-sEV measured by NTA (mean 196nm, mode 164nm) was larger than that measured by TEM (mean 89nm, mode 59nm). When comparing the overall size distribution (Figure 3.14b), I observed that EV smaller than 100nm were dominant in the TEM analysis while EV measured by NTA ranged from 100-200nm. Moreover, TEM was able to detect EV smaller than 50nm, which were not observed using NTA.

a)

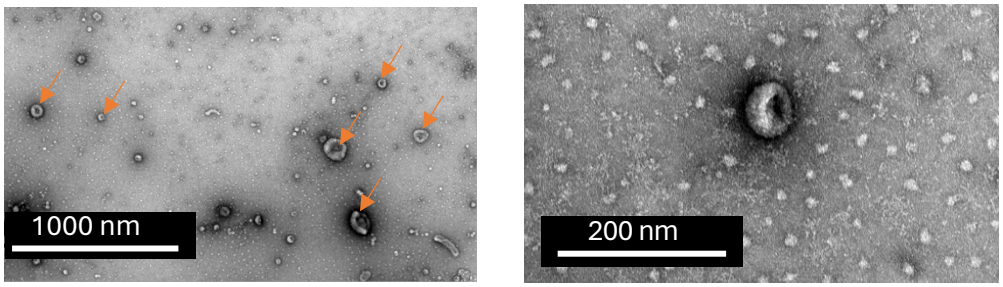

b)

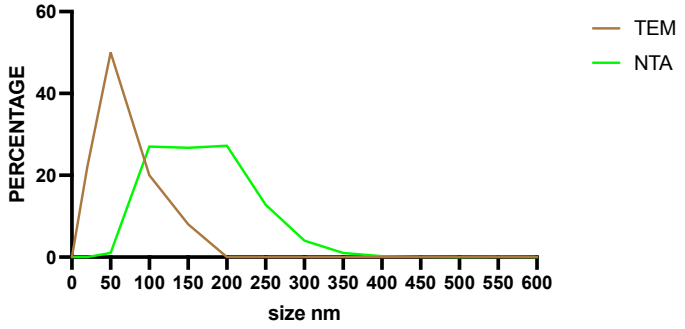

Figure 3.14. Comparison of PF-sEV size distribution as measured by TEM and NTA. a) Representative TEM image of PF-sEV. Orange arrows denote a selection of EV. Scale bars: 1000 nm (left), 200nm (right). b) Comparison of PF-sEV size as measured by TEM (brown line) and NTA (green line).

3.3.2.2 PF-sEV protein composition analysis by Western blotting

To further validate and characterize PF-sEV protein composition, Western blotting was performed to examine two cytosolic proteins syntenin, ALIX and two transmembrane proteins CD9 and CD81. The JESS Automated Western Blot System (Bio-Techne, USA) was employed as it requires less protein and therefore is a huge advantage given that only small quantities of protein are available per PF-sEV sample (around 7 µg EV from 500 µL PF).

PF-sEV isolated via the multi-step purification process (SEC, filtration, and ultracentrifugation) mentioned above were subjected to targeted protein analysis (Figure 3.15). Following optimization of primary antibody dilutions, all four proteins of interest (ALIX, CD9, CD81, and syntenin) were successfully visualized with a protein load of 4 µg PF-sEV. Notably, syntenin, identified as the most abundant sEV marker in PF-sEV, was also detectable at a reduced protein load of 0.4 µg.

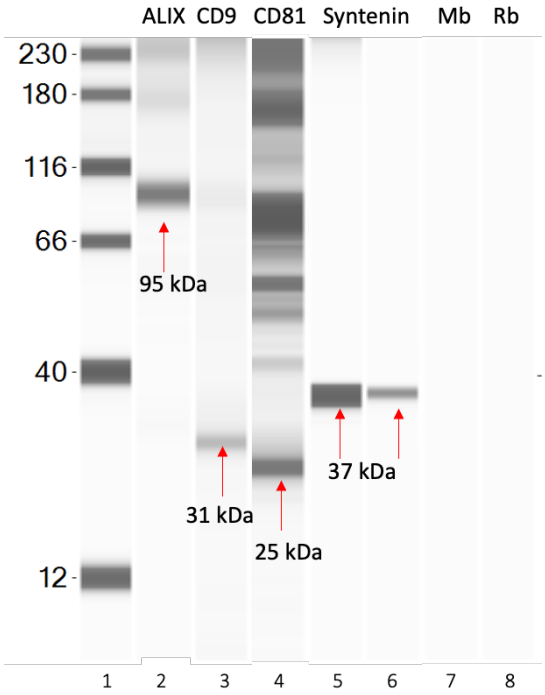

Figure 3.15. sEV marker detection in PF-sEV using the JESS Automated Western Blot System. Full western blot showing detection of sEV markers. Electrophoretic separation of PF-sEV proteins was performed with 4 µg (lanes 2-5) or 0.4 µg (lane 6) of protein loaded per lane. Primary antibody dilutions and targets include ALIX (95 kDa, 1:5; lane 2), CD9 (31 kDa, 1:2; lane 3), CD81 (25 kDa, 1:20; lane 4), and syntenin (37 kDa, 1:50; lanes 5 & 6). Negative controls consisted of anti-mouse (Mb; lane 7) and anti-rabbit (Rb; lane 8) secondary antibodies. Molecular weight markers were included (lane 1).

Due to the high sensitivity of the JESS system, albumin, a negative control for sEV preparation, was found to be unsuitable for analysis when loading 4 µg of PF cell lysates as a comparison. It caused overloading of the automated capillaries, resulting in experimental failure.

Consequently, conventional western blot analysis was employed. This method involves manual sample preparation and gel loading, with protein bands captured using a G:BOX imaging system . The technique was used to assess the expression of the highly abundant syntenin and albumin in PF-sEV isolated from three control subjects and three patients with endometriosis.

Ponceau S staining confirmed equivalent protein loading across all six samples (Figure 3.16a). Syntenin was detectable in all six PF-sEV samples with minimal detection in PF cell lysates (Figure 3.16b). While albumin bands were detectable in PF-sEV samples, a marked reduction in albumin levels was observed compared to PF cell lysates. Together, these results are indicative of effective sEV isolation. Additional characterisation of sEV markers revealed TSG101 expression in PF-sEV samples, though at lower levels compared to syntenin expression (Figure 3.16c).

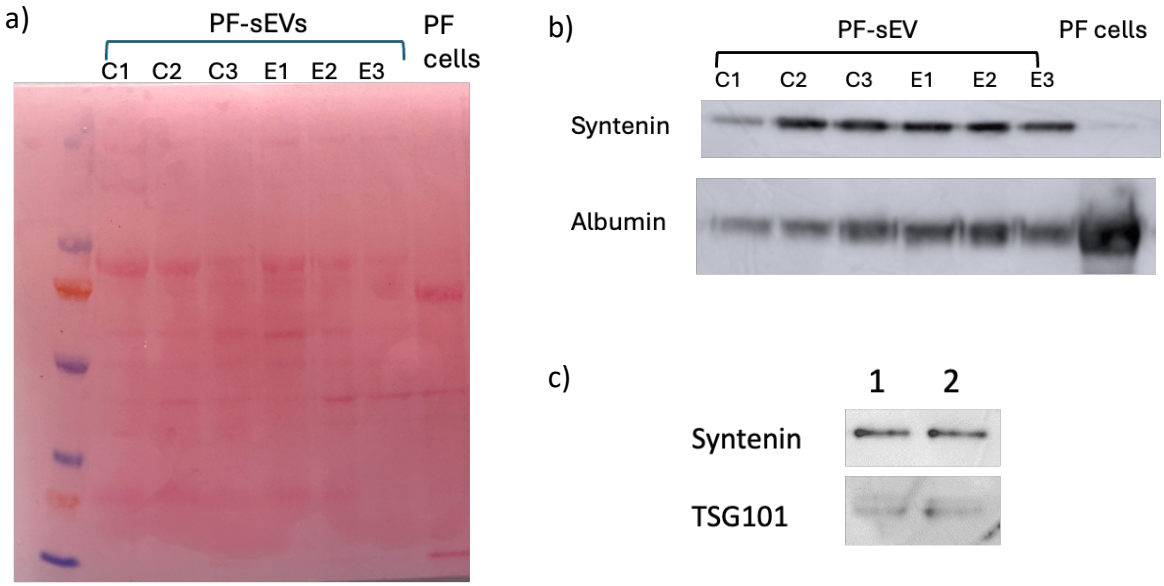

Figure 3.16. Western blot analysis of PF-sEV. a) Ponceau S staining of the membrane. b) Western blot analysis of syntenin and albumin expression in PF-sEV isolated from control and endometriosis patients (n=3) compared to PF cell lysates. C=control, E=endometriosis. c) Comparative analysis of syntenin and TSG101 expression in PF-sEV (n=2). Protein loading: 7µg per lane.

3.3.2.3 PF-sEV surface marker characterisation by the MACSPlex EV kit IO

Surface marker expression of PF-EV was assessed using the MACSPlex EV kit IO in 5 controls and 6 endometriosis samples. The analysis confirmed the expression of established sEV markers CD81, CD63, and CD9. All 37 surface markers in the panel were detected in PF-sEV, with considerable variability among samples (Table 3.4). Three sEV-enriched markers and nine additional markers (CD133/1, HLA-DR, EpCAM, CD24, CD29, CD44, CD14, CD49e, CD8) were consistently expressed across all 11 samples. The remaining 25 markers showed variable expression, being detected in 10% to 90% of the samples. CD4, CD56, CD105, and ROR1 were expressed in 10 out of 11 samples, with their absence noted in the same endometriosis sample. CD209 was the least expressed marker, present in only 2 samples.

All expressed markers had a mean nMFI above 0.01. Notably, higher expression frequency did not always correlate with higher nMFI. For instance, CD49e was expressed in all samples with a mean nMFI of 0.01, while CD3 was expressed in 7 out of 11 samples but had a mean

nMFI of 0.08. Apart from the sEV markers (CD81, CD9 and CD63), CD133/1, CD24, EpCAM, HLA-DR, and CD44 exhibited the highest mean nMFI levels.

To compare between endometriosis and control samples, CD1c was only expressed in 3 out of 5 control samples and not in any endometriosis samples. However, no significant differences in expression levels were observed between the two groups for the other markers.

Table 3.4. Expression of surface markers on PF-sEV using the MACSPlex EV kit IO. The expression profile and frequency of surface markers detected on PF-sEV across 11 samples.

Surface marker	Positive proportion	Mean nMFI ± SD	Surface marker	Positive proportion	Mean nMFI ± SD
CD8	11/11	0.087 ± 0.070	CD41b	8/11	0.018 ± 0.008
HLA-DRDPDQ	11/11	0.382 ± 0.375	CD42a	8/11	0.020 ± 0.008
CD24	11/11	0.711 ± 0.438	CD86	8/11	0.022 ± 0.011
CD326/EpCAM	11/11	0.462 ± 0.484	SSEA-4	8/11	0.021 ± 0.014
CD133/1	11/11	0.736 ± 0.909	CD62P	8/11	0.010 ± 0.011
CD44	11/11	0.175 ± 0.093	CD45	8/11	0.058 ± 0.037
CD29	11/11	0.091 ± 0.056	CD146	7/11	0.023 ± 0.005
CD14	11/11	0.071 ± 0.060	CD3	7/11	0.084 ± 0.106
CD9	11/11	0.854 ± 0.169	CD25	7/11	0.046 ± 0.037
CD63	11/11	0.476 ± 0.202	CD20	7/11	0.017 ± 0.011
CD81	11/11	1.670 ± 0.206	CD2	6/11	0.053 ± 0.037
CD49e	11/11	0.013 ± 0.010	CD142	6/11	0.020 ± 0.010
HLA-ABC	10/11	0.132 ± 0.063	CD19	6/11	0.020 ± 0.015
CD4	10/11	0.019 ± 0.009	CD69	5/11	0.016 ± 0.009
CD56	10/11	0.112 ± 0.085	CD31	4/11	0.017 ± 0.010
CD105	10/11	0.462 ± 0.484	CD11c	4/11	0.020 ± 0.008
ROR1	10/11	0.736 ± 0.909	CD1c	3/11	0.017 ± 0.014
CD40	8/11	0.175 ± 0.093	CD209	2/11	0.014 ± 0.001
MCSP	8/11	0.091 ± 0.056			

The characterisation revealed a diverse range of source cells for PF-sEV (Figure 3.17). Multiple cell populations were identified as potential origins of these PF-sEV, including epithelial cells (EpCAM), T cells (CD8, CD3), natural killer cells/ (CD56, also a neuronal

marker), endothelial cells (CD105, CD31), macrophages/monocytes (CD14), dendritic cells (CD25), mesenchymal stromal/stem cells (CD44, CD29, CD146) and embryonic stem cells (SEEA-4). The expression of mesenchymal stem cell markers CD44, CD29, and CD146, which have been previously documented in endometrial stromal cell populations (220-222), suggests the potential presence of endometrial stromal cell-derived sEV in the PF.

Several markers present on the surface of PF-sEV could be involved in signalling modulation, including antigen-presenting proteins (HLA-DR/HLA-ABC), adaptive immune evasion (CD24) (223, 224), and adhesion and migration markers (CD44) (165). The presence of these diverse markers suggests that PF-sEV may play multifaceted roles in intercellular communication and immune regulation within the PF microenvironment.

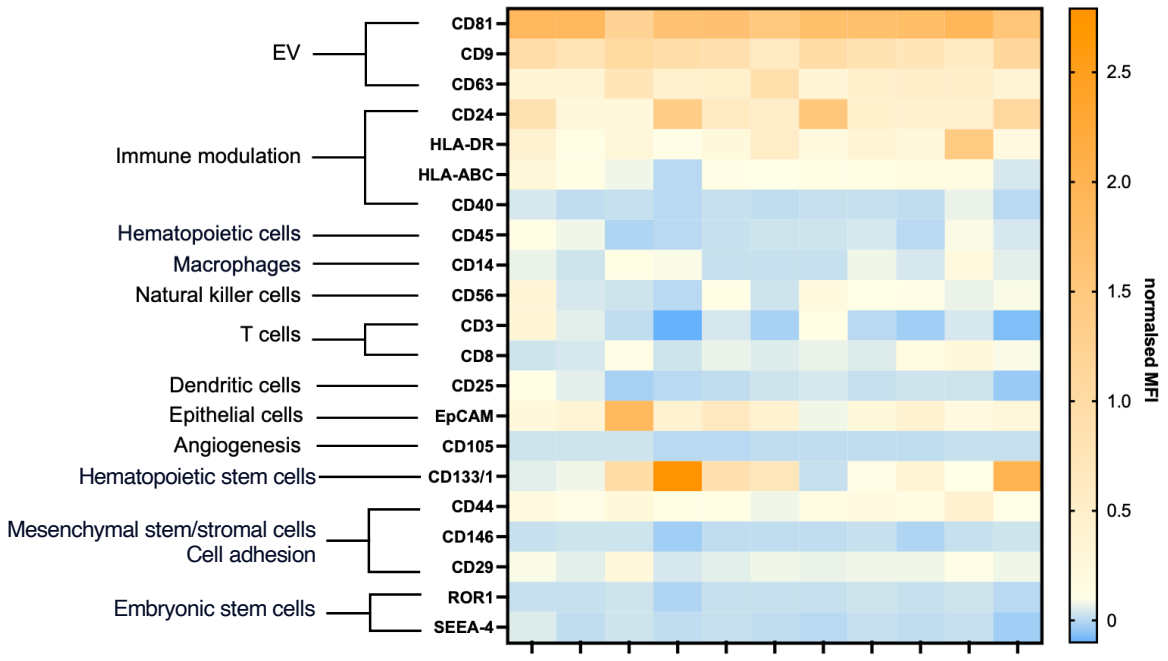

Figure 3.17. Potential cellular origins and functions of PF-sEV. This heatmap visualises the expression levels of various surface markers on PF-sEV determined by MACSPlex flow cytometry analysis. Colour intensity corresponds to the expression level (nMFI) of each marker (high expression: orange; moderate expression: yellow; low expression: blue).

Analysis of PF-sEV revealed a distinct profile compared to pMΦ-EV examined in Chapter 2 section 2.3.4. While PF-sEV presented fewer consistently expressed markers (12 vs 27), they exhibited a broader range of surface epitopes. Twenty-five markers were present in a subset

of PF-sEV samples, maintaining reasonable levels of nMFI>0.01. A few partially expressed markers have higher nMFI than markers expressed in all samples. This pattern suggests that the variability in marker expression among PF-sEV samples reflects diverse cellular origins and sample heterogeneity. In contrast, pMΦ-EV showed partial expression of markers, typically with very low nMFI<0.01. The partial expression observed in pMΦ-EV likely originates from background signal in the media.

3.3.3 The impact of hormone treatment (HT) on PF-sEV

This chapter aimed to determine the impact of HT on PF-sEV signatures. Initially, the analysis grouped all forms of HT together, comparing women on any hormones versus those with NHT in both endometriosis and control groups. Subsequently, it examined different types of HT specifically in endometriosis patients. Lastly, the HT resistant pain profile and potential correlation with PF-sEV was investigated.

3.3.3.1 HT effects on PF-sEV characteristics

A total of 34 PF samples from women using hormonal treatments (HT) were analysed in this study. These included 6 using the combined oral contraceptive pill (COCP), 10 using the progestin-only pill (POP), 12 fitted with intrauterine devices (IUD, Mirena), and 6 using GnRH agonist injections (Zoladex). These samples were matched for BMI and age with the no hormonal treatment (NHT) group. sEV were isolated from PF samples by SEC, filtration and ultracentrifugation, then characterized by NTA. To evaluate the potential effects of hormonal status and disease status on the sEV, the modal size and concentration s were compared. Interestingly, while disease status did not significantly affect PF-sEV characteristics analysed by NTA, hormonal status emerged as a significant factor influencing EV concentration. Women receiving HT showed significantly lower concentrations of PF-sEV compared to those with NHT in the endometriosis group ($P<0.05$) (Figure 3.18a). However, when examining EV mode size, no significant differences were observed (Figure 3.18b).

a)

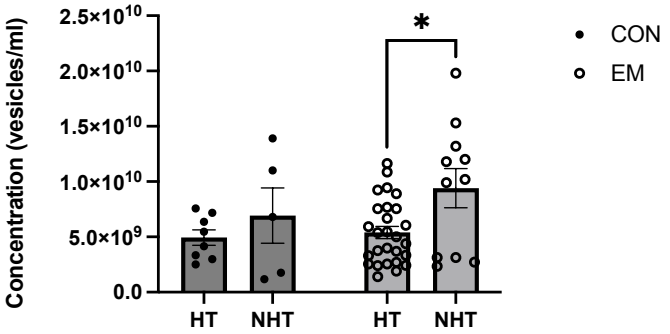

b)

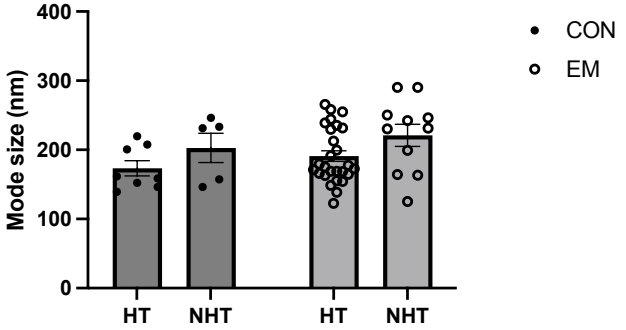

Figure 3.18. Effect of hormonal status and disease status on PF-sEV characteristics. a) sEV concentration and b) sEV mode size in endometriosis and control groups, comparing non-hormonal treatment (NHT) and hormonal treatment (HT) status. Control (NHT: n=5, HT: n=8), Endometriosis (NHT: n=11, HT: n=26). Two-way ANOVA with Turkey's multiple comparisons (Shapiro-Wilk test: $p > 0.05$), *$p<0.05$.

Surface marker analysis was conducted using the MACSPlex EV kit IO, with results compared using nMFI APC values. Principal component analysis (PCA) revealed distinct clustering between HT and NHT groups. The first two principal components collectively explained 46.12% of the total variance, with PC1 and PC2 accounting for 29.49% and 16.63%, respectively (Figure 3.19a). The primary contributors to both PC1 and PC2 are shown in Figures 3.19b and 3.19c.

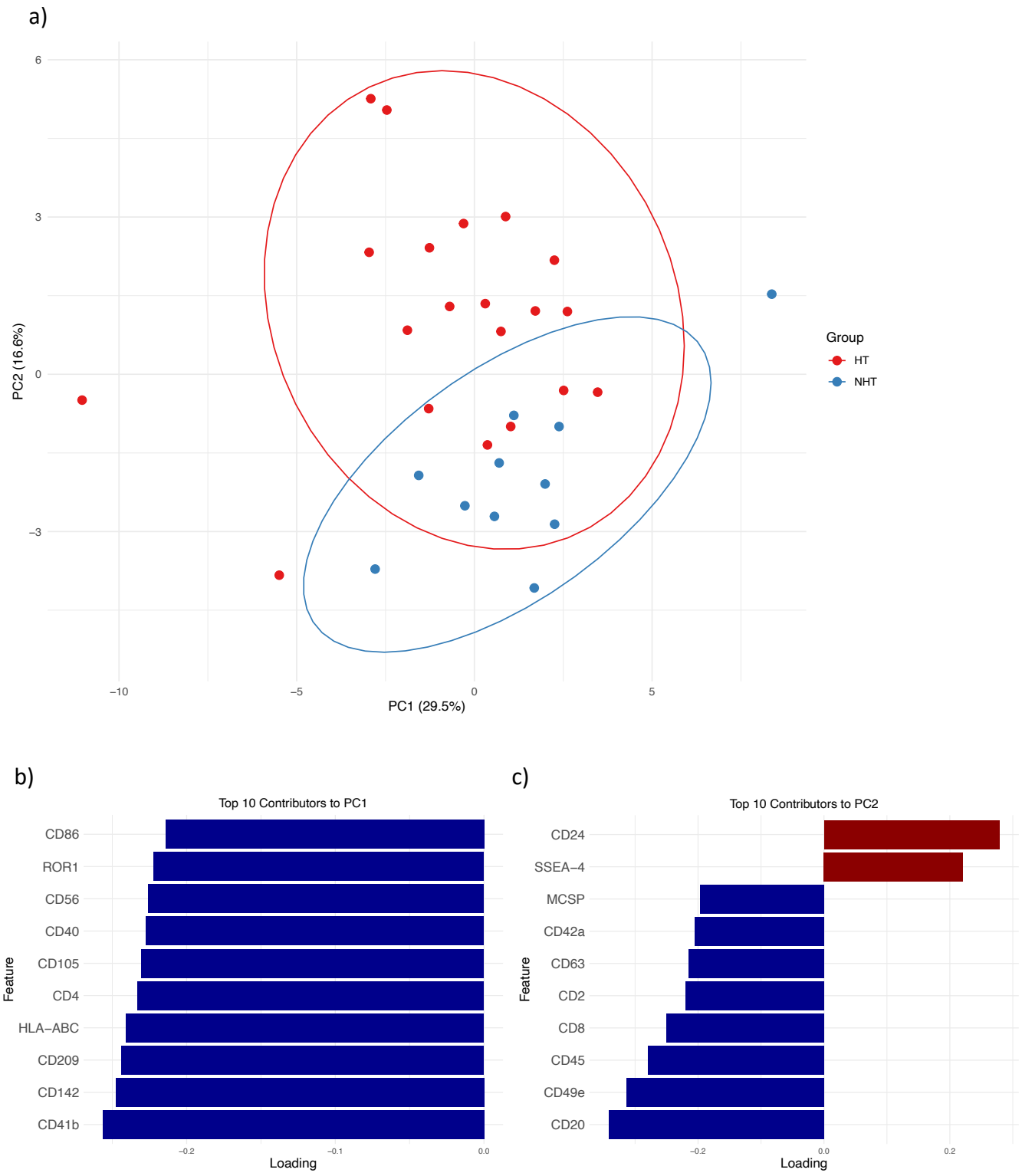

Figure 3.19. a) PCA of surface marker profiles in PF-sEVs measured by MACSplex EV kit IO. PC1 versus PC2 scores plot showing sample distribution across HT (red, n=26) and NHT (blue, n=11) groups. Ellipses represent 95% confidence intervals. b) Top 10 markers contributed to PC1. C) Top 10 markers contributed to PC2.

Individual marker comparison revealed that CD24 expression was significantly elevated in patients with HT compared to those with NHT in endometriosis ($p<0.005$) and control ($p<0.05$) groups (Figure 3.20a). CD24 expression showed a 2.51-fold increase in the HT group compared to the NHT group in endometriosis patients (HT: 1.67, NHT: 0.67), and a 2.10-fold increase in controls (HT: 1.53, NHT: 0.73). Conversely, EpCAM expression was significantly suppressed in the HT group compared to the NHT group (HT: 0.13, NHT: 0.23, $p=0.0027$) in endometriosis. Although EpCAM expression was 66% lower in the HT group compared to the NHT group in controls (HT: 0.236, NHT: 0.694), this was not statistically significant ($p=0.192$) (Figure 3.20b).

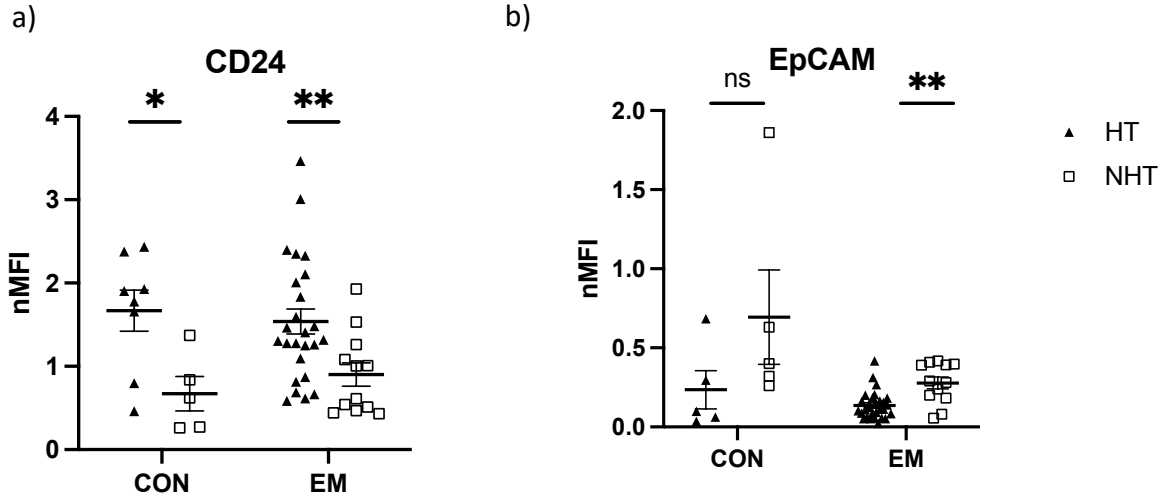

Figure 3.20. Change of surface marker expression on PF-sEV in endometriosis and control groups with and without hormonal treatment. a) CD24 expression. b) EpCAM expression. Dot plots show individual nMFI APC values. CON=control (NHT: n=5, HT: n=8); EM=endometriosis (NHT: n=11, HT: n=26). Unpaired two-tailed *t*-test (Shapiro-Wilk test: $p > 0.05$), *$p<0.05$, **$p<0.01$.

3.3.3.2 Comparison of different HT on PF-sEV characteristics

Following the overall analysis of HT effects in both endometriosis and control groups, I conducted a more detailed examination of specific HT types within the endometriosis group. The control group was excluded from this analysis due to insufficient representation across different HT categories. Specifically, the control group lacked subjects in the COCP category and had only two subjects in the GnRHa (Zoladex) group.

Within the endometriosis group (n=37), I compared the effects of COCP (n=6), POP (n=7), Mirena (n=9), and Zoladex (n=4) to NHT (n=11) on PF-sEV surface marker expression. Consistent with the overall HT analysis, CD24 expression on PF-sEV was significantly higher in all specific HT treatments compared to NHT (Figure 3.21a). Similarly, EpCAM expression was significantly lower in most specific HT groups compared to NHT (Figure 3.21b). While the Zoladex group showed lower EpCAM expression than NHT, this difference was not statistically significant ($p=0.08$). There were no significant differences in CD24 or EpCAM expression among the specific HT groups themselves.

Notably, CD133/1 expression, however, varied among HT methods: COCP (0.68±0.69) and POP (0.45±0.34) remained no different to NHT (0.61±0.52). However, the Mirena group (0.11±0.13) showed significantly suppressed CD133/1 expression compared to NHT ($p<0.05$), with an 82% reduction. In the Zoladex group, CD133/1 expression was minimal (0.0059±0.010), showing a dramatic 99% reduction compared to NHT. However, this difference was not statistically significant ($p=0.13$), likely due to the small sample size. These results are displayed in Figure 3.21c.

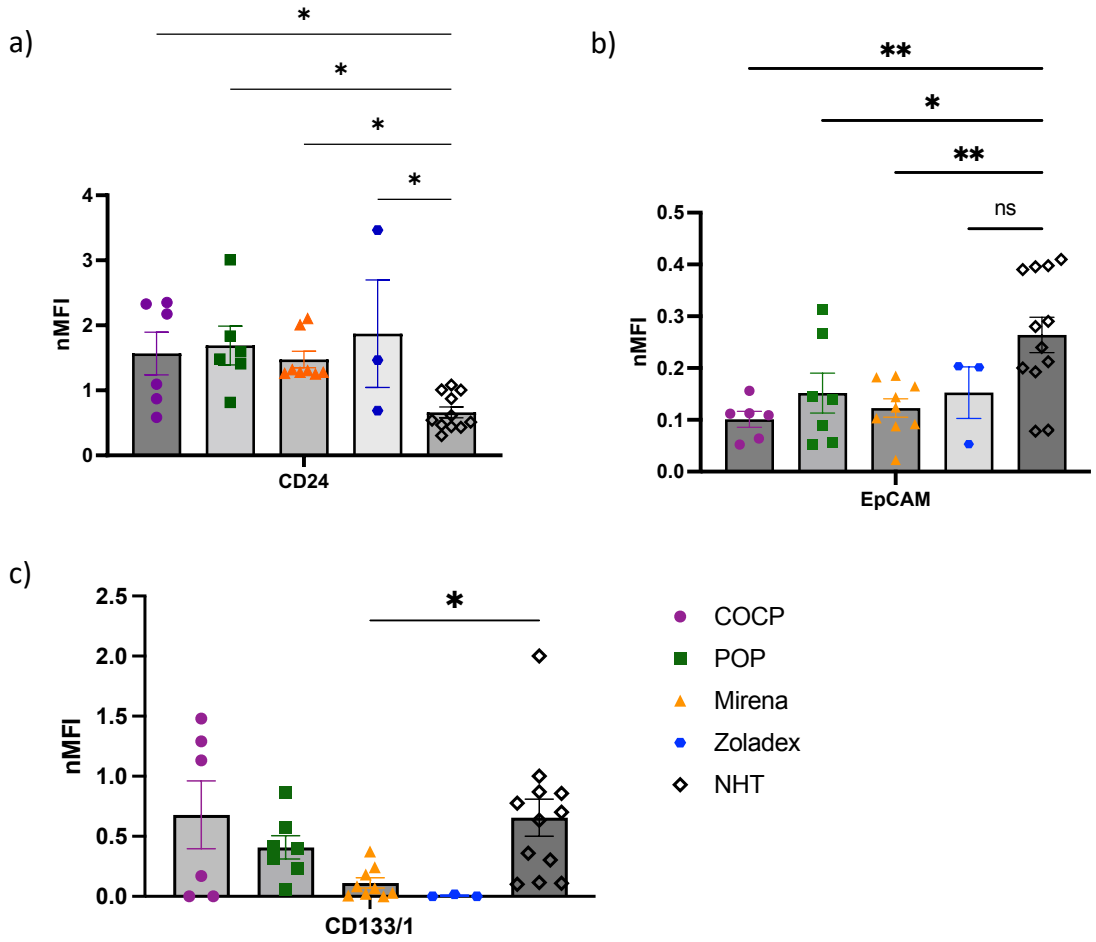

Figure 3.21. Comparison of surface marker expression on PF-sEV in endometriosis patients. a) CD24 expression on PF-sEV b) EpCAM expression on PF-sEV c) CD133/1 expression on PF-sEV. Expression of surface markers in HT groups were compared to NHT. Groups include: No hormone therapy (NHT, n=11), Combined oral contraceptive pill (COCP, n=6), Progesterone-only pill (POP, n=7), Mirena (n=9), and Zoladex (n=4). One-way ANOVA with Turkey's multiple comparison (Shapiro-Wilk test: $p > 0.05$), *$p<0.05$, **$p<0.01$.

3.3.3.3 HT-resistant pain analysis in endometriosis patients

Finally, as part of this study, the pain profile of endometriosis patients recruited by the ENDOX study was investigated. A total of 22 patients of whom had completed the pain questionnaire were selected (HT: n=16; NHT: n=6). Although BMI, age, and menstrual cycle were matched between HT and NHT groups, significant differences in level of acyclic pelvic pain experienced in the last 3 months were observed among endometriosis patients.

The HT group of endometriosis patients reported higher pelvic pain severity compared to the NHT group (Figure 3.22a). Pain severity was scaled from 0 to 10, with 0 being pain-free, 1-5 representing minimum/moderate pain, and 6-10 indicating moderate/severe pain. In the HT group of endometriosis patients (n=15), only one patient was pain-free and 11 patients (73%) reported severe pain. In contrast, in the NHT group of endometriosis patients (n=8), 5 patients (62.5%) were pain-free, while 3 patients reported some level of pain (Figure 3.22b).

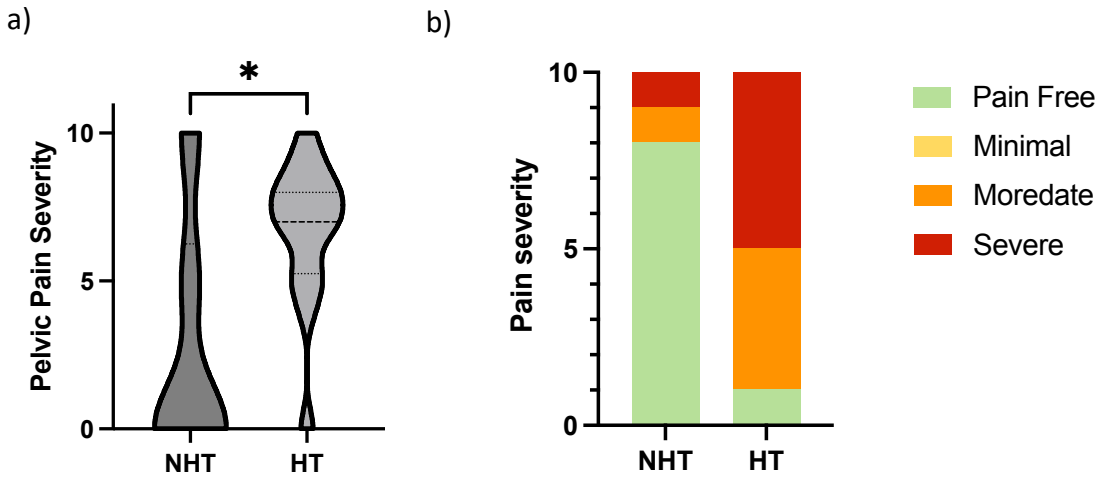

Figure 3.22. Comparison of acyclic pelvic pain severity in endometriosis patients. a) Pain severity scores in HT groups compared to NHT group. b) Distribution of pain severity categories in HT and NHT groups. Pain severity was scaled 0 to 10: 0 = pain-free, 1-3 = minimal, 4-6= moderate, 7-10 = severe. Non-hormonal treatment (NHT,n=6); Hormonal treatment (HT, n=16). Two-tailed Mann Whitney test (Shapiro-Wilk test: $p < 0.05$), *$p<0.05$.

Based on these findings, the HT group in endometriosis represented a cohort of patients with HT resistant EAP. To assess if PF-sEV signatures were indicative of HT resistant EAP, the correlation between EV concentration and MACSPlex EV marker expression with pain severity in the HT group was analysed. PF-sEV concentration was negatively correlated with pain severity in the HT group ($r=-0.056$, $p<0.05$), as illustrated in Figure 3.23. No correlation was observed between any of the EV MACSPlex markers and pain severity.

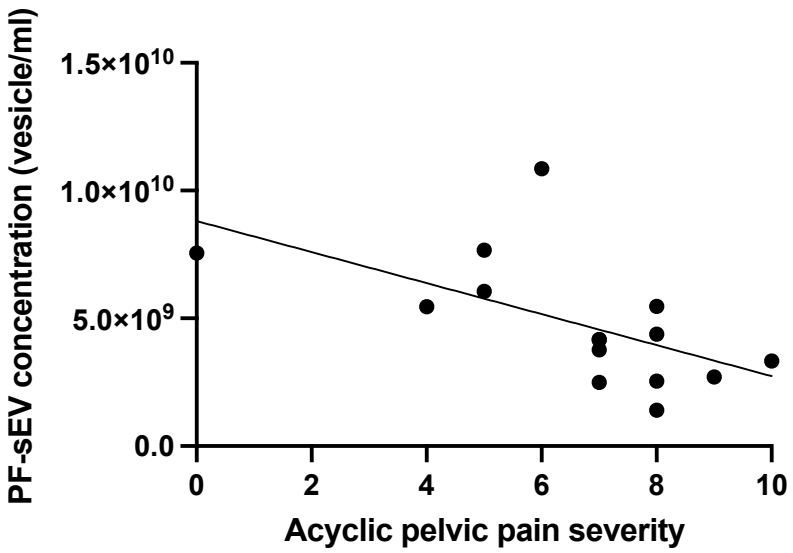

Figure 3.23. Analysis of PF-sEV concentration in relation to pain severity in endometriosis patients with HT. Scatter plot depicting PF-sEV concentration versus pain severity in endometriosis patients with HT (n=16). PF-sEV concentration was determined by NTA. Pain severity was assessed using a standardised 11-point numerical rating scale (0-10), where 0 represents no pain and 10 indicates the worst pain imaginable. Patients reported their worst acyclic pelvic pain levels over the past three months. The relationship between PF-sEV concentration and pain severity was evaluated using Pearson's correlation coefficient.

3.4 Discussion

3.4.1 SOP of PF-sEV isolation

This chapter demonstrated the effectiveness of a combined SEC, membrane filtration, and ultracentrifugation approach for isolating small extracellular vesicles from peritoneal fluid (PF-sEV). The results showed successful separation of EV and proteins from PF samples using both IZON Legacy and Gen 2 qEV original SEC columns.

Initially, using Legacy columns, EV were first detectable in fraction 6, with levels increasing and peaking in fraction 8, which showed the highest EV yield. Soluble protein levels became detectable but remained low in fraction 9, gradually increasing and reaching a peak in fraction 16. This clear separation between the EV-rich and protein-rich fractions demonstrates the effectiveness of the SEC method in isolating EV from peritoneal fluid. Fractions 6-9 were determined to be sEV-enriched, aligning with the manufacturer's recommendations. The transition to Gen 2 columns, while maintaining the same protocol, resulted in a shift of the EV peak to fraction 7, with increased EV collection in fraction 6 and reduced detectable soluble protein in fraction 9. Despite these changes, the sEV-enriched fractions remained consistent for PF samples.

A significant protocol update in 2024 changed the eluted fraction volume from 500µL to 400µL, leading to a re-evaluation of sEV-enriched fractions. This led to the exclusion of fraction 6, which now contained large EV with a mode size over 800nm. The new sEV-enriched fractions were determined to be inclusive of fractions 7-10, maintaining a size profile comparable to the previous protocols.

Throughout the study, protocols of IZON SEC columns were continuously optimised to accommodate updates in column technology and to maintain consistency in the isolation method. The experience emphasizes the importance of regular optimization when companies update their protocols and isolating EV from different biological fluids. Even small changes in the isolation process can result in significant differences in the EV population collected.

After identifying the sEV-enriched fractions, these fractions were pooled to maximize the yield of isolated vesicles. This step was particularly useful in removing larger EV from the first fraction of sEV-enriched fractions, which typically contained EV with a mode size around 300nm. Although the amount of these larger EV was minimal, the membrane filtration step contributed to a more homogeneous sEV population.

These isolated PF-sEV were then subjected to a titration experiment for the MACSPlex EV kit. In this experiment, EV counts ranging from $3.75x10^7$ to $1.5x10^9$ were tested. Results showed that low EV counts led to the missed detection of several markers with low expression like SSEA-4, CD146, and CD86. The expression profile remained stable between $1.88x10^8$ and $1.5x10^9$ EV, with no markers' expression levels exceeding the maximum detection range. This indicates that the assay maintained linearity even at higher EV inputs. Considering that $1x10^9$ EV is the typical lowest yield from 500µL of PF (the loading volume of one SEC column), $7.5x10^8$ EV were determined as the optimal PF-sEV input for the MACSPlex EV kit.

3.4.2 PF-sEV Characterisation

3.4.2.1 Size and concentration analysis by NTA and TEM

The analysis of 50 PF-sEV samples by NTA revealed significant variation in concentration, ranging from $3x10^9$ to $2x10^{10}$ vesicles/mL. This large variation is typical for PF-sEV, as demonstrated by previous studies. One study investigating PF-sEV from three patients found EV concentrations of 10^{10} to 10^{11}/mL, reaching up to 10^{12}/mL in a patient with ovarian cancer and ascites (225). Another study reported a range of $1x10^{11}$ to $9x10^{11}$ vesicles/mL among 29 samples (226).

The higher PF-sEV concentrations in these studies could be attributed to different isolation and characterisation methods. While the cited studies used ultracentrifugation alone, the current study employed SEC, filtration and ultracentrifugation, which may result in some EV

loss, but will result in a more purified preparation. Of the cited studies, study (51) used the same NTA instrument as current study, while study (225) used a different instrument (Nanosight LM10, Particle Characterization Laboratories, Inc., USA) for their measurements. Different NTA instruments in EV characterisation could lead to varying concentration measurements due to differences in their detection sensitivity and analysis parameters. As most studies, including this one, use frozen PF for analysis, samples are likely to have been frozen for different durations. Apart from patient heterogeneity, this variation in storage time may also contribute to the observed concentration differences.

Long-term storage effects on EV have been observed in plasma studies. One study investigating plasma samples stored at -80°C for up to 7 years revealed higher background under TEM compared to EV isolated from fresh plasma (227). Additionally, long-term storage of plasma could result in increased EV concentration as measured by NTA, possibly due to separation of EV aggregates or disintegration of large EV (228).

Ideally, handling fresh PF would be the best approach for analysis with no confounding variance in different storage durations. However, this is often impractical due to the time-consuming and labour-intensive nature of biological sample collection. The study investigating different storage conditions of plasma samples demonstrated that storage at -80°C was optimal for long-term preservation for EV isolation (229). Furthermore, isolating EV from frozen biological fluid samples, rather than isolating EV and freezing for future use is preferable (229). Therefore, aside from using fresh PF to isolate EV, frozen PF (-80°C) and subsequent EV isolation is an optimal method.

In the current study, no significant differences were observed between endometriosis patients and controls, or across different phases of the menstrual cycle. This finding contradicts Nazri et al. (58), who reported higher concentrations of sEV in the proliferative phase and disease stage I/II. Several factors may account for this discrepancy. Sample collection and processing is different as I analysed individual samples, whereas Nazri et al. used pooled samples. Where possible, it is always preferable to use individual samples for EV isolation to enable correlation with patient-specific clinical data. Considering the high variation of PF-sEV concentration among individuals, a potential dilution effect could occur

in pooled samples and affect results, especially when sample size is small (230). Additionally, whilst Nazri et al., stated that clear PF was used, the exclusion of lavage samples was not explicitly mentioned. I chose to exclude lavage PF as this would in turn dilute the number of EV, and make it difficult to compare between samples. Furthermore, the PF-sEV concentration reported in Nazri's study ($2x10^7$ to $1x10^9$ /mL) was considerably lower than in this study, further suggesting potential collection criteria differences.

Variations in sEV isolation and characterisation techniques between the two studies could also contribute to the observed differences. Different SEC columns were used, with Nazri's study employing the Exo-spin SEC column. Nazri's method also involved a precipitation step before column purification. This precipitation step, due to its low specificity, has been reported to co-isolate non-EV co-isolates into EV preparations (231, 232). Also, Nazri et al., used a smaller membrane filter (0.1 µm diameter) before SEC purification, whilst I performed SEC first, and then filtered the pooled sEV enriched fractions using a larger filter (0.2 µm diameter). Nazri performed two separate 16,000 x g centrifugation steps (before and after SEC with precipitation)), whilst the current methodology used in this study implemented a single 16,000 x g centrifugation prior to SEC. Moreover, to concentrate sEV after SEC, Nazri's method used a 100 kDA Amicon centrifugal filter unit, whereas in this study ultracentrifugation has been used. Finally, whilst both studies utilised the NanoSight NS500 instrument for NTA, Nazri et al., used an instrument fitted with a 488nm laser, whereas the current study uses a 405nm laser. Different instruments and settings can lead to variations in the measured size and concentration of EV (233, 234).

These factors highlight the importance of standardised protocols in EV research and the need for careful consideration of methodological differences when comparing results across studies.

Another factor contributing to the contradictory data is the reliance on self-reported cycle phase in both studies. Self-reporting can introduce variability due to recall bias and individual cycle differences, potentially leading to imprecise sample categorisation. This limitation highlights the need for more objective methods of cycle phase determination in future research with matched endometrial biopsies.

Two approaches for characterising sEV were compared: TEM and NTA. TEM images revealed minimal non-EV co-isolates in the background of PF-sEV preparation. TEM analysis consistently showed a smaller EV size compared to NTA. This discrepancy could be attributed to shrinkage of EV during the fixation process for TEM (235), potentially leading to underestimated sizes. Conversely, NTA faces limitations in detecting smaller EV, with some instruments struggling to resolve particles below 60 nm (233) or 90 nm (236), depending on specific settings.

NTA performance is intricately linked to the refractive index (RI) of its calibration material, typically silica beads (237). While these beads have a similar RI to EV, they are not identical (237). This slight difference can impact measurements, especially for smaller EV.
Despite these challenges, both methods offer distinct advantages. NTA provides rapid measurements and can detect lower concentrations of EV compared to TEM. TEM offers invaluable insights into EV morphology and sample purity. It can distinguish individual EV from aggregates and reveal the presence of non-EV co-isolates, providing a more comprehensive view of sample quality.

The complexities in accurately measuring sEV sizes highlight the need for a multi-faceted approach in EV research.

3.4.2.2 Protein composition characterisation by WB

WB was employed to characterize the protein composition of isolated PF-sEV, adhering to the MISEV guidelines (57). The use of the JESS automated Western blot system successfully demonstrated the presence of key sEV markers: syntenin, ALIX, CD9, and CD81. Notably, syntenin expression was detectable with as little as 0.4 µg of protein. This system provides a significant advantage for experiments with limited EV counts like PF-sEV. However, due to its high sensitivity, it is challenging to incorporate positive control cell lysates for negative markers like albumin, as required by MISEV guidelines (57). To address this, manual western blotting was utilized to show syntenin expression across multiple patient samples and to

demonstrate the reduction of albumin expression in sEV preparations compared to PF cell lysates. These results further confirmed that the isolated vesicles are indeed sEV.

3.4.2.3 Surface marker characterisation by the MACSPlex EV kit IO

The characterization of transmembrane sEV markers across samples was conducted using a bead-based flow cytometry assay with the MACSPlex EV kit IO. The presence of CD63, CD81, and CD9 was confirmed in all prepared PF-sEV samples. Beyond these three canonical markers, surface marker analysis revealed a diverse array of 34 markers, with EpCAM, CD133/1, HLA-DR, CD24, CD44, CD8, CD14, CD29, and CD49e consistently present. This indicates various cellular origins for PF-sEV, with endometrial epithelial cells, T cells, and antigen-presenting cells like macrophages being predominant sources. The shared high expression of HLA-DR, CD24, and CD44 in both pMΦ-sEV and PF-sEV confirms the dominant role of pMΦ-sEV in the PF. Notably, EpCAM and CD133/1 as the most abundantly expressed markers in PF-sEV also indicate significant endometrial origins.

These findings will be further investigated in Chapter 5, where the analysis of endometrial epithelial cells from eutopic and ectopic endometrium tissue and characterisation of their sEV will be presented. Other cell markers, such as CD56 (dendritic cells/neural cells), CD105 and CD31 (endothelial cells), mesenchymal stromal/stem cells (CD44, CD29, CD146) and CD41b and CD42a (platelets), were detected in subsets of PF-sEV with lower nMFI. It's important to note that these markers were also found on pMΦ-sEV.

The expression of HLA-DR, CD24, and CD44 by PF-sEV could indicate their role in the functional regulation of key cellular processes, as discussed below:

1) HLA-DR, a major histocompatibility complex class II (MHC-II) molecule, plays a crucial role in antigen presentation to CD4+ T cells (238). Its presence on PF-sEV suggests that these EV might participate in modulating adaptive immune responses within the peritoneal cavity. The interaction between HLA-DR on PF-sEV and T cell receptors (TCRs) on CD4+ T cells may influence T cell activation and differentiation.
2) CD24, a highly glycosylated cell adhesion protein, is implicated in oncogenic signalling and immune evasion (239). It is known to interact with Siglec-10,

inhibiting phagocytic activity of macrophages (240), repressing Toll-like receptors mediated inflammation (241) and impairing cytotoxicity of natural killer cells (242). The CD24/ Siglec-10 interaction via PF-sEV could be a pathway contributing to immune dysregulation in the peritoneal microenvironment of endometriosis.

3) CD44, an adhesion molecule, interacts with various ligands, including hyaluronic acid (HA), osteopontin, and matrix metalloproteinases (MMPs) (165). Notably, osteopontin levels are elevated in the endometrium of endometriosis patients (243) while MMP level (MMP-9 and MMP-2) are elevated in both PF and the endometrium of endometriosis patients (244-246). The interaction of CD44 and its ligands can influence processes such as cell migration, invasion, and signalling cascades involved in inflammation or tissue remodelling (165).

Further investigation to examine the functional roles of these markers and the expression on cells such as T cells, macrophages and endometrial cells within the peritoneal microenvironment is essential. The functional roles of PF-sEV and their ligands on macrophages will be studied in Chapter. This investigation may provide insights into how they influence key immune cells in the peritoneal cavity and potentially contribute to the pathogenesis of endometriosis.

The MACSPlex EV kit IO demonstrated superior sensitivity in surface marker detection compared to previous methods. While a prior study using ELISA detected EpCAM in only two (one healthy control and one ovarian cancer patient) out of six patients (50), my study consistently identified EpCAM across all samples. This enhanced sensitivity allows for better identification of low-abundance or variably expressed markers on EV. The discrepancy between the findings in the current study and those previous highlights the critical role of methodology in EV characterisation, suggesting that different techniques may lead to contrasting conclusions.

3.4.3 The impact of hormone treatment (HT) on PF-sEV

A key finding of this study was the significant impact of HT on PF-sEV, both concentrations and surface marker expression was altered. HT was found to suppress EV concentration and the expression of EpCAM, while upregulating the expression of CD24. These findings suggest a substantial modulation of cellular processes in the peritoneal microenvironment due to hormonal interventions.

HT typically inhibits endometrial proliferation and reduces inflammatory processes (247), this could lead to a decrease in sEV secretion, resulting in lower EV concentrations in the peritoneal fluid. EpCAM is a transmembrane glycoprotein expressed by endometrial epithelial cells. The inhibition of endometrial growth could result in fewer epithelial cells secreting EV and reduced EV secretion activity by epithelial cells. Consequently, this would lead to a lower proportion of EpCAM+ EV in the PF. These epithelial endometrial EV may originate from lesions or eutopic endometrium arriving in the PF via retrograde menstruation.

The upregulation of CD24 presents a more complex picture that warrants careful interpretation. Apart from roles in immune regulation, CD24 expression has been shown to be modulated by oestrogen. Previous studies have reported a negative correlation between CD24 and oestrogen levels in breast cancer (248) and with progesterone and oestrogen receptors in the endometrium (249).

The analysis of CD133/1 expression revealed variable effects among different HT types. CD133/1, a pentaspan transmembrane glycoprotein often used as a marker for stem and progenitor cells, has been associated with endometrial regenerative cells and potentially with endometriosis stem cells (250). Locally administered progestins (Mirena) suppressed CD133/1 expression most significantly compared to NHT implies that localized treatments may have more profound local effects on the peritoneal microenvironment. The negligible expression of CD133/1 in the Zoladex group is particularly intriguing, suggesting that GnRH agonists might have more potent effects on the stem cell population than progestins.

It is important to emphasize that sEV marker expression does not necessarily directly represent cellular expression. The relationship between sEV markers and their cellular counterparts can be positively correlated, negatively correlated, or show no correlation at all. This complexity underscores the need for careful interpretation of sEV marker data.

Moreover, there is currently limited research on how HT directly affect cellular expression of EpCAM, CD24 and CD133/1 in endometriosis. Additionally, hormone concentrations in the peritoneal microenvironment during HT remain largely undefined. Investigating these relationships is essential to fully understand whether changes in sEV marker profiles reflect underlying alterations in cell populations or EV release dynamics.

In this study, the HT group in endometriosis likely represents a hormone-resistant EAP cohort, as evidenced by higher pain severity and the small pain-free proportion compared to the NHT group.

Interestingly, EV concentration is negatively correlated with pelvic pain scores in endometriosis patients with HT. Further investigation is required to determine whether this correlation is related purely to pain severity or if it indicates a mechanism in hormone resistance. While CD24 itself is not a direct pelvic pain marker, as there was no correlation between its expression and pelvic pain levels, the increased CD24 expression in the HT group may indicate lower progesterone receptor expression and progesterone resistance in these patients, potentially explaining their resistance to HT and persistent pain.

To further elucidate the PF-sEV characteristics in response to HT and pelvic pain severity in endometriosis, a comparison of PF-sEV in pain-free HT patients to those experiencing pelvic pain during HT are required. Moreover, exploring the potential link between CD24 expression and progesterone receptor levels or function could shed light on the mechanisms of hormonal treatment resistance in endometriosis. Lastly, longitudinal studies tracking changes in PF-sEV profiles over the course of treatment could help identify potential biomarkers for treatment response or disease progression.

This study has limitations that should be addressed in future research. Grouping various COCP and POP with different active chemicals and dosages may have obscured subtle differences in their effects. The reliance on self-reported treatment information also introduces potential inaccuracies. Future studies should aim to analyse specific formulations separately and implement more rigorous verification of treatment regimens. As a pilot study, the sample size was limited. Increased sample sizes in future studies will enhance statistical power and the ability to detect more subtle effects, particularly when analysing different HT methods separately. Furthermore, the MACSPlex EV kit IO used for sEV characterization is only semi-quantitative. To gain more precise insights, it would be valuable to examine the differences in marker expression between endometriosis patients and controls using single EV flow cytometry.

In conclusion, this study provides the first detailed characterization of surface markers on PF-sEV in the context of endometriosis and HT, revealing significant treatment-induced alterations in EV profiles.

Chapter 4 The effect of PF-sEV on macrophage differentiation and functions

4.1 Introduction

The previous chapter demonstrated that PF-sEV express various immune-modulating markers such as HLA-DR and CD24, suggesting a potential role in regulating immune cell functions. Given the reported altered phenotypes of pMΦ (112), this chapter hypothesizes that PF-sEV from endometriosis patients modify pMΦ behaviour by reducing phagocytosis and altering cytokine profiles. These changes could contribute to the persistence and progression of endometriotic lesions by creating an environment more permissive for their growth.

4.1.1 An introduction to macrophage in vitro models

To test this hypothesis, a reliable and reproducible *in vitro* model is essential. While primary pMΦ provide invaluable insight into physiological conditions, they are not optimal for functional studies as they cannot be passaged, which restricts the scale and duration of experiments. Moreover, there is significant variability between patients in the quality and quantity of pMΦ obtained, as their isolation is highly dependent on PF collection conditions. The risk of blood contamination during surgery is particularly high in advanced endometriosis stages, where endometriomas and adhesions are present. This makes it harder to separate true pMΦ from blood monocytes that have entered the samples. These factors make pMΦ only a suboptimal cell population for standardised, large-scale studies to reliably examine the effects of PF-sEV on macrophage function.

To overcome these limitations, an *in vitro* cell model is often used by researchers which provides a more uniform and stable cellular background. Two well-established monocytic cell lines, THP-1 and U937, were selected and compared as *in vitro* models for pMΦ in this study. THP-1 cells are human monocytic cells derived from an acute monocytic leukaemia

patient (251), and U937 cells originate from a histiocytic lymphoma (252). Both cell lines have been used as *in vitro* models for macrophage studies in endometriosis (115, 253-255). Phorbol 12-myristate 13-acetate (PMA) is required to induce differentiation of U937 and THP-1 cells into macrophage-like cells by activating protein kinase C via diacylglycerol-responsive signalling. However, a significant challenge is the wide variation in PMA concentrations used that are reported in the literature, ranging from 2.5 ng/mL to 100 ng/mL (256, 257). This variation in PMA concentration has been shown to significantly affect the subsequent polarisation and functional characteristics of the differentiated cells (257, 258). High levels of PMA have been linked to overactivation of inflammatory and pro-inflammatory signalling pathways (257), while reduced PMA concentrations increase responsiveness to anti-inflammatory stimuli (253).

Importantly, the study in chapter 2 has revealed that pMΦ from endometriosis patients exhibit characteristics of M2-like macrophages, including high expression of CD163, CD206, HLA-DR, and high responsiveness to anti-inflammatory stimuli. Therefore, to accurately model these pMΦ *in vitro*, this study aims to systematically evaluate the effects of different PMA concentrations on U937 and THP-1 derived macrophages. The objective is to select an appropriate cell line and determine the minimal PMA concentration that allows for differentiation while maintaining sensitivity to subsequent signals. The cellular response to varied PMA concentrations will be assessed by examining morphology, adherence, and surface marker expression. Additionally, the study will evaluate optimal polarisation protocols for pro-inflammatory and anti-inflammatory macrophages to mimic pMΦ, using marker expression and cytokine secretion as key indicators.

This optimization will enhance the reliability and relevance of subsequent investigations into how PF-sEV might influence key aspects of macrophage biology, including phagocytic activity, cytokine production, polarisation state, and expression of functional surface markers.

4.1.2 Experimental Approach to Investigate Macrophage Phagocytosis

Phagocytosis is a fundamental function of macrophages, playing a crucial role in tissue homeostasis, pathogen clearance, and the resolution of inflammation (259). It is a complex process by which cells engulf and internalize large particles (>0.5 μm), including microorganisms, apoptotic cells, and cellular debris (260). This process involves recognition of the target, engulfment of the particle, and formation of a phagosome that matures and ultimately fuses with lysosomes for degradation of the internalized material (261). Impaired phagocytic activity of macrophages has been found in endometriosis patients and could potentially contribute to lesion growth (26, 262).

Traditionally, researchers used fluorescent labelled beads to examine phagocytic ability of macrophages (263-266). However, this presents several important pitfalls that researchers should carefully consider. One of the primary concerns is non-specific binding, where fluorescent beads can adhere to cell surfaces without being internalized, potentially leading to false-positive results. Another significant limitation is the lack of biological relevance. Synthetic beads do not accurately mimic physiological targets of phagocytosis, such as bacteria or apoptotic cells. This discrepancy may affect the engagement of specific receptors and downstream signalling pathways, potentially yielding results that do not fully reflect *in vivo* phagocytic processes. Additionally, the traditional bead assay typically provides endpoint measurements, making it challenging to assess the dynamics of phagocytosis over time without performing multiple experiments.

To address these issues and better investigate the effect of PF-sEV on phagocytosis, this study will employ pHrodo *E. coli* bioparticles, with principles illustrated in figure 4.1. These bioparticles offer several advantages over traditional methods. They fluoresce brightly in acidic phagosomes but minimally at neutral pH, providing a clear distinction between phagocytosed and surface-attached particles and particles internalized by other routes. Being E. coli-derived, they mimic natural targets more closely than synthetic beads. The pH-dependent fluorescence significantly reduces false positives and allows for real-time, kinetic measurements of phagocytosis by confocal microscopy (267), flow cytometry (267, 268) and

novel imaging system like IncuCyte ZOOM® real time imaging platform (Sartorius, Germany) (269).

In the experimental setup, THP-1 M0 and M2 (IL-4+IL-13 stimulated) macrophages will be used as models. This approach is chosen because pMΦ consist of monocyte-derived macrophages and tissue resident macrophages (112). Tissue-resident macrophages have been found to exhibit an M2-like phenotype (270). The M0 model represents newly infiltrated monocyte derived macrophages that have not yet polarised into pro-inflammatory or anti-inflammatory subtypes. Cells will be treated with PF-sEV from surgically confirmed endometriosis patients or symptomatic non-endometriosis controls, followed by incubation with pHrodo *E. coli* bioparticles. These particles are assessed quantitatively by flow cytometry and qualitatively by confocal microscopy imaging, providing complementary data on phagocytic activity.

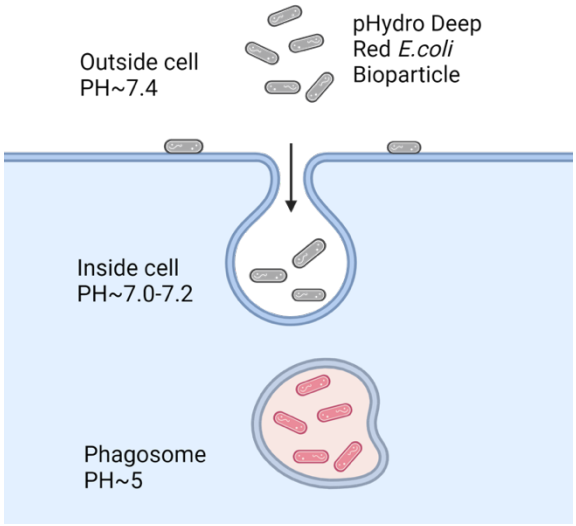

Figure 4.1 Mechanism of pHrodo *E. coli* bioparticles for assessing phagocytic activity. These bioparticles are non-fluorescent at neutral pH when outside the cell or attached to the cell surface. If internalized into the cell but not enclosed within a phagosome, the bioparticles remain in a neutral pH environment and do not fluoresce brightly. Upon phagocytosis, the bioparticles are internalized into early phagosomes with a pH of approximately 6.2, where they begin to fluoresce. As the phagosome matures and becomes more acidic, the fluorescence intensity of the pHrodo dye increases, reaching its maximum in the highly acidic environment of mature phagolysosomes. The fluorescence intensity correlates with the degree of phagocytosis, allowing for quantitative assessment by flow cytometry.

4.1.3 Potential phagocytosis evasion mechanism: "Don't Eat Me" Signals

Recent advances in cancer research have provided valuable insights into the mechanisms by which abnormal cells can evade phagocytosis, and these findings may have important implications for understanding endometriosis. Tumour cells have been shown to express "don't eat me" signals, which interact with inhibitory receptors on macrophages to suppress phagocytosis including CD24/Siglec10, CD47/SIRP-α, and PD-L1/PD-1 (181) (Figure 4.2).
The Interaction between these "don't eat me" signals and their corresponding inhibitory receptors on macrophages triggers a common inhibitory mechanism. Binding to these inhibitory receptors leads to phosphorylation of cytoplasmic immunoreceptor tyrosine-based inhibition motifs (ITIMs) (181). This phosphorylation results in the recruitment and activation of src homology-2 (SH2)-domain containing protein tyrosine phosphatases (SHP-1 and SHP-2) (271, 272). These activated phosphatases then inhibit dephosphorylation and accumulation of myosin-II at the phagocytic synapse (271, 273) leading to inhibition of phagocytosis.

The CD47/SIRP-α pathway is perhaps the most well-studied. CD47, a widely expressed cell surface glycoprotein (274), interacts with SIRP-α which is expressed in all myeloid cell types including macrophages (275). In many cancers, CD47 is overexpressed, facilitating immune evasion (276, 277). The therapeutic potential of targeting this pathway has been demonstrated in cancer studies, where CD47-blocking antibodies enhance macrophage-mediated phagocytosis of tumour cells (278). Interestingly, expression of CD47 in cancer cell derived EV has been involved in immune evasion from macrophages (279-282).

Drawing parallels to endometriosis, recent studies have reported elevated CD47 expression in the ectopic endometrium of patients with the condition (283, 284). Blocking of CD47 has been found to promote clearance of endometrial stromal cells by macrophages (283). Furthermore, pMΦ isolated from women with endometriosis exhibit increased expression of SIRP-α than patients without endometriosis (285).

While the PD-L1/PD-1 pathway is primarily known for its role in T cell inhibition, it also affects macrophage function (286). PD-L1, often upregulated on tumour cells, binds to PD-1 on macrophages, leading to suppression of phagocytic activity. The interaction has been found to be mediated by sEV in glioblastoma (287). In addition, PD-L1 and PD-1 is upregulated in ectopic and eutopic endometrium from patients with endometriosis (288).

The CD24/Siglec-10 pathway represents another important mechanism of phagocytosis inhibition. CD24, a small, heavily glycosylated cell surface protein often overexpressed in cancers, interacts with Siglec-10 on macrophages (223). pMΦ from ovarian cancer patients express significantly more Siglec-10 compared to those of non-cancerous individuals (223). Currently, the expression of Siglec-10 on pMΦ of endometriosis patients is unknown, and warrants investigation. Furthermore, given the analysis in chapter 3 showed the presence of CD24 in PF-sEV in endometriosis patients, they may interact with Siglec-10 on pMΦ.

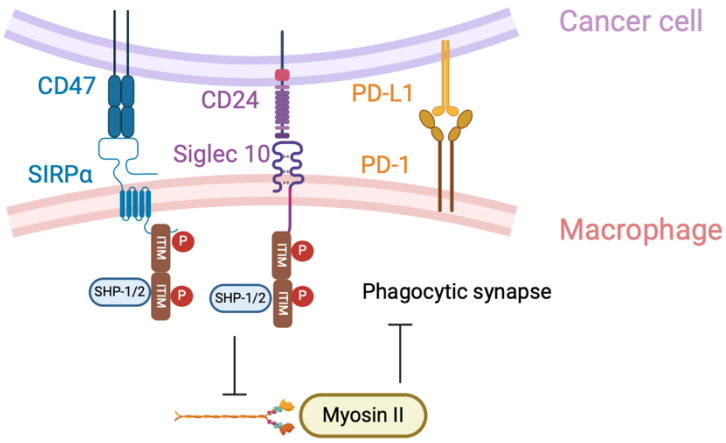

Figure 4.2. Molecular mechanisms of "don't eat me" signals in cancer-macrophage interactions. The hree key inhibitory signalling axes CD47/SIRPα, CD24/Siglec-10, and PD-L1/PD-1 between cancer cells and tumour-associated macrophages (TAMs). Ligand binding induces phosphorylation of immunoreceptor tyrosine-based inhibitory motifs (ITIMs) on TAM receptors. This leads to recruitment and activation of SHP-1/2 phosphatases, potentially inhibiting phagocytosis by preventing Myosin II dephosphorylation.

Based on these findings, I hypothesize that PF-sEV regulate macrophage phagocytic activity via the CD47/SIRP-α axis, as well as through other pathways such as PD-L1/PD-1 and CD24/Siglec-10. To test this hypothesis, this chapter will examine the effect of PF-sEV from endometriosis patients versus controls on macrophage phagocytosis using pHrodo

bioparticles. It will also investigate the expression of CD47 and PD-L1 on PF-sEV, and SIRP-α, PD-1, and Siglec-10 expression on macrophages. Finally, blocking experiments using pHrodo bioparticles will be conducted in the *in vitro* model to elucidate the role of these pathways in modulating macrophage phagocytosis in endometriosis.

3.2.1 Macrophage cytokine secretion in endometriosis

As discussed previously, aberrant cytokine profiles have been reported in the peritoneal microenvironment of endometriosis and implicated in the pathogenesis and progression of the disease (184, 289).

Macrophages are known to exhibit remarkable plasticity in their cytokine secretion profiles, depending on their activation state and environmental cues (114). In endometriosis, activated macrophages secrete a diverse array of molecules into the peritoneal microenvironment (290). These include IL-1, fibronectin, IGFI, IL-6, IL-8, IL-12, TGF, VEGF and TNF (1, 290).Despite the established importance of macrophage-derived cytokines in endometriosis, the precise mechanisms regulating their production remain to be fully elucidated.

This study hypothesizes that PF-sEV from endometriosis patients modulate macrophage cytokine production differently compared to PF-sEV from healthy controls, potentially contributing to a lesion-favouring microenvironment. Furthermore, macrophages polarized into M1 or M2 subtypes may respond differently to these PF-sEV, reflecting the complex interplay between sEV and macrophage phenotypes in endometriosis. To test this hypothesis, this study aims to assess the cytokine secretion profiles of THP-1 differentiated macrophages in response to PF-sEV from endometriosis patients and healthy controls and determine if THP-1 derived M0 macrophages polarised into M1 or M2 macrophages respond differently to PF-sEV. The research will utilize a combination of techniques, including cytometric bead array (CBA) and ELISA, to measure a wide range of cytokines. These cytokines include TGF-β1, IL-1β, IL-8, IL-10, IL-6, MCP-1, and VEGF, all of which are known to be altered in endometriosis and potentially contribute to disease progression.

4.2 Methods

4.2.1 Cell Culture of U937 and THP-1 derived macrophages

U937 and THP-1 derived macrophages (purchased directly for this study from ATCC) were cultured in complete growth media consisting of RPMI-1640 (Thermo Fisher Scientific, USA; Sigma Aldrich, USA) supplemented with 10% (v/v) FCS, P/S, and 0.05mM 2-mercaptoethanol (THP-1 only). Cells were cultured at 37°C with 5% O_2 and maintained between $5x10^5$ and $1.5x10^6$ cells/mL for up to 30 passages.

4.2.2 Macrophage differentiation and polarisation of U937 and THP-1 derived macrophages

$5x10^5$ or $1x10^6$ cells/well U937 and THP-1 derived macrophages were seeded in a single well of a 12 well plate (Nunc) and treated with treated with 2.5, 5, 10, 20, 50, or 100 ng/mL PMA (Sigma Aldrich, USA) for 24-48h to induce differentiation. PMA was dissolved in dimethyl sulfoxide (DMSO), control groups (0ng/mL PMA) were treated with 100ng/mL DMSO. After differentiation, cells were washed three times with PBS and rested in complete growth media without PMA for 24h. For M1 polarisation, cells were treated with 100 ng/mL lipopolysaccharide (LPS, Sigma Aldrich, USA) and 20ng/mL interferon gamma (IFN-γ, PeproTech, USA) in 500µL growth media for 24h. M2 polarisation was induced by treating with 20ng/mL Interleukin 4 (IL-4, PeproTech, USA) with or without 20ng/mL Interleukin 13 (IL-13, PeproTech, USA) for 24-48h. Cultured macrophages were detached from plates by incubation with Accutase® (Innovative Cell Technologies, USA) for 30 mins at 37 degree. Cells were analysed by flow cytometry.

4.2.3 Cell adherence assay

After 48h of PMA treatment, supernatants were collected, and cells were washed gently 3 times with PBS. Each PBS wash was then combined with the supernatants to determine the

number of non-adherent cells. The non-adherent cells were centrifuged at 400 x g for 3 mins and resuspended in 200µl of PBS. Cell numbers were counted, and the adherence rate calculated: (Total cell number – non-adherence cell number)/ Total cell number.

4.2.4 Cell morphology and size

Cell morphology was examined 24h and 48h after PMA treatment using contrast phase microscopy (CKX53; OLYMPUS, Japan). Three representative images were captured, and 10 cells were randomly selected in each image (30 cells) and sizes were analysed by ImageJ software.

4.2.5 PF sample collection

A total of 48 PF samples (age: 35.2 ± 6.1 years, BMI: 25.2 ± 4.2 kg/m^2; mean ± SD) from the FENOX and ENDOX studies were used in this study. All samples were pure (no lavage) with minimal blood contamination. Thrirty-three frozen PF samples (patient numbers 1-43) were used for PF-sEV isolation. Samples 1-24 were used for the phagocytosis assay. Samples 1 and 25-33 were used for CD47 co-expression experiments. All frozen PF samples were processed and stored as described in Chapter 3, Section 2.1. 3. Fresh PF samples (patient numbers 7, 34, 35) were used for pMΦ culture to assess phagocytic functions. An additional 3 fresh PF samples (patient numbers 36-38) were used for culturing pMΦ to characterise "don't eat me" signal receptors. Detailed patient information for each sample is provided in Table 4.1.

Table 4.1. Clinical characteristics of PF samples. Clinical data for 38 PF samples collected from patients are presented. The table includes patient number (1-38), Endometriosis stage (0-4, according to rASRM classification), age (years), BMI, exogenous hormone use (N: no, Y: yes), menstrual cycle phase (proliferative/secretory), and sample preservation condition (fresh or frozen). N/A indicates unavailable information.

Patient number	Endometriosis stage (0-4)	Hormone use	Menstrual phase	Age	BMI	Sample preservation

1	0	N	Secretory	32	23	Frozen
2	0	N	Secretory	37	29	Frozen
3	0	N	Secretory	35	24	Frozen
4	0	N	Secretory	38	21	Frozen
5	0	N	Secretory	23	19	Frozen
6	0	N	Secretory	20	29	Frozen
7	0	N	Secretory	43	31	Frozen/Fresh
8	1	N	Secretory	38	31	Frozen
9	1	N	Secretory	25	24	Frozen
10	1	N	Secretory	36	22	Frozen
11	1	N	Secretory	32	23	Frozen
12	1	N	Secretory	25	34	Frozen
13	2	N	Secretory	40	24	Frozen
14	2	N	Secretory	34	24	Frozen
15	2	N	Secretory	45	26	Frozen
16	2	N	Secretory	36	21	Frozen
17	2	N	Secretory	30	22	Frozen
18	2	N	Secretory	38	33	Frozen
19	3	N	Secretory	32	25	Frozen
20	3	N	Secretory	29	24	Frozen
21	4	N	Secretory	29	20	Frozen
22	4	N	Secretory	43	22	Frozen
23	4	N	Secretory	42	31	Frozen

24	4	N	Secretory	34	29	Frozen
25	1	N	N/A	26	22	Frozen
26	2	N	N/A	32	33	Frozen
27	3	N	N/A	31	19	Frozen
28	4	N	N/A	36	20	Frozen
29	1	N	Proliferative	34	23	Frozen
30	0	N	N/A	29	25	Frozen
31	0	N	Secretory	22	30	Frozen
32	0	N	N/A	38	23	Frozen
33	0	N	Secretory	32	23	Frozen
34	0	N	N/A	33	27	Frozen
35	1	Y	Proliferative	34	23	Frozen
36	0	N	N/A	22	30	Frozen
37	0	N	Secretory	33	27	Frozen
38	4	N	Proliferative	36	20	Frozen
39	0	N	Proliferative	38	23	Frozen
40	3	N	Proliferative	31	19	Frozen
41	2	N	N/A	32	33	Frozen
42	1	N	Secretory	26	22	Frozen
43	0	N	N/A	29	25	Frozen
44	1	N	Secretory	29	29	Fresh
45	0	N	Secretory	33	24	Fresh
46	2	N	N//A	23	26	Fresh

47	1	Y	Secretory	24	N/A	Fresh
48	1	Y	N/A	41	N/A	Fresh

4.2.6 PF-sEV isolation

PF-sEV were isolated as described in Chapter 3, Section 3.2.2. In brief, frozen PF samples were thawed at 37°C and centrifuged at 16,000g for 30 minutes. EV from the supernatants were isolated though SEC columns (qEVoriginal 35nm Gen, IZON, New Zealand). The sEV-enriched fractions were collected, pooled, and filtered through a 0.2 µm PVDF membrane. Subsequently, the filtrate was concentrated by ultracentrifugation.

4.2.7 pMΦ isolation and culture

pMΦ were isolated from pure PF (2 mL-5 mL) obtained from 4 endometriosis patients and 2 control patients in the FENOX study. The isolation and culture procedures were carried out as previously described in Chapter 2 Section 2.2.2. The macrophages were cultured *in vitro* for 4 days. From these samples, 3 endometriosis pMΦ samples were analysed for 'Don't eat me' signal receptors. An Additional 1 endometriosis pMΦ sample and 2 control pMΦ samples were assessed using the phagocytosis assay. Both analyses were performed using flow cytometry.

4.2.8 Phagocytosis assay using pHrodo Deep Red E.coli bioparticles

Phagocytic activity was assessed using pHrodo Deep Red *E. coli* Bioparticles for Phagocytosis (Thermo Fisher Scientific, USA). Bioparticles were reconstituted in PBS (1 mg/mL), sonicated for 10 minutes before use, and stored at 4°C for up to 7 days.

4.2.8.1 Titration of bioparticle concentration and macrophage subtype comparison

A titration experiment (0-50 µg/mL bioparticles) was performed by an MSc student, Aya Akhatova, under my supervision. M0 THP-1-derived macrophages ($2x10^5$ cells/well in 48-well plates), differentiated as described in Section 4.2.2, were incubated with bioparticles for 1 hour. Phagocytic activity was also compared across M0, M1, and M2 THP-1 macrophages (polarised as detailed in Section 4.2.2) using 20 µg/mL bioparticles for 1 hour. Three independent experiments were conducted for optimisation.

4.2.8.2 Effect of PF on macrophage phagocytosis

THP-1-derived M0 and M2 macrophages were treated with 5% (v/v) PF from endometriosis patients (stage I/II: n=11, stage III/IV: n=6) or healthy controls (n=6) for 24 hours, followed by incubation with 20 µg/mL bioparticles for 1 hour. Additionally, pMΦ were isolated from PF as described in Chapter 2 Section 2.2.2 from one control and one endometriosis patient. These pMΦ were treated with 5% (v/v) PF from endometriosis patients and controls (n=3) for 24 hours.

4.2.8.3 Effect of PF-sEV on macrophage phagocytosis

THP-1 derived M0 and M2 macrophages were treated with PF-sEV from controls (n=6) and endometriosis patients (stage I/II: n=6; stage III/IV: n=7) at $1x10^{10}$ EV/mL in RPMI media containing PS and 10% EV-depleted FBS (prepared as described in Chapter 2, Section 2.2.3) for 24 hours. pMΦ from one control patient were treated with $1x10^{10}$ EV/mL PF-sEV from control and endometriosis patients (n=3) for 24h. PF-sEV were isolated as detailed in Chapter 3, Section 3.2.2 and quantified by NTA.

4.2.8.4 Effect of EV-depleted PF on macrophage phagocytosis

PF was added to a final concentration of 5% (v/v) in RPMI EV-free media (1% P/S, 10% EV-depleted FBS). The 5% PF media was transferred to Ultra Clear ultracentrifuge tubes (5 mL; Beckman coulter, USA) and EV were depleted via ultracentrifugation (150,000 × g, 4 h) in an

Optima XE-90 ultracentrifuge (Beckman Coulter, USA) equipped with SW55-Ti swinging bucket rotor (Beckman Coulter, USA). THP-1 derived M0 and M2 macrophages were treated with 5% (v/v) EV-depleted PF from endometriosis patients (stage I/II, stage III/IV, n=6 each) or healthy controls (n=5) for 24 h.

For each experiment, macrophages (THP-1 derived M0 and M2 macrophages) with no additional treatment were incubated with bioparticles under the same conditions and used as reference controls. Macrophages without bioparticle exposure or additional treatment served as negative controls. The phagocytic activities were examined by confocal microscopy and flow cytometry.

4.2.9 Visualization of phagocytosis using confocal microscopy

Pooled sEV-enriched fractions (PF sample of one endometriosis patient) in fPBS obtained after SEC column isolation (IZON, New Zealand) were stained using a PKH26 Red Fluorescent Cell Linker Kit (Sigma Aldrich, USA). Briefly, 2µl of PKH26 dye was incubated with the sEV-enriched fractions in 1mL of Diluent C for 5 mins at room temperature. The reaction was stopped by adding 1mL of 1% (v/v) bovine serum albumin (BSA, Sigma Aldrich, USA) in PBS for 1 min. PKH26-labeled sEV were made up to 13mL with fPBS in an Ultra-clear centrifuge tube (13.2 ml, Beckman Coulter, USA) and pelleted by ultracentrifugation at 150,000 x g (max) for 2 h using a SW 44 Ti swinging bucket rotor in an Optima XE-90 ultracentrifuge (Beckman Coulter, USA).

To control for potential non-specific fluorescence from free dye or dye aggregates, a parallel preparation was made using fPBS without PF-sEV, subjected to the same PKH26 staining procedure and ultracentrifugation. The resulting solution served as a negative control.

The pellets from both the PF-sEV preparation and the negative control were resuspended in 20 µl fPBS and incubated with THP-1 derived macrophages in 8-well chamber slides (ibidi, Thermo Fisher Scientific, USA) overnight, then washed with PBS.

Macrophages were then treated with 20µg/mL pHrodo E.coli Deep Red bioparticles for 1 h and washed 3 times with PBS. Macrophages were incubated with Wheat Germ Agglutinin (WGA)-Alexa flour 488 (1:1000 dilution, Thermo Fisher Scientific, USA) for 10 mins at 37°C, followed by 3 PBS washes. Cells were fixed with formaldehyde 4% aqueous solution (VWR, USA) for 10 min at 37°C, washed 3 times with PBS, then permeabilized with 0.5% (v/v) TWEEN for 15 min at 4°C. After 3 final PBS washes, mounting medium containing DAPI (Abcam, UK) was added. Macrophage phagocytosis was visualized using a LSM 900 Airyscan 2 confocal microscope (Zeiss, Germany), with assistance from Dr. James Bancroft at the Wellcome Centre for Human Genetics.

4.2.10 Flow cytometry

4.2.10.1 Analysis of THP-1 and U937 derived macrophages

Cells were washed with PBS at 300 x g for 5 mins and stained with FIXABLE Blue LIVE&DEAD viability dye (Thermo Fisher Scientific, USA) at 1:1000 dilution for 15mins at room temperature in the dark. Cells were centrifugated (300 x g, 5 mins) and further incubated with antibodies (table 4.2) in 2% (v/v) FCS PBS at 4°C for 30mins in the dark and washed three times with PBS at 300 x g, 5 mins. Stained cells were analysed using an LSRII flow cytometer (BD Biosciences, USA).

Table 4.2. List of antibodies assessing THP-1 polarisation and differentiation

	ISOTYPE	CLONE	FLUOROPHORE	COMPANY
CD14	Mouse IgG1, κ	63D3	APC/Cy7	Biolegend
HLA-DR	Mouse IgG2a, κ	L243	Alexa flour 700	Biolegend
CD80	Mouse IgG1, κ	2D10	Brilliant Violet 785™	Biolegend
CD206	Mouse IgG1, κ	15-2	APC	Biolegend
CD163	Mouse IgG1, κ	GHI/61	Brilliant Violet 711™	Biolegend
LIVE/DEAD			Brilliant Violet 421™	Thermo Fisher Scientific

4.2.10.2 Measurement of cytokine levels of THP-1 derived macrophages after PF-sEV incubation using a Cytometric Bead Array

$5x10^5$ THP-1 derived macrophages were seeded per well in 24 well plates and differentiated to macrophages by 5ng/mL PMA for 48h and rested in rested in complete RPMI medium (supplemented with 10% FBS, 1% P/S) without PMA for 24h. $1x10^{10}$ PF-sEV were added for 24h. The supernatant was collected and centrifugated at 500 x g for 3 mins. Cytokine levels in fresh cell culture supernatants were quantified using the Cytometric Bead Array (CBA) Human Inflammatory Cytokines Kit with additional VEGF and MCP-1 beads (BD Biosciences, USA), following the manufacturer's protocol. In brief, 50 µL of cell supernatant from each sample was added to mixed capture beads and PE detection diluents and incubated for 3 h at room temperature. After washing with wash buffer by centrifugation (200 x g, 5 mins), samples were resuspended in 300 µL wash buffer and analysed using an LSRII flow cytometer (BD Biosciences, USA). The acquired data was then processed using the CBA analysis software (BD Biosciences, USA). The concentration of each cytokine was determined by comparing the PE fluorescence intensity of the sample to the standard curve generated for each analyte. The remaining cell supernatants were kept at -20°C for later ELISA.

4.2.10.3 Measurement of phagocytic activity of macrophages

Following bioparticle incubation, macrophages were detached using Accutase (Sigma-Aldrich, USA) for 10-30 minutes at 37°C. Cells were then immediately placed on ice to halt phagocytosis, washed with 2% (v/v) FCS in PBS (300 × g, 5 min, 4°C), and resuspended in ice-cold PBS for flow cytometric analysis performed using an LSRII flow cytometer (BD Biosciences, USA). The phagocytic activity was determined by examining the mean fluorescence intensity (MFI) of the APC channel in the positive population, with a minimum of 10,000 events recorded per sample.

Experimental controls included untreated THP-1 derived macrophages (negative control for gating) and cells pre-treated with 10 µM cytochalasin D (Sigma-Aldrich, USA) for 10 minutes

prior to bioparticle addition (phagocytosis inhibition control). Macrophages treated solely with bioparticles served as reference controls for each experiment.

For THP-1 macrophages, the APC mean fluorescence intensity (MFI) from triplicate wells of bioparticle-only treated cells was established as the reference value. Experimental data (PF, PF-sEV, and EV-depleted PF treatments) were expressed as fold change relative to this reference. For pMΦ, raw MFI values were utilised.

4.2.10.4 Measurement of co-expression of CD47/PD-L1 with other markers on PF-sEV using the MACSPlex EV kit IO

The co-expression of CD47 and PD-L1 with other markers on PF-sEV was detected using a modified MACSPlex EV kit IO protocol (291).

An Initial titration experiment using PF-sEV isolated from pooled PF of three endometriosis patients were prepared at concentrations of $1x10^9$ and $2x10^9$ EV/mL in fPBS. MACSPlex capture beads (15 µl) were incubated with PF-sEV overnight at room temperature with rotation at 12 rpm. After washing (3000 x g, 5 mins), PF-sEV were incubated for 1 hour at room temperature with rotation at 12 rpm with the detection antibody - either 5 µl of anti-CD47-APC (CC2C6, Biolegend, USA) or 5 µl anti-PD-L1-APC (29E.2A3, Biolegend, USA).

A further CD47 co-expression titration experiment was conducted by an MSc student, Malak Amer, using PF-sEV isolated from three individual endometriosis patients. Input PF-sEV concentrations of $2x10^9$ EV/mL, $4x10^9$ EV/mL, and $6x10^9$ EV/mL were tested. A final input concentration of $6x10^9$ EV/mL was used to examine CD47 co-expression in 5 control and 5 endometriosis patients with patient information listed in Table 4.1 (patient number:25-34). To control for non-specific binding, capture beads with the detection antibody alone were analysed as a negative control. APC Median Fluorescence Intensity (MFI) was detected by flow cytometry (Northern Lights, Cytek Biosciences, USA). A marker was considered positive if the MFI value was higher than both the respective control (mIgG or REA) and the negative control.

4.2.10.5 Measurement of 'Don't eat me' signal receptors on macrophages.

The expression of 'Don't eat me' signal receptors (SIRP-α, Siglec-10 and PD-1) was assessed on pMΦ isolated from 3 endometriosis patients and THP-1 derived macrophages. The expression of these receptors was measured using specific antibodies (or the respective isotype control) as listed in Table 4.4 using a Northern Lights Flow cytometer (Cytek Biosciences, USA).

Table 4.3 Antibodies for 'Don't eat me' receptors on macrophages

MARKER	ISOTYPE	CLONE	FLOUROPHORE	COMPANY
SIGLEC-10	Mouse IgG1, κ	5G6	PE	Biolegend, UK
PD-1	Mouse IgG1, κ	NAT105	PE	Biolegend, UK
CD47	Mouse IgG1, κ	CC2C6	APC	Biolegend, UK
ISOTYPE CONTROL	Mouse IgG1, κ	MOPC-21	APC	Biolegend, UK
ISOTYPE CONTROL	Mouse IgG1, κ	MOPC-21	PE	Biolegend, UK

4.2.11 Enzyme-linked immunosorbent assay (ELISA)

Samples were diluted in PBS if necessary to ensure all samples were within the working range of the ELISA. The 96-well ELISA plates were read using a FLUOstar Omega microplate reader (BMG LABTECH, UK) with an absorbance of 450nm.

4.2.11.1 Measurement of cytokine secretion of THP-1 derived macrophages after polarisation

$5x10^5$ THP-1 derived macrophages were seeded per well in 24 well plates and differentiated and polarised into M1 and M2 macrophages as described in section 4.2.2. Cell culture supernatants (500µl each) were collected and centrifuged at 500 x g for 3 mins to remove

cells. Cytokine levels (IL-1β, TGF-β1, IL-10 and IL-8) were detected using Duoset ELISA kits (R&D SYSTEMS, USA) as per the manufacturer's instructions.

4.2.11.2 Measurement of cytokine secretion of THP-1 derived macrophages after PF-sEV treatment

The level of IL-6, IL-10 and TGF- β1 in the cell culture supernatants that were assessed by CBA were also examined using Duoset ELISA kits (R&D SYSTEMS, USA) as per the manufacturer's instructions.

4.2.12 CD47 Blocking experiment

PF-sEV were isolated from control and endometriosis patients (n=5) by SEC columns (Gen 2, qEV Original 35nm columns, IZON, New Zealand) as described in Chapter 3 Section 2.2. sEV enriched fractions were pooled (1.6mL) and filtered (0.2um PVDF membrane) and incubated with 10µl of anti-CD47 antibody (B6H12, Thermo Fisher Scientific, USA) or the respective Mouse IgG1 isotype control (MOPC-21, Biolegend, USA) overnight at 4°C with rotation at 12rpm. The CD47 blocked PF-sEV or Isotype control PF-sEV were washed with 13mL fPBS and unbound antibody was removed by ultracentrifugation at 150,000 x g (max) for 2h using a SW 44 Ti swinging bucket rotor in an Optima XE-90 ultracentrifuge (Beckman Coulter, USA). The superntant was discarded and the PF-sEV pellets were resuspended in 40µl fPBS. CD47 blocked PF-sEV and Isotype control PF-sEV were quantified by NTA. $1x10^{10}$ EV/mL were added to EV-depleted media (RPMI1640 media with 1% PS and 10% (v/v) EV-depleted) and incubated with THP-1 derived M2 macrophages for 24h. THP-1 derived M2 macrophages were then washed with PBS and treated with 20 µg/mL pHrodo deep red E.coli bioparticles for 1h and assessed for phagocytosis as previously described in section 4.2.7 and section 4.2.9.3 using flow cytometry (Northern Lights, Cytek Biosciences, USA).

4.2.13 Statistical analysis

Statistical analyses were performed using GraphPad Prism software. Normality of data distribution was assessed using the Shapiro-Wilk test. One-way ANOVA with Tukey's post-hoc test was used to assess the effects of PMA concentrations on cell size, marker expression, and cell adherence. Two-way ANOVA followed by Tukey's post-hoc test was employed to assess the effects of two variables (EV depletion and disease status) on phagocytic activity. Paired t-tests were used for comparing related groups, such as NTA analysis of whole PF versus EV-depleted PF within each disease group. Data are presented as mean ± SD. A p-value < 0.05 was considered statistically significant.

4.3 Results

4.3.1 Optimisation of a protocol for in vitro macrophage differentiation and polarisation.

4.3.1.1 Cell morphology of PMA-induced THP-1 and U937 derived macrophages

THP-1 and U937 cells were differentiated into macrophages like cells by incubation with an increasing dose of PMA ranging from 2 to 100ng/mL. Cell morphology was recorded at 24h and 48h post-treatment. Both cell lines exhibited significant morphological changes in response to PMA treatment. Cell adherence was observed after just 24h of incubation, even at the lowest PMA concentration of 2ng/mL. THP-1 derived macrophages became noticeably enlarged and elongated, with the appearance of short cytoplasmic protrusions (Figure 4.3). While U937 cells also became enlarged, they maintained a more rounded shape compared to THP-1 derived macrophages (Figure 4.4).

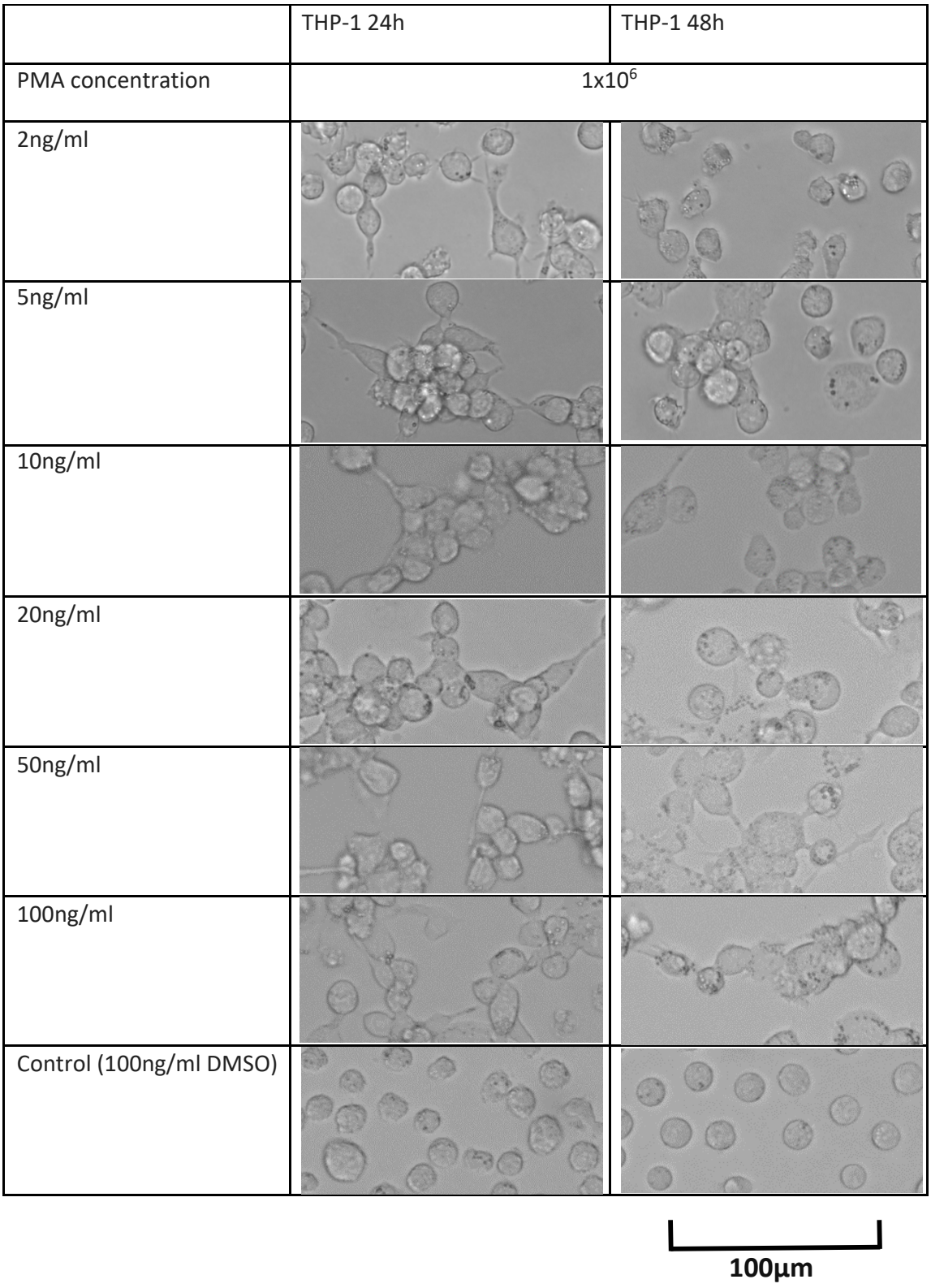

Figure 4.3. Morphological changes of THP-1 derived macrophages. Representative bright-field microscopy images of THP-1 derived macrophages treated with 2-100 ng/mL PMA for 24h and 48h. Scale bar = 100 µm.

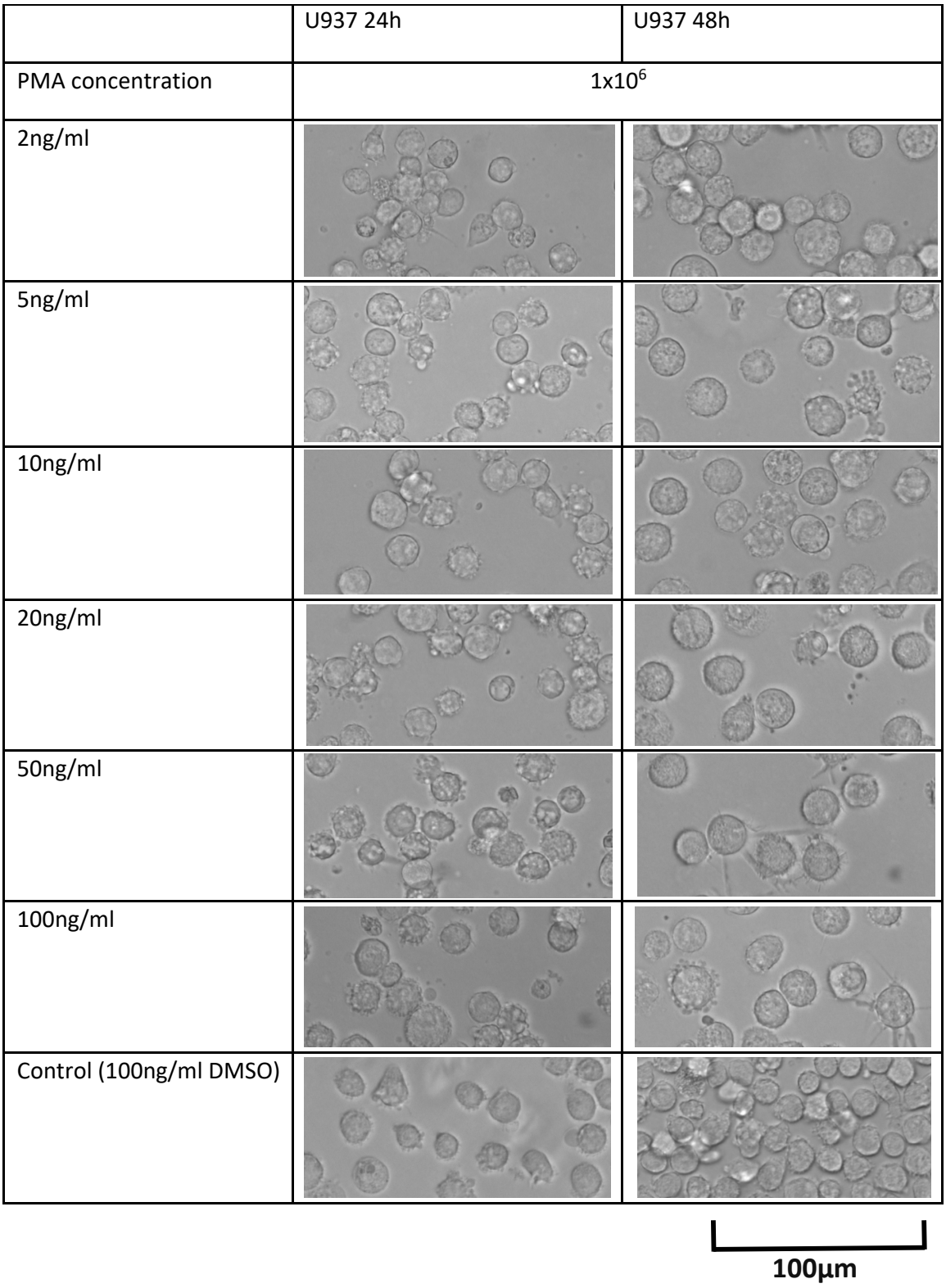

Figure 4.4. Morphological changes of U937 derived macrophages. Representative bright-field microscopy of U937 cells treated with 2-100 ng/mL PMA for 24h and 48h. Scale bar = 100 µm.

Quantitative assessment of THP-1 and U937 cells was performed using ImageJ software. THP-1 derived macrophages exhibited a gradual, dose-dependent increase in size in response to PMA treatment (Figure 4.5a). Compared to untreated THP-1 derived macrophages, those incubated with PMA concentrations of 5ng/mL or above were significantly larger in diameter. This increase in cell size peaked at 20ng/mL PMA and then plateaued.

Unlike THP-1 derived macrophages, the diameter of U937 cells were significantly increased when treated with 2ng/mL of PMA compared to untreated cells (Figure 4.5b). Higher concentrations of PMA resulted in increased average cell sizes and peaked at 10ng/mL PMA.

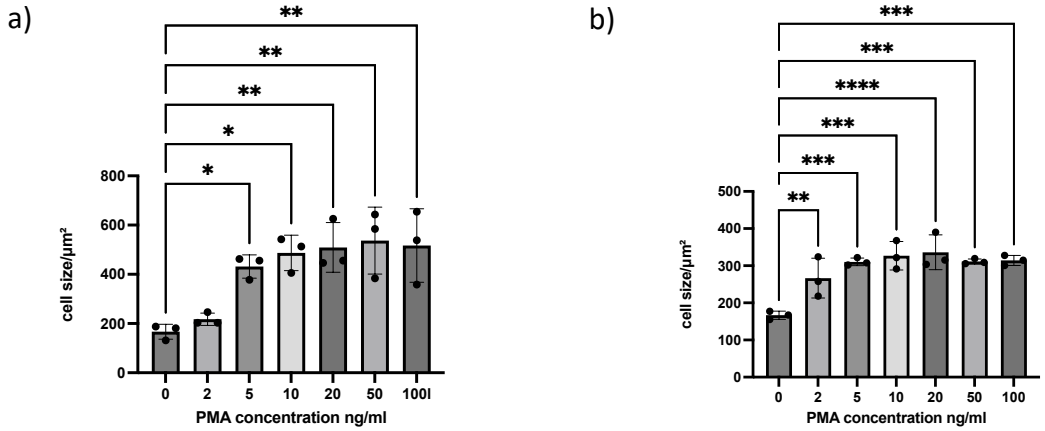

Figure 4.5. Quantitative size analysis of PMA-induced THP-1 and U937 derived macrophages (n=3). Average size (μm^2) of a) THP-1 and b) U937 derived macrophages treated with an increasing concentration of PMA (0-100 ng/mL) for 48h. Data represent the mean ± SD from three independent biological experiments.. One-way ANOVA with Turkey's multiple comparisons (Shapiro-Wilk test: $p > 0.05$) for THP-1 and Kruskal-Wallis test with Dunn's multiple comparisons (Shapiro-Wilk test: $p < 0.05$) for U937, *P<0.05, **P<0.01, ***P<0.001, ****P<0.0001. *P<0.05, ****P<0.0001.

4.3.1.2 Cell adherence of PMA-induced THP-1 and U937 derived macrophages

Cell adherence is a fundamental indicator of differentiation. THP-1 derived macrophages showed a gradual increase in adherence with increasing PMA concentrations (Figure 4.6a). As expected, very few THP-1 derived macrophages (20 % ± 14%, mean± SD) underwent adherence in the absence of PMA. At 2ng/mL PMA, the adherence rate increased to 57% ±

28% (mean± SD) (p>0.05) to untreated cells. It was noticeable that cells easily detached during the washing procedure. Compared to untreated cells, the adherence rate significantly increased to 81% ± 16% (mean± SD) at 5ng/mL PMA (p<0.001), 85% ± 10% (mean± SD) at 10ng/mL PMA (p<0.001), and above 90% for PMA concentrations between 20-100ng/mL (p<0.001).

For U937 derived macrophages, untreated cells have an adherence rate of 6% ± 4% (mean± SD). Treatment with 2ng/mL PMA resulted in a significant higher adherence rate of 83% ± 19% (mean± SD) (P<0.0001) (Figure 4.6b). At higher PMA concentrations (5-100ng/mL), the adherence rate increased to over 95% (P<0.0001).

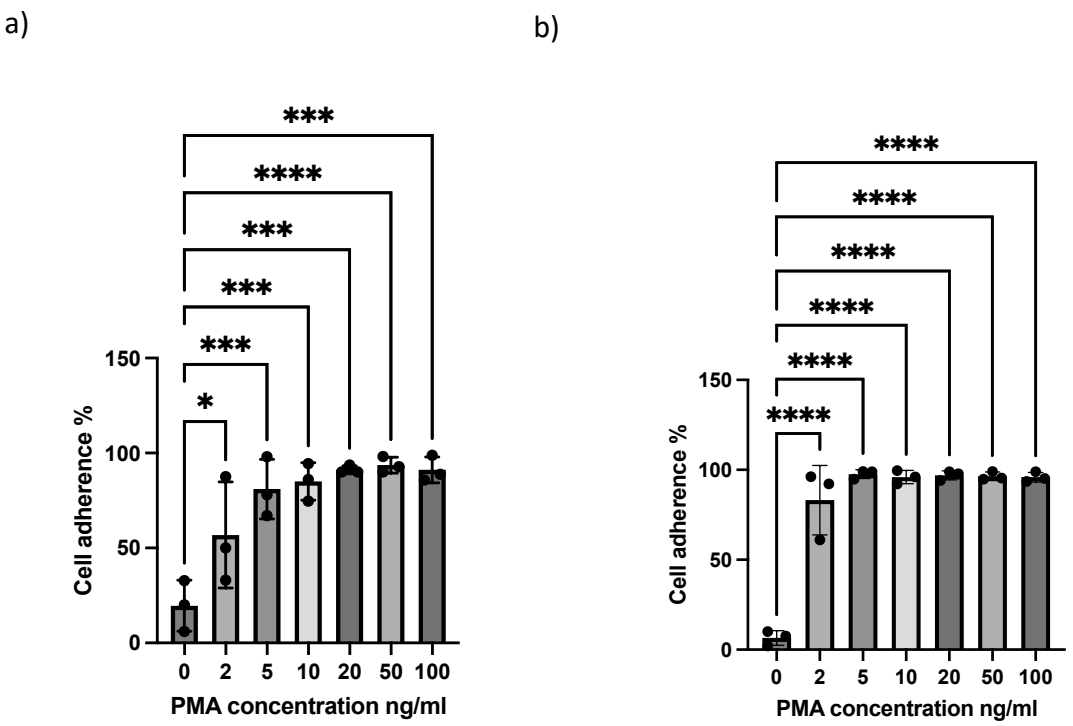

Figure 4.6. Cell adherence rates of PMA-induced THP-1 and U937 derived macrophages (n=3). Adherence rates of a) THP-1 derived macrophages and b) U937 derived macrophages treated with an increasing concentration of PMA (0-100 ng/mL) for 48h. Data represent the mean ± SD from three independent experiments, each consisting of three wells seeded with 5×10^5 THP-1 derived macrophages combined per treatment group. One-way ANOVA with Turkey's multiple comparisons (Shapiro-Wilk test: p > 0.05), *P<0.05, ***P<0.001, ****P<0.0001.

Together, these results demonstrate distinct responses of U937 and THP-1 derived macrophages to PMA treatment in terms of both cell size and adherence. U937 cells show a more rapid and uniform response, reaching a plateau in both size and adherence at lower PMA concentrations. In contrast, THP-1 derived macrophages exhibit a more gradual, dose-dependent response, requiring higher PMA concentrations to achieve significant changes in size and stable adherence.

4.3.1.3 Comparison of THP-1 cell seeding densities for PMA-Induced differentiation.

The influence of initial THP-1 cell seeding density on PMA-induced differentiation was also investigated as one study has shown that THP-1 cell confluency affects their response to PMA (292). THP-1 were seeded at two different densities: $5x10^5$ and $1x10^6$ cells per well in 12-well plates. No obvious changes in cell morphology (Figure 4.7a) or cell adherence rate (Figure 4.7b) were observed between these two seeding densities. On this basis, $1x10^6$ cells per well in 12-well plates were set as the standardised seeding density for subsequent analysis.

a)

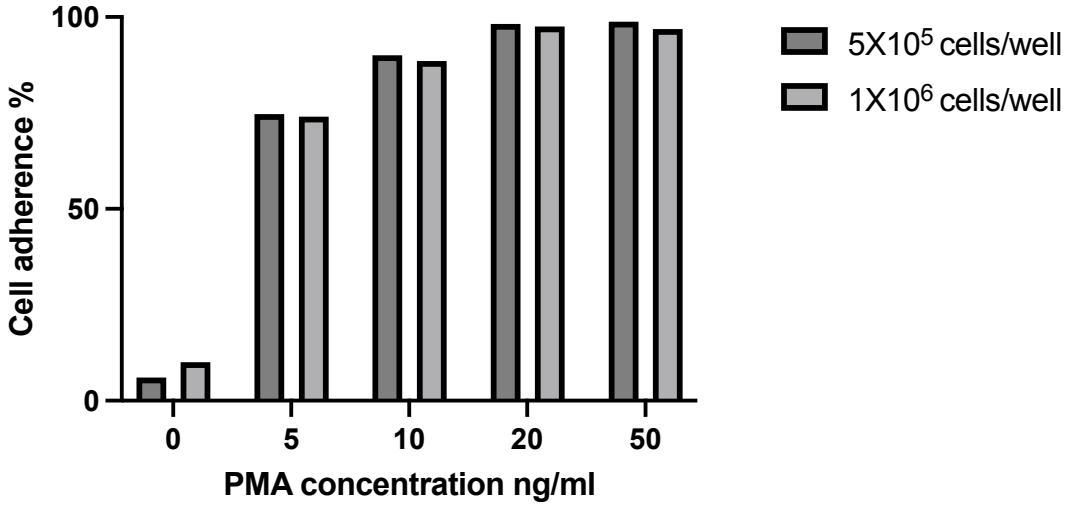

b)

	24h		48h	
Cell density	$5x10^5$	$1x10^6$	$5x10^5$	$1x10^6$
5ng/ml PMA				
10ng/ml PMA				
20ng/ml PMA				
50ng/ml PMA				
50ng/ml DMSO				100 µm

Figure 4.7. Effect of initial THP-1 cell seeding density on PMA-induced differentiation. a) Representative bright-field microscopy images of THP-1 derived macrophages seeded at $5x10^5$ and $1x10^6$ cells/well in 12-well plates and treated with PMA (5-50ng/mL) or DMSO control (50ng/mL) for 48h. Scale bar = 100 µm. b) Quantification of THP-1 cell adherence following PMA treatment. Cells were seeded at $5x10^5$ and $1x10^6$ cells/well in 12-well plates and exposed to 0-100ng/mL PMA for 48h. n=1.

4.3.1.4 CD14 expression of PMA-induced THP-1 and U937 derived macrophages

Differentiation induced by PMA treatment in both U937, and THP-1 derived macrophages was further assessed by examining the expression of CD14 using flow cytometry. CD14 is a cell surface marker commonly used to identify monocytes and macrophages, and its upregulation is often associated with monocyte-to-macrophage differentiation in cell lines (257, 293). For THP-1 (Figure 4.8a), untreated cells expressed negligible CD14, which was increased with 2ng/mL PMA, but not significantly ($p>0.05$). Only treatment with 5ng/mL and 10ng/mL PMA induced significantly higher ($p<0.05$) CD14 expression compared to untreated cells. Higher concentrations of PMA (20-100ng/mL) did not significantly ($p>0.05$) upregulate CD14 expression compared to untreated cells, and CD14 expression steadily decreased with increasing concentrations. For U937 (Figure 4.8b), CD14 expression peaked at 2 ng/mL PMA and gradually declined with increasing PMA concentrations (5-100 ng/mL). All PMA-treated U937 cells exhibited significantly higher CD14 expression ($p<0.0001$) compared to untreated cells.

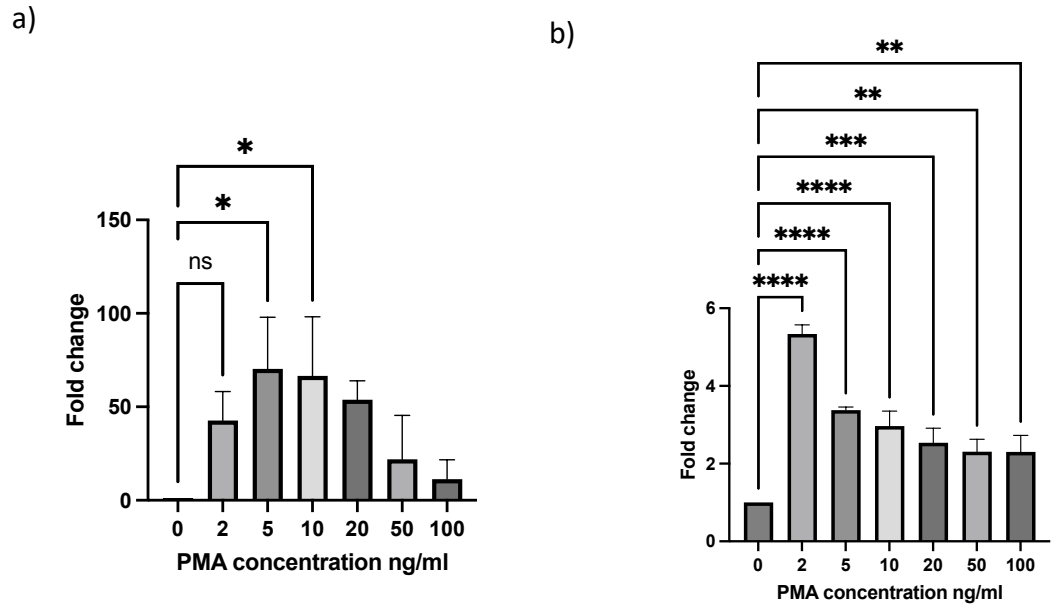

Figure 4.8. Flow cytometry analysis of CD14 expression in differentiated THP-1 and U937 cells (n=3). Fold change in CD14 expression of a) THP-1 derived macrophages and b) U937 cells, treated with PMA (0-100 ng/mL) for 48h. Data are presented as fold change relative to undifferentiated THP-1 cells (PMA free), calculated by dividing the MFI of THP-1-derived macrophages under different conditions by the average MFI of undifferentiated THP-1 cells from three replicates. Bars = mean ± SD. One-way ANOVA with Turkey's multiple comparisons (Shapiro-Wilk test: $p > 0.05$), *$p<0.05$, **$p<0.01$, ***$p<0.001$, ****$p<0.0001$.

Based on the analysis of cell morphology, cell size, cell adherence, and CD14 expression treatment with 2ng/mL PMA induced differentiation in both cell lines, but was not stable, especially in THP-1 derived macrophages. Significant differences in cell morphology, size, adherence and CD14 expression was consistently observed in both cell lines differentiated with 5ng/mL PMA compared to untreated cells. CD14 expression exhibited a dose-response effect with PMA, it increased at lower PMA concentrations and then notably declined at higher concentrations. This observation indicates that different PMA dosage may affect other marker expression. To assess the effect of PMA-mediated activation of THP-1 and U937 polarisation, 5ng/mL and 10ng/mL PMA were chosen for polarisation studies.

4.3.1.5 Polarisation of PMA-differentiated THP-1 and U937 Cells

PMA-differentiated cells (M0) were polarized into M1 and M2 subtypes with LPS + IFN-γ and IL-4 + IL-13 stimulation respectively for 24h. A 6-colour macrophage characterization flow panel was used to assess the expression of markers (pan-marker: CD14; M1: CD80, CD86, HLA-DR; M2: CD163, CD206). The study compared the polarisation efficacy in both THP-1 and U937 cell lines, as well as the impact of different PMA concentrations (5 ng/mL and 10 ng/mL) on the polarisation process.

For THP-1 derived macrophages, LPS + IFN-γ stimulation effectively induced M1 polarisation, as evidenced by significantly higher expression of HLA-DR, CD80, and CD86 compared to both M0 and M2 phenotypes (Figure 4.9a, b, c). This effect was consistent across both PMA concentrations tested. Interestingly, CD86 expression was significantly higher in M1 macrophages differentiated with 10 ng/mL PMA compared to those differentiated with 5 ng/mL PMA ($P<0.01$), suggesting that higher PMA concentrations may enhance certain aspects of M1 polarisation.

Regarding M2 polarisation in THP-1 derived macrophages, the results were less pronounced and showed some dependency on PMA concentration. CD206 expression, a key M2 marker, was significantly higher in IL-4 stimulated cells compared to M1 and M0, but only when

differentiated with 5 ng/mL PMA (P<0.0001) (Figure 44d). This suggests that lower PMA concentrations may be more conducive to M2 polarisation. CD163 expression did not show significant elevation compared to M0 (Figure 4.9e).

CD14 expression in THP-1 derived macrophages remained relatively stable and high in M0 and M2 subgroups but was significantly lower in M1 macrophages (P<0.001) (Figure 4.9f).

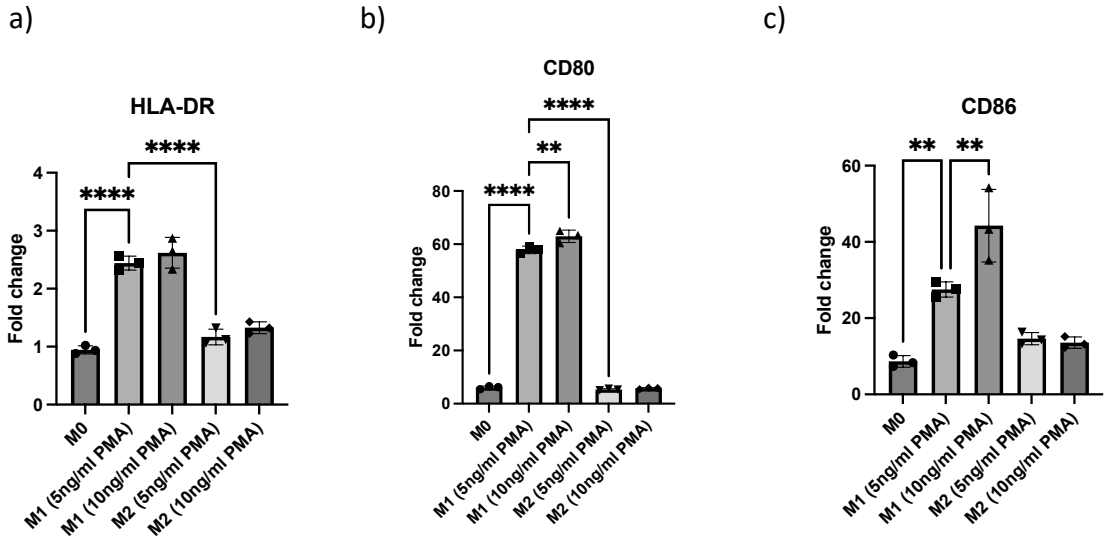

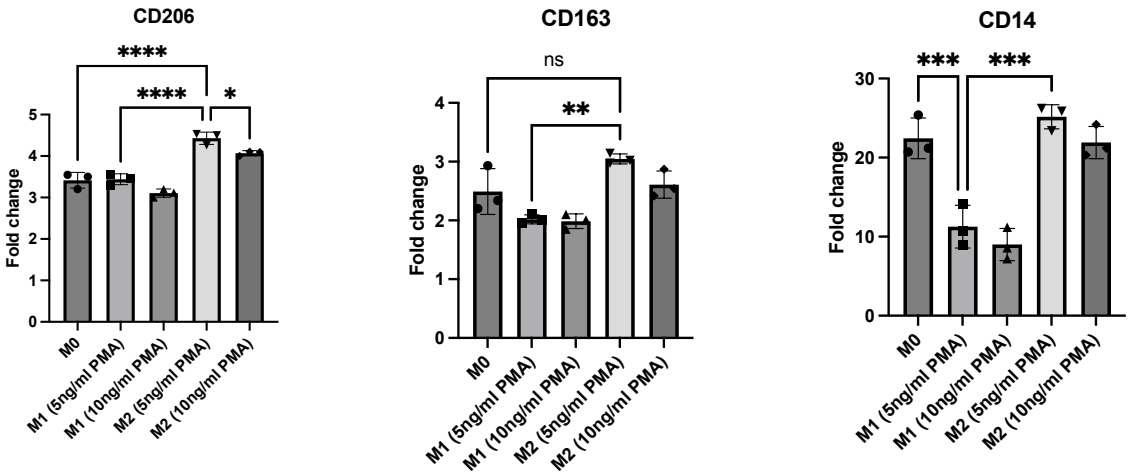

Figure 4.9. Flow cytometry analysis of macrophage polarisation markers in PMA-differentiated THP-1 derived macrophages (n=3). THP-1 derived macrophages were differentiated with 5 ng/mL or 10 ng/mL PMA for 48h, then polarized to M1 (LPS + IFN-γ) or M2 (IL-4 + IL-13) phenotypes for 24h. Expression of a) HLA-DR (M1 marker), b) CD80 (M1 marker), c) CD86 (M1 marker), d) CD206 (M2 marker), e) CD163 (M2 marker), f) CD14 (pan-macrophage marker) was analysed. Data are presented as fold change relative to undifferentiated THP-1 cells (PMA free), calculated by dividing the MFI of THP-1-derived macrophages under different conditions by the average MFI of undifferentiated THP-1 cells from three replicates. Bars = mean ± SD. One-way ANOVA with Turkey's multiple comparisons (Shapiro-Wilk test: $p > 0.05$), *$p<0.05$, **$p<0.01$, ***$p<0.001$, ****$p<0.0001$.

U937 cells demonstrated similar trends in M1 polarisation to THP-1 derived macrophages. Compared to both M0 and M2 macrophages, LPS + IFN-γ stimulation significantly increased the expression of HLA-DR ($P<0.0001$ for both), CD80 ($P<0.0001$ for both), and CD86 ($P<0.0001$ vs M0, $P<0.01$ vs M2) (Figure 4.10a, b, c).However, U937 cells exhibited higher baseline levels of CD206 and CD163 expression compared to THP-1 derived macrophages. The response to IL-4 stimulation for M2 polarization was less pronounced in U937 cells. Specifically, CD206 expression was significantly higher in M2 compared to M0 ($P<0.05$), but not when compared to M1 at 5ng/mL PMA concentration (Figure 45d). CD163 expression showed a significant increase in M2 compared to M1 ($P<0.05$), but this elevation was not significant when compared to M0 (Figure 4.10e).

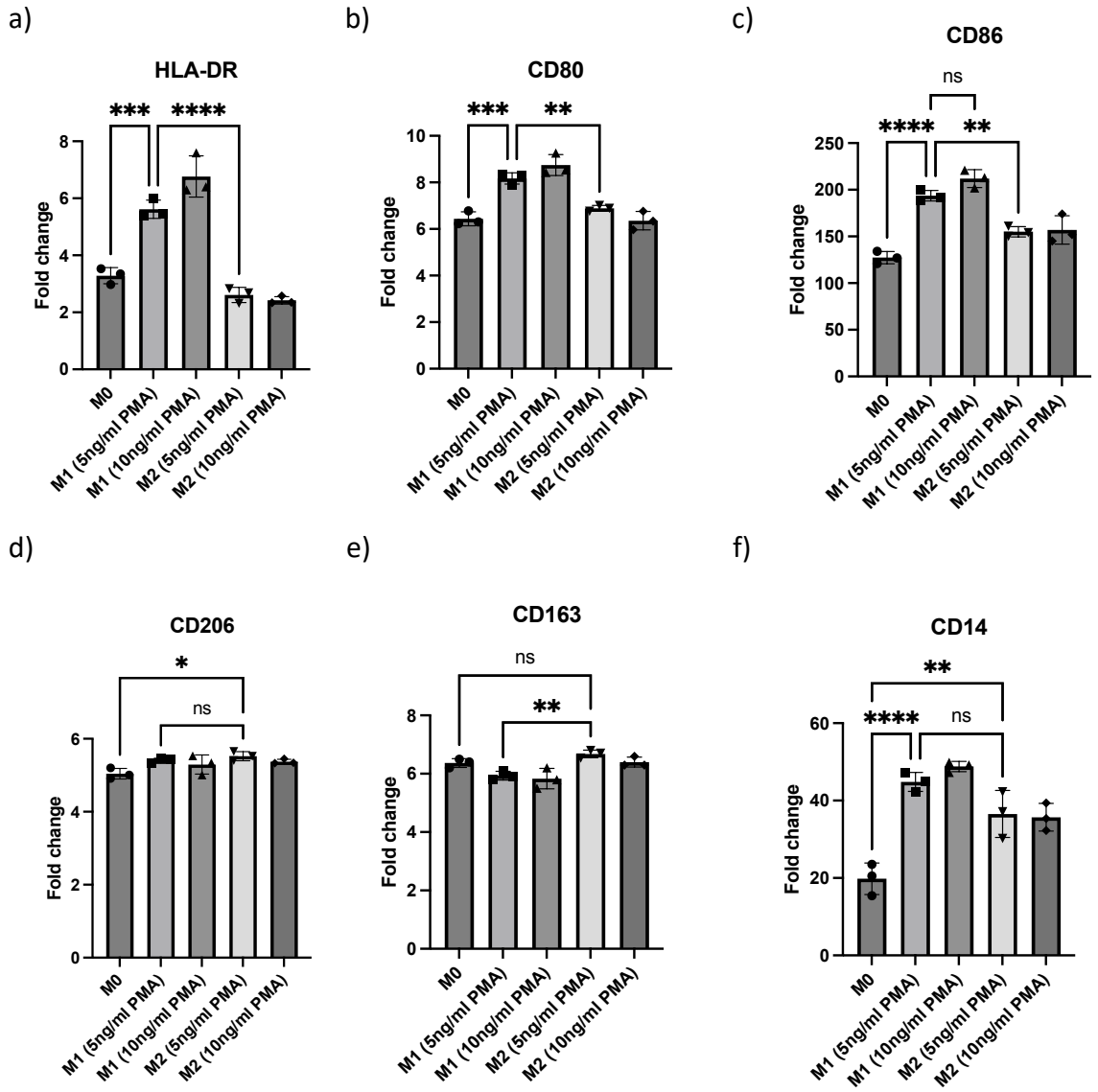

Figure 4.10. Flow cytometry analysis of macrophage polarization markers in PMA-differentiated U937 cells (n=3). U937 cells were differentiated with 5 ng/mL or 10 ng/mL PMA for 48h, then polarized to M1 (LPS + IFN-γ) or M2 (IL-4 + IL-13) phenotypes for 24h. Expression of a) HLA-DR (M1 marker), b) CD80 (M1 marker), c) CD86 (M1 marker), d) CD206 (M2 marker), e) CD163 (M2 marker), f) CD14 (pan-macrophage marker) was analysed. Data are presented as fold change relative to undifferentiated cells. Bars = mean ± SD. One-way ANOVA with Turkey's multiple comparisons (Shapiro-Wilk test: $p > 0.05$),, *$p<0.05$, **$p<0.01$, ****$p<0.0001$.

An interesting distinction between the two cell lines was observed in CD14 expression patterns. Unlike THP-1 derived macrophages, both M1 and M2 polarization increased CD14 expression in U937 cells (Figure 4.10f). Based on these results, LPS and IFN- γ stimulation successfully induce M1 marker expression (CD80, CD86 and HLA-DR), while IL-4 stimulation

was sufficient to induce CD206 in THP-1 derived macrophages but not in U937 cells and failed to induce expression of CD163 in both cell lines. Importantly, increased PMA dosage favoured M1 polarisation (expression of CD80, CD86, HLA-DR) and suppressed M2 polarisation (CD206) in both cell lines. Therefore, 5ng/mL PMA was chosen for subsequent macrophage differentiation.

THP-1-derived macrophages, morphologically similar to pMΦ, both exhibited cytoplasmic protrusions, whereas U937-derived macrophages maitained a spherical shape.

pMΦ were observed to be heterogeneous, activated and highly responsive to stimulants. IL-4 stimulation led to obvious elevation of CD206 expression as shown in Chapter 2 Section 3.2. THP-1 derived macrophages demonstrate greater plasticity compared to U937 cells, making them a preferred model for studying pMΦ biology. This plasticity is evident in their dose-responsive expression of macrophage markers when exposed to PMA and polarizing stimuli. THP-1 derived macrophages show superior responsiveness to IL-4 stimulation, indicating a greater capacity to adopt M2-like phenotypes, which is crucial for studying pMΦ. In contrast, U937 cells appear to have lower plasticity. They exhibit high baseline activation, potentially masking subtle changes in response to polarising factors. Given these observations, THP-1 derived macrophages were chosen as the preferred model for further studies.

4.3.1.6 Optimisation of M2 polarisation protocol for differentiated THP-1 derived macrophages

To improve M2 polarization, particularly CD163 expression, different reported stimulation protocols were compared in THP-1 derived macrophages. The study assessed the effects of IL-4 alone and IL-4+IL-13 in combination, with stimulation durations of 24h and 48h.
For CD206 expression, extending the stimulation time to 48h significantly enhanced CD206 expression compared to 24h, regardless of whether IL-4 was used alone or in combination with IL-13 ($P<0.0001$). Additionally, both IL-4 and IL-4+IL-13 treatments at 48h resulted in significantly higher CD206 expression compared to M0 ($P<0.0001$) (Figure 4.11a). The highest CD206 expression was observed with the IL-4+IL-13 combination at 48h.

IL-4 stimulation alone, whether for 24h or 48h, did not significantly increase CD163 expression compared to M0 cells (Figure 4.11b). The addition of IL-13 and extending stimulation time to 48h were both crucial for inducing CD163 expression. Only the IL-4+IL-13 combination stimulated for 48h resulted in significantly higher CD163 expression compared to M0 cells ($P<0.01$).

Based on these results, the IL-4+IL-13 combination with a 48h stimulation period was determined to be the most effective in inducing both CD206 and CD163 expression. This protocol was therefore set as the standardised method for M2 polarisation in subsequent experiments.

a)

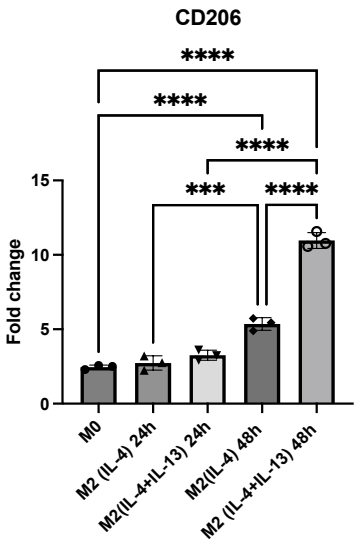

b)

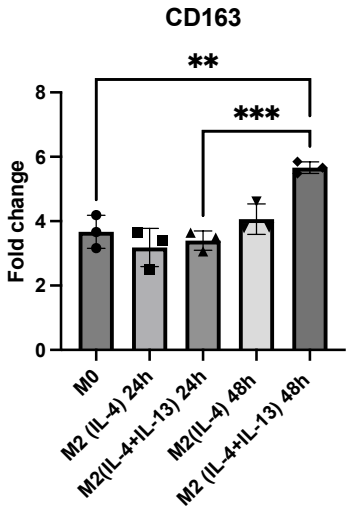

Figure 4.11. Flow cytometry analysis of optimising M2 polarisation in differentiated THP-1 derived macrophages (n=3). THP-1 derived macrophages were differentiated to M0 with PMA, then stimulated with different M2 polarization protocols: IL-4 alone or IL-4+IL-13 in combination, for either 24h or 48h. Expression of M2 markers was analysed by flow cytometry: a) CD206 expression, b) CD163 expression. Data are presented as fold change relative to undifferentiated THP-1 derived macrophages. Bars = mean ± SD. One-way ANOVA with Turkey's multiple comparisons (Shapiro-Wilk test: $p > 0.05$),, **$p<0.01$, ***$p<0.001$, ****$p<0.0001$.

Finally, cytokine secretion of polarised THP-1 M1 and M2 macrophages was assessed. Pro-inflammatory IL-1β levels were significantly higher in M1 subgroups (P<0.01) (Figure 4.12a), while anti-inflammatory TGF-β1 levels were significantly higher in M2 subgroups (P<0.0001 vs M0, P<0.05 vs M1) (Figure 4.12b), further confirming successful polarisation of macrophages.

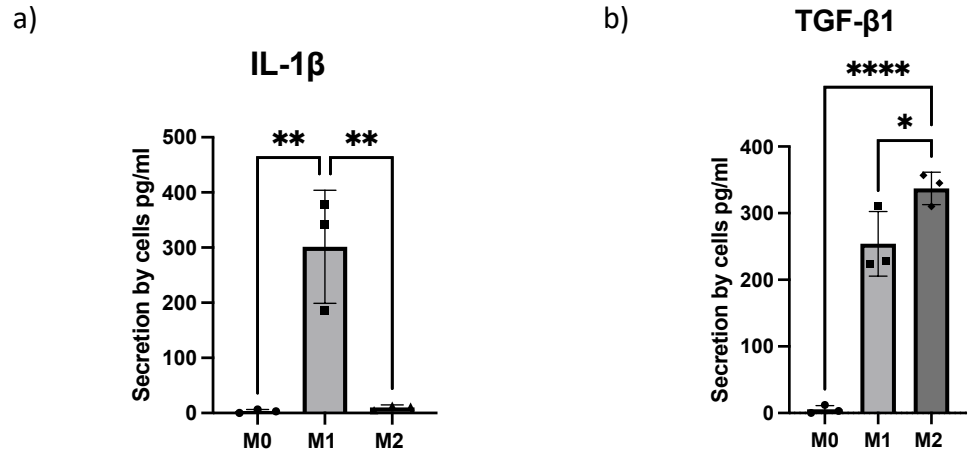

Figure 4.12. Cytokine secretion profiles of M1 and M2 macrophages (n=3). THP-1 cells were differentiated into macrophages (M0) using PMA, then polarised to M1 (LPS + IFN-γ) for 24 h or M2 (IL-4 + IL-13) for 48 h. Cytokine levels of a) IL-1β, b) TGF-β1 in cell culture supernatants were measured by ELISA. Bars = mean ± SD. One-way ANOVA with Turkey's multiple comparisons, *p<0.05, **p<0.01, ****p<0.0001.

4.3.2 The effect of PF on macrophage phagocytic activity

Impaired phagocytic activity of pMΦ has been shown in endometriosis patients, potentially contributing to immune evasion of endometriotic lesions (262). This section investigated the effect of PF on the phagocytic activity of macrophages.

4.3.2.1 Optimisation of the macrophage phagocytosis assay

Using THP-1 derived macrophages and pHrodo *E. coli* Deep Red bioparticles, a series of preliminary experiments were conducted to determine the ideal parameters for assessing phagocytosis. This was performed as part of Aya Akhatova's MSc in Clinical Embryology research project.

First, using flow cytometry, a titration of pHrodo *E. coli* Deep Red bioparticles was performed to assess the optimal concentration to use for downstream experiments. A dose response effect on phagocytic activity was observed with increasing concentrations of bioparticles as shown by the percentage positive THP-1 derived macrophages (Figure 4.13a) and the increase in MFI (Figure 4.13b). The optimal concentration of bioparticles was established at 20 µg/mL, with a 1 h incubation time. This combination was sufficient to reach a plateau for the percentage of positive phagocytic cells (Figure 4.13a) while the overall phagocytic activity, as measured by examining the MFI , did not plateau under these conditions (Figure 4.13b). To validate the flow cytometry assay's specificity for measuring phagocytosis, visual confirmation using confocal microscopy demonstrated that the fluorescently bright bioparticles were only found inside THP-1 derived macrophages, with no fluorescence observed outside the cells (Figure 4.13c).

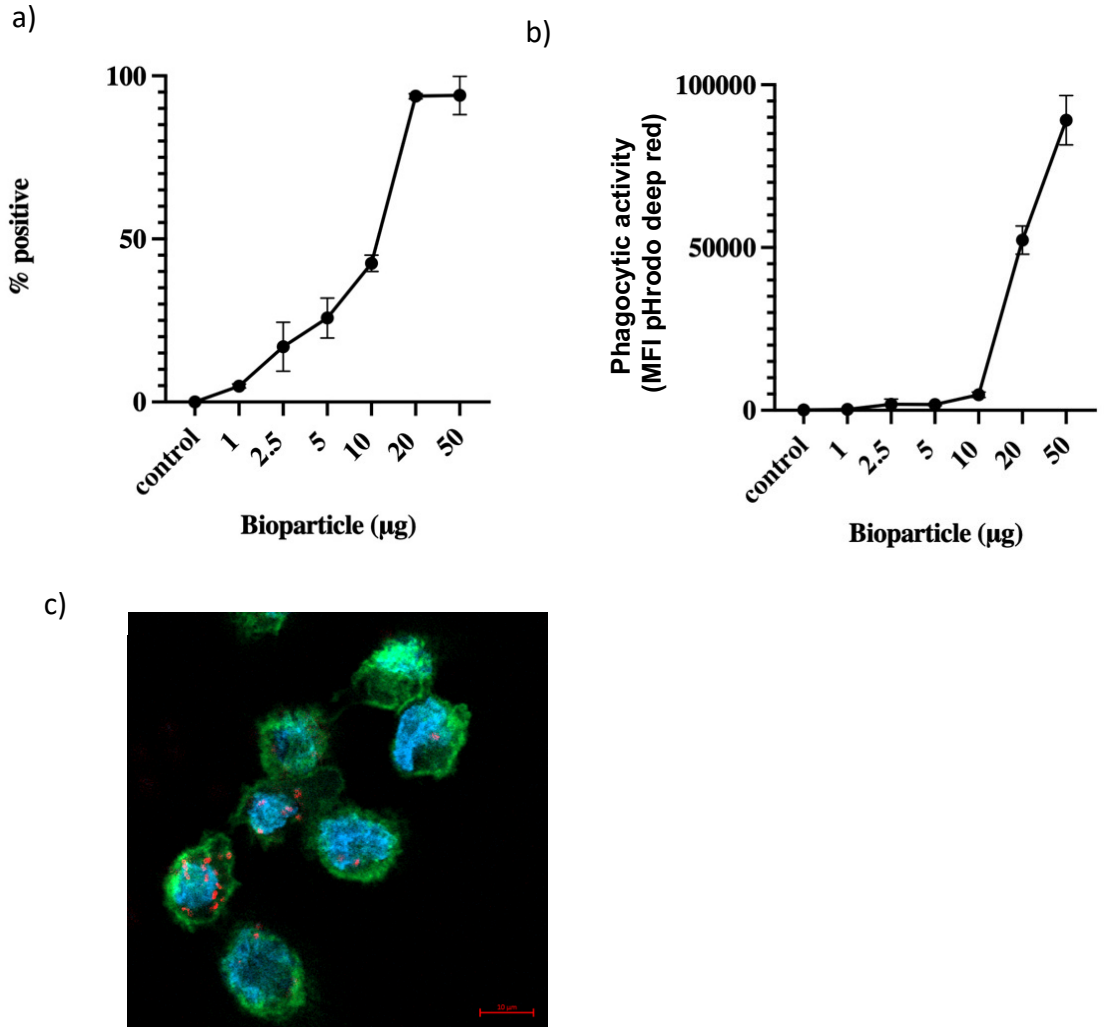

Figure 4.13. Optimization of the macrophage phagocytosis assay using pHrodo *E. coli* deep red bioparticles. THP-1 derived M0 macrophages were incubated with 1-50µg/mL of pHrodo *E. coli* deep red bioparticles for 1 hour. Phagocytosis was assessed by flow cytometry and confocal microscopy: a) Percentage of phagocytic THP-1 derived macrophages at different bioparticle concentrations. Bars = mean ± SD (n=3). b) MFI at different bioparticle concentrations, indicating overall phagocytic activity. Bars = mean ± SD (n=3). c) Representative confocal microscopy image showing internalised pHrodo *E. coli* deep red bioparticles (bright red). Cell nuclei were stained with DAPI (blue) and cell membranes with WGA (green). Scale bar = 10 µm.

4.3.2.2 Comparison of phagocytic activity in THP-1 derived M0, M1 and M2 macrophages

A comparative analysis of phagocytic activity among different THP-1 derived macrophages (M0, M1, and M2) revealed significant functional differences. M0 and M2 macrophages exhibited strong phagocytic activity, which was decreased by treating with cytochalasin D, a

known inhibitor of phagocytosis (Figure 4.14). M0 and M2 macrophages treated with cytochalasin D showed a significant reduction in phagocytic activity (mean ± SD) by 89% ± 3.5% and 95% ± 1.2%, respectively (P<0.0001). In contrast, M1 macrophages exhibited significantly weaker phagocytic activity compared to M0 and M2 phenotypes (P<0.0001) (Figure 4.14). Cytochalasin D treatment had no significant effect on M1 phagocytosis.
This observation underscores the fundamental differences in phagocytic capacity among macrophage subtypes and led to the decision to focus subsequent phagocytosis studies on M0 and M2 macrophages.

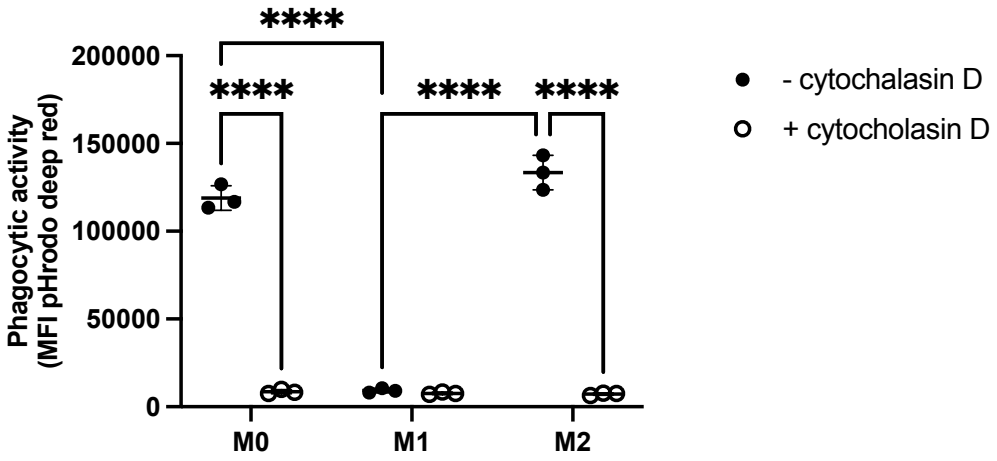

Figure 4.14. Comparative flow cytometry analysis of phagocytic activity in THP-1 derived M0, M1, and M2 macrophages n=3. THP-1-derived macrophages (M0, M1, and M2) were incubated with pHrodo *E. coli* deep red bioparticles (20 µg/mL, 1 hour) with or without cytochalasin D pre-treatment. Bars = mean ± SD. Two-way ANOVA with Turkey's multiple comparisons (Shapiro-Wilk test: p > 0.05), ****p<0.0001.

4.3.2.3 Investigating the effect of PF from endometriosis and control patients on macrophage phagocytosis by flow cytometry

This section examined how PF from endometriosis and control patients influenced the phagocytic activity of M0 and M2 macrophages.

To determine the optimal PF concentration, a series of dose-response experiments were conducted as part of Aya Akhatova's MSc project. THP-1 derived M0 macrophages were treated with PF concentrations ranging from 2% to 50% (v/v) in culture media for 24 hours. Cell viability was then assessed using flow cytometry and trypan blue staining. These

experiments revealed that 5% (v/v) PF was the optimal concentration, as higher levels led to cell detachment and increased granularity, indicating reduced viability (data not shown). Twenty-three PF (5% v/v) samples were chosen for further experiments, categorized as follows: 6 controls (women without endometriosis), 11 patients with endometriosis stages I/II, and 6 patients with endometriosis stages III/IV.

The phagocytic activity of macrophages was assessed after treatment with PF from different groups. For M0 macrophages, the phagocytic activity of those treated with PF from stage III/IV endometriosis (n=6) was significantly lower than both control (n=6) ($P<0.01$) and endometriosis stage I/II PF (n=11) ($P<0.05$). However, M0 treated with PF from endometriosis stage I/II did not show a difference compared to the control group. Importantly, the phagocytic activity of M2 macrophages treated with endometriosis PF (both stage I/II and III/IV) was significantly lower than that observed in M2 macrophages treated with control PF ($P<0.01$) (Figure 4.15b).

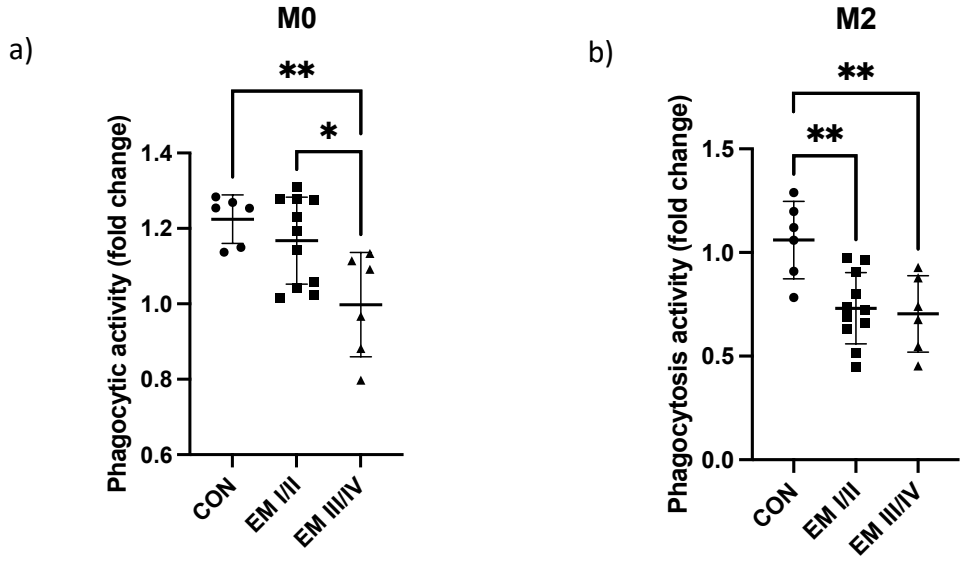

Figure 4.15. Flow cytometry analysis of phagocytic activity in THP-1 derived macrophages treated with PF from control and endometriosis patients THP-1-derived a) M0 and b) M2 macrophages were treated with 5% (v/v) PF from control or endometriosis patients (stage I/II and stage III/IV) for 24 hours. Phagocytic activity was assessed using pHrodo *E. coli* deep red bioparticles and compared as fold change to a) untreated cells and among different PF groups (control (CON): n=5, endometriosis stage I/II (EM I/II): n=11, endometriosis stage III/IV (EM III/IV): n=6). Fold change was calculated by dividing the pHrodo deep red MFI of PF-treated cells by the mean pHrodo deep red MFI of untreated cells from three wells. Data are presented as mean ± SD. One-way ANOVA with Turkey's multiple comparisons (Shapiro-Wilk test: $p > 0.05$), *$P<0.05$, **$P<0.01$.

4.3.2.4 Investigating the effect of PF from Endometriosis and Control Patients on Macrophage Phagocytosis using pMΦ

Next, I validated these findings using primary human pMΦ. First, I examined the phagocytic activity of primary pMΦ isolated from two patients: one control patient and one endometriosis stage I patient. Notably, macrophages derived from the endometriosis patient exhibited lower phagocytic activity compared to those from the control patient (Figure 4.16a). This observation aligns with clinical findings of impaired macrophage function in endometriosis patients (262).

Next, the phagocytic activity of the control and endometriosis primary pMΦ were examined following treatment with either 5% (v/v) PF from control patients (n=3) or endometriosis stage IV patients (n=3). The control primary pMΦ responded similarly to THP-1 derived macrophages, whereby there was a significant reduction in phagocytic activity when treated with PF from endometriosis patients compared to treatment with PF from control patients (Figure 4.16b). In contrast, treatment with PF had no effect on the phagocytic activity of primary pMΦ isolated from the endometriosis patient (Figure 4.16b).

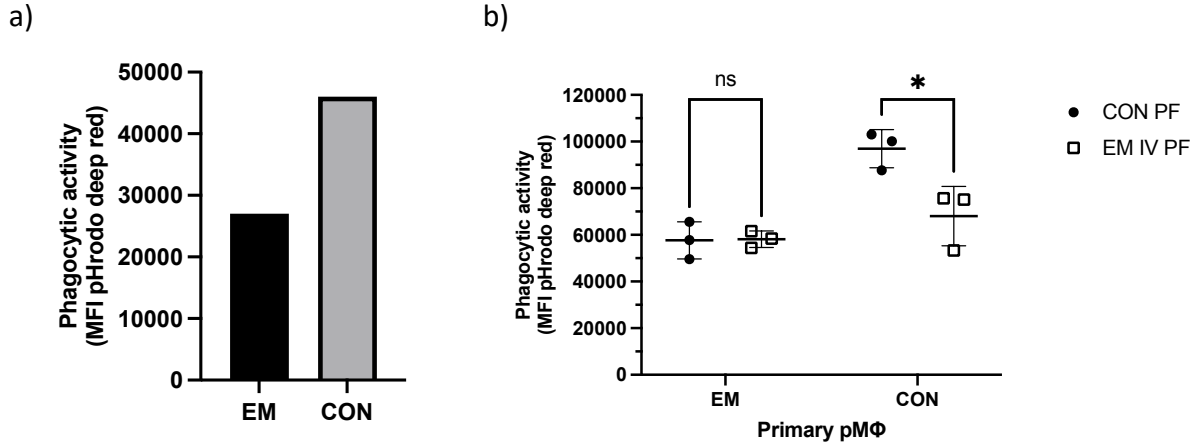

Figure 4.16. Flow cytometry analysis examining the effect of PF on phagocytic activity of primary pMΦ. Primary pMΦ were isolated from a control patient and a patient with stage I endometriosis. Phagocytic activity was assessed using pHrodo *E. coli* deep red bioparticles by flow cytometry at a) baseline and b) after 24h treatment with 5 % (v/v) PF from control patients and endometriosis stage IV patients (n=3). EM=endometriosis patients; CON=control patients. Bars = mean ± SD. Two-way ANOVA with Turkey's multiple comparisons (Shapiro-Wilk test: $p > 0.05$), *$p<0.05$.

4.3.3 The effect of PF-sEV on macrophage phagocytosis

Given that PF from endometriosis patients significantly suppresses macrophage phagocytosis, I next investigated whether PF-sEV from these patients contribute to this observed suppression of macrophage phagocytic activity.

4.3.3.1 Examining the interaction of PF-sEV and pHrodo *E.coli* deep red bioparticles with macrophages by confocal microscopy

First, the uptake of PF-sEV ($1x10^{10}$ EV/ml) and pHrodo *E.coli* deep red bioparticles by macrophages were visualised under confocal microscopy (Figure 4.17). PKH26-labeled PF-sEV were located on the surface and inside THP-1 derived M0 macrophages. The visualization also demonstrated that the same cells capable of engulfing the pHrodo *E. coli* deep red bioparticles also interacted with the PKH26-labeled PF-sEV.

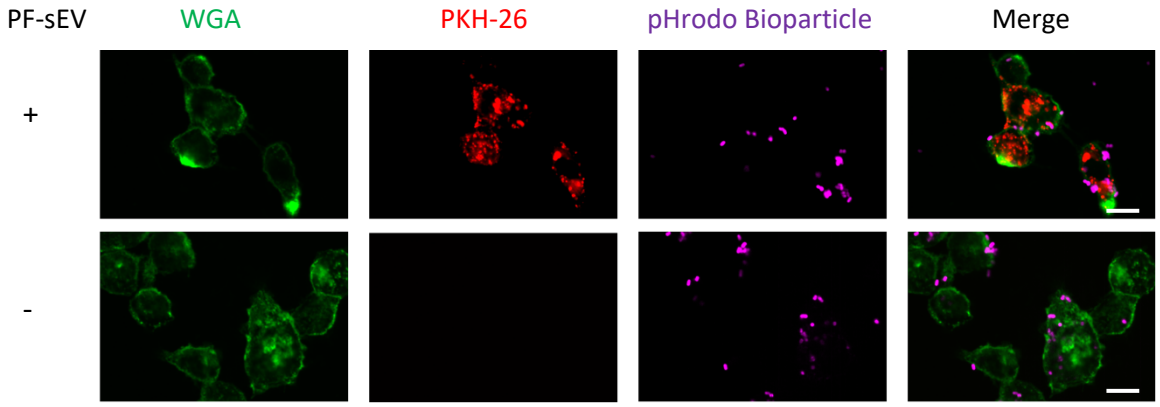

Figure 4.17. Visualisation of the Uptake of PF-sEV by macrophages and co-localization with phagocytosed *E. coli* bioparticles by confocal microscopy. THP-1-derived M0 macrophages were incubated with pHrodo *E. coli* deep red bioparticles (Purple) in the presence (+) or absence (-) of PF-sEV (PKH-26 labelled, red) pre-treatment for 24h. Cell membranes were stained with WGA (Wheat Germ Agglutinin, Green). Scale bar=10 µm.

4.3.3.2 Investigating the effect of PF-sEV on phagocytic activity of THP-1 derived M0 and M2 macrophages by flow cytometry

The direct effects of PF-sEV on macrophage phagocytosis were again assessed using THP-1 derived M0 and M2 macrophages and pHrodo *E.coli* deep red bioparticles. Macrophages

were treated with PF-sEV for 24h at a physiological concentration of $1x10^{10}$ EV/mL, as determined in Chapter 3.

In M0 macrophages, PF-sEV from both stage I/II and stage III/IV endometriosis patients significantly suppressed phagocytic activity compared to PF-sEV from control patients (P<0.01 and P<0.05, respectively) (Figure 4.18a). M2 macrophages treated with PF-sEV from endometriosis patients again exhibited significantly lower phagocytic activity compared to those treated with PF-sEV from control patients (stage I/II: P<0.01; stage III/IV: P<0.05) (Figure 4.18b). While there was no statistically significant difference between the effects of stage I/II and stage III/IV PF-sEV, those from stage I/II led to a greater average reduction in phagocytic activity but with more variation compared to stage III/IV PF-sEV.

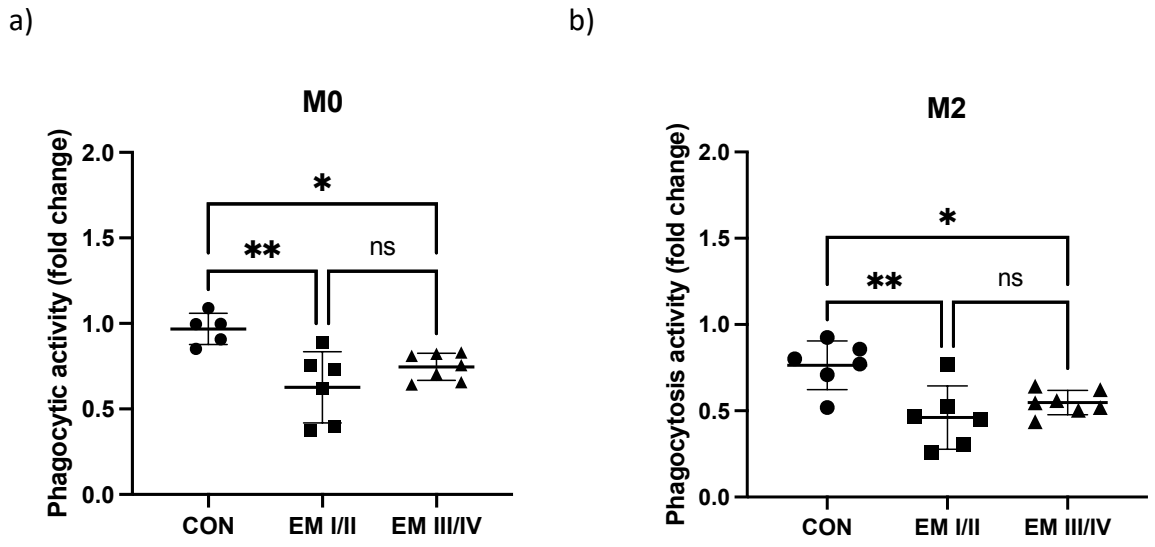

Figure 4.18. Flow cytometry analysis of phagocytic activity in THP-1 derived macrophages treated with PF-sEV from control and endometriosis patients. THP-1-derived a) M0 and b) M2 macrophages were treated with $1x10^{10}$ EV/mL PF-sEV from control or endometriosis patients (stage I/II and stage III/IV) for 24 hours. Phagocytic activity was assessed using pHrodo *E. coli* deep red bioparticles and compared as fold change to different PF-sEV groups (control (CON): n=5, endometriosis stage I/II (EM I/II): n=6, endometriosis stage III/IV (EM III/IV): n=7). Fold change was calculated by dividing the deep red MFI of PF-sEV-treated cells by the mean deep red MFI of untreated cells from three wells. Data are presented as mean ± SD. One-way ANOVA with Turkey's multiple comparisons (Shapiro-Wilk test: p > 0.05), *P<0.05, **P<0.01.

4.3.3.3 Investigating the effect of PF-sEV from endometriosis and control patients on macrophage phagocytosis using pMΦ

To validate suppression of phagocytic activity of PF-sEV from endometriosis patients observed in the THP-1 derived macrophages, I examined the effect of PF-sEV on pMΦ from one control patient. The flow cytometry results showed that incubation with PF-sEV from endometriosis stage IV patients significantly suppressed the phagocytic activity of the pMΦ compared to incubation with PF-sEV from control patients ($P<0.05$) (Figure 4.19).

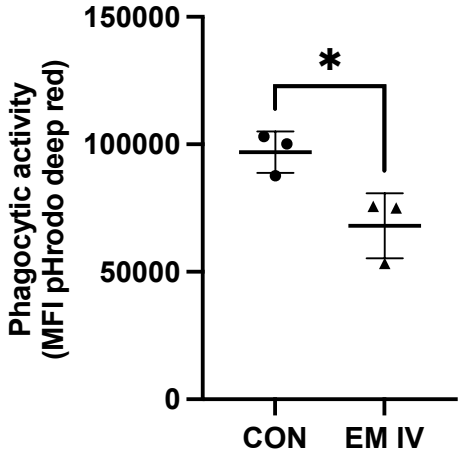

Figure 4.19. Flow cytometry analysis of the effect of PF-sEV on phagocytic activity of primary pMΦ. Primary pMΦ were isolated from a control patient. Phagocytic activity was assessed using pHrodo *E. coli* deep red bioparticles by flow cytometry after 24h treatment with $1x10^{10}$ PF-sEV from control patients (CON) and endometriosis stage IV patients (EM IV) (n=3). Bars = mean ± SD. Unpaired two-tailed *t*-test (Shapiro-Wilk test: $p > 0.05$), *$p<0.05$.

4.3.3.4 Investigating the effect of EV depletion on the phagocytosis-modulating effects of PF

The previous experiments demonstrated that PF-sEV, particularly from endometriosis patients, have a suppressive effect on macrophage phagocytic activity. To further investigate these findings, I compared the effects of PF and EV-depleted PF on THP-1 derived M0 and M2 macrophages.

EV depletion of PF was achieved through ultracentrifugation at 150,000g for 4 hours. To confirm the efficacy of this depletion process, NTA was performed. NTA results

demonstrated a significant reduction in EV levels in the depleted PF (P<0.0001) (Figure 4.20). On average, 89% ± 32% (mean ± SD) of EV were depleted.

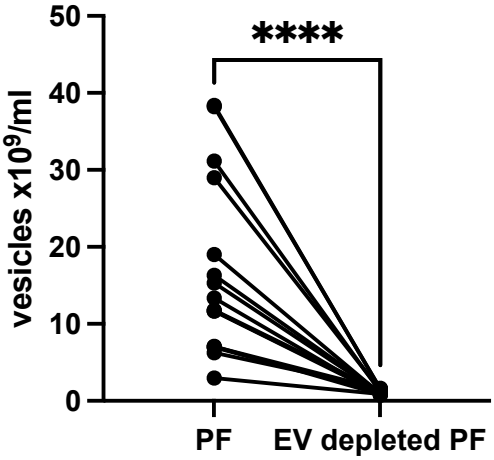

Figure 4.20. Efficacy of EV depletion from PF samples (n=16). NTA of EV concentration of PF samples before and after ultracentrifugation at 150,000g for 4 hours. Each line represents an individual PF sample. Paired two-tailed Wilcoxon-test (Shapiro-Wilk test: p < 0.05), ****p<0.0001.

Following the EV depletion process, 5% (v/v) of EV-depleted PF were added to THP-1 derived M0 and M2 macrophages for 24h and phagocytosis activity was assessed.

In M0 macrophages, for control patients, the depletion of sEV did not significantly alter the phagocytic activity compared to PF (Figure 4.21a). In contrast, for the endometriosis group (stage I/II and stage III/IV), EV-depleted PF led to significantly higher phagocytic activity compared to PF in M0 macrophages (P<0.0001, P<0.05 respectively) (Figure 4.21a).

In M2 macrophages, similar patterns were observed. EV depletion did not affect the PF-mediated regulation of phagocytic activity in the control group while EV depletion led to significantly higher phagocytic activity in stage I/II and stage III/IV (P<0.0001, P<0.01 respectively) (Figure 4.21b).

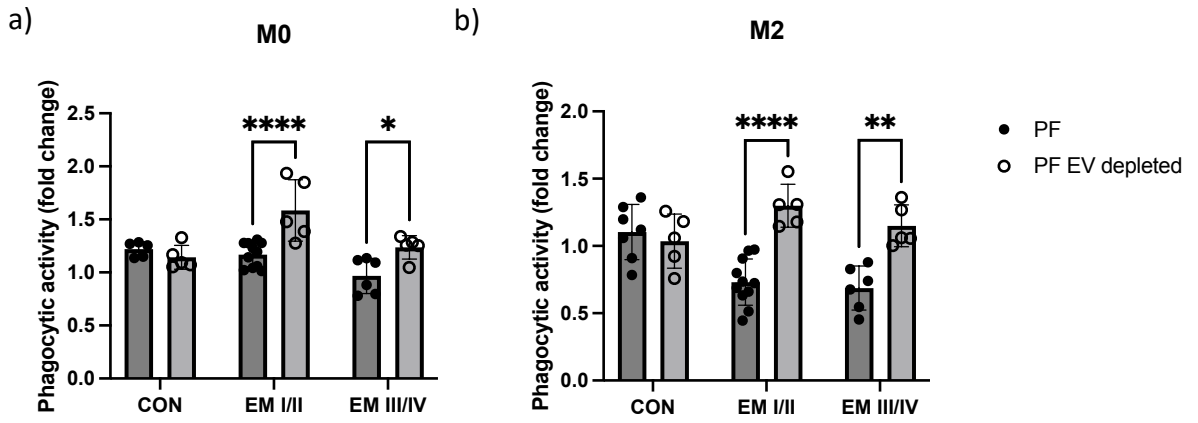

Figure 4.21. Effect of EV-depleted PF on phagocytic activity of THP-1 derived macrophages. THP-1-derived a) M0 and b) M2 macrophages were treated with 5% (v/v) EV-depleted PF from control (n=5) and endometriosis patients (stages I/II and III/IV; n=6) for 24 hours. Phagocytic activity was assessed using pHrodo *E. coli* deep red bioparticles by flow cytometry and compared PF and EV-depleted PF treated cells. Fold change was calculated by dividing the deep red MFI of PF-sEV-treated cells by the mean deep red MFI of untreated cells from three wells. Data are presented as mean ± SD. Two-way ANOVA with Turkey's multiple comparisons (Shapiro-Wilk test: $p > 0.05$), *P<0.05, **P<0.01, ****P<0.0001.

4.3.4 The effect of PF-sEV on macrophage cytokine secretion

While phagocytosis is a key component of macrophage-mediated immune responses, the secretion of cytokines plays a vital role in regulating inflammatory and immunoregulatory processes in the peritoneal microenvironment. Therefore, in this section I investigated the impact of PF-sEV on cytokine production of macrophages.

The study employed a combination of CBA and ELISA techniques to assess cytokine secretion in THP-1-derived macrophages. THP-1 derived M0, M1 and M2 macrophages were treated with $1x10^{10}$ EV/mL of PF-sEV isolated from one control patient and one endometriosis patient.

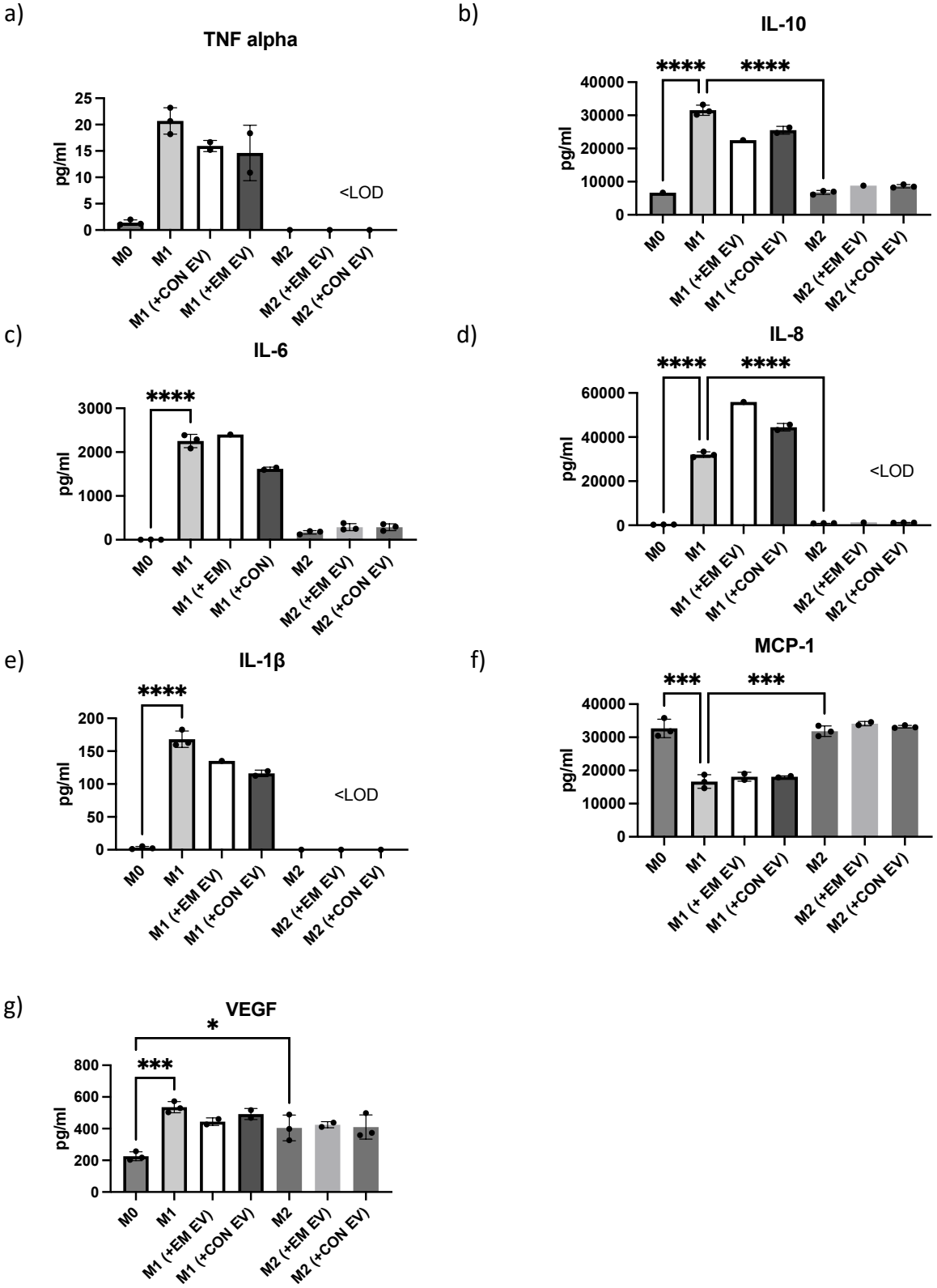

Figure 4.22. Cytokine secretion profiles of THP-1-derived macrophages in response to PF-sEV treatment. The secretion of a) TNF-alpha, b) IL-6, c) IL-1β, d) IL-10, e) IL-8, f) MCP-1, and g) VEGF of THP-1 derived macrophages (M0, M1, M2) and THP-1 derived macrophages (M1, M2) treated with PF-sEV from one control and one endometriosis patient were assessed by CBA array. Bars = mean ± SD. LOD, limit of detection. One-way ANOVA with Turkey's multiple comparisons (Shapiro-Wilk test: $p > 0.05$), *P<0.05, ***P<0.001, ****P<0.0001.

The analysis revealed distinct cytokine profiles among untreated M0, M1 (LPS+IFN- γ stimulated), and M2 (IL-4 +IL-13 stimulated) macrophages (Figure 4.22). TNF-alpha, IL-6, and IL-1β were exclusively detectable in M1 macrophages, consistent with their pro-inflammatory phenotype (Figure 4.22a, c, e). IL-10, IL-8, MCP-1, and VEGF were detected in both M1 and M2 macrophages (Figure 4.22b, d, f, g). IL-8 secretion is significantly higher in M1 than M2 macrophages (Figure 4.22e). Surprisingly, IL-10, the anti-inflammatory cytokine secretion was significantly higher in M1 than M2 macrophages (Figure 4.22b). Generally, cytokine levels were elevated in M1 or M2 macrophages compared to M0 macrophages, with some exceptions. MCP-1 secretion was suppressed in M1 macrophages compared to M0 but remained at similar levels between M0 and M2 (Figure 4.22f).

Treatment with PF-sEV led to changes in cytokine profiles. In M1 macrophages, PF-sEV incubation suppressed IL-10, IL-1β, and TNF-alpha secretion compared to untreated cells. Conversely, IL-8 and MCP-1 secretion were increased after PF-sEV treatment in M1 macrophages. Interestingly, IL-6 secretion showed a differential response: PF-sEV from endometriosis patients led to elevation compared to untreated M1 macrophages, while PF-sEV from control patients led to suppression. In M2 macrophages, all cytokine secretions were elevated after PF-sEV incubation, suggesting a general enhancement of the M2 phenotype.

ELISA validation of IL-10 and IL-6 secretion confirmed the trends observed in the CBA, although absolute values were lower, likely due to sample freezing (Figure 4.23a, b). Additionally, TGF- β1 levels, assessed by ELISA, were significantly higher in M2 macrophages compared to M0 macrophages (Figure 4.23c). Notably, PF-sEV treatment led to an 8-fold increase in TGF- β1 secretion levels in M2 macrophages.

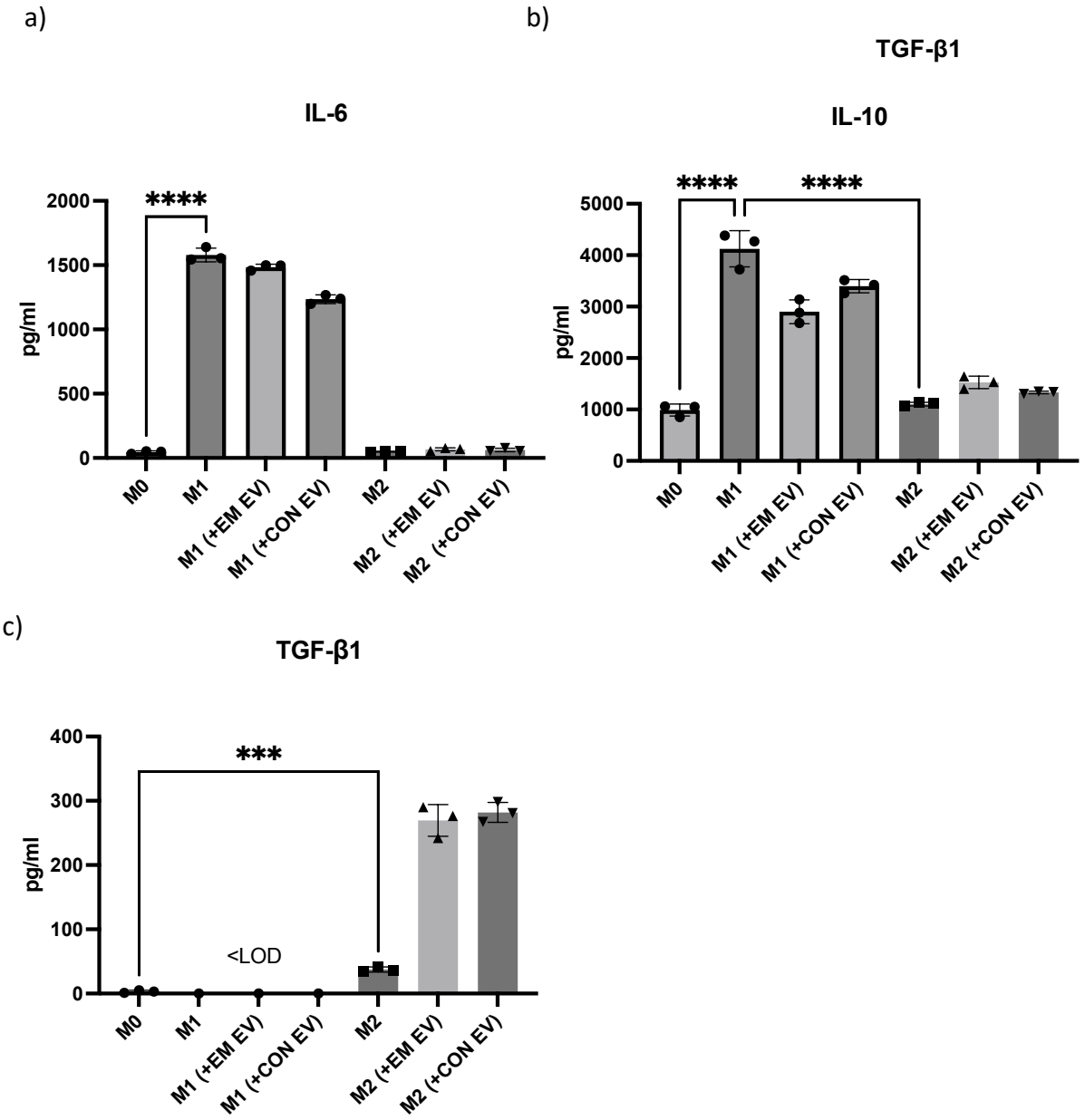

Figure 4.23. Cytokine secretion by THP-1-derived macrophages. The secretion of a) IL-10, b) IL-6, and c) TGF-β1 of THP-1 derived macrophages (M0, M1, M2) and THP-1 derived macrophages (M1, M2) treated with PF-sEV from one control and one endometriosis patient were assessed by ELISA. Bars = mean ± SD. One-way ANOVA with Turkey's multiple comparisons (Shapiro-Wilk test: $p > 0.05$), ***P<0.001, ****P<0.0001.

It is important to note that statistical analysis was only performed for untreated M0, M1, and M2 macrophages, while PF-sEV groups were analysed for trends without statistical analysis due to limited sample size (n=1 per group).

4.3.5 Investigation of 'don't eat me' signals in PF-sEV meditated regulation of macrophage phagocytosis

As previously demonstrated in Section 4.3.3, PF-sEV from endometriosis patients significantly suppress the phagocytic activity of macrophages. To understand the molecular mechanisms underlying this suppression, I focused on the role of 'don't eat me' signals, CD24/Siglec-10, CD47/SIRP-α, and PD-L1/PD-1, which are known regulators of phagocytosis (181). Previous PF-sEV characterisation by MACSPlex EV kit IO has shown high expression of CD24, one of the 'don't eat me' signals. Therefore, I first explored the expression of additional 'don't eat me' ligands, CD47 and PD-L1, on PF-sEV. Following analysis examined their corresponding receptors Siglec-10, SIRP-α and PD-1 on macrophages. Furthermore, I conducted blocking experiments to determine whether these signalling pathways play a functional role in regulating the phagocytic activity of macrophages.

4.3.5.1 Expression of 'don't eat me' ligands on the surface of PF-sEV

To expand the analysis to include CD47 and PD-L1, which are not part of the standard MACSPlex EV kit IO panel, I employed a modified protocol adapted from the literature (291). Initial experiments were conducted using pooled PF-sEV samples at concentrations of $1x10^9$ EV/mL and $2x10^9$ EV/mL for both CD47 and PD-L1 detection (Figure 4.24). CD47 analysis demonstrated a clear dose-response effect. At $1x10^9$ EV/mL, six markers (CD9, CD81, CD44, CD24, CD133/1, HLA-DR) showed higher MFI compared to negative control (PBS) and isotype controls (Figure 4.24a). Increasing the concentration to $2x10^9$ EV/mL expanded the number of positive markers to 12, adding ROR-1, CD29, CD8, CD14, EpCAM, and CD40 to the list (Figure 4.24a). This concentration-dependent increase in detectable markers suggests that CD47 is present on PF-sEV and can be reliably detected using this modified protocol.

In contrast, the detection of PD-L1 on PF-sEV was hindered by technical limitations (Figure 4.24b). Flow cytometric analysis revealed no dose-response effect between $1x10^9$ and $2x10^9$ EV/mL concentrations in MFI expression. Moreover, the selection of positive markers was prevented due to high MFI values in the negative control. These technical challenges

highlighted the need for further optimisation when trying to analyse PD-L1 using the MACSPlex EV kit IO.

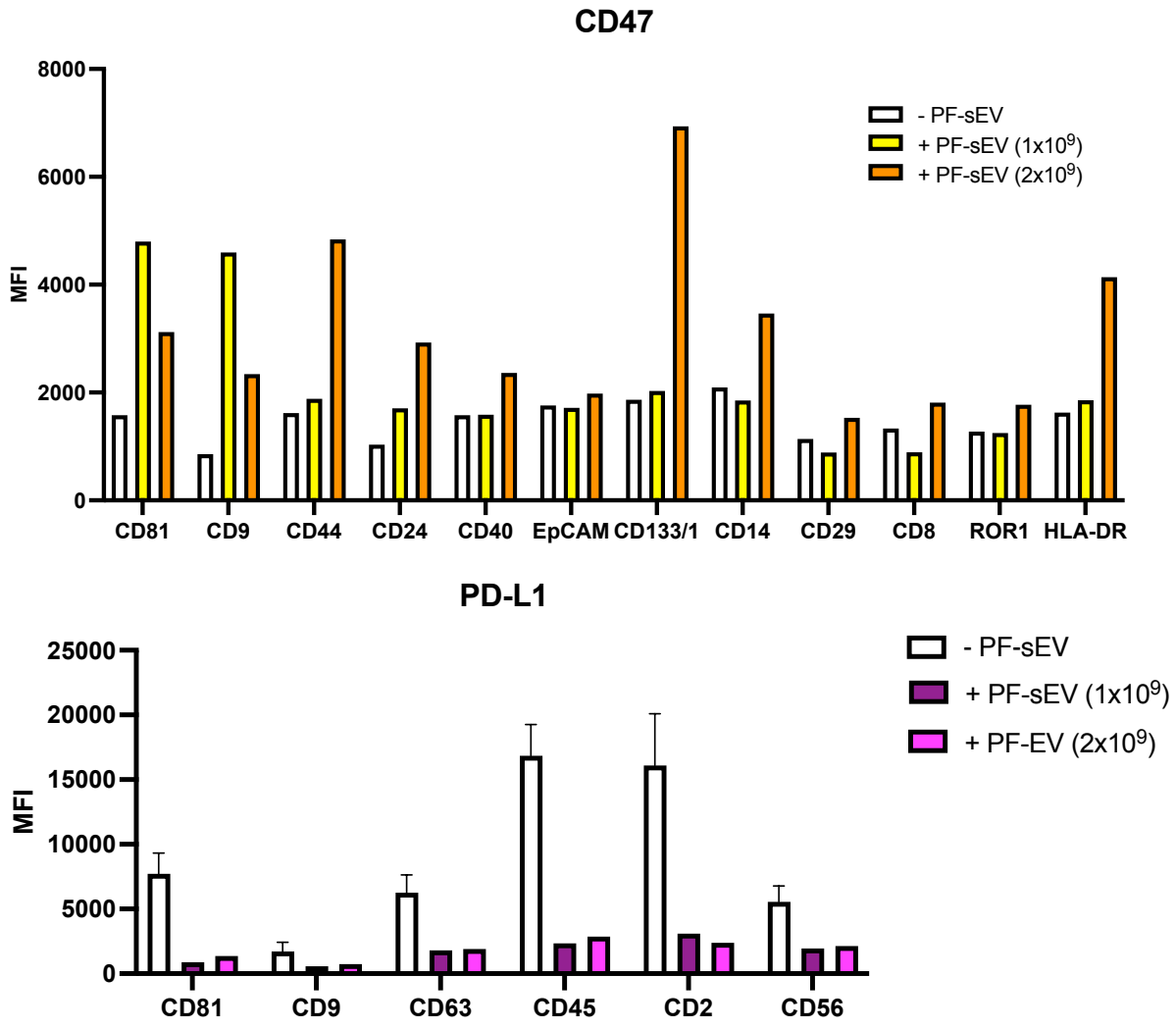

Figure 4.24. Flow cytometry analysis of co-expression of CD47 and PD-L1 with various markers on PF-sEV utilising a modified MACSPlex EV protocol. The co-expression of CD47 and PD-L1 with a panel of 37 markers in the MACSPlex EV kit IO was assessed. Pooled PF-sEV (n=1) were analysed at concentrations of $1x10^9$ and $2x10^9$ EV/mL. PF-sEV were incubated with capture beads from the MACSPlex EV kit and subsequently with a) anti-CD47 APC antibody or b) anti-PD-L1 APC antibody. For PD-L1, the negative control represents the mean of two measurements ± SD. Capture beads with detection antibody alone served as a negative control (- PF-sEV) to evaluate non-specific binding. Markers were considered positive if their signal exceeded both the respective isotype control (mIgG or REA) and the negative control.

4.3.5.2 Investigating the co-expression of CD47 on PF-sEV in control and endometriosis patients

Following the initial detection of CD47 on pooled PF-sEV samples, the expression pattern in individual patient samples was assessed by an MSc student. To establish the optimal PF-sEV concentration for reliable CD47 detection, a titration experiment was performed using samples from three endometriosis patients. The experiment tested concentrations of $2x10^9$, $4x10^9$, and $6x10^9$ EV/mL, with positive markers identified and listed for each concentration (Figure 4.25).

The results revealed a concentration-dependent increase in the number of markers co-expressed with CD47. At both $2x10^9$ and $4x10^9$ EV/mL, 16 proteins demonstrated co-expression with CD47. However, when the concentration was increased to $6x10^9$ EV/mL, the number of co-expressed markers rose to 19. Moreover, the highest concentration yielded the most consistent results across the three patients, with seven proteins consistently expressed, compared to three at $4x10^9$ EV/mL and two at $2x10^9$ EV/mL. Therefore, $6x10^9$ EV/mL was chosen for the following analysis of 5 endometriosis patients and 5 controls.

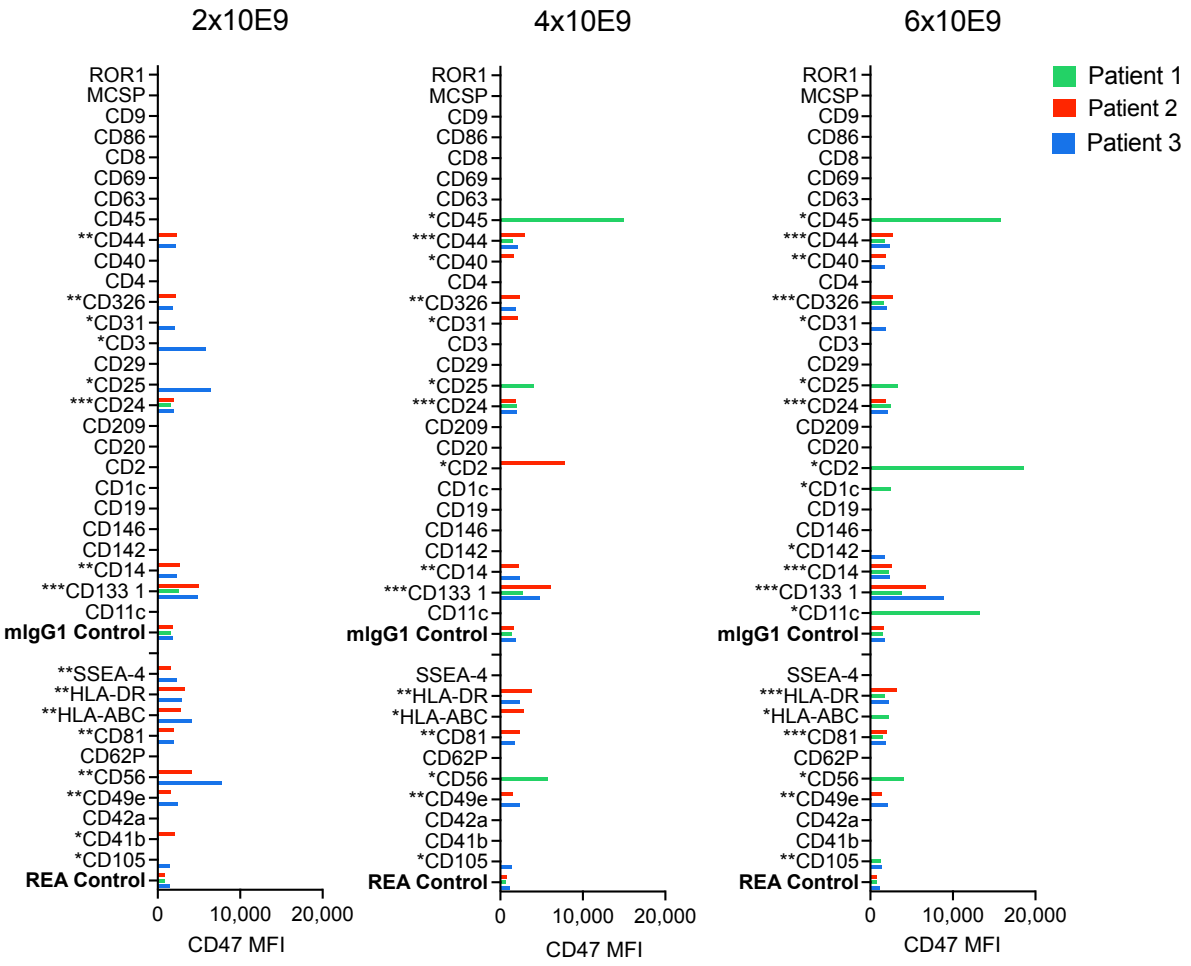

Figure 4.25. Titration experiment of PF-sEV input for CD47 co-expression using the MACSPlex EV kit IO (n=3). PF-sEV were isolated from three individual endometriosis patients: Patient 1 (green), Patient 2 (red), and Patient 3 (blue). The co-expression of markers with CD47 on PF-sEV of each patient's sample was analysed at three different concentrations: a) $2x10^9$ EV/mL, b) $4x10^9$ EV/mL, and c) $6x10^9$ EV/mL. *** = expressed by three patients; ** = expressed by two patients; * = expressed by one patient. Data produced by an MSc student.

CD47 was present on PF-sEV in all 10 patients (Figure 4.29). In total, CD47 was shown to be co-expressed with 34 of the 37 markers examined, whereby 22 of these were found in both control and endometriosis patients. These include CD81, CD9, CD133/1, EpCAM, CD24 and CD14 (Figure 4.26). A small proportion of markers co-expressing CD47 were found exclusively in control or endometriosis patients.

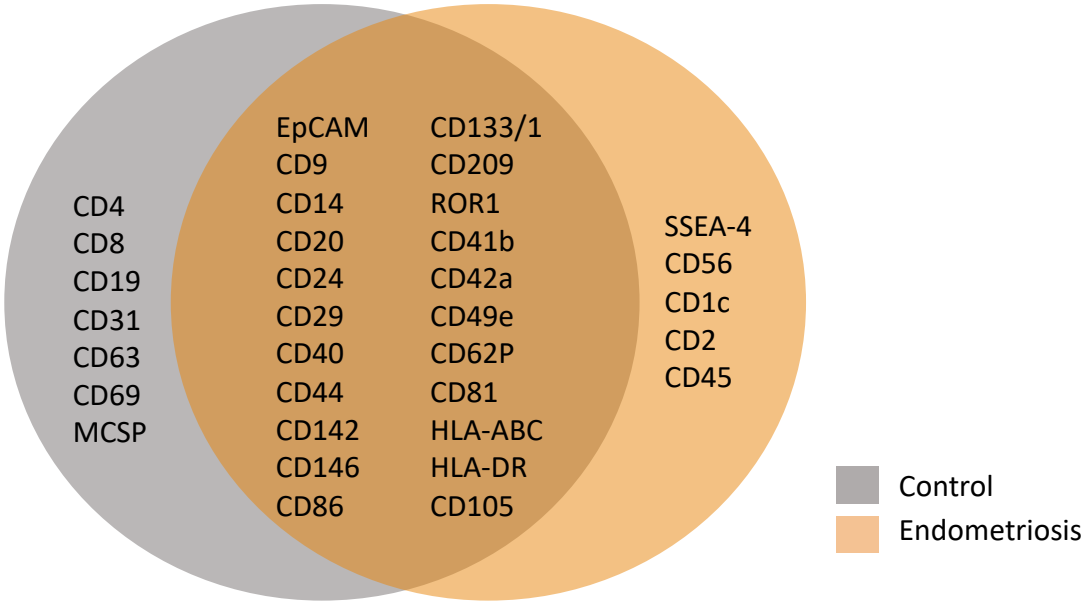

Figure. 4.26. Co-expression analysis of CD47 on PF-sEV in control and endometriosis patients. A Venn diagram was constructed to visualize the distribution of co-expressed markers with CD47 on PF-sEV between the control (n=5) and endometriosis (n=5) groups. Data produced by an MSc student.

4.3.5.3 Expression of *'don't eat me' receptors* on macrophages

Given that PF-sEV express CD24 and CD47, next, I examined whether macrophages express the respective receptors. The findings in Section 4.3.3 demonstrate that PF-sEV from endometriosis patients have a suppressive effect on phagocytic activity in both M0 and M2 macrophages, with the effect being more pronounced in M2 macrophages. As M2-like subtypes have been linked to the pathogenesis of endometriosis, this section explored the potential mechanisms by which PF-sEV regulate macrophage phagocytosis, focusing on THP-1 derived M2 macrophages.

The expression of the corresponding receptors of CD24 (Siglec-10), CD47 (SIRP-α) and PD-L1 (PD-1) were examined on both THP-1 derived M2 macrophages and primary pMΦ from three endometriosis patients using flow cytometry. In THP-1 derived M2 macrophages, SIRP-α was highly expressed (Figure 4.27a), while Siglec-10 expression was found to be absent (Figure 4.27c). PD-1 expression was not detected in THP-1 derived macrophages (Figure 4.27e).

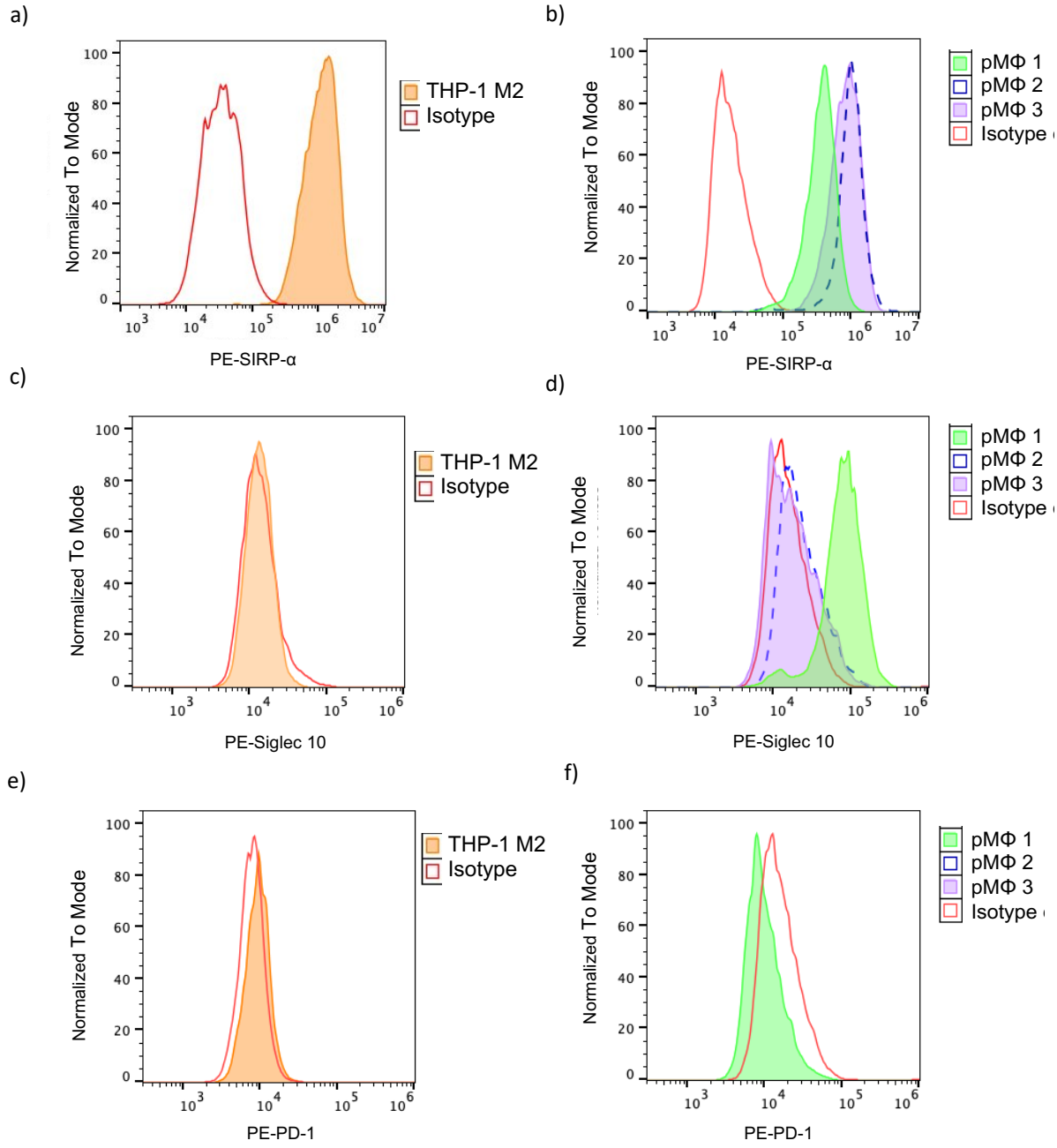

Figure 4.27. Expression of Siglec-10, SIRP-α, and PD-1 on macrophages. Histograms showing flow cytometry analysis of receptor expression relevant to the respective isotype control (red line): SIRP-α expression on a) THP-1 derived M2 macrophages and b) pMΦ (n=3, pMΦ1-3), Siglec-10 expression on c) THP-1 derived M2 macrophages and d) pMΦ pMΦ (n=3, pMΦ1-3), PD-1 expression on e) THP-1 derived M2 macrophages and f) pMΦ pMΦ (n=1, pMΦ1).

Regarding primary pMΦ, SIRP-α was highly expressed in all three pMΦ samples (Figure 4.27b). Siglec-10 expression showed variability among pMΦ samples, with pMΦ 1 showing

a 70% positive population, while no expression was detected in pMΦ 2 and 3 (Figure 4.27d). Similar to THP-1 derived macrophages, PD-1 expression was not detected in any of the pMΦ samples (Figure 4.27f).

These results showed that CD47 is expressed on the surface of PF-sEV, and its receptor SIRP-α is highly expressed on THP-1 derived M2 macrophages and primary pMΦ, suggesting physiological relevance. In contrast, although CD24 is highly expressed on PF-sEV, Siglec-10 expression varied between primary pMΦ and was absent on THP-1 derived macrophages. PD-L1 was not detected on PF-sEV and PD-1 was absent on both THP-1 derived M2 macrophages and primary pMΦ.

Given these findings, CD47-SIRP-α interaction could be a potential mechanism for PF-sEV-mediated regulation of macrophage function that could be investigated in a THP-1 *in vitro* model. To test this hypothesis, I next aimed to block the CD47-SIRP-α interaction to further investigate the mechanism.

4.3.5.4 Investigating the effect of blocking CD47 on PF-sEV on regulating macrophage phagocytosis

To target CD47-mediated SIRP-α signalling, CD47 on the surface of PF-sEV (n=9: 4 control and 5 endometriosis (3 stage III/IV and 2 stage I/II)) was disrupted using a blocking anti-CD47 monoclonal antibody (anti-CD47 PF-sEV) or with an isotype-matched mouse IgG control (IgG PF-sEV).

The phagocytic activity of THP-1 derived M2 macrophages was assessed following treatment with IgG PF-sEV or anti-CD47 PF-sEV from endometriosis patients or controls. M2 macrophages treated with IgG PF-sEV from endometriosis patients showed a significant reduction ($P<0.01$) in phagocytic activity compared to those treated with IgG PF-sEV from control patients (Figure 4.28), aligning with previous findings shown in Figure 4.20b in Section 4.3.3.2.

Macrophages treated with anti-CD47 PF-sEV from endometriosis patients showed elevation of phagocytic activity compared to those treated with IgG PF-sEV from endometriosis patients (Figure 4.28), indicating the potential role of CD47 in regulating macrophage phagocytosis in endometriosis. The phagocytic activity of macrophages treated with anti-CD47 PF-sEV from endometriosis patients approached levels similar to those treated with IgG PF-sEV from control patients, suggesting that CD47 blockade could potentially normalize the impaired phagocytic function associated with endometriosis.

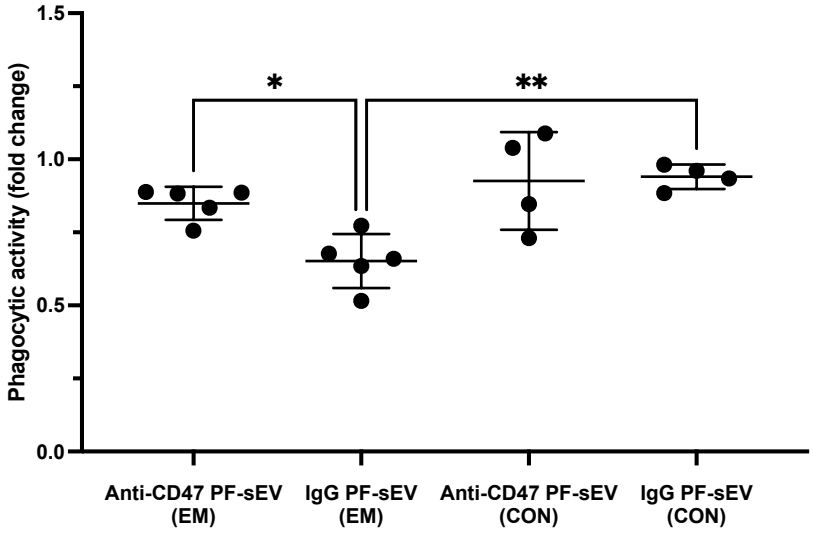

Figure 4.28. Flow cytometry analysis of the effect of blocking CD47 on PF-sEV on regulating macrophage phagocytosis. THP-1 derived M2 macrophages were treated with PF-sEV from endometriosis patients (EM, n=5: 3 stage III/IV and 2 stage I/II) or controls (CON, n=4), pre-incubated with either IgG (control) or anti-CD47 antibodies. Phagocytic activity was assessed using pHrodo *E. coli* Deep Red bioparticles. Fold change was calculated by dividing the deep red MFI of PF-sEV-treated cells by the mean deep red MFI of untreated cells from three wells. Bars = mean ± SD. One-way ANOVA with Turkey's multiple comparisons (Shapiro-Wilk test: $p > 0.05$), *P<0.05, **P<0.01.

4.4 Discussion

4.4.1 Variability in macrophage behaviour across in vitro models and protocols

In this chapter, I first investigated an *in vitro* model of macrophage differentiation and polarisation using U937 and THP-1 cell lines. PMA successfully induced differentiation in both cell lines, as evidenced by morphological changes, increased cell size, enhanced adherence and increased expression of CD14. However, the two cell lines exhibited distinct sensitivity patterns to PMA concentration.

U937 cells showed high sensitivity to PMA, reaching maximum differentiation at a relatively low concentration (2 ng/mL), with minimal additional changes at higher concentrations. In contrast, THP-1 derived macrophages displayed a more gradual, dose-dependent response to PMA, requiring a minimum concentration of 5 ng/mL for differentiation, with continued morphological changes and CD14 expression observed at higher concentrations, aligned with previous study (257).

Both U937 and THP-1 derived macrophages expressed M1 phenotypes after 24h of LPS and IFN- γ stimulation at 5ng/mL and 10ng/mL of PMA. When using IL-4 for stimulation, U937 was less responsive than THP-1 in expressing CD206. THP-1 derived macrophages differentiated using 10 ng/mL PMA were less responsive to CD206 expression compared to those differentiated with 5 ng/mL PMA. There was no increased CD163 expression detectable in both cell lines using these protocols. The results are consistent with reports from the literature that high PMA concentrations hindered M2 polarisation(253).

The expression pattern of CD14 on these two cell lines also revealed interesting findings. Low doses of PMA led to increased CD14 expression compared to undifferentiated cells, indicating maturation. However, with increasing PMA concentration, CD14 levels gradually decreased, especially in THP-1 derived macrophages. This may explain discrepancies in CD14 expression reported in the literature, as studies often use different PMA concentrations. For instance, one study demonstrated decreased CD14 expression in THP-

1 derived macrophages after PMA differentiation using 100 ng/mL PMA (256), while another reported increased CD14 expression following 20 ng/mL PMA stimulation (257).

The observations of CD14 expression after LPS stimulation provide additional insight. Although CD14 is a co-receptor for LPS and its upregulation was expected (294), high concentrations of LPS (100ng/mL) downregulated CD14 expression in THP-1 derived macrophages in this study. This could be due to accelerated internalization of CD14 in response to high levels of LPS (295). Similarly, PMA stimulation, which activates inflammatory signalling cascade genes, may lead to CD14 internalisation at higher concentrations. Another explanation is CD14 shedding observed after PMA stimulation (296). Interestingly, U937 cells exhibited CD14 downregulation at much lower PMA concentrations (5ng/mL) than THP-1 derived macrophages, with expression remaining constant despite further PMA increases. This suggests that U937 cells may be more sensitive to PMA-activated pro-inflammatory signalling pathways compared to THP-1 derived macrophages. The precise mechanism behind CD14 regulation in response to PMA stimulation and inflammatory stimuli requires further investigation to fully elucidate these cell line-specific differences.

Regarding macrophage polarisation, both U937 and THP-1 derived macrophages expressed M1 phenotypes after 24h LPS and IFN- γ stimulations at 5ng/mL and 10ng/mL PMA. However, significant differences were observed in response to IL-4 stimulation, which typically induces an M2 phenotype. U937 derived macrophages were found to have higher baseline CD206 and CD163 expression after PMA activation compared to THP-1 derived macrophages. Despite of this, U937 cells were less responsive to IL-4 stimulation in terms of further increasing CD206 expression. Moreover, 10 ng/mL PMA-differentiated THP-1 derived macrophages were less responsive to CD206 expression compared to those differentiated with 5 ng/mL PMA. This finding aligns with existing literature indicating that high PMA concentrations can hinder M2 polarisation, as reported in previous studies (253, 297).

Notably, CD163 expression elevation was not evident in either cell line with 24-hour protocols. However, 48-hour stimulation with IL-4 + IL-13 induced more robust M2 marker

expression, especially CD163, consistent with literature reporting higher mRNA expression of CD163 and CD206 compared to 24-hour stimulation (297). If CD163 is of particular interest, alternative polarization protocols could be considered. CD163 has been found to be more highly expressed in M2c subtypes stimulated by IL-10 than in M2a subtypes stimulated by IL-4 (298).

The experiments highlight the complex and cell-specific regulation in response to different stimuli, potentially reflecting distinct cellular activation mechanisms or thresholds in these monocytic cell lines. Considering the importance of anti-inflammatory subtypes in endometriosis, THP-1 derived macrophages were selected for subsequent experiments. 5ng/mL PMA and 48h IL-4 and IL-13 stimulation were chosen for M2 polarisation. 5ng/mL PMA was chosen for differentiation, and 48-hour stimulation with IL-4 and IL-13 was selected for M2 polarisation. Building upon this *in vitro* model, and the effects of PF and PF-sEV on macrophage phagocytosis and cytokine secretion were investigated. Fc receptor blocking was not included in the flow cytometry protocol, which may have led some degree of non-specific binding. This should be considered when interpreting the results.

4.4.2 Modulation of macrophage phagocytosis is both stage-dependent and phenotype-dependent in endometriosis

4.4.2.1 Optimisation

The study utilised pHrodo *E.coli* deep red bioparticles to quantitatively assess macrophage phagocytic activity. This methodology was validated in THP-1 derived macrophages through confocal microscopy. pHrodo *E.coli* deep red bioparticles exhibited pH-sensitive fluorescence, emitting signals only upon phagocytosis inside cells, with no fluorescence detected outside cells, thus confirming its efficacy. Flow cytometric analysis revealed a distinct dose-dependent response in phagocytosis, further corroborating the assay's sensitivity and reliability.

When comparing phagocytic activity of THP-1 derived M0, M1 and M2 macrophages, M2 and M0 macrophages demonstrated high phagocytic activity, while M1 macrophages showed low activity, possibly due to the suppression of phagocytic function by LPS stimulation (299). Based on these findings, M0 and M2 macrophages were selected as models for subsequent *in vitro* studies to mimic infiltrated monocyte-derived macrophages and tissue-resident macrophages in the peritoneal microenvironment of endometriosis, respectively (112).

4.4.2.2 The effect of PF on macrophage phagocytosis

The differential effects of PF on macrophage phagocytosis revealed to be both stage-dependent and phenotype dependent.

For M0 macrophages, treatment with PF from endometriosis rASRM stages III/IV have a significantly lower phagocytic activity compared to controls, whereas treatment with PF from stage I/II did not affect phagocytic activity. This suggests a dynamic change in the peritoneal microenvironment as the disease progresses, potentially reflecting a suppressive immune environment in later stages. This shift in the immune environment reflects the evolving nature of the disease, transitioning from an initial inflammatory response to a more established, growth-promoting state in later stages, which has been reported by many studies (300-302).

In THP-1 derived M2 macrophages, PF treatment from endometriosis patients (both rASRM stage I/II and stage III/IV) suppressed phagocytic activity compared to M2 macrophages treated with PF from control patients. The contrasting effects of PF from stage I/II patients on M0 and M2 macrophages highlighted the complexity of the peritoneal microenvironment in endometriosis. This divergence suggested that different macrophage subtypes might respond to stimuli differently. The distinct responses of M0 and M2 macrophages to the same PF indicated that the progression of endometriosis might be influenced by specific interactions between various macrophage phenotypes and the changing peritoneal environment, rather than by a uniform shift in macrophage function.

This was supported by the observed heterogeneity of pMΦ, which displayed both pro-inflammatory and anti-inflammatory characteristics (26, 118).

To validate the suppressive effect of PF from endometriosis patients observed in THP-1 derived macrophages, the effect of PF-sEV was also examined on pMΦ isolated from an endometriosis patient and a control patient. The results of pMΦ from the control patient confirmed the suppressive effect of PF from endometriosis patients on phagocytic activity observed in THP-1 derived macrophages. pMΦ from endometriosis patients exhibited lower baseline phagocytic activity than the control. While this finding is limited by the small sample size, it aligns with literature reporting impaired phagocytosis in pMΦ from endometriosis patients (26, 262). In addition, pMΦ from the endometriosis patient were unresponsive to phagocytic activity after stimulation with PF. This suggests intrinsic alterations in these cells that persist even when environmental stimuli are removed, pointing to possible long-term or epigenetic changes in their functions.

These findings on the effects of PF led to further investigation into the specific role of PF-sEV.

4.4.2.3 The effect of PF-sEV on macrophage phagocytosis

Direct treatment with PF-sEV revealed significant suppression of phagocytic activity in both THP-1 derived M0 and M2 macrophages, irrespective of the disease stage. This effect was particularly pronounced in M2 macrophages. Interestingly, the effects of PF-sEV differed from those observed with PF treatment, especially in M0 macrophages. While PF from rASRM stage I/II endometriosis patients did not significantly supress phagocytic activity, PF-sEV from stage I/II endometriosis patients did compared to PF-sEV from controls. This discrepancy suggests the presence of non-EV components in PF with phagocytosis-enhancing properties, counteracting the suppressive effects of PF-sEV.

To validate these findings observed in THP-1 derived macrophages, the effect of PF-sEV was also examined in pMΦ isolated from a control patient. The results corroborated the suppressive effect of PF-sEV from endometriosis patients on phagocytic activity. Specifically,

incubation with PF-sEV from endometriosis stage IV patients significantly suppressed the phagocytic activity of pMΦ compared to incubation with PF-sEV from control patients.

These findings collectively highlight the potent immunomodulatory role of PF-sEV in endometriosis, particularly their ability to suppress macrophage phagocytic function. The consistency of this effect across different macrophage models (THP-1 derived and primary pMΦ) emphasize its potential significance in the pathophysiology of endometriosis.

4.4.2.4 The effect of EV depletion on PF-mediated phagocytosis regulation

To further investigate the role of PF-sEV in modulating macrophage function, an alternative approach was employed. Instead of directly treating macrophages with isolated PF-sEV, I examined how the removal of these EV from PF affected macrophage phagocytosis.

In control patients, the depletion of PF-sEV did not significantly alter phagocytic activity compared to untreated cells or compared to PF in both M0 and M2 macrophages. This suggests that under normal conditions, PF-sEV may not play a major role in regulating macrophage phagocytosis.

Conversely, in endometriosis samples, PF-sEV removal significantly increased macrophage phagocytic activity compared to the PF group, indicating that endometriosis PF-sEV carry factors that actively suppress macrophage function irrespective of stage in both M0 and M2 macrophages.

The suppressive effect of PF-sEV from endometriosis patients was confirmed by the EV depletion study. For rASRM stage III/IV endometriosis, the PF-sEV suppressive effect is reflected in PF treatment, indicating its dominant role. However, in rASRM stage I/II endometriosis, the PF-sEV suppressive effect is not shown in PF-treated M0 macrophages. This indicates the potential counter-stimulatory effect in non-EV components, such as the presence of stimulatory factors like cytokines in the PF. For instance, IL-6, which is elevated in endometriosis PF (60, 61), has been shown to promote macrophage phagocytosis (62,

63). The role of these non-EV components in early-stage endometriosis requires further investigation.

4.4.2.5 Comparison with an existing study

One study attempted to investigate the effect of ectopic endometrial lesion EV on phagocytosis of macrophages, claiming that 'ectopic endometrium EV reduce phagocytic capacity of macrophages' (149). While this conclusion aligns with our current study, their experimental approach had several limitations.

The study by Huang et al. showed that THP-1 M0 macrophages were less likely to uptake PKH26 fluorescently labelled sEV from ectopic endometrium tissues compared to sEV from healthy serum samples. This approach has some drawbacks. EV uptake involves multiple routes, including membrane fusion and micropinocytosis as stated in Chapter 3 Section 1, not simply phagocytosis. Therefore, reduced uptake of labelled EV cannot be directly equated to reduced phagocytic activity. Methodologically, the study relied on confocal microscopy and fluorescent beads, and failed to distinguish between fluorescently labelled sEV inside cells or on the surface. Moreover, their evidence is presented without quantification, which limits the robustness of the conclusions. Furthermore, the study does not provide direct evidence of how sEV interaction affects the macrophages' ability to phagocytose other particles or cells.

In contrast, my current study employed a more robust methodology. Instead of assessing EV uptake, THP-1 -derived macrophages were pre-treated with PF-sEV and then tested for phagocytic activity using pHrodo *E.coli* deep red bioparticles. The bioparticles only fluoresce once inside macrophages, eliminating the ambiguity of surface-bound particles. Quantification was performed via flow cytometry, providing a more objective and quantifiable assessment of phagocytic activity. This approach allows for a more direct and quantitative measurement of how PF-sEV may affect macrophage phagocytic function, addressing the limitations of the previous study and providing stronger evidence for the conclusions.

4.4.3 PF-sEV affect cytokine secretion of macrophages

The next part of the study investigated the cytokine secretion profiles of THP-1-derived macrophages, revealing distinct patterns among M0, M1, and M2 phenotypes using CBA kits. After stimulation with LPS+IFN- γ or IL-4+IL-13, several notable changes in cytokine secretion levels were observed compared to M0 macrophages.

The secretion levels of IL-8, IL-10, and VEGF were found to be higher in stimulated macrophages compared to M0 macrophages. TNF-alpha, IL-6, and IL-1β were only detectable after LPS+IFN- γ stimulation, which is consistent with an M1 phenotype. In contrast, TGF-β1 was only detectable after IL-4+IL-13 stimulation, aligning with an M2 phenotype. MCP-1 levels decreased after treatment with LPS+IFN- γ.

An unexpected finding was that IL-10 expression was higher in M1 than M2 macrophages. IL-10 is generally considered an anti-inflammatory cytokine, often associated with M2 macrophages (303, 304). Additionally, higher cytokine secretion levels were observed in THP-1-derived M1 than M2 macrophages. These findings could be THP-1 specific or indicate suboptimal stimulation protocols for cytokine analysis. Future studies should consider time course analyses for each cytokine, as secretion levels may vary with stimulation duration (305), potentially clarifying these observations.

My study also examined the effects of PF-sEV on macrophage responses. Cells were pre-treated with PF-sEV for 24 hours before stimulation. Interestingly, PF-sEV pre-treatment made the cells less responsive to LPS+IFN- γ but more responsive to IL-4+IL-13, resulting in lower cytokine secretion levels in M1 and higher cytokine secretion in M2 compared to cells with no PF treatment. Apart from IL-8 and MCP-1, PF-sEV treatment led to higher secretion levels of these two factors in both M1 and M2 macrophages.

Importantly, potential disease-specific effects were observed in the study. PF-sEV from control subjects induced less IL-6 secretion, while PF-sEV from endometriosis patients induced more IL-6 secretion in M1 macrophages compared to untreated cells. This finding

suggests that the content or properties of PF-sEV may differ between symptomatic controls and those with endometriosis, potentially contributing to the inflammatory environment associated with the disease.

To validate the CBA results, IL-10 and IL-6 levels were confirmed by ELISA with three replicates per sample, indicating the reliability of the array data.

While these findings provide valuable insights into the effects of PF-sEV on macrophage cytokine secretion, it's crucial to interpret them with caution due to the limited sample size. The PF-sEV groups had only one sample per group (n=1), which significantly limits the generalizability of the results. Further studies with larger sample sizes will be essential to validate these observations and explore potential inter-individual variations in PF-sEV-mediated effects on macrophage function.

4.4.4 PF-sEV suppress phagocytosis via CD47/SIRP-α axis

Given the findings of the suppressive effect of PF-sEV from endometriosis patients on macrophage phagocytosis, subsequent investigations into 'don't eat me' signals focused on THP-1-derived M2 macrophages.

The CD47/SIRP-α pathway presented stronger evidence, with the existing literature reporting elevated expression of CD47 in endometriosis lesions (283, 284) and SIRP-α in pMΦ (285) in endometriosis. A modified MACSPlex EV kit IO protocol was employed to characterise the co-expression of CD47 with various markers on PF-sEV. Initial titration experiments demonstrated the success of these protocols in examining CD47 expression on PF-sEV. The experiments showed a dose-dependent response, with CD47 co-expression signal intensity increasing with PF-sEV concentration.

The co-expression analysis of CD47 was expanded as part of a separate MSc project by Malak Amer (under my co-supervision), incorporating 5 endometriosis patient and 5 control samples. CD47 was co-expressed in all 10 samples and commonly co-expressed with 22 out

of 34 markers including EpCAM, CD133/1, CD81, CD9 and CD24 in both endometriosis and control patients.

To further investigate the relevance of the CD47/SIRP-α axis in endometriosis and to assess the potential use of THP-1-derived macrophages as an *in vitro* model, SIRP-α expression was evaluated on both THP-1-derived M2 macrophages and pMΦ. The expression of SIRP-α was confirmed on both cell types. Based on these findings, I hypothesized that CD47 on PF-sEV interacts with SIRP-α on pMΦ, suppressing their phagocytic activity. To test this hypothesis, I investigated the interaction using THP-1-derived M2 macrophages as an *in vitro* model. The role of CD47/SIRP-α axis was examined by blocking CD47 on PF-sEV and observing the effects on macrophage phagocytosis.

The study attempted to investigate CD24/Siglec-10 and PD-1/PD-L1 pathways but faced limitations. The difficulties encountered in detecting PD-L1 on PF-sEV was due to non-specific binding of the antibody to the MACSPlex capture beads. The problem has been reported in previous research (143), therefore highlighting the technical challenges in studying EV-associated proteins beyond the pre-established panels using the MACSPlex EV kit IO. It emphasizes the need for optimized detection methods for each new detection antibody, as the standard protocols may not be universally applicable to all proteins of interest. It's receptor, PD-1 expression was not detected in pMΦ, but with only one sample (n=1), further optimization and replication are necessary. In addition, THP-1 did not express PD-1, thus, an alternative *in vitro* model is required.

In Chapter 2, CD24 was shown to be highly expressed on PF-sEV, as detected by the MACSplex EV kit IO. The study then aimed to characterize Siglec-10, the binding partner of CD24, on pMΦ from endometriosis patients. In a limited sample size of three, only one sample showed Siglec-10 expression in a proportion of pMΦ, while the other two exhibited no expression. Due to the small sample size, no definitive conclusions could be drawn about the role of CD24/ Siglec-10 as potential signalling pathways in regulating phagocytosis. Further studies including a larger sample size are necessary to properly characterize Siglec-10 expression on pMΦ in endometriosis, which have been shown to be elevated in ovarian cancer patients (223).

This chapter provides valuable insight into how PF-sEV suppress phagocytosis of macrophages via the CD47/SIRP-α axis. However, it's important to note that PF-sEV originate from multiple cell sources. The observation of suppressive effects in PF-sEV from endometriosis patients, but not in controls, indicates specific cell sources or phenotypes of these sEV, potentially coming from endometriosis lesions. sEV derived from ectopic endometrial stromal cells and ectopic endometrium tissues have been reported to polarize macrophages to M2 like phenotypes via EV (149, 150, 306). However, research on ectopic endometrial epithelial cell-derived sEV remains limited. Given that CD47 is co-expressed with EpCAM, ectopic endometrial epithelial cells emerge as a potential source of these immunomodulatory sEV. These aspects will be investigated in the next chapter.

4.4.5 Future Work

The sample size of this pilot study, particularly for the cytokine secretion profile analysis, offers an opportunity for expansion in future studies to further validate and extend these findings. Increasing the sample size in subsequent research would strengthen the statistical power and enhance the robustness of the result, revealing subtle effects that might be missed in a smaller sample cohort.

While pHrodo *E. coli* deep red bioparticles provided a reliable method for assessing phagocytic activity, they do not fully represent the pathophysiological processes in endometriosis. Macrophages should be phagocytosing endometrial tissues rather than bacterial particles. To increase clinical relevance, future work should focus on assessing the phagocytosis of endometrial stromal and epithelial cells.

The *in vitro* approach used in this study, while enabling controlled experiments, has limitations in fully representing the complex peritoneal environment found *in vivo*. Important factors such as cell-cell interactions, tissue architecture, and dynamic changes in the microenvironment are not adequately captured in this simplified model. Recent advancements in tissue engineering have led to the development of more

sophisticated models, such as hydrogel systems incorporating endometrial stromal and epithelial cells (307). Future research could focus on implementing them with macrophage and EV co-culture. This integrated approach would more closely mimic the intricate cellular interplay and environmental conditions present in the peritoneal cavity of endometriosis patients.

Current methods for measuring CD47 expression using the MACSPlex kit IO as co-expression with other EV markers have provided important data, but it's difficult to quantify and compare PF-sEV CD47 expression between endometriosis and control patients. While existing studies propose models for quantification (143), absolute expression levels of the protein of interest are still unknown. The challenges encountered in PD-L1 expression experiments highlight the complexity of these methods with cross-reacting between detection antibody and capture beads. Implementing single EV flow cytometry analysis in future studies could address these limitations in protein quantification and provide more precise measurements.

This study has identified CD47 as a potential mediator of PF-sEV effects on macrophage phagocytic activity, however, the precise molecular mechanisms underlying these changes warrant future investigation. The traditional M1/M2 classification of macrophages, while useful as a preliminary framework, is now considered outdated due to its oversimplification of macrophage phenotypes. Advances in transcriptomics have emphasised the value of expression profiling, which provides a more comprehensive and unbiased understanding of macrophages in disease microenvironment. Future studies combining EV RNA sequencing and proteomics analyses with single cell transcriptomic analysis of lesions could provide a comprehensive view of transcriptional changes, protein expression alterations, and signalling cascades activated by PF-sEV exposure. Integrating these diverse data sets would construct a more complete picture of the molecular events triggered by PF-sEV interaction with macrophages, potentially revealing novel therapeutic targets.

Interestingly, beyond direct interaction with inhibitory receptors, "don't eat me" signals like PD-L1 have been shown to transfer to the membrane of PD-L1-negative breast cancer cells via EV, facilitating immune evasion (308). This raises the intriguing possibility that EV-CD47

might similarly transfer to CD47 negative endometrial cells, potentially extending its immunomodulatory effects. Future studies should investigate whether such a transfer mechanism exists for CD47 in endometriosis.

In conclusion, while this study has provided important new insights into the role of PF and PF-sEV in modulating macrophage function in endometriosis, there is significant scope for future research to build upon these findings. Addressing the limitations identified and pursuing the suggested avenues for future work will contribute to a more comprehensive understanding of the complex immunological landscape of endometriosis, potentially leading to new diagnostic and therapeutic strategies for this challenging condition.

Chapter 5 Characterisation and functional analysis of endometrial epithelial organoid derived-sEV

5.1 Introduction

The endometrium, the inner lining of the uterus, plays a crucial role in reproductive health and is a site of significant interest in the study of various gynaecological disorders, including endometriosis (309, 310). Its structure includes the luminal epithelium (LE), which forms a single layer of pseudostratified cells lining the uterine cavity. Beneath this, a network of branching glandular epithelium (GE) consists of columnar cells. These epithelial structures are embedded in a supportive matrix of stromal fibroblasts. The endometrium also hosts various immune cells and is supplied by an intricate network of both blood and lymphatic vessels (311, 312).

Endometrial epithelial cells are characterised by columnar morphology and apical-basal polarity (313). The apical domain faces the uterine lumen and is specialized for secretion, absorption, and interaction with the external environment. It features microvilli to increase the surface area and tight junctions (313), marked by proteins like ZO-1, which forms a barrier between cells and controls paracellular transport (314). This domain is critical for the cyclical secretion of substances that support embryo implantation (315). The basal domain adheres to basement membrane and is characterised by components like laminin (316). This domain is crucial for cell-matrix adhesion and closely interacts with underlying stroma.

The endometrial epithelium responds to sex hormones that change during menstrual cycles (317), and plays a crucial role in embryo implantation (318). During the proliferative phase, rising oestrogen levels promote proliferation and growth of the endometrial epithelium, preparing it for potential implantation (317, 319). In the secretory phase, progesterone dominance induces maturation and differentiation into secretory and ciliated cells creating an environment conducive to embryo implantation (320). If implantation does not occur,

the drop in both hormones triggers menstruation, whereby the functional layer of the endometrium is shed (319, 320).

Endometriosis lesions, which are postulated to originate from endometrial tissue that is refluxed into the pelvic cavity via retrograde menstruation (321), also predominantly consist of endometrial stroma and glandular epithelium. (1, 322) (Figure 5.1). While these structures maintain a degree of polarity and glandular-like features, they exhibit significant morphological variations that set them apart from the typical glandular formations found in the eutopic endometrium (323, 324). Excessive oestrogen formation and activity within the lesion microenvironment has been linked to lesion growth (1).

Most published research focusing on endometriosis specific sEV has studied those derived from stromal cells, as they are easy to grow *in vitro* and are the most abundant cell type in the endometrium (310) and endometriosis lesions (325). sEV from ectopic endometrial stromal cells in endometriosis lesions have been found to promote lymph-angiogenesis, immune cell infiltration (326) and regulate macrophage polarisation (150). However, studies of sEV from endometrial epithelial cells from endometriosis patients are still lacking despite their potential importance. Epithelial cells harbour more oncogene mutations than stromal cells (327), and recent advances in spatial transcriptomics of endometriotic lesions have revealed that the endometrial epithelium plays a crucial role in modulating the local immune environment, particularly in relation to macrophages (328). Understanding EV profiles of endometrial epithelial cells may better explain how these cells contribute to endometriosis progression and presentation.

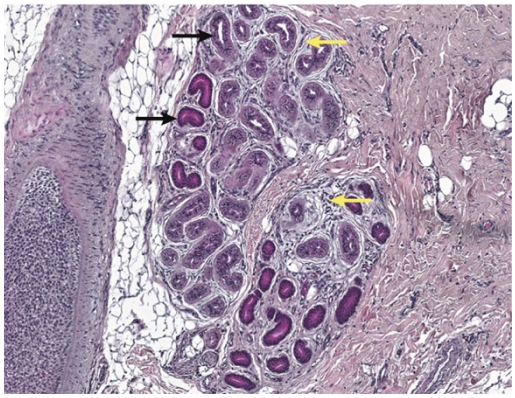

Figure 5.1. Histological section of a deep endometriosis lesion. Glandular epithelial cells are indicated by black arrows, while stromal cells are marked with yellow arrows. Magnification ×200. Adapted from Zondervan et al. 2018 (1).

Traditionally, research on epithelial cells has relied on 2D cell culture models. However, primary endometrial epithelial cells cannot easily and repeatably be passaged in 2D culture, and lose characteristics of *in vivo* endometrium, including polarity and responses to hormonal stimuli (329). To address these limitations, researchers have developed 3D culture systems supported by a gel matrix supplemented with essential growth factors. Endometrial epithelial organoids (EEO), 3D structures of endometrial epithelial cells, were first developed in 2017 (330, 331). EEO offer key advantages, including the ability to be passaged and maintain their structure over extended periods, making them ideal for long-term studies. This characteristic is particularly valuable for research into sEV, which often requires extended culture periods to generate sufficient material for analysis.

Another significant feature of EEO is their ability to recapitulate the polarised structure of the endometrial epithelium, with distinct apical and basal sides. It has been demonstrated that secretions from the apical and basal sides differ in their composition of metabolites and other biologically active molecules (332).

Furthermore, EEO can respond to hormonal stimuli *in vitro* that mimic the menstrual cycle, with oestrogen addition followed by progesterone. In response to progesterone, morphological changes and expression of secretory phase-specific markers progestogen-associated endometrial protein (PAEP) and secreted phosphoprotein one (SPP-1) are comparable to *in vivo* endometrium (330, 331).

One of the most significant advantages of EEO is their ability to be grown from ectopic endometriosis lesions, mimic diseases phenotypes and disease associated traits (107) and preserve DNA methylation alteration patterns (333). This capability allows for more physiologically relevant studies of endometrial pathology. Additionally, different expression of glycodelin A has been found in EEO from eutopic endometrium of endometriosis patients and healthy controls (334). While research on sEV specifically in endometriosis EEO is still limited, studies on related conditions provide valuable insights. For instance, sEV derived from EEO of adenomyosis, an endometrial disorder related to endometriosis in which epithelial and stomal cells grow into the myometrium, have been found to carry miRNAs involved in embryo implantation (335). This suggests that pathological changes affect EEO sEV profiles.

Given these findings, I propose sEV profiles of EEO will be affected by their polarity, hormone stimulation and endometriosis disease states. To investigate these hypotheses, I will implement standardized protocols for processing samples from eutopic endometrium collected via endometrium biopsy from both healthy women and those with endometriosis, as well as from endometriotic lesions, to grow EEO. In addition, the growth of EEO from fresh and frozen samples will be compared, the ability to grow EEO from frozen lesion tissue would be of great advantage, but methods are not published in the literature.

sEV isolation and characterisation will be based on established protocols mentioned in previous chapters, with modifications to accommodate the unique features of EEO cultures. I will use NTA and TEM to assess size distribution and concentration and the MACSPlex EV kit IO (Miltenyi Biotec, Germany) for surface marker expression analysis to comprehensively characterise the sEV.

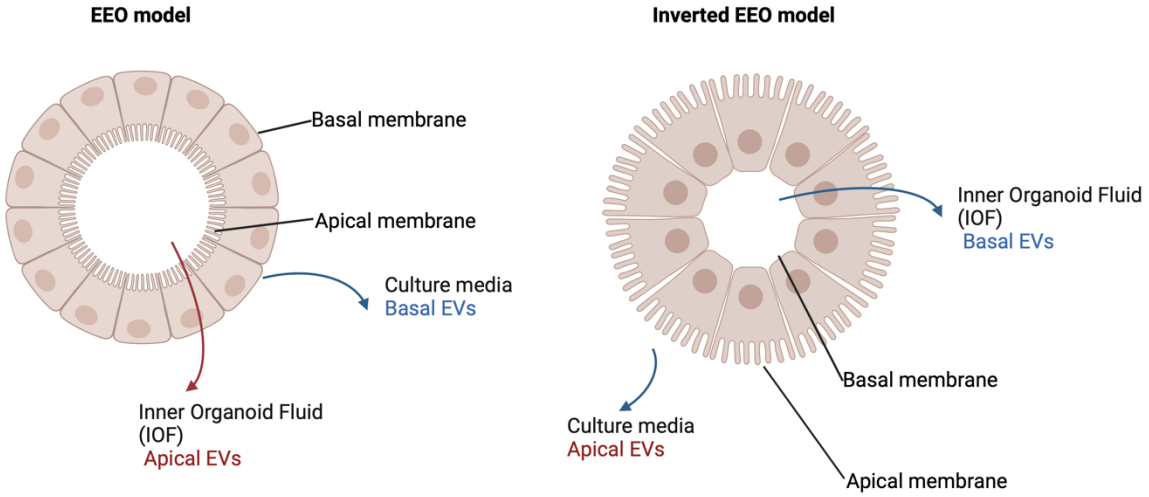

Figure 5.2. Schematic representation of EEO models. a) Standard EEO model with the apical side facing inward. Inner organoid fluid (IOF) contains apical EV while conditioned media (CM) surrounding EEO contains basal EV. b) Inverted EEO model with the apical side facing outward. Apical EV collected from CM while basal EV collected from IOF.

As the EEO model is a 3D structure with the apical side facing inward, analysing the apical side secretome requires collection of inner organoid fluid (IOF) (Figure 5.2). To address this challenge, I will compare two methods for accessing apical-side EV. One method will use centrifugation without breaking the cells, which has shown no difference in metabolite profiles when compared to collection by microneedle (332). However, sEV isolation may be altered by the extra centrifugation step required. Therefore, I will additionally utilise the inverted model (336), in which EEO are removed from the supporting gel matrix and the cell polarity flips over time, allowing for the collection of apical-side EV from culture media surrounding the EEO (Figure 5.2). This comparative approach will help eliminate potential collection-related differences between basal and apical EV, ensuring that any observed distinctions are truly representative of their biological origins rather than artifacts of the isolation process.

Current hormone stimulation protocols have successfully shown the change of marker expression and morphology of EEO in response to progesterone comparable to endometrium change during secretory phase *in vivo* (330, 331). I will introduce hormone stimulation and assess whether progesterone alter sEV characterisation.

sEV profiles in PF from ovarian cancer patients are altered and correlate with clinical outcomes (226). EEO-sEV from endometriosis may also modify the peritoneal microenvironment. My previous findings, as detailed in Chapter 4, demonstrated that PF-sEV suppress phagocytic activity. Importantly, CD47, a key mediator in this process, is co-expressed with EpCAM in sEV, implying their epithelial origin. These observations led to the hypothesis that EV derived from endometriotic lesion EEO may have a suppressive effect on the phagocytic activity of macrophages in the peritoneal microenvironment. Functional analysis with THP-1 derived macrophages and pHrodo *E.coli* deep red bioparticles will be conducted as previously described.

To gain a better understanding of sEV-mediated communication and cellular origins in the peritoneal microenvironment, EEO-sEV profiles will be integrated with those from peritoneal macrophages and PF-sEV analysed by standardised protocols in previous chapters. This comprehensive approach will allow me to compare sEV characteristics across different cellular sources, including their size distribution and surface marker expression. By analysing these profiles, I aim to identify source-specific sEV signatures that can serve as cell origin markers.

This chapter aims to provide a comprehensive characterisation and functional analysis of sEV derived from EEO, examining both basal and apical side released EV using standard EEO and inverted models. The influence of hormonal stimulation on sEV production and characteristics will also be analysed. Moreover, sEV from EEO grown from three distinct sources will be compared: ectopic EEO from endometriotic lesions and eutopic EEO from eutopic endometrium of endometriosis patients and controls. By elucidating the unique properties of these organoid-derived sEV, including their size distribution, concentration, and surface markers, I aim to establish a foundation for understanding their potential roles in endometrial biology and pathology in endometriosis.

5.2 Methods

5.2.1 Sample collection and processing

Women were recruited for sample collection under ethics approvals from the Oxford Research Ethics Committee C (ref:08/H0606/94, 18/SC/0216 and 17/SC/0664 (FENOX). Endometrium samples were obtained using an Endocell Disposable endometrial cell sampler (Wallach Surgical devices, USA), while endometriosis lesions were collected during laparoscopic surgery. Women with a Mirena coil were excluded from endometrium sample collection.

Both endometrial and endometriosis lesion samples were processed within 1h of collection. The samples were chopped with a scalpel into approximately 1mm^2 pieces. These processed samples were either stored in CS10 solution (STEMCELL Technologies, Canada) at -80°C or used fresh for immediate culture.

Samples from a total of 11 patients (age: 30.2 ± 9.6 years; BMI: 28.7 ± 7.8 kg/m^2; mean ± SD) were used in the study (Table 5.1). All lesions selected to establish EEO were peritoneal lesions, no ovarian endometrioma were included.

Table 5.1 Patient characteristics and sample information for eutopic endometrium and endometriosis lesion samples. The table presents data from 11 patients, including endometriosis (EM) stage (0-4) according to rASRM guidelines (337), menstrual cycle stage, hormone use status, age, BMI, successful establishment of eutopic and ectopic EEO and the location of peritoneal lesions sampled. Y=yes, N=no, N/A=not applicable/available

Patient number	EM staging (0-4)	EEO type			Menstrual cycle stage	Hormone use	Age (years)	BMI
		Eutopic endometrium	Ectopic lesion	Ectopic lesion location				
1	0	Y	N	N/A	Proliferative	N	23	20
2	0	Y	N	N/A	Proliferative	N	21	39
3	0	Y	N	N/A	Secretory	N	39	N/A
4	2	Y	Y	Ovarian fossa	Secretory	Y	34	32

5	4	Y	Y	Peritoneal sidewall	Proliferative	N	24	32
6	1	Y	Y	Pouch of Douglas	N/A	Y	18	19
7	2	Y	Y	Ovarian fossa	N/A	N	23	27
8	4	N	Y	Recto-vaginal	N/A	Y	38	43
9	2	N	Y	Ovarian fossa	N/A	Y	47	26
10	3	Y	N	N/A	Proliferative	N	26	24
11	2	Y	N	N/A	Secretory	N	40	25

5.2.2 EEO establishment and culture

Frozen endometrium or lesions were thawed and centrifuged at 500 x g for 5min. Tissues were enzymatically digested in pre-warmed advanced DMEM/F12 media (Thermo Fisher Scientific, USA) containing 1 mg/mL Collagenase V (Sigma-Aldrich, USA) on a rotator (16 rpm) at 37°C for 30-60 min. For eutopic endometrium samples, digested tissue was filtered through a 100µm cell strainer and then a 40µm cell strainer (Corning, USA). Glandular epithelial cells were collected by backwashing the 40µm strainer with 50mL advanced DMEM/F12 media. For lesion samples, digested tissue was passed through a 70µm cell strainer (Corning, USA), and the 50mL filtrate was collected. The collected filtrates were centrifuged (500 x g, 5 min). Supernatants were removed, and pellets were resuspended in Matrigel (Corning, USA). Droplets (20µL) were deposited in each well of 48-well plates (Corning, USA). Organoids were cultured in expansion media (ExM). ExM was based on Turco's protocol (330) with minor modification (Table 5.2). ROCK inhibitor (10 µM) Y27632 (Abcam, UK) was added in ExM for the first 3 days of each passage. Media were changed every 2-3 days.

Eutopic EEO were derived from eutopic endometrium samples from endometriosis patients and control patients. Ectopic EEO were derived from lesion samples of endometriosis patients. Low retention pipette tips (Rainin, USA) and LoBind tubes (Eppendorf, Germany) were used to avoid organoid attachment throughout all procedures. Unless otherwise stated, organoids of low passage number (P3−P5) were used for experiments.

For cryopreservation, established organoids were released from Matrigel using cell recovery solution (Corning, USA) and collected using 1000 µL wide-bore tips (Rainin, USA). After centrifugation (600 x g, 6 min), organoids were resuspended in Recovery™ Cell Culture Freezing Medium (Thermo Fisher Scientific, USA) and stored at -80°C.

Table 5.2. Expansion media (ExM) for EEO culture. Reagent, supply company, and the final concentration in the media.

Reagent	Company	Final Concentration
Advanced DMEM/F12	Thermo Fisher	1X
B27 Supplement minus Vitamin-A	Thermo Fisher	1X
Recombinant human Noggin	Peprotech	100ng/mL
Recombinant human FGF-10	Peprotech	10ng/mL
N2 Supplement (100X)	Thermo Fisher	1X
N-Acetyl-cysteine	Sigma Aldrich	1.25mM
Primocin	InvivoGen	100µg/mL
Recombinant human Rspondin-1	Peprotech	500ng/mL
Nicotinamide	Sigma Aldrich	2mM
Recombinant human EGF	Peprotech	50ng/mL
ALK-4,-5,-7 Inhibitor, A83-01	Tocris	500nM
Insulin-Transferrin-Selenium (100X)	Thermo Fisher	1X
bEGF	Peprotech	2ng/mL
SB202190	Sigma Aldrich	10µM
GlutaMax (100X)	Thermo Fisher	1X
β-Estradiol	Sigma Aldrich	1nM

5.2.2.1 Comparison of mechanical passage and single cell passage

Cell passage was performed every 7-12 days dependant on organoid formation and size. For mechanical organoid passage, Matrigel-embedded organoids were mechanically scraped using 200µl pipette tips (Ranin, USA), centrifuged (600 x g, 6 min), and resuspended in 150µl advanced DMEM/F12 media. Organoids were dissociated by pipetting 300 times, followed by another centrifugation (600 x g, 6 min) and further dissociated by pipetting 80 times. Dissociated organoids were resuspended in Matrigel and plated as 20µL droplets.

For single cell organoid passage, EEO were treated with cell recovery solution (Corning, USA) for 45-60 min at 4°C to dissolve Matrigel and collected by centrifugation (600 x g, 6min). The recovered organoids were next dissociated into single cells using TrypLE (Thermo Fisher Scientific, USA) in rotation for 30 min at 37°C. The resulting cell mixture was filtered through a 40 µm cell strainer. Cells were counted, then centrifuged at 300 x g for 5 min. The cell pellet was resuspended in Matrigel at a concentration of 500-1000 cells/µL.

5.2.2.2 Establishment of the inverted EEO model

To establish the inverted EEO model, organoids were first passaged using the single-cell passage method described in 5.2.2.1. Cells were seeded at a density of 500 cells/µL of Matrigel and cultured for 7 days. After this initial culture period, organoids were transferred to the inverted EEO model following a published protocol (336). In brief, EEO were released from Matrigel using cell recovery solution (45-60 min at 4°C) and collected by 1000 µL wide bore tips. After gentle rotation at 4°C for 1 hour, the free EEO were centrifuged (600 x g, 6 min), washed with PBS, and resuspended in ExM supplemented with 10 µM ROCK inhibitor Y27632 (Abcam, UK). These EEO are then cultured in ultralow-attachment plates (Corning, USA) in suspension.

5.2.3 sEV isolation from EEO cultures

For EV collection experiments, organoids were passaged using the single-cell passage method described in 5.2.2.1. Cells were seeded at a density of 800 cells/µL of Matrigel in 22 wells of 48-well plates. EV-depleted ExM (prepared by ultracentrifugation at 150,000 x g for 4h) was used for culture.

In the EEO model, basal sEV were collected from conditioned media (CM) while apical sEV were collected from the internal organoid fluid (IOF). In the inverted EEO model, apical sEV were collected from the CM. EV were collected from the CM or IOF after 72h of EEO culture. For analysis using the MACSPlex EV kit IO and NTA, CM and IOF were collected from day 4

to day 7 of culture. For functional analysis (phagocytosis assay), CM were collected from day 7 to day 10 of culture.

For IOF collection from the EEO model, a protocol adapted from a published method was employed (332). The process is illustrated in Figure 5.4. Briefly, 11 wells of 48-well plates were washed with PBS, and 500 µL of cell recovery solution was added to each well. After incubation at 4°C for 1 h to dissolve the Matrigel, free organoids were collected and centrifuged at 300 x g for 5 min. The supernatant was discarded, and organoids were resuspended in 300 µL chilled fPBS and vortexed for 5 min. A final centrifugation step at 3750 x g for 15 min at 4°C was performed to obtain the IOF, which was made up to a standardised total volume of 5 mL with fPBS.

Following the acquisition of 5 mL CM and IOF, both fluids were subjected to a standardised protocol for sEV isolation. Initially, cell debris was removed by centrifugation at 1500 x g for 10 min, followed by elimination of large EV at 16,000 x g for 30 min. Subsequently, the fluid was transferred to ultra-clear centrifugate tubes (5 mL, Beckman Coutler, USA) and pelleted via ultracentrifugation at 150,000 x g for 2 h using a SW 55 Ti swinging bucket rotor in an Optima XE-90 ultracentrifuge (Beckman Coulter, USA) and resuspended in 500 µL of fPBS. The collected EV were further purified by SEC columns (qEV original 35nm columns Gen 2, IZON Science, New Zealand) as described in Chapter 3 Section 2.2. The resulting sEV-enriched fractions were concentrated by an additional 2 h / 150,000 x g ultracentrifugation and resuspended in 50µL PBS for the phagocytosis assay or 300 µL for MACSPlex EV analysis.

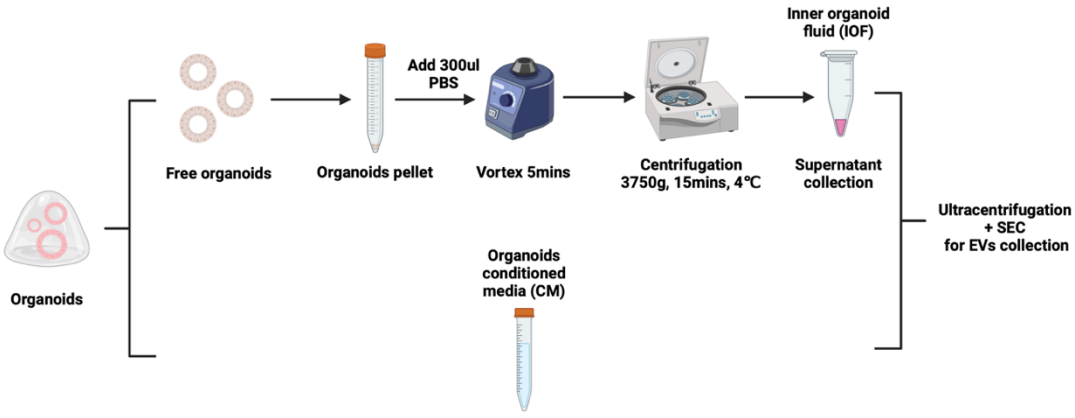

Figure 5.4. The workflow of sEV isolation from EEO cultures. Schematic showing the process of isolating sEV from conditioned media (CM) and Inner Organoid Fluid (IOF).

5.2.3.1 Comparison of different methods in isolating apical sEV.

Apical sEV were isolated from IOF in eutopic EEO from one control patient (n=1) using four methods: 1) The standard protocol (ultracentrifugation + SEC + ultracentrifugation) described in Section 5.2.3, 2) 150,000 x g 2h ultracentrifugation, 3) double ultracentrifugation, and 4) ultracentrifugation followed by 0.2µm PVDF membrane filtration. Additionally, using the same patient's cells, apical sEV were collected from an inverted EEO model. In this inverted model, sEV were isolated from the CM using the standard protocol (ultracentrifugation + SEC + ultracentrifugation).

5.2.4 Hormonal cycling of EEO

Hormonal cycling of EEO was performed using β-estradiol (E2, Sigma Aldrich, USA), progesterone (P4, Sigma Aldrich, USA), and adenosine 3',5'-cyclic monophosphate (cAMP, Sigma Aldrich, USA) following established protocols (330, 331) (Figure 5.3). Eutopic EEO from a control patient were passaged and cultured for the first 7 days in ExM supplemented with 1 nM E2 to mimic the proliferative phase. For the following 7 days, to simulate the secretory phase, the medium was changed to contain 0.1 nM E2 and 50 ng/mL P4 (331). Alternatively, 1µM cAMP was added to the culture medium with P4 (330). CM and IOF were collected in 48h incubation DAY 5-7 and Day 12-14 to isolate sEV as described in 5.2.3 for downstream analysis.

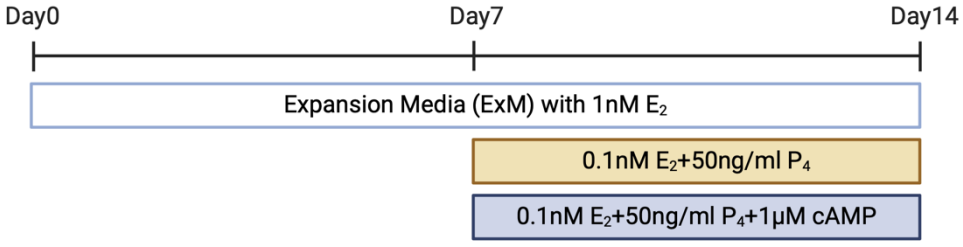

Figure 5.3. Schematic representation of hormonal cycling protocol for EEO culture. The 14-day cycle consists of two phases: (1) Proliferative phase: Days 1-7, ExM supplemented with 1 nM E2. (2) Secretory phase: Days 8-14, medium changed to contain 0.1 nM E2 and 50 ng/mL P4. An alternative protocol adds 1µM cAMP along with P4 in the secretory phase. E2: β-oestradiol; P4: progesterone; cAMP: 8-bromoadenosine 3', 5'-cyclic monophosphate.

5.2.5 Immunofluorescence staining confocal microscopy

Organoids were prepared for antibody staining by culturing for 7-12 days on an 8-well microscopy chamber slide (ibidi, Thermo Fisher Scientific, USA). Once ready, whole-mount staining was performed on EEO within Matrigel. Briefly, organoids were washed with PBS and fixed for 30 min using 4% (v/v) formaldehyde aqueous solution (VWR, USA) at room temperature, followed by permeabilisation using 0.5% Triton X-100 in PBS for 30 min. After blocking with 5% BSA/0.2% Triton X-100/0.05% Tween-20 in PBS for 2-3 h, the organoids were incubated with primary antibodies (pan-Cytokeratin (AE1/AE3, Invitrogen, USA), E-Cadherin (HECD-1, Invitrogen, USA), EpCAM (VU1D9, Invitrogen, USA), ZO-1 (1A12, Invitrogen, USA), Laminin (A5, Invitrogen, USA), and SPP-1 (EPR21139-316, Abcam, UK) at a 1:100 dilution and incubated overnight at 4℃. The following day, organoids were washed three times with PBS and incubated with appropriate Alexa Fluor-conjugated secondary antibodies (1:500 dilution) for 2-3 h hour at room temperature. Organoids were then mounted using mounting media with DAPI (Abcam, UK). Z-stack images were acquired using a Leica TCS SP8 confocal laser scanning microscope with assistance from Dr. James Bancroft at the Wellcome Centre for Human Genetics. All imaging parameters were kept constant across samples to allow for comparison for SPP-1.

5.2.6 Phagocytosis assay

THP-1 cells were seeded at $2x10^5$ cells/well in 48-well plates and differentiated and polarised into M2 macrophages as described in Chapter 4 Section 2.2. The phagocytic activity of macrophages were tested using pHrodo *E.coli* deep red bioparticle Conjugate for Phagocytosis (Thermo Fisher Scientific, USA) as described in Chapter 4 Section 2.8, after different treatments as described in the following sections.

5.2.6.1 The effect of EEO-sEV on macrophage phagocytosis

EEO-sEV were isolated from 5.5 mL of CM collected from 22 wells of 48-well plates using the method described in 5.2.3. As a control, an equivalent volume of EV-depleted ExM was subjected to the identical isolation protocol. EEO-sEV were quantified by NTA and all samples were diluted to equivalent volumes using fPBS. THP-1 derived M2 macrophages were treated with 2×10^9 EV/mL of EEO-sEV or ExM-sEV isolated from 5.5 mL EV-depleted ExM in EV-depleted RPMI media. Macrophages were incubated with the treatments for 24 hours before assessing phagocytic activity as described in Chapter 4 Section 2.8.

5.2.6.2 The effect of EV depletion of EEO CM on macrophage phagocytosis

For the EV depletion experiment, CM was harvested following a 72h incubation of EEO. The CM was centrifuged at 1,500 × g for 10 min to remove cellular debris. Subsequently, 5 mL of this CM was ultracentrifuged at 150,000 × g for 4h at 4°C as described in Section 5.2.3 to deplete EV. The efficacy of EV depletion was assessed via NTA. THP-1 derived M2 macrophages, cultured in 48-well plates, were treated with 200 µL of either complete CM or EV-depleted CM per well.

Reference controls were established for each experiment type. For EEO-sEV experiments, three wells of macrophages were treated with EV-depleted RPMI media containing an equivalent amount of fPBS. In EV depletion experiments, three wells of macrophages were treated with EV-depleted ExM.

5.2.7 Flow cytometry

5.2.7.1 Measurement of surface markers on EEO-sEV by the MACSPlex EV kit IO

The MACSPlex EV kit IO (Miltenyi Biotec, Germany) was used to analyse surface marker expression of EEO-sEV.

The study included compared basal sEV collected from eutopic EEO of control patients (n=3) with basal sEV from eutopic and ectopic EEO of endometriosis patients (n=6), as described in Chapter 2, Section 2.8.2.

The analysis further compared basal and apical sEV from hormone-treated eutopic EEO of a control patient in the proliferative and secretory phases, as described in Section 5.2.4.

CD47 expression was not included in the original panel of the MACSplex EV kit IO, therefore co-expression on ectopic EEO-sEV from one endometriosis patient was measured by utilising a modified MACSPlex protocol (291) as described in Chapter 4 Section 2.10.6.

For all experiments, a standardised input of 1×10^9 EV/mL was used for the MACSPlex analysis of EEO-sEV.

5.2.7.2 Measurement of phagocytic activity of macrophages.

After incubating for 1 h with pHrodo *E.coli* deep red bioparticles, THP-1 M2 macrophages were lifted using Accutase for 15-30 min at 37 °C. The phagocytic activity was assessed by flow cytometry (Northern Lights, Cytek Biosciences, USA) and analysed as fold change by comparing the mean fluorescence intensity (MFI) of pHrodo *E. coli* Deep Red bioparticles in THP-1 derived M2 macrophages pre-treated with EEO-EV or CM to the mean MFI of pHrodo *E. coli* Deep Red bioparticles in untreated THP-1 derived M2 macrophages (bioparticle only, n=3) following methods described in Chapter 4 Section 4.2.10.3.

5.2.8 NTA

The method was used as described in Chapter 2 Section 2.2.4. NTA was employed for multiple purposes:

5.2.8.1 EV quantification for flow cytometry

NTA was used to determine the concentration of EEO-sEV. Subsequently, $1x10^9$ EV/mL were used as the input for the MACSPlex EV kit IO flow cytometry analysis.

5.2.8.2 Comparison of isolation methods for apical sEV

NTA was used to compare apical sEV collected from one control EEO by different isolation methods from the EEO model and from the inverted EEO model mentioned in Section 5.2.6.1 above.

5.2.8.3 Hormonal stimulation effects

NTA was used to assess changes in basal and apical sEV after hormonal stimulation described in Section 5.2.3.

5.2.8.4 Characterisation of sEV properties across EEO types and secretion polarity

NTA was used to assess differences in sEV concentration and size between different types of EEO (Eutopic EEO from controls: n=3, eutopic and ectopic EEO from endometriosis patients: n=6) and between basal and apical sides (n=3 for each of the 3 EEO types).

5.2.8.5 Assessment of EV depletion efficacy in EEO CM

The EEO CM were pooled into three types: 1) eutopic EEO from control patients (n=3), 2) eutopic EEO from endometriosis patients (n=5), and 3) ectopic EEO (n=3). The concentration of EV in these pooled samples was assessed by NTA. EV in the unused conditioned media were then depleted by ultracentrifugation at 150,000 x g for 4h. The EV-depleted conditioned media samples (n=11) were analysed individually (with no dilution) using NTA.

5.2.9 TEM

Basal sEV were collected from 22 wells of a 48-well plate and showed average concentration of $5x10^9$ EV/mL by NTA, while apical sEV were collected from 11 wells of the same plate with average concentration of $5x10^{11}$ EV/mL. These sEV were isolated from eutopic EEO derived from both an endometriosis patient and a control subject, as well as from ectopic EEO from one endometriosis patient. The morphological characteristics of collected sEV were assessed using TEM according to protocols detailed in Chapter 2 Section 2.2.5 and performed by Errin Johnson at the Sir William Dunn School of Pathology.

5.2.10 Statistical analysis

Two-way ANOVA was used to assess the effects of EEO types and secretion side on EV concentration and modal size, followed by Tukey's HSD test. For all other comparisons, one-way ANOVA or t-tests were applied as appropriate, depending on the number of groups being compared. $P<0.05$ was considered significant. Statistical analyses were performed using GraphPad Prism.

5.3 Results

5.3.1 Optimisation of EEO models for endometriosis research

5.3.1.1 Establishment of EEO from eutopic endometrium and endometriosis lesion samples

Following published protocols for the establishment of EEO *in vitro* (107, 330), I established EEO lines from frozen endometrial samples (n=15), with a 100% success rate (data not shown). For ectopic EEO grown from endometriosis lesions, no specific protocol had been published. Unlike eutopic endometrium samples, microscope observation of lesion samples showed no typical gland-like structures after digestion (data not shown). This indicated a lower presence of epithelial cells and potential structural differences in lesion samples. To address this, fresh samples were used to minimize cell loss during the freezing/thawing cycle. Digestion times were extended, varying from 40 to 60 min depending on sample size, to effectively break down the fibrosis often present in these samples (338). A 70 µm cell strainer was employed to maximize the collection of epithelial cells.

As presented in Figure 5.5, EEO grown from eutopic endometrium exhibited visible gland-like structures 1-2 days post-seeding. Eutopic EEO demonstrated rapid growth, increasing from an initial diameter of 20 µm to over 200 µm over a period of 6 days. In contrast, ectopic EEO from lesions resulted in a higher presence of background cells and debris compared to endometrium samples (Figure 5.5). Ectopic EEO were not visible on day 2, and their size remained less than 100 µm by day 8, indicating slower growth and development compared to eutopic EEO. Eutopic EEO required passage after 7-10 days, while ectopic EEO required 14 to 20 days in P0.

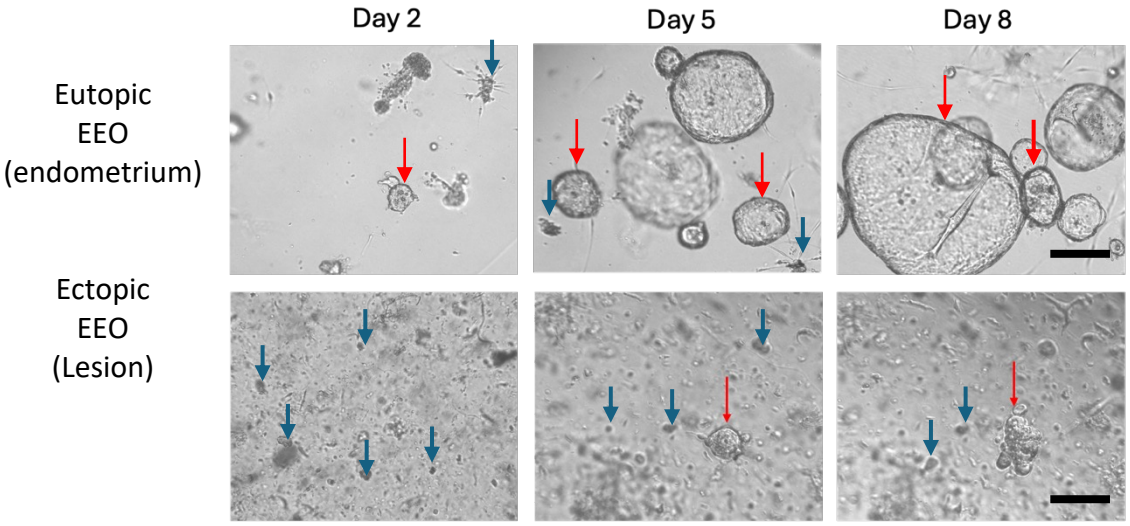

Figure 5.5. Growth comparison of EEO derived from eutopic endometrium and endometriosis lesion. Representative bright-field microscopy images showing the development of EEO from eutopic and lesion samples at day 2, 5, and 8 post-establishment. Red arrows indicate organoid like structure and blue arrows indicate background cells and debris. Scale bar = 100 µm.

Eutopic endometrium samples collected from women on hormonal treatment (HT) initially yielded fewer organoids in P0 due to the suppression of endometrium growth and endometrium thinning (339). However, after passaging (P1 to P5), no obvious differences in growth rate or morphology were observed between EEO established from eutopic samples (with or without HT) and ectopic samples (Figure 5.6), which is consistent with existing literature (330).

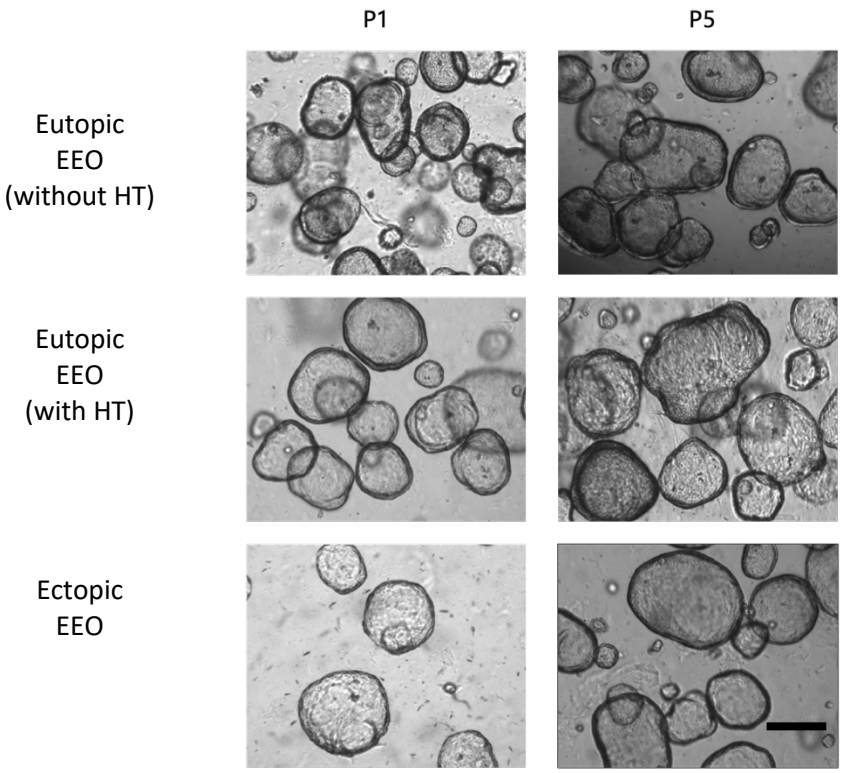

Figure 5.6. Comparison of EEO growth and morphology across passages from different sample types. Representative bright-field microscopy images of EEO derived from eutopic endometrium (with and without hormonal treatment) and ectopic endometrium (lesions) at passages P1 and P5. Scale bar = 100 µm. HT= hormonal treatment.

To confirm that EEO from eutopic endometrium and endometriosis lesion samples both are formed by cells of endometrial epithelial origin, immunohistochemistry was performed on eutopic EEO (endometriosis: n=1, control: n=1) and ectopic EEO (n=1), investigating the expression of pan-Cytokeratin, E-cadherin, and EpCAM. EpCAM was used to verify the endometrial epithelial origin, as mesothelial cells that linethe peritoneal cavity are EpCAM negative (340). All 3 EEO types were positive for EpCAM, pan-Cytokeratin, and E-cadherin (Figure 5.7). Importantly, each of the three EEO types formed a lumen, presenting hollow structures with no cells at the centre.

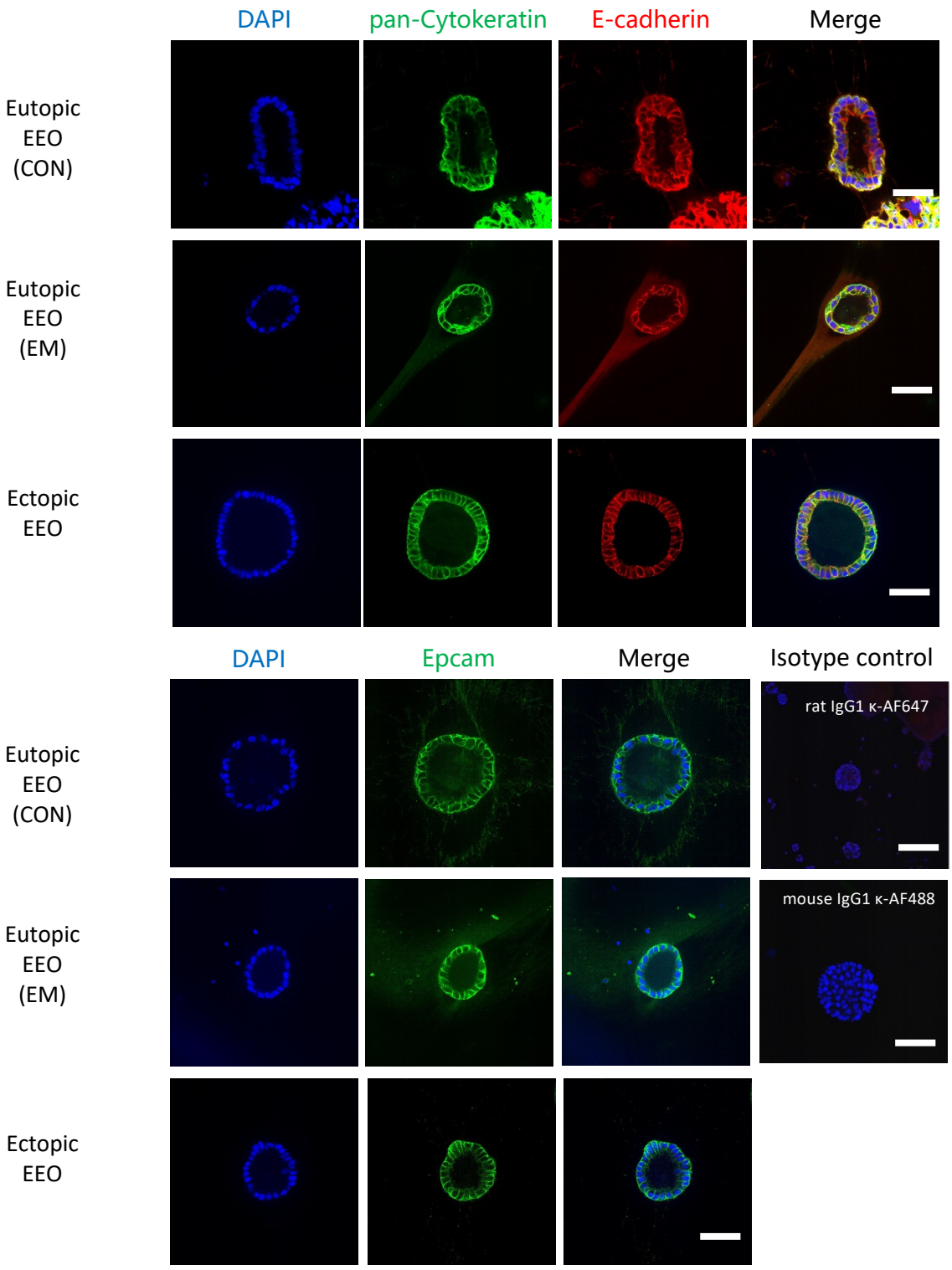

Figure 5.7. Immunofluorescence analysis of the epithelial and endometrial origin of EEO. Representative confocal microscopy images of eutopic EEO from endometriosis (EM) and control (CON) patients, and ectopic EEO at P3. Samples were stained for epithelial markers pan-Cytokeratin (green) and E-cadherin (red) in one set of images, and for the endometrial epithelial marker EpCAM (green) in a separate set. Nuclei were stained with DAPI (blue) in both sets. Specificity was confirmed by isotype controls: for pan-Cytokeratin and EpCAM, and rat IgG1 κ-AF647 for E-cadherin staining. Scale bar = 50 µm.

Different methods of passage were compared to optimise the growth and maintenance of EEO. Initially, mechanical passaging was used, which involved breaking organoids into pieces by pipetting through a 200 μL pipette tips. This method was quick and efficient, requiring EEO passage again after approximately 7 days. However, it resulted in new organoids of varying sizes within the same well, leading to inconsistencies in growth (Figure 5.8). The heterogeneity in organoid size could complicate standardization across experiments and introduce variability in results.

As an alternative, a method using TrypLE to create single-cell suspensions was developed. It produced organoids of more uniform size (Figure 5.8). Additionally, it allowed for cell counting before seeding, therefore providing more precise control over seeding density. However, as EEO formed from single cells rather than organoid pieces, this method resulted in slower initial growth compared to mechanical EEO passage. Despite the longer time required for organoid formation, this approach led to a longer interval between passage events. This extended growth period may be particularly beneficial in scenarios where long observation times are required, allowing for extended experimental windows without the need for intervention. Through optimization, it was determined that seeding 800 cells in 20μL of Matrigel allowed for robust growth over a 12-day period before passage was required.

Based on these findings, a strategic approach for passaging EEO was adopted. Mechanical passage was used for early stages of culture due to its speed and efficiency. However, for specific applications such as sEV collection, single-cell passage was used.

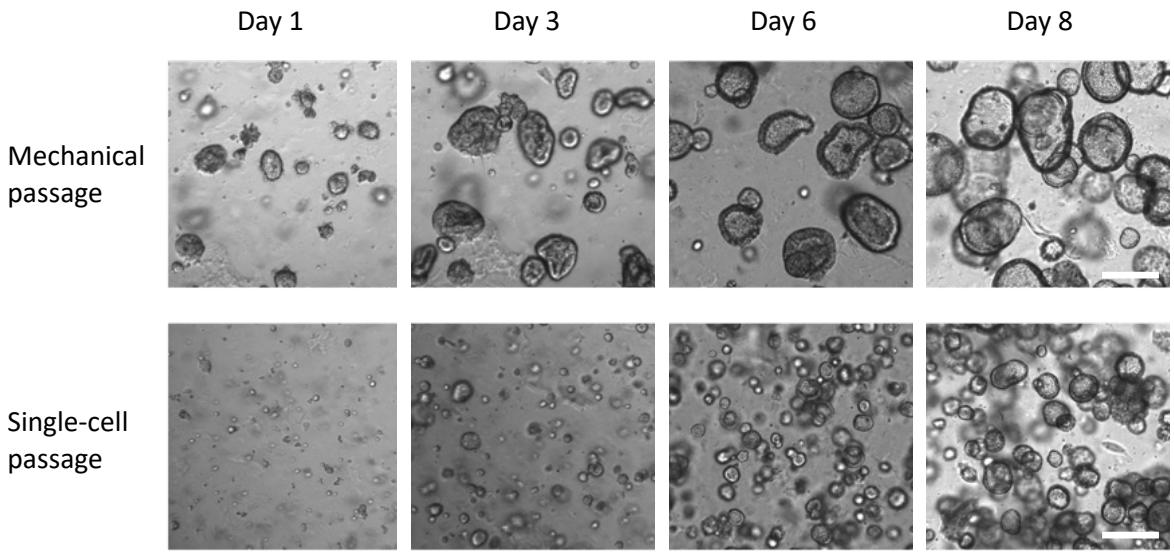

Figure 5.8. Comparison of EEO growth using different passaging methods. Representative bright-field microscopy images showing EEO growth from days 1, 3, 6 and 8 produced by mechanical passage (top) and single-cell passage (bottom). Scale bar = 100 µm.

5.3.1.2 Establishment of an inverted EEO model from eutopic EEO

In addition to optimising passage methods, an inverted 'apical-out' model for EEO was explored using a published protocol (336). This model inverts the typical organoid structure, exposing the apical surface of the epithelium to the external environment. Upon implementation, obvious differences in morphology were observed under bright field microscopy. The inverted organoids appeared more diffused and folded compared to standard organoids (Figure 5.9a), providing a visual indication that the apical side potentially with cilia was facing outwards.

The inverted structure of these EEO was confirmed through immunofluorescence staining and analysis under confocal microscopy. Specifically, antibodies against ZO-1, a tight junction protein typically located on the basal side of epithelial cells, and Laminin, an extracellular matrix protein associated with the apical surface in this inverted model, were used. The staining patterns observed confirmed the inversion of the EEO, with ZO-1 localised to the interior and Laminin to the exterior of the organoids (Figure 5.9b).

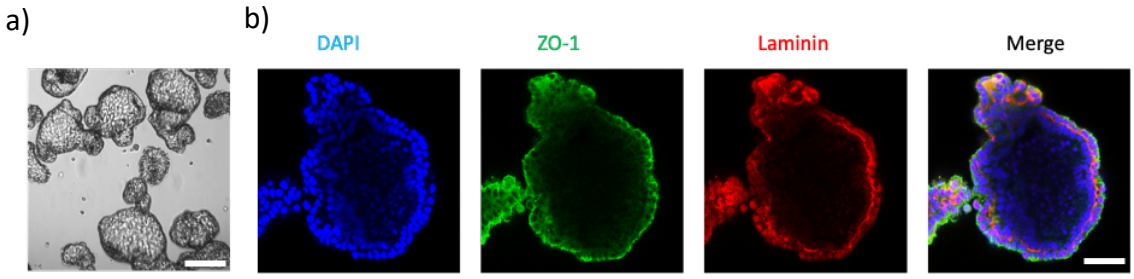

Figure 5.9. Structural and immunofluorescence analysis of inverted EEO. a) Representative bright-field microscopy image of inverted EEO. Scale bar = 100 µm. B) confocal microscopy images of Immunofluorescence staining of inverted EEO with ZO-1 (green) and Laminin (red) expression. Nuclei are stained with DAPI (blue). Scale bar = 50 µm.

5.3.1.3 Examination of hormonal responsiveness of eutopic EEO

Next, I tested the responsiveness for eutopic EEO to hormone stimuli. In the human endometrium, epithelial cells undergo morphological and functional changes including expression of secretory protein like SPP-1 in response to progesterone during the secretory phase of the menstrual cycle (330, 331).

Eutopic EEO from one control patient were first incubated in ExM with E2 for 7 days and treated with additional progesterone (P4) for another 7 days following an established protocol (331) to mimic menstrual cycle.

This treatment increased the expression of SPP-1 compared to oestrogen treated EEO, as demonstrated by confocal microscopy (Figure 5.12), confirming the hormonal responsiveness of the EEO.

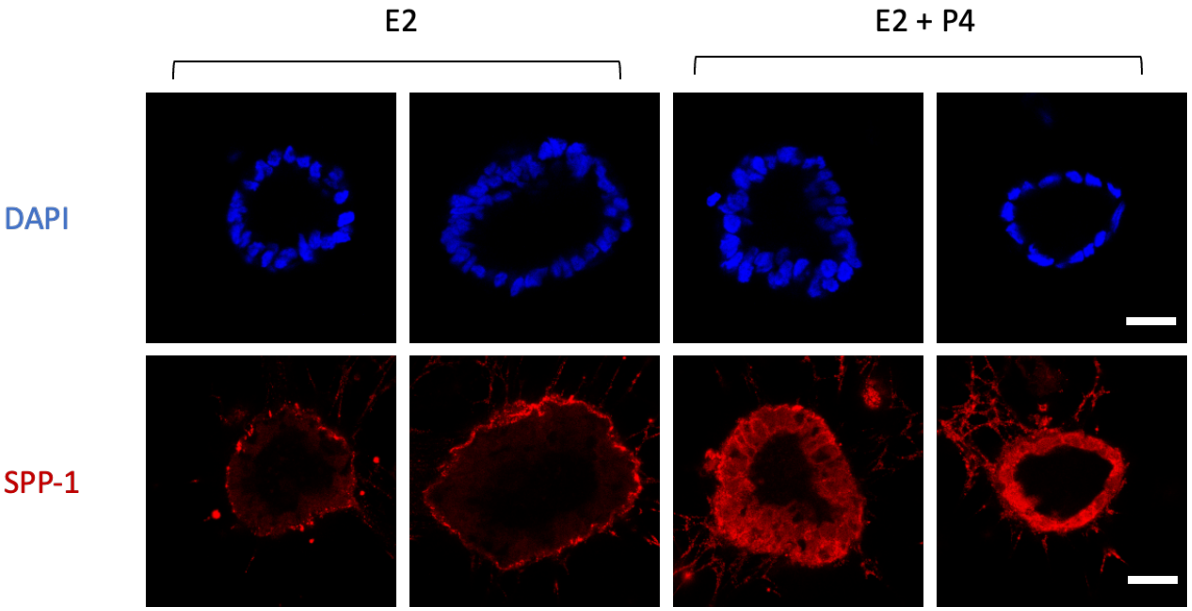

Figure 5.12 Immunofluorescence analysis of hormone-driven SPP-1 expression in EEO. EEO were first grown in ExM with 1nM E2 for 7 days, then treated for an additional 7 days with: ExM with 1nM E2, ExM with 0.1nM E2 + 50ng/mL P4. The SPP-1 expression was examined by confocal microscopy in E2-treated EEO (left) and E2+P4 treated EEO (right). Scale bar = 50µm.

5.3.2 Characterisation of EV secreted from basal epithelium of endometrium

5.3.2.1 Characterisation of size and concentration of EEO basal sEV

To collect EV released from the basal side of the endometrial epithelium, Eutopic EEO from endometriosis patients, Eutopic EEO from control patients and Ectopic EEO were seeded in Matrigel and cultured for 4 days. In total, conditioned media (5.5 mL) from each type of EEO was collected from 22 wells of 48-well plates after a 72-hour period (days 4-7). The EV were concentrated by ultracentrifugation and further purified using SEC. NTA revealed no significant differences in size (137 ± 7nm, 128 ± 28nm,130 ± 38nm; mean ± SD) (Figure 5.10a) or concentration ($2.52x10^7$ ± $1.56x10^6$ EV/well, $3.37x10^7$ ± $9.02\ x10^6$ EV/well, $2.56x10^7$ ± $6.06x10^6$ EV/well; mean ± SD) among eutopic EEO from endometriosis and controls, and ectopic EEO respectively (Figure 5.10a,b). These findings were confirmed by TEM, which also revealed EV of <200 µm in size, as indicated by the red arrows. TEM images showed a

clear background indicating minimal soluble protein contamination of the preparations (Figure 5.10c).

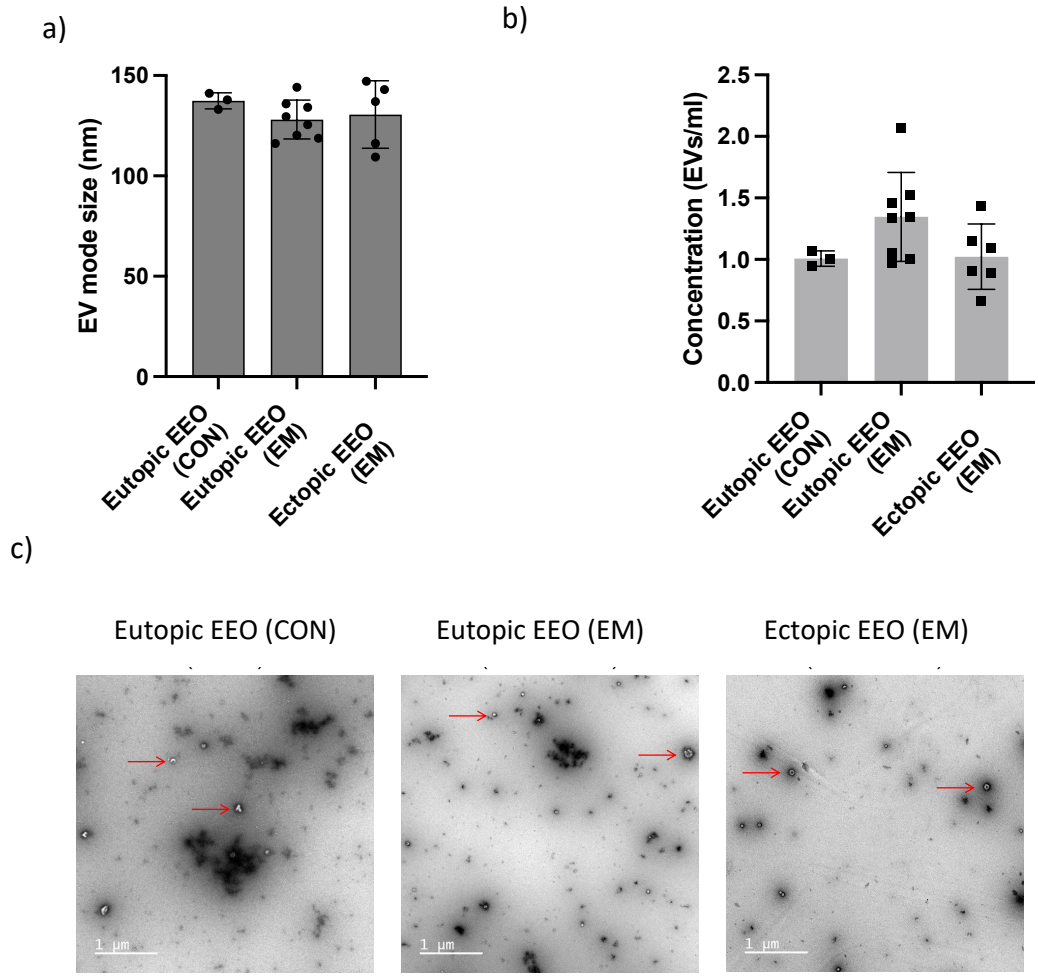

Figure 5.10. Characterisation of basal sEV derived from EEO. a) Representative NTA size distribution profiles of basal sEV isolated from control, eutopic, and ectopic EEO (n=3). B) Representative TEM image of basal sEV (red arrows) isolated from EEO. Scale bar = 1 µm.

5.3.2.2 Characterisation of surface marker expression on EEO basal sEV using the MACSPlex EV kit IO.

The MACSPlex EV kit IO was used to characterise the surface markers of the EV. A total of 22 markers were detected on all 15 samples of EEO-basal sEV (Table 5.2). As expected, the sEV-enriched tetraspanin markers CD81, CD9, and CD63 were detected, confirming the presence of characteristic EV proteins. Basal EEO EV expressed even higher CD133/1 (mean nMFI of 3.6) and EpCAM (mean nMFI of 2.5) than the three tetraspanin EV markers. In

addition to these highly expressed markers, several other proteins were found to be abundantly present on the EEO basal EV. These include a set of immunomodulation and functional markers, including CD29, CD24, CD44, HLA-DR and CD146. The expression levels of these proteins were also noteworthy, with nMFI values above 0.1. From the 15 samples examined, 14 markers were only detected in a subset of samples (Table 5.2) with very low mean nMFI (<0.0005), possibly due to background noise from media. An exception was CD45, which was expressed in 13 out of 15 samples examined, with a mean nMFI of 0.00178. CD62P was not detected in any samples.

Table 5.2. Surface marker expression of EEO basal sEV. EEO basal sEV were examined in 15 samples.

Marker	Number of positive samples	Mean nMFI ± SE	Marker	Number of positive samples	Mean nMFI ± SE
CD3	15/15	0.0014 ± 0.00287	CD142	15/15	0.06819 ± 0.1093
CD105	15/15	0.00605 ± 0.00678	CD69	15/15	0.00653 ± 0.01514
CD56	15/15	0.00254 ± 0.00476	CD29	15/15	0.55055 ± 0.47281
HLA-DR	15/15	0.07174 ± 0.33277	CD19	02/15	0.00017 ± 8e-05
ROR1	15/15	0.00461 ± 0.01491	CD4	03/15	5e-05 ± 7e-05
CD49e	15/15	0.00922 ± 0.01572	CD8	03/15	0.00017 ± 0.00021
CD25	15/15	0.0013 ± 0.00194	CD1c	03/15	0.00021 ± 7e-05
CD40	15/15	0.00774 ± 0.02676	CD2	04/15	0.00045 ± 0.0005
CD63	15/15	0.52416 ± 0.161	CD209	07/15	0.00031 ± 0.00056
HLA-ABC	15/15	0.02029 ± 0.03919	MCSP	01/15	0.00012
SSEA-4	15/15	0.08652 ± 0.23466	CD11c	06/15	0.00025 ± 0.00076
CD9	15/15	0.96317 ± 0.37479	CD14	04/15	0.00014 ± 0.00036
CD41b	15/15	0.0093 ± 0.01797	CD20	05/15	0.00053 ± 0.00143
CD146	15/15	0.06833 ± 0.11855	CD31	08/15	0.00058 ± 0.00085
CD81	15/15	1.51274 ± 0.34257	CD45	13/15	0.00178 ± 0.0027
CD133/1	15/15	3.61931 ± 5.27442	CD86	6/15	0.00049 ± 0.00083
CD326	15/15	2.52711 ± 1.90547	CD42a	11/15	0.00043 ± 0.00153
CD44	15/15	0.10511 ± 0.12874	mIgG1 Control	15/15	0.00022 ± 0.00221
CD24	15/15	0.10605 ± 0.19098	REA Control	15/15	0.0005 ± 0.00167

When comparing eutopic EEO from endometriosis patients (n=6) and controls (n=3) and ectopic EEO (n=6), differences in surface marker expression were observed. The table 5.3 provides an overview of the expression patterns for the three EEO types.

Table 5.3 Surface marker expression on EEO-sEV. The mean nMFI and SD of surface markers on sEV from eutopic EEO from control (CON) (n=3) and endometriosis patients (EM) (n=6) and ectopic EEO from endometriosis patients (EM) (n=6). Group difference was analysed by a one-way ANOVA, with *P < 0.05 indicating statistical significance.

	Eutopic EEO (CON)		Eutopic EEO (EM)		Ectopic EEO (EM)		Group difference	
	Mean	SD	Mean	SD	Mean	SD	P value	F value
CD3	0.0017	0.0009	0.0013	0.0004	0.0013	0.0010	0.77	0.30
CD105	0.0047	0.0009	0.0058	0.0015	0.0070	0.0020	0.18	2.00
CD56	0.0025	0.0007	0.0021	0.0004	0.0030	0.0018	0.46	0.80
HLA-DR	0.0632	0.0765	0.0534	0.0810	0.0943	0.1035	0.73	0.30
ROR1	0.0037	0.0020	0.0033	0.0024	0.0064	0.0053	0.38	1.00
CD49e	0.0079	0.0019	0.0093	0.0036	0.0098	0.0055	0.82	0.20
CD25	0.0015	0.0005	0.0013	0.0004	0.0012	0.0006	0.67	0.40
CD40	0.0058	0.0027	0.0047	0.0037	0.0117	0.0092	0.19	1.90
CD63	0.4824	0.0315	0.5225	0.0279	0.5467	0.0447	0.08	3.10
HLA-ABC	0.0121	0.0063	0.0205	0.0085	0.0242	0.0119	0.25	1.50
SSEA-4	0.0752	0.0375	0.0990	0.0654	0.0797	0.0715	0.83	0.20
CD9	0.9970	0.0362	0.9334	0.0952	0.9760	0.1212	0.63	0.48
CD41b	0.0110	0.0017	0.0124	0.0045	0.0053	0.0025	0.0099*	6.90
CD146	0.0492	0.0148	0.0665	0.0201	0.0798	0.0418	0.39	1.00
CD81	1.5207	0.0652	1.5443	0.0774	1.4773	0.1071	0.45	0.90
CD133/1	3.5650	0.5542	2.8477	0.7421	4.4181	1.7428	0.13	2.40
EpCAM	3.0913	0.2199	2.3954	0.5179	2.3767	0.3889	0.07	3.30
CD44	0.0851	0.0238	0.0883	0.0144	0.1319	0.0349	0.0233*	5.20
CD24	0.1376	0.0452	0.0949	0.0509	0.1014	0.0513	0.48	0.70
CD142	0.0434	0.0303	0.0702	0.0243	0.0785	0.0277	0.22	1.80
CD69	0.0060	0.0021	0.0038	0.0018	0.0095	0.0042	0.0214*	5.40
CD29	0.5216	0.0920	0.4693	0.0525	0.6463	0.1272	0.0234*	5.20

CD44 expression showed significantly higher levels (mean nMFI ± SD) in ectopic EEO-EV (0.13 ± 0.03) compared to eutopic EEO from endometriosis patients (0.085 ± 0.02) ($p<0.05$). While the mean CD44 expression in eutopic EEO from control patients (0.085 ± 0.01) was similar to that of eutopic EEO, the difference between ectopic and control EEO did not reach statistical significance. This lack of significance between ectopic and control groups may be due to the small sample size (n=3) and resulting statistical power limitations (Figure 5.11a). Similarly, CD29 and CD69 showed significantly higher expression in ectopic EEO compared to eutopic EEO from endometriosis patients ($p<0.05$), while eutopic EEO from control patients (0.522 ± 0.053) displayed intermediate levels (Figure 5.11b&c). In contrast, CD41b expression was significantly lower in ectopic EEO-sEV while its expression remains at similar levels between sEV from eutopic EEO of control and endometriosis patients (Figure 5.11d). Interestingly, EpCAM expression (mean nMFI ± SD) was highest in eutopic EEO from control patients (nMFI 3.106 ± 0.220) compared to both eutopic EEO-EV from endometriosis patients (2.395 ± 0.518) and ectopic EEO-EV (2.377 ± 0.389). These differences approached but did not reach statistical significance ($p=0.0849$ and $p=0.0763$, respectively) (Figure 5.11e). This pattern is complex, suggesting potential alterations in epithelial characteristics between normal and endometriosis-affected tissues.

Most markers, such as CD44, CD29, and CD69, showed significantly different expression in ectopic EEO-sEV compared to eutopic EEO-sEV from both endometriosis and control patients. This suggests that sEV derived from ectopic lesions exhibit a distinct surface marker profile, reflecting alterations associated with the ectopic growth. However, for EpCAM, the pattern differed, as sEV from eutopic endometrium in control patients exhibited uniquely higher expression compared to sEV from both ectopic lesions and eutopic endometrium in endometriosis patients, indicating potential alterations in eutopic endometrium associated with endometriosis.

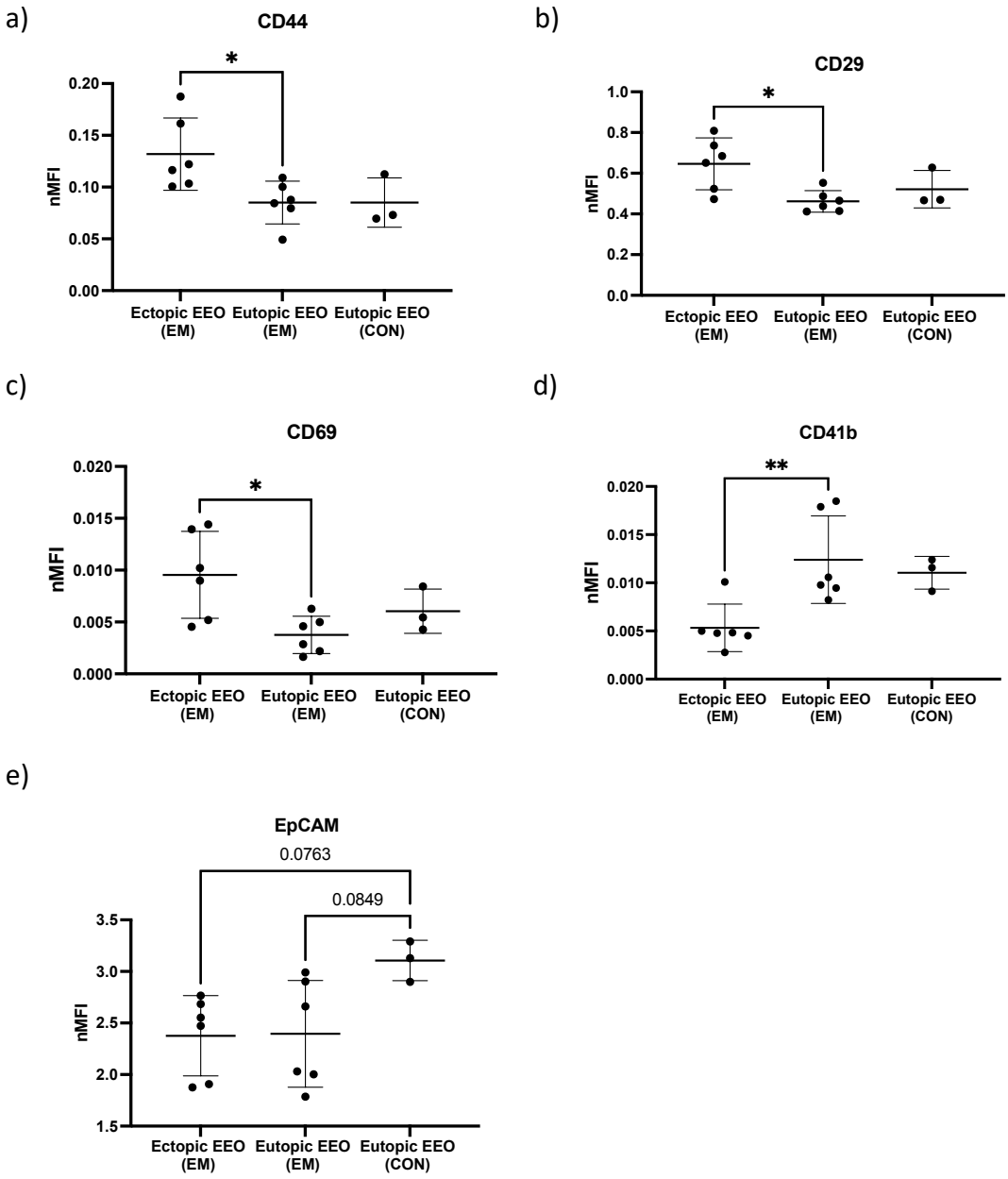

Figure 5.11 Differential expression of surface markers in sEV derived from eutopic EEO from endometriosis and control patients and ectopic EEO. MACSPlex analysis compare the expression levels of specific markers among three groups: eutopic EEO-sEV from CON (n=3) and EM (n=6), and ectopic EEO-sEV from EM (n=6). Markers analysed include: a) CD44, b) CD29, c) CD69, d) CD41b and e) EpCAM. Data presented as mean ± SD. CON=control, EM=endometriosis. One-way ANOVA with Turkey's multiple comparisons (Shapiro-Wilk test: $p > 0.05$), *P<0.05, **P<0.01

5.3.2.3 Characterisation of basal sEV from eutopic EEO in response to hormone stimulation

I next sought to investigate if the nature of EV secreted changes in response to hormone stimulation mimicking the menstrual cycle, following the established protocol (331).

Basal sEV were collected from eutopic EEO from one control patient treated with E2, E2+P4, and E2+P4+cAMP by ultracentrifugation and SEC and analysed by NTA (Figure 5.13a). No significant changes were observed in size (E2: mode 136 nm, mean 236 nm; E2+P4: mode 128 nm, mean 243 nm; E2+P4+cAMP: mode 133 nm, mean 246 nm) or concentration (E2: $2.2x10^8$ EV/well; E2+P4: $2.2x10^8$ EV/well; E2+P4+cAMP: $2.0x10^8$ EV/well) across the different hormone treatments. Additionally, examination of sEV surface markers using the MACSplex EV detection kit revealed no notable differences in marker expression among the various hormone treatment conditions (Figure 5.13b)

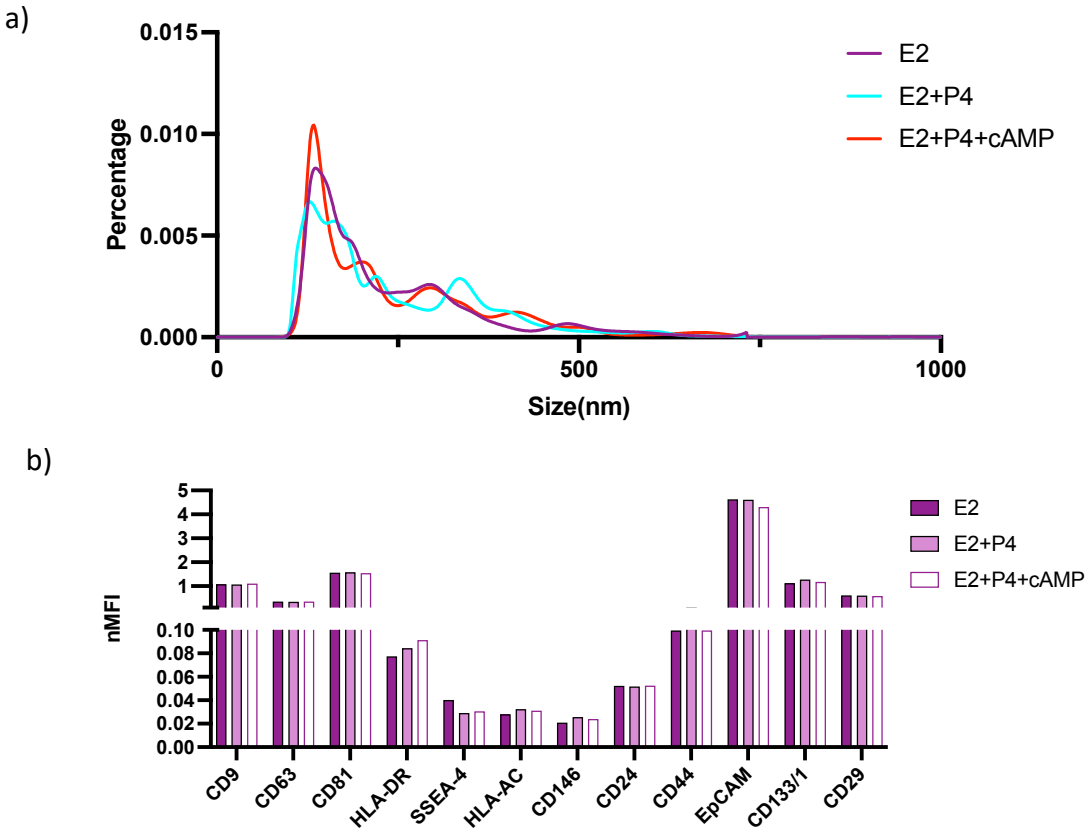

Figure 5.13. Characterisation of basal EV secreted by hormone stimulated EEO. a) The size distribution profile of EEO basal sEV analysed by NTA. B) Surface marker expression of EEO basal sEV measured by the MACSPlex EV kit IO. n=1.

5.3.3 Characterisation of EV secreted from the apical epithelium of the endometrium

5.3.3.1 Characterisation of size and concentration of EEO apical sEV and comparison with basal EEO sEV

To analyse sEV secreted from the apical membrane of endometrial epithelial cells, I first used a protocol in which IOF is collected through centrifugation (332) in a standard EEO model. In brief, this collection method involved centrifugation of EEO. sEV were then isolated from the IOF using the same methodology as for the basal side sEV with ultracentrifugation and SEC column , to allow comparison.

The size distribution of apical sEV was analysed using NTA, a bimodal size distribution was visualised with two peaks at 130 nm and 300 nm (Figure 5.14a). Specifically, the concentration of EV (mean ± SD) produced from all three types of EEO was similar (eutopic EEO from control patients; $1.5x10^9 \pm 3.5\ x10^8$ EV/well, eutopic EEO from endometriosis patients; $1.3x10^9 \pm 5.7\ x10^8$ EV/well, and ectopic EEO; $7.9x10^8 \pm 4.9\ x10^8$ EV/well). The mode sizes (mean ± SD) were 303 ± 24 nm, 284 ± 25 nm, and 137 ± 22 nm for eutopic EEO from control and endometriosis patients, and ectopic EEO, respectively.

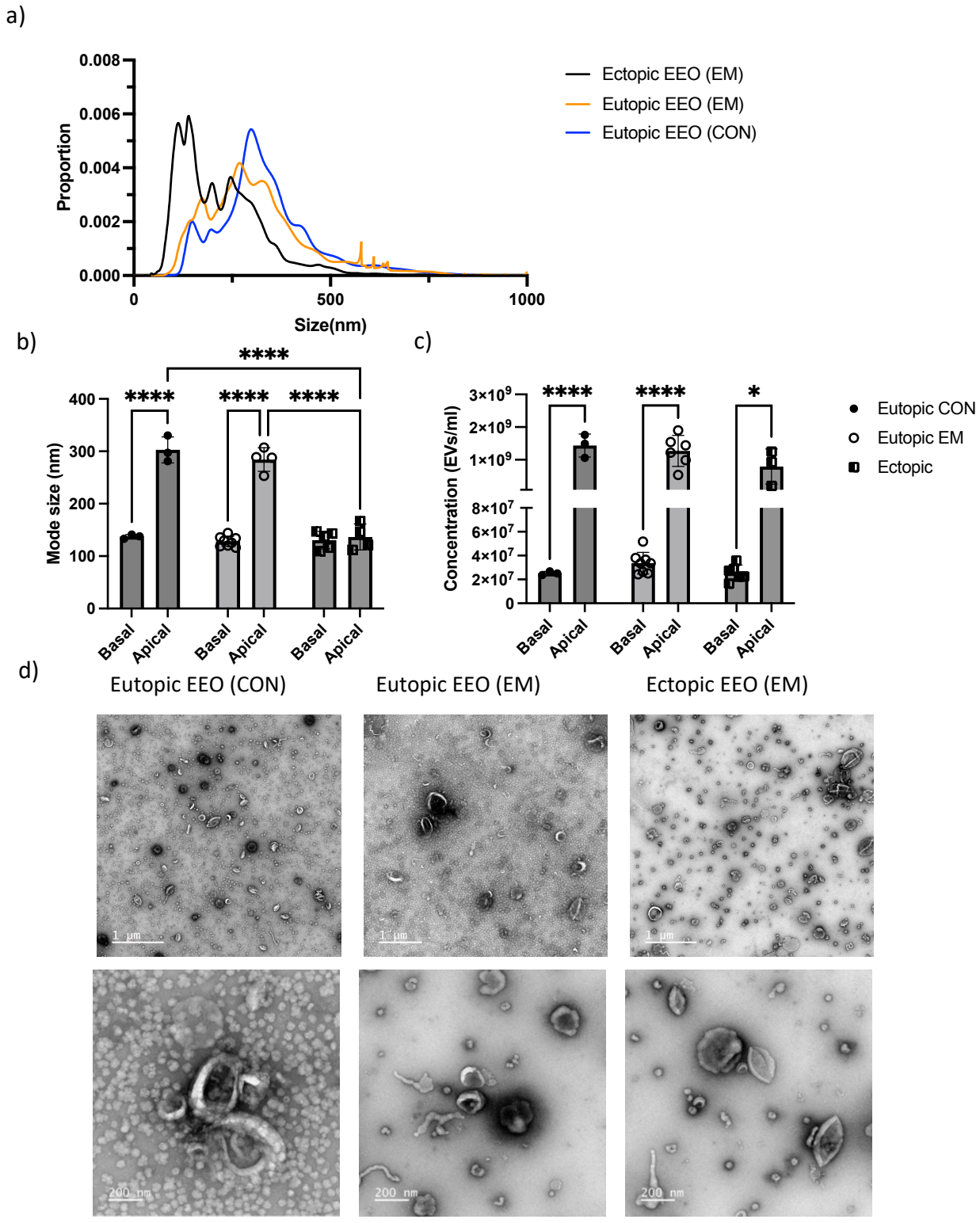

Figure 5.14 Characterisation of apical sEV from EEO. a) size distribution profile of apical sEV from eutopic EEO and ectopic EEO from endometriosis patients (n=4) and eutopic EEO from control patients (n=3) measured by NTA. B) modal size and c) concentration comparison of sEV from different EEO types and secretion sides. D) Representative TEM images of apical sEV. Scale bars: 1 µm (top), 200 nm (bottom). Bars = mean ± SD. Two-way ANOVA with Turkey's multiple comparisons (Shapiro-Wilk test: $p > 0.05$), *P<0.05, ****P<0.0001.

Two-way ANOVA was performed to assess the effects of EEO type and secretion side on sEV size. Both factors significantly affected the mode size of sEV. Apical sEV were significantly larger than basal sEV in control and eutopic EEO ($p<0.0001$), while remaining similar in size in ectopic EEO ($p>0.05$) (Figure 5.14b). Ectopic EEO sEV had a significantly smaller mode size compared to eutopic EEO from both endometriosis and control patients ($p<0.0001$) (Figure 5.14b) potentially due to the smaller 300nm peak population shown in the size distribution profile (Figure 5.16a). The concentration of EV did not vary between different EEO preparation types, but there was significantly higher EV released from the apical compared to basal membrane of all three EEO types (Figure 5.14c).

Visualisation of EV from the apical membrane utilising TEM confirmed the presence of vesicles with characteristic EV structure, including both double membrane and cup shape characteristics, in apical samples (Figure 5.14d), confirming that these are indeed EV and not aggregates or co-isolates. These apical EV were observed to be larger in size compared to the basal EV samples (Figure 5.14b), which supported the NTA findings.

5.3.3.2 Examination of the effect of isolation methods on EEO apical sEV characteristics

To ensure the robustness of these findings, various isolation methods were compared. NTA revealed similar size distribution profiles of apical EV isolated by ultracentrifugation followed by SEC (modal size 334nm) (Figure 5.15a), ultracentrifugation alone (modal size 350nm) (Figure 5.15b), two consecutive rounds of ultracentrifugation (modal size 348nm) (Figure 5.15c), and ultracentrifugation combined with 0.22µm membrane filtration (modal size 364nm) (Figure 5.15d). Regardless of the isolation technique used, the presence of large EV was consistently observed.

Recognising that the IOF collection method involved additional vortexing and centrifugation steps, which could potentially impact EV collection, I used an alternative approach to further validate these observations. This inverted EEO model allows for the direct collection of apical EV from the CM. NTA of EV collected using this alternative approach reaffirmed the presence of large EV in the apical side secretions, with a modal size of 353 nm (Figure 5.15e).

Furthermore, these apical EV demonstrated a high concentration ($2.1x10^9$ vesicle/well), consistent with the initial findings.

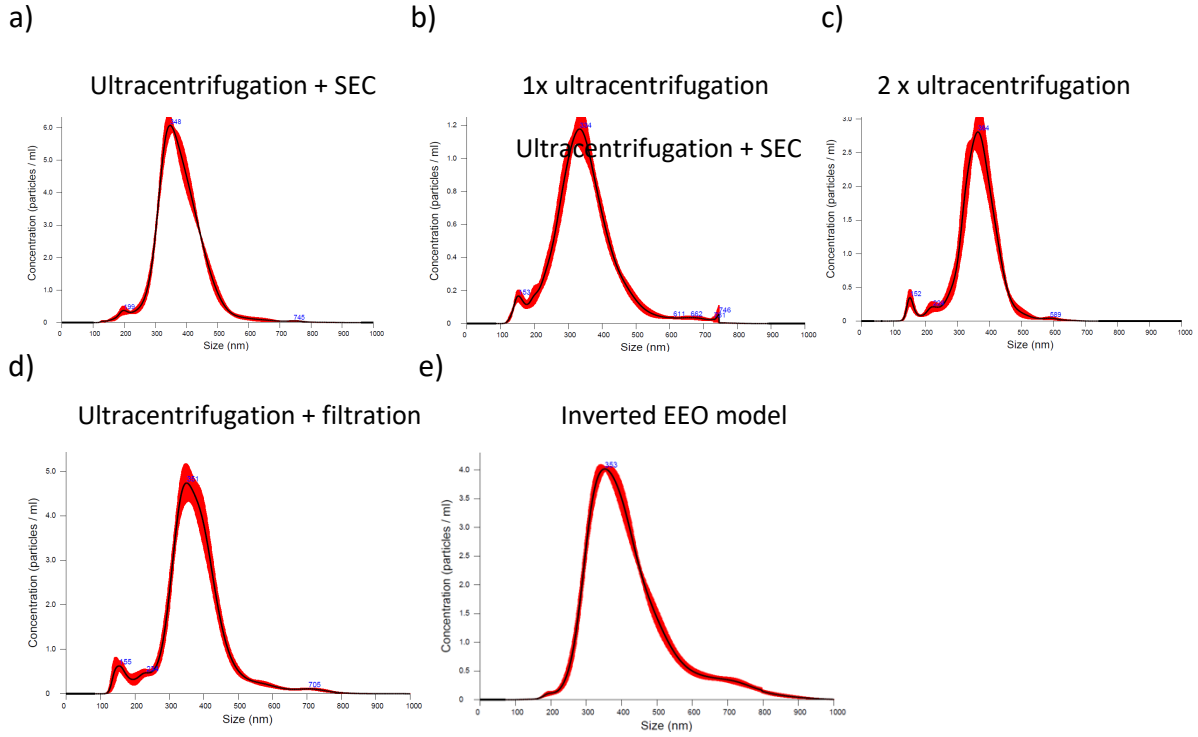

Figure 5.15 Validation of large apical EV using different isolation methods and collection approaches. NTA size distributions of apical EV isolated from IOF by a) ultracentrifugation +SEC, b) Ultracentrifugation, c) 2 x ultracentrifugation, d) ultracentrifugation + filtration. e) NTA profile of EV from conditioned media from inverted EEO model.

5.3.3.3 Characterisation of surface marker expression on EEO apical sEV by the MACSPlex EV kit IO.

Flow cytometry analysis of sEV using the MACSPlex EV kit IO revealed a low expression of sEV enriched markers on apical sEV. Specifically, I observed a 100-fold lower expression of CD81, CD9, and CD63 on apical sEV compared to basal sEV, when the same sEV input was loaded (Figure 5.16). This observation was consistent across different collection methods and models, with a similar trend observed in apical sEV isolated from the conditioned media using the inverted EEO model. Importantly, this marked difference was not limited to these three canonical sEV markers. The expression of other markers in the MACSPlex panel that are typically highly expressed on the basal side, such as CD133/1 and EpCAM, was also lower on apical EV.

It's important to note that the MACSPlex analysis methodology is based on the selection of EV expressing CD81, CD9, and CD63. Therefore, this observation suggests that only a small proportion of the apical sEV express these sEV-enriched markers. It indicates that the apical EV are a distinct subpopulation with different surface marker profiles compared to the basal EV.

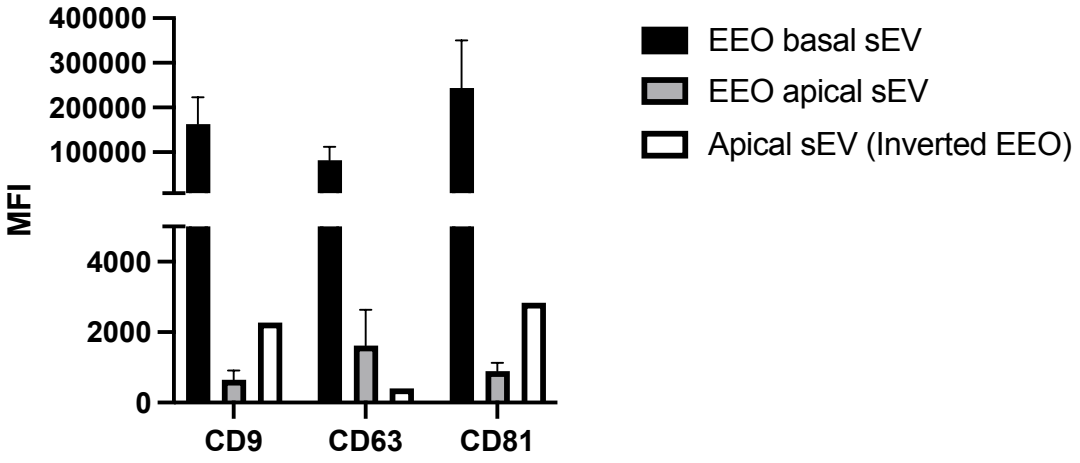

Figure 5.16. MACSPlex analysis of sEV markers on apical and basal sEV. Expression levels of CD81, CD9, and CD63 on apical sEV compared to basal sEV. Data represent mean MFI ±SD (n=2) for EEO basal sEV and EEO apical sEV, and MFI (n=1) for apical sEV from inverted EEO model.

The lower expression of CD81, CD63, and CD9 poses challenges for data normalisation. Typically, normalisation is based on the average of these three markers, but in this case, such normalization would result in abnormally high nMFI values. Consequently, these values would not be comparable to the basal sEV data, potentially leading to misinterpretation of results. Therefore, further protein marker expression characterisation using the MACSPlex EV kit IO was not performed for apical EV.

5.3.3.4 Characterisation of apical sEV from eutopic EEO in response to hormone stimulation

Lastly, I investigated the effect of hormone-stimulated differentiation on apical EV secretion. Interestingly, while I observed no difference in the overall concentration of EV, I did note a change in the size distribution profile (E2: mean 277nm, mode: 112nm, E2+P4: mean: 192nm, mode: 105nm; E2+P4+cAMP: 229nm, 112nm). Specifically, the peak at 300nm was

reduced and peak at 100nm was elevated with E2+P4 and P4+cAMP stimulation (Figure 5.17). The median size (D50) values were 305nm for E2, 120 nm for E2+P4, and 185 nm for E2+P4+cAMP, with an approximate 50% reduction in median size, again indicating a shift towards smaller EV under progesterone stimulation.

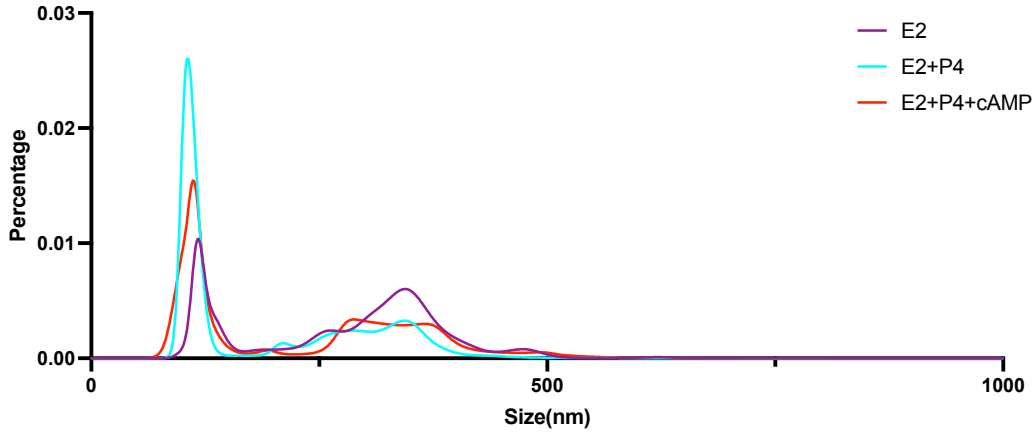

Figure 5.17. Size distribution profile of EEO apical sEV secretion. Size distribution profiles of apical EV under different hormonal conditions measured by NTA. N=1.

5.3.4 Investigation of the effect of sEV from basal endometrium on macrophage function

5.3.4.1 Examining of the effect of EEO basal sEV on the phagocytic activity of macrophages

In Chapter 4 Section 4.3.3, I identified that PF-sEV from endometriosis patients suppressed the phagocytic activity of macrophages. PF-sEV highly expressed EpCAM indicating their potential endometrial epithelial origins. This section further investigates the effect of basal sEV from ectopic EEO and eutopic EEO from endometriosis patients and controls on the phagocytic activity of THP-1 M2 macrophages as alternatively activated macrophages have been found to be predominant subtypes that facilitate lesion growth with impaired phagocytic activity in peritoneal microenvironment (112, 113).

To avoid the influence of EV present in the media, EEO were placed in EV depleted media for the 72 hours of EV generation. In Chapter 4, PF-sEV were used at a concentration of 1×10^{10} EV/mL to reflect the total EV load typically present in patient PF, and this was sufficient to

impair phagocytic activity. However, these sEV originate from a heterogeneous mix of cell types. To specifically assess the impact of an endometrial epithelial cell-derived population while maintaining a physiologically relevant concentration, sEV isolated from EEO were used at a concentration of 2×10^9 EV/mL in this chapter. $2x10^9$ EV/mL of sEV isolated by ultracentrifugation and SEC column were added to the culture and phagocytosis by M2 macrophages was assessed by flow cytometry, utilizing pHrodo *E.coli* deep red bioparticles (Figure 5.18). Phagocytic activity of M2 macrophages treated with sEV from eutopic EEO from control patients, showed no difference to the ExM group. M2 macrophages treated witheutopic EEO sEV from endometriosis patients showed significantly lower phagocytic activity compared to the ExM group ($p<0.01$). M2 macrophages treated with sEV from the ectopic EEO demonstrated the most dramatic effect, with an 84 ± 4% reduction in phagocytic activity, which was significantly lower than both the ExM ($p<0.0001$) and eutopic groups ($p<0.001$).

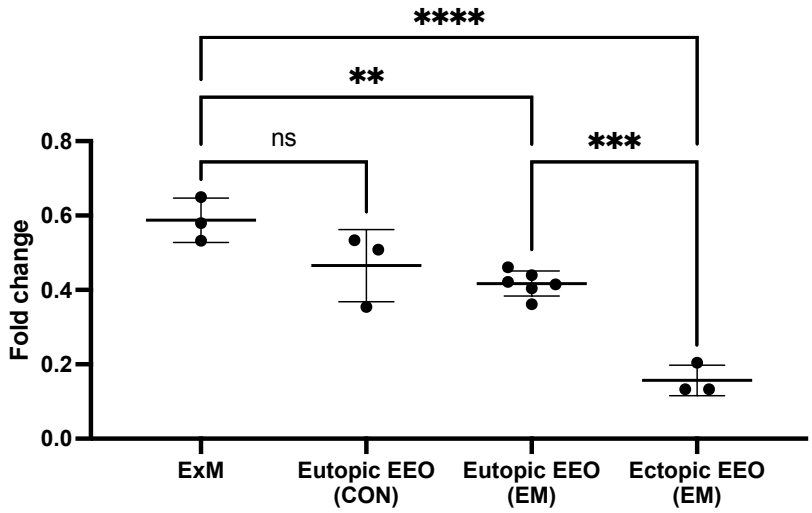

Figure 5.18. Direct effect of basal EEO sEV on THP-1 M2 macrophage phagocytic activity. Phagocytic activity of THP-1 M2 macrophages after 24-hour treatment with $2x10^9$ EV/mL of basal sEV isolated from eutopic EEO from control patients (CON), eutopic EEO from endometriosis patients (EM), and ectopic EEO from endometriosis patients (EM). EV-depleted ExM was used as a control. Phagocytic activity was assessed using pHrodo *E.coli* deep red bioparticles. Bars= mean±SD. One-way ANOVA with Turkey's multiple comparisons (Shapiro-Wilk test: $p > 0.05$), **P<0.01, ***P<0.001, ****P<0.0001.

5.3.4.2 Confirmation of EEO basal sEV-mediated suppression of phagocytic activity through EV depletion experiments.

Next, I performed EV depletion experiments to validate the role of sEV in modulating macrophage phagocytic activity, comparing the effects of complete conditioned media with those of EV-depleted conditioned media from EEO cultures.

The conditioned media (CM) from each EEO type was applied directly to THP-1 derived M2 macrophages for 24 hours or underwent 4 hours of ultracentrifugation to deplete EV before being applied to THP-1 derived M2 macrophages. Ultracentrifugation removed approximately 90% of EV, leading to significantly less EV in EV-depleted CM as measured using NTA ($p<0.001$) (Figure 5.19).

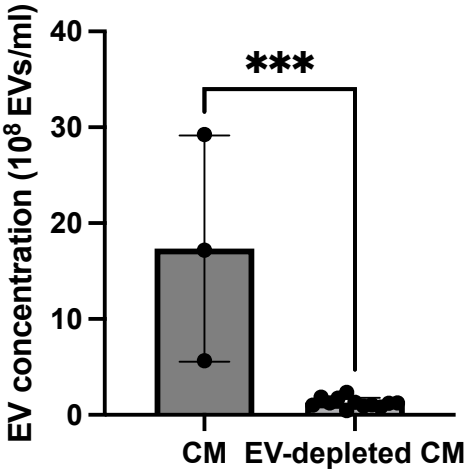

Figure 5.19. Efficacy of sEV depletion in EEO conditioned media by ultracentrifugation. NTA was used to quantify EV in conditioned media (CM) from EEO before and after ultracentrifugation. Conditioned media were collected from eutopic EEO of control patients (n=3), eutopic EEO of endometriosis patients (n=5), and ectopic EEO (n=5). Samples were pooled by type for initial EV quantification. EV depletion was performed by ultracentrifugation at 150,000 x g for 4 hours. EV-depleted samples (n=13) were analysed individually. Bars represent mean ± SD of EV concentration. Unpaired two-tailed *t*-test (Shapiro-Wilk test: $p > 0.05$),***$P<0.01$.

Following 24h treatments with conditioned media and EV-depleted conditioned media, the phagocytic activity of THP1-derived M2 macrophages was assessed. The results showed that conditioned media suppressed the phagocytic activity of macrophages compared to the

ExM treated group, with the most pronounced suppression observed in the ectopic EEO group (Figure 5.20). This suppression was partially alleviated by EV depletion in both the eutopic and ectopic groups, but not in the control EEO group (Figure 5.20).

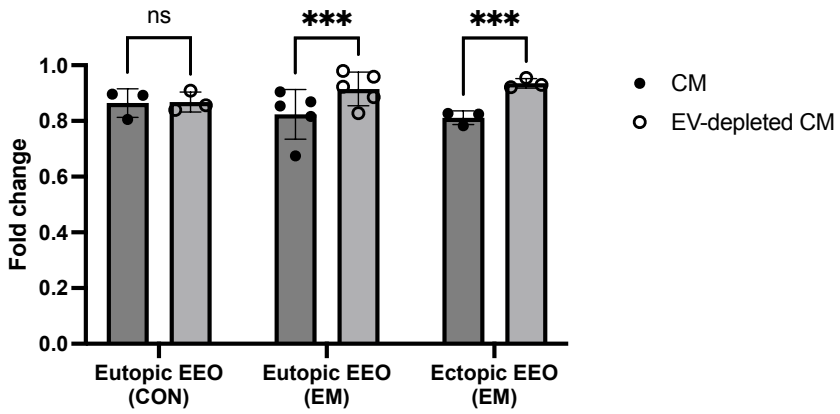

Figure 5.20. Effect of EV depletion on THP-1-derived M2 macrophage phagocytic activity. THP-1 M2 macrophages were treated with conditioned media (CM) or EV-depleted CM from eutopic EEO from control (n=3) and endometriosis patients (n=5), and ectopic EEO (n=3) cultures for 24h. Phagocytic activity was assessed using pHrodo *E.coli* deep red bioparticles and flow cytometry. Data are presented as fold change relative to untreated M2 macrophages in EV-depleted ExM (bioparticle only), calculated by dividing the MFI of pHrodo *E. coli* Deep Red bioparticles in THP-1-derived M2 macrophages pre-treated with EEO-EV or CM by the average MFI in untreated M2 macrophages from three replicates. Bars= mean ± SD. Two-way ANOVA with Turkey's multiple comparisons (Shapiro-Wilk test: $p > 0.05$), ***$P<0.001$.

5.3.4.3 Characterisation of CD47 expression on EEO basal sEV by the MACSPlex EV kit IO

The CD47/SIRP-alpha axis has been implicated in the suppression of macrophage phagocytic activity, as previously investigated in Chapter 4 Section 4.3.5. The earlier findings demonstrated that CD47 was co-expressed with EpCAM on PF-sEV (Figure 4.23, Chapter 4 Section 4.3.5). Given the observed suppression of macrophage phagocytic activity by EEO-sEV and the high expression of EpCAM on these sEV, I hypothesised that CD47 may also be present on EEO-derived sEV, potentially contributing to this suppressive effect. Using the same modified MACSPlex EV protocol presented in Chapter 4, the analysis of EEO basal sEV

showed CD47 co-expression with 10 markers including EpCAM, CD133/1, CD24, CD81 (Figure 5.21)

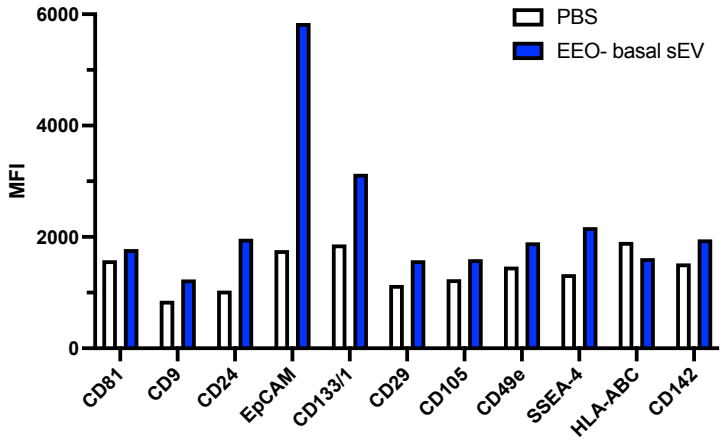

Figure 5.21. Flow cytometry analysis of co-expression of CD47 with various markers on EEO basal sEV utilising the modified MACSPlex EV protocol (n=1)**.** The co-expression of CD47 with a panel of 37 markers in the MACSPlex EV kit IO was assessed. Ectopic EEO-sEV (n=1) were analysed at concentrations of $1x10^9$ EV/mL. PF-sEV were incubated with capture beads from the MACSPlex EV kit IO and subsequently with anti-CD47 APC antibody. Capture beads with detection antibody alone served as a negative control (- EEO-basal sEV) to evaluate non-specific binding. Markers were considered positive if their signal exceeded both the respective isotype control (mIgG or REA) and the negative control.

5.3.5 Integrated analysis of sEV in the peritoneal microenvironment in endometriosis

To gain a comprehensive understanding of the sEV present in the peritoneal microenvironment of endometriosis patients, I conducted an integrated analysis of sEV derived from various sources, analysed in the above chapters. This analysis included PF-sEV, pMΦ-sEV, and both basal and apical EEO-sEV from ectopic and eutopic endometrium of endometriosis patients (Figure 5.22).

NTA was performed to characterize the size distribution of sEV from these different sources. PF-sEV demonstrated a modal size of 220 ± 53nm, with a broad size distribution: approximately 50% of EV were smaller than 200nm, while the other 50% ranged between 200nm to 500nm. This diverse size profile likely reflects the heterogeneous cellular origins of PF-sEV in the complex peritoneal environment.

Interestingly, sEV derived from different cell sources exhibited distinct size distributions. pMΦ-sEV showed the smallest modal size of 128 ± 20nm, with a remarkably uniform size distribution – 95% of these EV were smaller than 200nm. This homogeneity suggests a consistent vesicle production process in pMΦ.

Eutopic and ectopic EEO basal sEV displayed similar a modal size of 128 ± 10nm and 130 ± 17nm respectively, characterized by a single peak. Compared to pMΦ-sEV, EEO basal EV contained a higher proportion of larger EV exceeding 200nm.

The most pronounced differences were observed in apical EEO-sEV, which exhibited a bimodal size distribution. Notably, ectopic EEO apical EV contained fewer large EV compared to eutopic EEO and demonstrated a smaller modal size (137 ± 25 nm) than eutopic (284 ± 22 nm). This distinction between ectopic and eutopic EEO-sEV suggests that ectopic epithelial cells exhibit differences to eutopic epithelium.

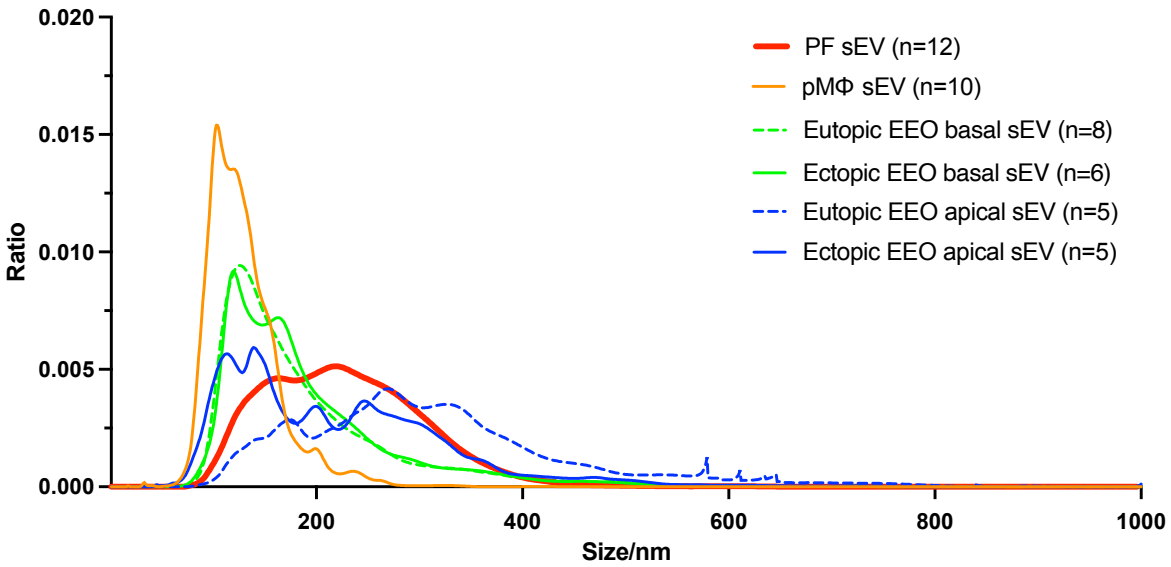

Figure 5.22. Comparative size distribution profiles of sEV from various sources in the endometriosis peritoneal microenvironment. NTA size distribution profiles of sEV derived from PF; pMΦ; eutopic EEO, basal and apical; Ectopic EEO, basal and apical.

Comparative analysis of sEV surface marker expression was also performed. For the comparison between sEV derived from pMΦ and EEO, i focused only on markers present in all samples of each type, as these represent *in vitro* cultures of single cell types. This approach allowed me to exclude any potential background contamination and focus on cell-type-specific markers. For PF-sEV, all markers expressed in any sample are included to provide a comprehensive characterisation of the diverse EV population in PF, which originates from multiple cell types *in vivo.*

The overlapping and intersection of surface markers were displayed in figure 5.23. The analysis revealed differential expression patterns between pMΦ and EEO sEV. Markers such as CD14, CD45, CD86, CD4, CD8, CD2, CD11c, MCSP, and CD31 were present in pM-sEV but absent in EEO-sEV. Conversely, CD133/1, CD326, CD146, and CD69 were expressed on EEO-sEV but not on pMΦ-sEV. These distinct marker profiles reflect the different cellular origins of these EV and may serve as useful identifiers in future studies.

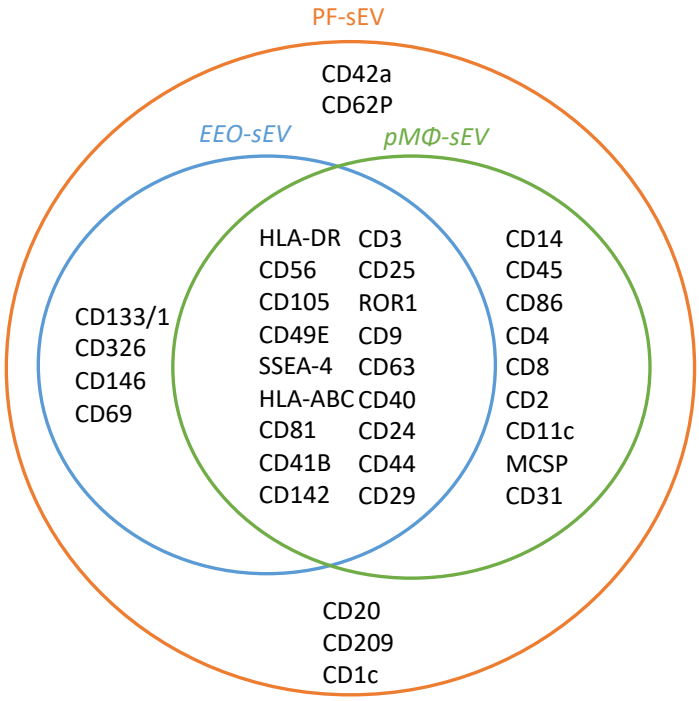

Figure 5.23. Surface marker expression profile of sEV from different sources in the endometriosis peritoneal microenvironment. Venn diagram showing the distribution and overlap of surface markers on sEV derived from PF, pMΦ and EEO basal side.

I observed that the majority of marker expression levels were lower than the three well-established sEV-enriched markers: CD81, CD9, and CD63, thereby producing a nMFI expression lower than 1. However, there were some notable exceptions. In pMΦ-sEV, HLA-DR expression was remarkably high, measuring six times higher than the average expression of CD81, CD9, and CD63. Similarly, in EEO basal EV, EpCAM and CD133/1 expression levels were five times and two times higher, respectively, than the average of the three enriched markers. These highly abundant markers may serve as excellent indicators of cellular origins in future studies. Although HLA-DR is higher in pMΦ-sEV, its expression was also found in EEO-sEV. A combination of markers including CD14, CD86, and CD45 may be necessary to confidently confirm pMΦ origin.

Interestingly, both pMΦ and EEO-sEV expressed markers typically associated with other cell types, albeit at low levels. These included CD3 (typically associated with T cells), CD56 (associated with NK cells), and CD105 (associated with endothelial cells). This observation underscores the complexity of EV surface marker expression and highlights the intricate nature of intercellular communications. It also suggests that the presence of a marker does not necessarily indicate the cellular origin of the vesicle, emphasizing the need for careful interpretation of sEV marker profiles.

Our analysis also revealed that several markers (CD42a, CD62P, CD20, CD209, and CD1c) were absent in both pMΦ and EEO-sEV but present in PF-sEV. CD42a and CD62P are well-known platelet markers, and their presence aligns with a recent study demonstrating platelet activation signalling pathways and elevated platelet markers in sEV from the PF of endometriosis patients (341). The presence of CD20, CD209, and CD1c, which are associated with B cells and adaptive immunity, indicates that B cells and T cells, along with macrophages, play a role in immune regulation within the peritoneal microenvironment of endometriosis patients.

5.4 Discussion

This chapter presents successful establishment and characterisation of EEO from both eutopic endometrial tissues and ectopic endometriosis lesions, as well as the analysis of their sEV profiles, in endometriosis patients for the first time.

5.4.1 Successful establishment of an EEO model in endometriosis research

This study has successfully replicated and extended EEO models based on published protocols (107, 330) in endometriosis research. The methodology demonstrated high reproducibility and replicability, yielding a 100% success rate in generating EEO from cryopreserved eutopic endometrium samples of control subjects, endometriosis patients, and individuals undergoing HT (Mirena coil excluded). The establishment of EEO from eutopic endometrium across all patient cohorts underscores the robustness of the protocol in endometriosis-focused investigations.

For eutopic endometrium, the optimized protocol modified from Turco's protocol (330) involving 30-minute collagenase V digestion and 40µm filtration to separate stromal cells and epithelial cells. Gland-like epithelial cells were retained on the cell strainer and collected by backwashing. This method resulted in clear epithelial cultures with minimal stromal contamination, as confirmed by phase-contrast microscopy in P0.

Literature on ectopic EEO growth in endometriosis research is very limited. Only two studies (107, 333) have reported the successful growth of ectopic EEO from endometriosis lesions. This current investigation successfully cultivated ectopic EEO from endometriosis lesions of various stages, peritoneal locations, and hormone therapy status. The study corroborated Boretto et al.'s observations (107) while employing a different tissue digestion protocol, further validating the possibility of growing ectopic EEO from diverse endometriosis lesions.

Unlike eutopic endometrium, endometriosis lesions exhibited resistance to tissue dissociation even after prolonged digestion periods exceeding 1h. Microscopic examination

revealed no gland-like structures, indicating distinct tissue architecture, and large undigestible tissue chunks persisted. To address these challenges, the study modified the protocol by employing collagenase V digestion for 1-1.5 h dependent on lesion type and sizes, followed by filtration of large indigestible tissues using a 100µm cell strainer. This approach, combined with the use of fresh samples, yielded an 80% success rate in ectopic EEO cultivation. The investigation revealed a potential requirement for distinct protocols compared to eutopic EEO growth, underscoring the heterogeneity in tissue dissociation and morphology among endometriosis lesions. The use of TrypLE instead of filtration in Boretto's protocol may offer an alternative method for dissociating undigestible tissue chunks. These findings emphasise the necessity for a comprehensive evaluation to modulate digestion time and protocols based on various clinical parameters such as lesion types (red, blue) and size. Such optimization is crucial for ensuring reproducibility and comparability of ectopic EEO models in endometriosis research.

I observed reduced initial growth rate of ectopic EEO in P0, a phenomenon also reported by Boretto et al. (27). However, this difference was not apparent after subsequent passages. This initial growth disparity could be attributed to harsher dissociation protocols and lower cell viability. Alternatively, the ExM, while containing essential factors for eutopic endometrium growth (330), may not be optimal for the initial establishment of ectopic EEO cultures. Boretto et al. investigated the effect of several key components already included in ExM on ectopic EEO growth, they identified that the removal of noggin and EGF compromised ectopic EEO development (27). Future work could explore whether ectopic EEO requires higher doses of noggin and EGF.

Additionally, R-spondins, key modulators of Wnt-signaling (342), play an essential role in epithelial cell growth (343). Dysrelulation of Wnt-signalling was associated with endometriosis (344, 345). Apart from R-spondin 1, which is implemented in current protocols, R-spondin 3 has been found to stimulate intestinal epithelial regeneration (346) and has been used together with R-spondin 1 in intestinal organoid growth (347, 348). The latest proteome-wide association study has found R-spondin 3 to be associated with endometriosis (349). either alone or in combination, might better support lesion organoid growth. Based on these findings, R-spondin 3, either alone or in combination with R-spondin

1 in organoid culture, requires further investigation as it might better support lesion organoid growth.

5.4.2 Characterisation of EEO-sEV

I have revealed the first EEO-sEV characterisation from endometriosis lesions and the first apical sEV characterisation of eutopic and ectopic EEO.

5.4.2.1 Eutopic EEO-sEV are influenced by polarity and hormonal stimulation

Significantly higher sEV concentrations were released from the apical side, with 100 times more sEV secreted compared to the basal side. In addition, the mode sizes of apical sEV are significantly larger than those from the basal side. The size distribution profile revealed basal side EV showed one peak at 130nm, while apical EV displayed a distinct bimodal distribution with a prominent peak at 300 nm, indicating differential EV secretion patterns between the apical and basal surfaces. The results were consistent between apical sEV collected from IOF in EEO and conditioned media from inverted EEO. The presence of larger EV was confirmed by TEM. The marker expression again confirmed the different populations of EV secreted from the basal and apical side of EEO. When analysing by the MACSPlex EV kit IO, apical sEV exhibited low expression of sEV-enriched markers CD9, CD81, and CD63. This observation supports the hypothesis that apical sEV likely represent a different subpopulation of EV compared to basal sEV. The low expression of these markers rendered MACSPlex analysis unsuitable for apical EV, preventing a direct comparison with basal EV profiles.

In eutopic endometrium, the apical side plays a crucial role in the reproductive process, as it has direct contact with the uterine lumen and, potentially, the embryo during implantation. The apical surface of endometrial epithelial cells is known to form pinopodes, which are dome-shaped protrusions that appear on the cell surface during the window of implantation in response to progesterone (350, 351). Their potential functions are believed to secrete EV to support embryo-endometrial interactions and the implantation process

(352, 353). The presence of larger EV (around 300 nm) secreted from the apical side of eutopic and control EEO may be related to this function.

The differential composition of apical and basal EV likely reflects the organized protein sorting and targeting processes within epithelial cells (354, 355). This sorting process, which directs proteins to either apical or basolateral membranes, may similarly influence EV cargo packaging. The cytoskeleton, particularly polarised microtubules, guides EV to specific membrane domains (313). Regulatory proteins like specific SNARE complexes play a crucial role in polarised exocytosis (356-358) and are also involved in EV secretion (359). This suggests that similar mechanisms might regulate the fusion of EV-containing multivesicular bodies with either the apical or basal plasma membrane.

5.4.2.2 Hormonal stimulation affects apical sEV from eutopic EEO

Another crucial facet of endometrial research is the impact of hormonal cycling. Addition of P4 and cAMP successfully differentiated control eutopic EEO to express SPP-1. Surprisingly, I did not observe changes in basal sEV concentration, size, or marker expression. This could indicate that differentiation primarily affects the apical side, which interfaces with the embryo. Indeed, I observed a reduction in the 300nm peak population of apical EV after hormone stimulation, though this finding is limited by a very small sample size (n=1). The inability of the MACSPlex EV kit IO to assess markers for apical sEV, prevented a comprehensive analysis of surface marker profiles to assess apical sEV changes after hormone-induced differentiation. These constraints highlight the need for alternative approaches, particularly proteomics and transcriptomics, to fully characterize hormone-induced changes in EV populations.

While protocols exist for simulating menstrual cycle hormonal changes in eutopic EEO (330), there is a notable absence of protocols replicating the specific hormonal milieu of the peritoneal cavity where endometriotic lesions reside. Abnormal oestrogen production in the peritoneal cavity has been linked to lesion growth and maintenance (2). This approach would allow for more physiologically relevant studies of lesion EEO, potentially revealing

important insights into lesion behaviour, drug responses, and the mechanisms underlying endometriosis progression.

5.4.2.3 EEO-sEV present an endometriosis lesion specific profile

Ectopic EEO-EV from endometriosis lesions showed differences to eutopic EEO. While the apical and basal side EV showed distinct size profiles in eutopic EEO. The apical sEV from ectopic EEO presented with a significantly smaller mode size compared to eutopic EEO, the mode size was similar to basal sEV. Since cell polarity plays a crucial role in determining secretion profiles in eutopic endometrium, the similarities observed may result from the dysregulated functions and impaired polarity of endometrial epithelial cells in endometriotic lesions.

Analysis of surface marker expression revealed distinct patterns in basal side EV, particularly in relation to endometriosis-associated markers. CD44 and CD29 were significantly higher in ectopic EEO-EV compared to eutopic and control. CD44, a cell-surface glycoprotein, is involved in cell-cell interactions, cell adhesion, and migration (165). By interacting with peritoneal mesothelial cell (PMC)-associated hyaluronan, CD44 in cancer cells (ovarian (360) and gastric cancer (361)) and endometrial cells (362) has been found to be responsible for the attachment to mesothelium. Decreased development of endometriotic lesions was observed in CD44 knockout mice (363). Soluble CD44 is high in PF of endometriosis (364, 365). CD29, also known as integrin β1, plays a role in cell adhesion and signalling (366) and contributes to ovarian cancer cell adhesion to mesothelium (360).

The elevated expression of these markers in ectopic EEO sEV suggests enhanced adhesive and migratory properties, which may contribute to the establishment and survival of endometriotic lesions. Furthermore, the high expression of CD44 and CD29 has been linked to epithelial-mesenchymal transition (EMT) (367). Epithelial-mesenchymal transition (EMT) is a process where epithelial cells lose their polarity and cell connections, gaining increased mobility like mesenchymal cells. This transformation has been linked to the progression of endometriosis (367). EpCAM, an epithelial cell adhesion molecule, was highest in control

eutopic EEO-sEV and lowest in ectopic EEO-sEV (p=0.07). The lower expression in ectopic EEO might indicate a loss of epithelial characteristics, possibly related to EMT.

The patterns observed in eutopic EEO-EV present an intriguingly mixed profile. Some markers (CD44 and CD29) showed similarity with ectopic EEO-EV, EpCAM was more akin to control eutopic EEO-EV. This heterogeneous expression pattern could be indicating fundamental differences in the eutopic endometrium of women with endometriosis compared to those without the disease, even before lesion formation. This aligns with previous findings that eutopic endometrial tissue in women with endometriosis carries a distinct RNA profile in sEV compared to controls (185). The mixed profile also reflects the influence of the peritoneal microenvironment on ectopic lesions, explaining why some markers in eutopic EEO-sEV remain similar to controls while others change.

The comprehensive analysis of EEO sEV underscores the polarised nature of epithelial cells, revealing distinct characteristics between apical and basal EV populations. This finding emphasizes the critical importance of considering polarised EV secretion when investigating EV-mediated intercellular communication in endometrial function and endometriosis pathophysiology. Endometriotic lesions display epithelial components that retain a glandular organization, yet these structures exhibit distinct morphological characteristics and variations that differ from the typical glands observed in the eutopic endometrium (323, 324). The distinct sEV profile of ectopic EEO compared to that of eutopic EEO in this chapter, indicate functional differences between these cell populations. To further elucidate the molecular differences between eutopic and ectopic EEO-sEV, as well as between their apical and basal compartments, future studies should use comprehensive RNA sequencing and proteomic analyses.

Additionally, given the observed elevated levels of markers like CD44 and CD29 in ectopic EEO sEV, a comparative analysis of the cellular expression of these markers between eutopic and ectopic EEO should be conducted. Comparison of cellular and EV expression of these markers could reveal insights into cargo selection and EV loading mechanisms and provide a broader picture of the distinct molecular profile of endometriosis lesions.

5.4.3 The effect of EEO-sEV on macrophage phagocytosis

As PF-sEV analysis revealed high expression of EpCAM in Chapter 3 Section 3.2.3, which was also found to be high on ectopic EEO-sEV, I hypothesize that ectopic EEO-sEV constitute a large proportion of PF-sEV and contribute to phagocytic suppression.

The functional studies on macrophage phagocytosis revealed a suppressive effect of both eutopic and ectopic EEO-sEV from endometriosis patients, with ectopic EEO showing the most pronounced effect. Eutopic EEOEV may aid in initial establishment, while ectopic EEO-sEV may assist in maintenance by evading immune surveillance. These findings from the EV experiment were supported by EV-depletion experiments.

Preliminary data suggested the co-expression of CD47 on ectopic EEO-sEV, raising intriguing questions about whether the CD47/SIRPα axis I identified may be specific to EEO-sEV. Future studies should incorporate CD47 blocking experiments to confirm the functional role of the CD47/SIRPα axis in EEO-sEV-mediated phagocytosis suppression. Additionally, studies to deplete EpCAM+/CD133/1+ sEV in the PF-sEV population may help identify if the suppression is solely coming from EEO-sEV or if other sEV in PF-sEV also have a suppressive effect on the phagocytic activity of macrophages.

Regarding which macrophages have been influenced, apart from pMΦ, lesion derived epithelial sEV may influence lesion-resident macrophages, derived endometrial macrophages, and monocyte-derived macrophages, which have been found to have a pro-disease role in endometriosis (123). For eutopic epithelium, in addition to potentially traveling to the peritoneal cavity through retrograde menstruation, they may also affect macrophages in the eutopic endometrium in cell modelling during menstruation and embryo implantation (368).

5.4.4 Integrated EV analysis in the peritoneal microenvironment of endometriosis

Lastly, the size distribution and surface markers of sEV from different sources (pMΦ, EEO, and PF) were integrated to provide a comprehensive picture of the peritoneal microenvironment and identify cell-specific markers. The results revealed that each cell source secretes different EV, resulting in a broad size distribution of PF-sEV. This diversity underscores the importance of careful data analysis when studying EV in complex biological environments.

The study identified CD133/1 and CD326 as potential markers for endometrial epithelial cells, while CD14, CD45, and HLA-DR were associated with pMΦ. Interestingly, some markers were found in PF-sEV but not in pMΦ or EEO-sEV (both ectopic and eutopic), suggesting contributions from other cell types. These markers were linked to platelets (CD62p, CD42a) (369) and components of adaptive immunity (CD1c (370), CD20 (371)), such as T cells and B cells. Interestingly, CD209, typically expressed in macrophages (372), was not detected in pMΦ but was present in PF-sEV. This discrepancy could be attributed to either altered properties of macrophages *in vitro* or the presence of a small subpopulation of CD209-positive macrophages in the PF that was not captured in the isolated pMΦ.

However, several limitations of this analysis should be noted. The current analysis could not distinguish between eutopic epithelial-EV and ectopic epithelial-EV, or determine which population consists of a larger EV population.

The characterisation of endometrial stromal cell-derived sEV is also crucial as they represent the largest cell population in the endometrium and play key roles in both normal endometrial function and endometriosis pathogenesis (373). While CD44, CD29, and CD146 (mesenchymal stromal/stem cell marker) are found present in endometrial stromal cells (220-222), these markers serve multiple functions, including roles in cell adhesion and phagocytosis. Additionally, these markers have been detected in macrophages (374-376) and were also found in pMΦ-sEV profiles in our current research, indicating they are not

exclusively specific to stromal cells. The current characterisation is less definitive due to the lack of CD10, a sensitive and specific endometrial stromal cell marker (377, 378), in the panel. Future incorporation of more specific stromal markers such as CD10 or CD90 into the characterisation panel, combined with parallel analysis of EVs isolated directly from ex vivo endometrial stromal cells, will help confirm and validate the stromal signature in these populations. Future work can also investigate whether the EEO core is hypoxic, which may lead to changes in EV profiles, by staining EEO with a hypoxia dye such as Image-iT Green (ThermoFisher, USA).

Additionally, while the MACSPlex technique provides valuable semi-quantitative data on EV surface markers, it does not allow for precise quantification of marker proportions within the whole EV population. This limitation highlights the potential benefit of complementary single EV flow cytometry approaches in future studies to provide a more detailed and quantitative characterisation of EV subpopulations.

This chapter demonstrated the value of organoid models in endometriosis research and presents the first comprehensive analysis of EEO sEV in endometriosis, revealing an essential role of endometrial epithelial cells in endometriosis. Key findings include the impact of EEO polarity on EV secretion, identification of endometriosis-specific EV markers, and potential hormone influences on EV characteristics. The research also suggests important roles for EV in modulating macrophage function. These findings open new avenues for research in understanding and managing this complex condition.

Chapter 6 Conclusion

In Chapter 1, I proposed three main hypotheses:

1. PF-sEV originate from diverse cell types, including pMΦ and endometriosis lesions.
2. PF-sEV could serve as biomarkers for environmental changes in the peritoneal microenvironment, such as disease progression or hormonal status.
3. PF-sEV, especially those derived from endometrial epithelial cells, have distinct effects on macrophage differentiation and function, contributing to the pathogenesis of endometriosis.

To address these hypotheses, this thesis has provided a comprehensive characterisation of surface markers on sEV in the peritoneal microenvironment of endometriosis, utilising multiplex bead-based flow cytometry. The study encompassed sEV from both biological fluids and *in vitro* cell cultures, offering a multifaceted view of these vesicles in endometriosis. Beyond characterisation, this research also explored the functions of these sEV, particularly their role in macrophage regulation.

Specifically, in Chapter 2, the study focused on sEV derived from pMΦ ex vivo. This chapter first revealed high expression of CD206 and CD163 in $CD14^{high}CD16^{high}$ pMΦ in endometriosis patients and revealed high expression of immunomodulation markers including HLA-DR, and CD24 and macrophage markers like CD14, CD86 and CD45 on pMΦ-derrived sEV. Notably, HLA-DR expression on these sEV was found to positively correlate with cellular markers, while CD14 did not show such a correlation.

Investigation of PF-sEV demonstrated considerable inter-patient variability in concentration and surface marker expression. Immune cell markers that have been shown in pMΦ-sEV, including HLA-DR, CD14, and CD24, were consistently present, while EpCAM and CD133/1 indicated endometrial epithelial cell markers were also found in PF-sEV. Hormonal

treatment was found to affect the sEV profile, suppressing EpCAM expression and elevating CD24, with CD133/1 showing variability among different types of HT.

Utilising THP-1 cells as a model of macrophages, PF-sEV from endometriosis patients were found to suppress their phagocytic activity. CD47 was co-expressed with EpCAM on PF-sEV, and blocking CD47 led to attenuation of suppression, indicating a crucial role for this interaction.

The study then focused on endometrial epithelial derived sEV using organoid models. EEOs were successfully developed from endometriosis lesions, with basal epithelium EEOs expressing lesion-specific surface marker profiles. Both ectopic and eutopic EEO-sEV demonstrated high EpCAM expression and no CD14 expression, suggesting EpCAM could be an indicator of cell origin in PF-sEV. Importantly, EEO-sEV from lesions also suppressed phagocytic activity of macrophages.

Finally, the research revealed that apical and basal EEOs from eutopic endometrium and ectopic endometriosis lesions have different EV profiles, and this polarity may be disrupted in lesions, reflected in less pronounced differences between apical and basal EV in ectopic EEOs. These findings collectively enhance our understanding of the complex role of sEV in endometriosis and offer potential avenues for future diagnostic and therapeutic interventions.

The comprehensive analysis conducted in this thesis has contributed to a published literature review examining the current understanding of pMΦ-sEV biology in endometriosis pathophysiology (56), which identified critical knowledge gaps in the field. Furthermore, the novel findings regarding sEV surface marker characterisation and their immunomodulatory effects on macrophage phagocytosis are currently being prepared for peer-reviewed publication.

This conclusion chapter will synthesize these findings in relation to the initial hypotheses and discuss their implications for our understanding of endometriosis.

6.1 Cellular origins of sEV in the peritoneal microenvironment of endometriosis

A key finding of this research is the distinct expression patterns of surface markers on sEV in the peritoneal microenvironment of endometriosis, indicating their different cellular origins. This diversity in sEV origins provides valuable insights into the complex cellular interactions occurring in this disease.

From *in vitro* culture studies, I have identified cell specific markers for pMΦ and endometrial epithelial cells. CD14 and HLA-DR could serve as indicators of pMΦ, which highly express these markers. In contrast, endometrial epithelial cell-derived sEV showed high expression of EpCAM and CD133/1. This distinction allows for the potential identification of sEV cellular origins within the PF based on surface markers.

In EV characterisation directly from primary PF, sEV profiles demonstrated high expression of HLA-DR, CD133/1, and EpCAM, indicating a dominant role of sEV from endometrial epithelial cells and antigen-presenting cells in the peritoneal microenvironment. This finding suggests that these cell types may be significant contributors to the sEV population in endometriosis.

The constant expression of CD8 and high frequency of CD4 (10 out of 11 samples) in PF-sEV revealed a potential role for T cell-derived sEV, adding another layer of complexity to the cellular origins of sEV. T cells are the second largest immune cell population in peritoneal fluid (20%) after macrophages (26). Investigating the EV profile from different T cell subtypes in endometriosis will be important in understanding the role of the adaptive immune system in the disease. Furthermore, the study identified markers indicative of other cell types, including platelets (CD42a), neural cells/NK cells (CD56), suggesting a diverse range of cellular contributors to the sEV population in the peritoneal microenvironment.

Apart from endometrial epithelial cells and immune cells, another potential origin of PF-sEV is endometrial stromal cells which are dominant in endometrium and lesions (373). The MACSPlex EV analysis revealed markers associated with mesenchymal stem/stromal cells (CD44, CD29, and CD146) in PF-sEV, suggesting potential origin from endometrial stromal cells where these markers are known to be present (220-222). However, the interpretation of these results is complex since these markers serve multiple biological functions, including cell adhesion, and are not exclusively specific to stromal cells (374-376). Their expression in other cell types like macrophages (374-376) and detection in pMΦ-sEV profiles complicates the definitive identification of stromal cell-derived sEV in PF-sEV profiles.

This challenge of marker specificity extends beyond stromal cell markers. Most markers analysed in the study were not exclusively expressed by one cell type. For instance, CD24 is highly expressed by both pMΦ-sEV and EEO-sEV, whilst HLA-DR is expressed in both, but at different abundances. This overlap demonstrates that relying on single cell markers is insufficient for determining sEV cellular origins. Instead, a panel of positive and negative markers, considering both presence and relative abundance, is necessary to accurately confirm cell origins.

Additionally, the semiquantitative nature of the MACSPlex EV kit IO (143) further limits our ability to precisely quantify the proportions of sEV from different cell types. To address these limitations, single EV flow cytometry analysis could be employed to quantify the proportion of EV secreted from each cell type based on marker expression and choose markers of interest freely. This could provide a more accurate picture of the cellular origins of sEV in the peritoneal microenvironment. Future incorporation of more specific endometrial stromal markers such as CD10 or CD90 (377, 378) into the characterisation panel, combined with parallel analysis of EV isolated directly from *ex vivo* endometrial stromal cells, will help confirm and validate the stromal signature in these populations.

Moreover, comparative studies between endometriosis patients and controls could reveal how the proportions of sEV from different cell types change in the disease state. Single EV flow cytometry allows multi-colour antibody labelling (379, 380), and would therefore enable future investigation into the co-expression of markers such as CD44 and CD29 on

EpCAM+ EV to identify ectopic lesion origins. This could lead to further investigation on how these cells regulate endometriosis development via EV secretion.

Further investigation into the functional roles of sEV from different cellular origins could enhance our understanding of how various cell types contribute to the pathogenesis of endometriosis through EV-mediated communication.

6.2 Mechanisms of endometriosis progression

This thesis uncovered an impairment in the phagocytic activity of macrophages when exposed to PF-sEV and EEO-sEV. This effect is likely mediated through the CD47/SIRP-alpha pathway and may originate from endometrial epithelial cells in lesions. By inhibiting macrophage function, sEV could contribute to the creation of an immunosuppressive microenvironment that favours the survival and growth of endometriotic tissue.

To further support these findings, future experiments could examine the effect of removing EpCAM+ EV from PF-sEV on mediating phagocytic activity. This would help confirm whether this regulation is solely from endometrial epithelial cells or if EV derived from other cells also contribute to the suppression.

The expression of various immunomodulation markers on PF-sEV suggests the immune regulation may extend beyond phagocytosis. The high expression of HLA-DR on PF-sEV observed in this study suggests a potential role in communicating with T cells. pMΦ-sEV which highly expressed HLA-DR could be important in T cell regulation. Notably, EEO-sEV also expressed HLA-DR. A recent study revealed that ectopic epithelial cells from ovarian endometriosis patients expressed higher levels of HLA-DR and stimulate CD4+ T cells (381). sEV may also be involved in this process. Future experiments investigating how PF-sEV and EEO-sEV affect T cell activation and cytotoxicity may provide crucial insights into the complex immune dynamics of endometriosis.

The elevation of CD44 and CD29 in lesion EEO-sEV may indicate differences in the adhesive and proliferative abilities of these cells in facilitating the attachment and growth of endometrial cells at ectopic sites. By interacting with peritoneal mesothelial cells, CD44 and CD29 have been reported to contribute to ovarian cancer cell adhesion (360) and CD44 in endometriosis lesion development (362, 363). Given that EV serve as a route for transferring "don't eat me" signal markers to facilitate immune evasion (308), 68), it is worth investigating whether CD44 and CD29 can be transferred via EV to eutopic endometrial epithelial cells, potentially enhancing their adhesion capabilities.

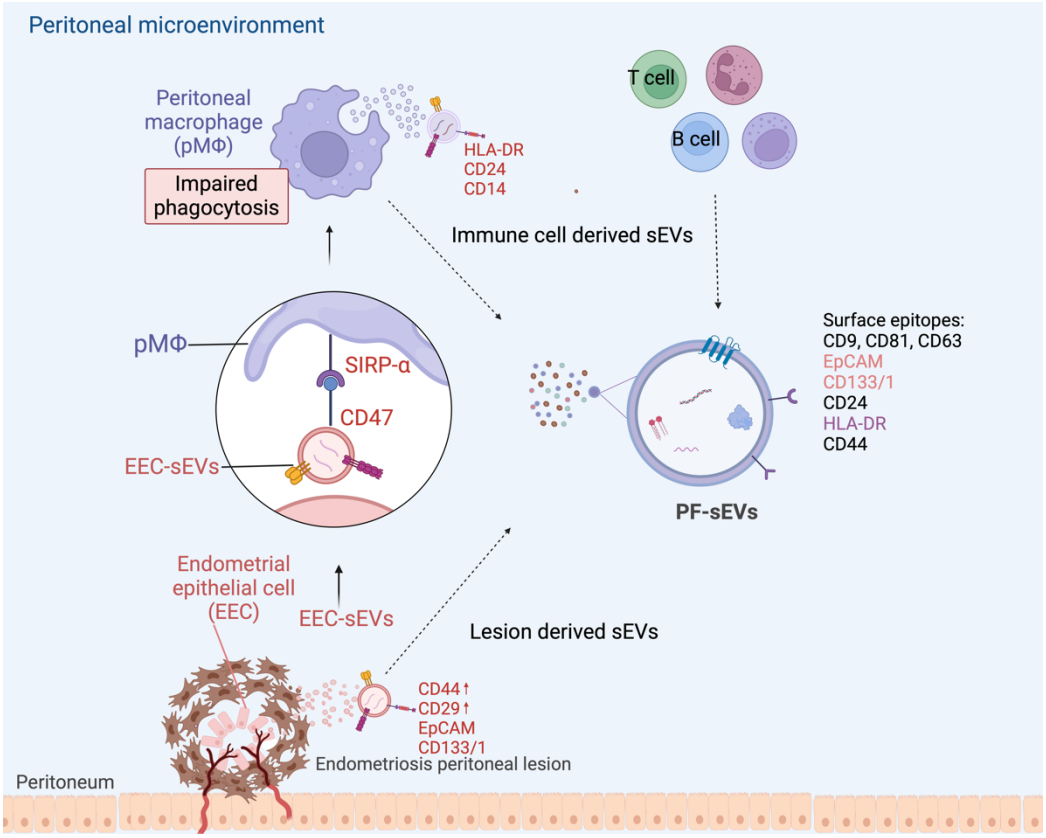

Figure 6.1 Main findings of sEV interaction in peritoneal microenvironment of endometriosis. Peritoneal fluid derived sEV (PF-sEV) originate from diverse cellular sources, including immune cells, endometrial epithelial cells, and endothelial cells, and highly express EpCAM, CD133/1, CD24, HLA-DR and CD44. The surface marker expression varies depending on cellular origin, with endometrial epithelial-derived sEV enriched in EpCAM and CD133/1, while lesion-derived sEV exhibit higher levels of CD44 and CD24. Macrophage-derived sEV express CD14, CD24, and HLA-DR. Ectopic endometrial epithelial cells (EEC) secrete EEC-derived sEV (EEC-sEV), which express CD47 and interact with SIRP-α on peritoneal macrophages (pMΦ), leading to impaired phagocytosis.

Figure 6.1 summarise main findings in the DPhil project and Figure 6.2 illustrates these potential sEV-mediated mechanisms in endometriosis, including macrophage inhibition, T cell interaction, and enhanced adhesion of endometrial cells.

Further exploration of protein composition and sEV RNA modifications, as well as associated signalling pathways, will be crucial in deepening our understanding of the mechanisms involved in endometriosis. Proteomic and transcriptomic analyses of sEV could reveal novel molecular signatures associated with the disease, potentially leading to the identification of new therapeutic targets and biomarkers.

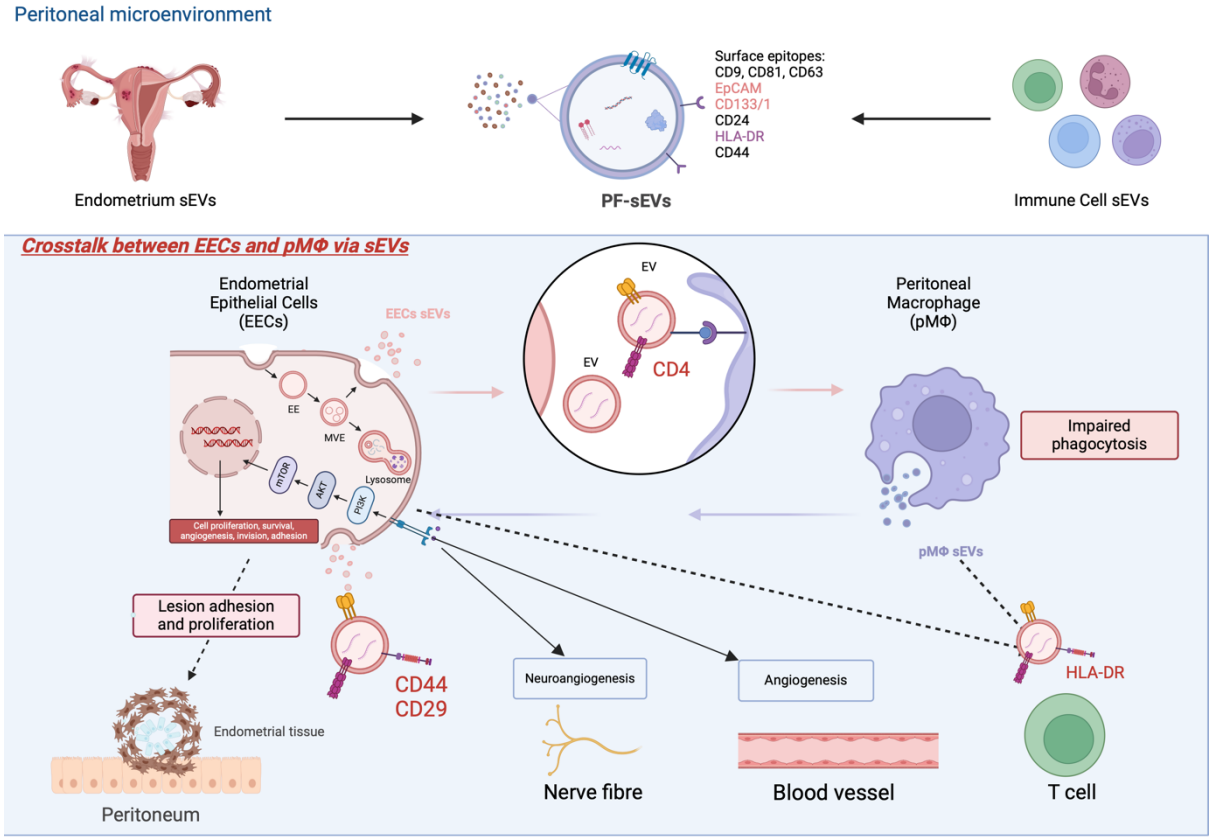

Figure 6.2. Established and potential sEV-mediated mechanisms in endometriosis progression in the peritoneal cavity. This schematic illustrates the diverse roles of sEV in endometriosis progression. sEV in PF primarily originate from immune cells, eutopic and ectopic endometrial cells. Previous studies revealed endometrial stromal EV promote macrophage polarisation, angiogenesis, and neuroangiogenesis, while pMΦ-sEV promote stromal cell growth. The current study demonstrates inhibition of macrophage phagocytosis by ectopic endometrial epithelial-derived sEV via the CD47/SIRP-alpha pathway, fostering an immunosuppressive environment. Potential pathways also include HLA-DR-expressing sEV from pMΦ and epithelial cells interacting with T cells, potentially modulating their activation and function. Additionally, transfer of adhesion molecules (CD44, CD29) via sEV may enhance endometrial tissue adhesion capabilities to peritoneal mesothelial cells in lesion establishment.

6.2 EV as a Biomarker in endometriosis

The potential of sEV as biomarkers for endometriosis is promising yet complex. Current research reveals that sEV profile differences between ectopic and eutopic EEO are not consistently reflected in PF-sEV profiles of endometriosis patients and controls. This discrepancy underscores the high heterogeneity of EV populations in biological fluids and highlights the impact of confounding factors, such as varying storage times of PF samples, on EV characterisation.

Observed HT-induced changes in sEV profiles, including the suppression of EpCAM, elevation of CD24 expression, and differential effects on CD133/1, demonstrate EV' sensitivity to environmental changes. This sensitivity suggests potential for monitoring treatment efficacy and hormone resistance development.

While informative, the invasive nature of PF collection limits its suitability for routine biomarker testing. Future studies should prioritise translating these findings to more accessible biological fluids such as blood, urine, or saliva. Additionally, menstrual effluent, given its direct relationship to the endometrium, merits investigation for unique endometriosis markers.

It's important to acknowledge that there's still a long way to go in this field. The differences observed in *in vitro* models can be easily masked in complex biological fluids due to the presence of EV from multiple sources and other confounding factors. Replication of findings across studies is challenging due to technique specificity in EV isolation and characterization. This challenge highlights the need for more sensitive and specific detection techniques with standardised protocols. Investigating lesion derived EV may be particularly helpful. Exploration of advanced techniques like single EV flow cytometry could provide more detailed insights into EV subpopulations specific to endometriosis.

Appendix

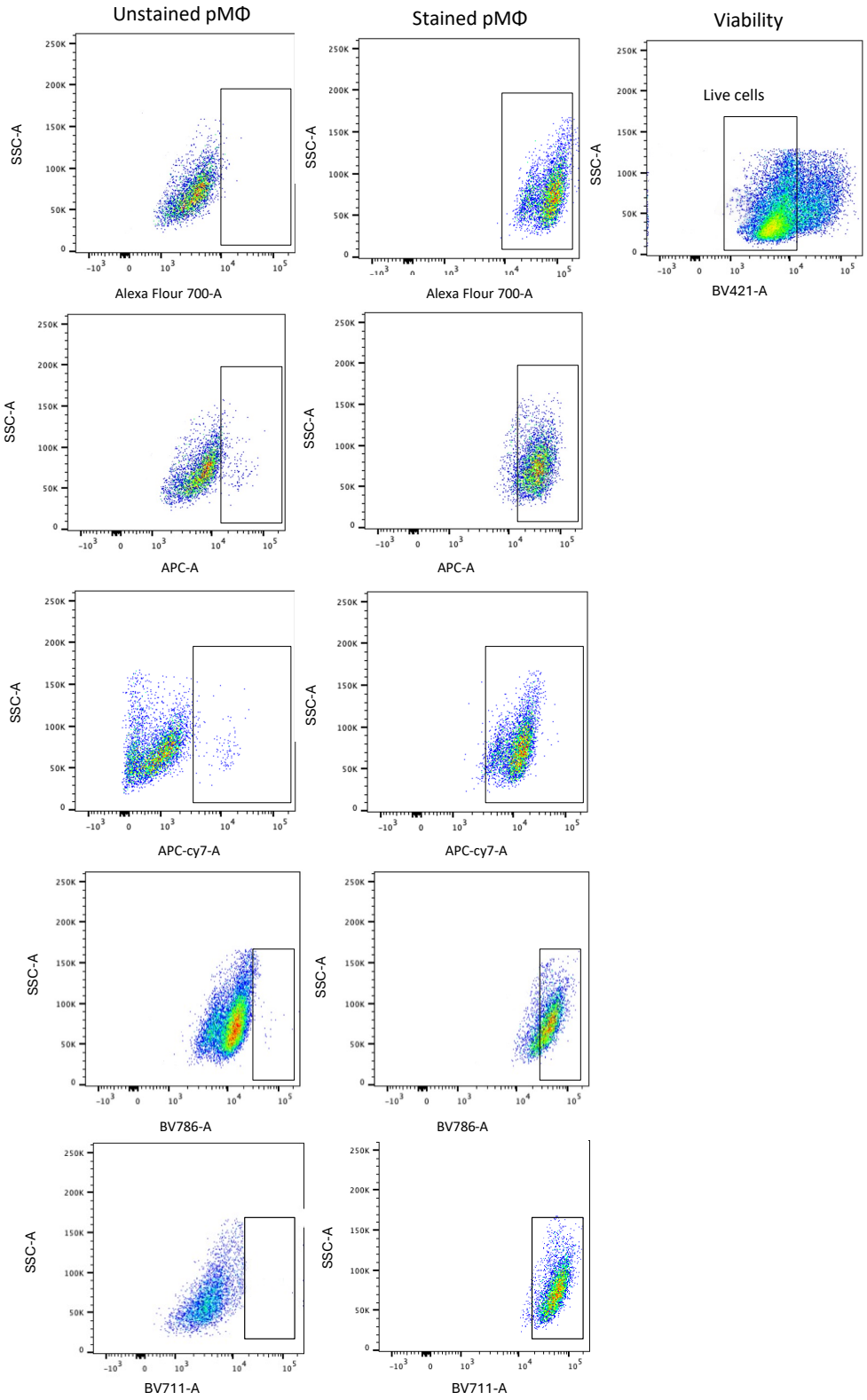

Figure 1. Gating controls for pMΦ characterisation panel. Live and heat-killed pMΦ were stained with viability dye to define live cell gates. Unstained and fully stained pMΦ (with compensation) were used to gate marker-positive populations.

References

1. Zondervan KT, Becker CM, Koga K, Missmer SA, Taylor RN, Viganò P. Endometriosis. Nat Rev Dis Primers. 2018;4(1):9.
2. Zondervan KT, Becker CM, Missmer SA. Endometriosis. N Engl J Med. 2020;382(13):1244-56.
3. Prescott J, Farland LV, Tobias DK, Gaskins AJ, Spiegelman D, Chavarro JE, et al. A prospective cohort study of endometriosis and subsequent risk of infertility. Human Reproduction. 2016;31(7):1475-82.
4. Canis M, Donnez JG, Guzick DS, Halme JK, Rock JA, Schenken RS, Vernon MW. Revised American Society for Reproductive Medicine Classification of Endometriosis: 1996. Fertility & Sterility. 1997;67(5):817-21.
5. Tuttlies F, Keckstein J, Ulrich U, Possover M, Schweppe K, Wustlich M, et al. ENZIAN-score, a classification of deep infiltrating endometriosis. Zentralblatt fur Gynakologie. 2005;127(5):275-81.
6. Adamson GD, Pasta DJ. Endometriosis fertility index: the new, validated endometriosis staging system. Fertility and Sterility. 2010;94(5):1609-15.
7. Nisenblat V, Bossuyt PM, Farquhar C, Johnson N, Hull MLJCDoSR. Imaging modalities for the non-invasive diagnosis of endometriosis. 2016(2).
8. Becker CM, Bokor A, Heikinheimo O, Horne A, Jansen F, Kiesel L, et al. ESHRE guideline: endometriosis†. Human Reproduction Open. 2022;2022(2).
9. Johnson NP, Hummelshoj L, Adamson GD, Keckstein J, Taylor HS, Abrao MS, et al. World Endometriosis Society consensus on the classification of endometriosis. Human reproduction. 2017;32(2):315-24.
10. Nnoaham KE, Hummelshoj L, Webster P, d'Hooghe T, de Cicco Nardone F, de Cicco Nardone C, et al. Impact of endometriosis on quality of life and work productivity: a multicenter study across ten countries. Fertility & Sterility. 2011;96(2):366-73.e8.
11. Becker CM, Gattrell WT, Gude K, Singh SS. Reevaluating response and failure of medical treatment of endometriosis: a systematic review. Fertility & Sterility. 2017;108(1):125-36.
12. Agarwal SK, Chapron C, Giudice LC, Laufer MR, Leyland N, Missmer SA, et al. Clinical diagnosis of endometriosis: a call to action. American journal of obstetrics and gynecology. 2019;220(4):354.e1-.e12.
13. Vigano P, Candiani M, Monno A, Giacomini E, Vercellini P, Somigliana E. Time to redefine endometriosis including its pro-fibrotic nature. Human Reproduction. 2018;33(3):347-52.
14. Maybin JA, Critchley HOD. Menstrual physiology: implications for endometrial pathology and beyond. Human Reproduction Update. 2015;21(6):748-61.
15. Bulun SE, Wan Y, Matei D. Epithelial Mutations in Endometriosis: Link to Ovarian Cancer. Endocrinology. 2019;160(3):626-38.
16. Sampson J. Peritoneal endometriosis due to menstrual dissemination of endometrial tissue into the peritoneal cavity. American journal of obstetrics and gynecology. 1927;14:422-69.
17. Halme J, HAMMOND MG, HULKA JF, RAJ SG, TALBERT LM. Retrograde menstruation in healthy women and in patients with endometriosis. Obstetrics & Gynecology. 1984;64(2):151-4.

18. Rahmioglu N, Mortlock S, Ghiasi M, Møller PL, Stefansdottir L, Galarneau G, et al. The genetic basis of endometriosis and comorbidity with other pain and inflammatory conditions. Nat Genet. 2023;55(3):423-36.
19. Symons LK, Miller JE, Kay VR, Marks RM, Liblik K, Koti M, Tayade C. The Immunopathophysiology of Endometriosis. Trends in Molecular Medicine. 2018;24(9):748-62.
20. Guo M, Bafligil C, Tapmeier T, Hubbard C, Manek S, Shang C, et al. Mass cytometry analysis reveals a distinct immune environment in peritoneal fluid in endometriosis: a characterisation study. BMC Medicine. 2020;18(1):3.
21. Zou G, Wang J, Xu X, Xu P, Zhu L, Yu Q, et al. Cell subtypes and immune dysfunction in peritoneal fluid of endometriosis revealed by single-cell RNA-sequencing. Cell & Bioscience. 2021;11(1):1-17.
22. Orkin SH, Zon LI. Hematopoiesis: an evolving paradigm for stem cell biology. Cell. 2008;132(4):631-44.
23. Chuang PC, Wu MH, Shoji Y, Tsai SJ, Ireland. Downregulation of CD36 results in reduced phagocytic ability of peritoneal macrophages of women with endometriosis. The Journal of Pathology: A Journal of the Pathological Society of Great Britain. 2009;219(2):232-41.
24. Chuang P-C, Lin Y-J, Wu M-H, Wing L-YC, Shoji Y, Tsai S-J. Inhibition of CD36-dependent phagocytosis by prostaglandin E2 contributes to the development of endometriosis. The American Journal of Pathology. 2010;176(2):850-60.
25. Gibson DA, Collins F, De Leo B, Horne AW, Saunders PT. Pelvic pain correlates with peritoneal macrophage abundance not endometriosis. Reproduction & Fertility. 2021;2(1):47-57.
26. Zou G, Wang J, Xu X, Xu P, Zhu L, Yu Q, et al. Cell subtypes and immune dysfunction in peritoneal fluid of endometriosis revealed by single-cell RNA-sequencing. Cell & Bioscience. 2021;11(1):98.
27. Podgaec S, Abrao MS, Dias JA, Jr, Rizzo LV, de Oliveira RM, Baracat EC. Endometriosis: an inflammatory disease with a Th2 immune response component. Human Reproduction. 2007;22(5):1373-9.
28. Takamura M, Koga K, Izumi G, Hirata T, Harada M, Hirota Y, et al. Simultaneous Detection and Evaluation of Four Subsets of CD4+ T Lymphocyte in Lesions and Peripheral Blood in Endometriosis. 2015;74(6):480-6.
29. Wang X-Q, Zhou W-J, Luo X-Z, Tao Y, Li D-J. Synergistic effect of regulatory T cells and proinflammatory cytokines in angiogenesis in the endometriotic milieu. Human Reproduction. 2017;32(6):1304-17.
30. Li M-Q, Wang Y, Chang K-K, Meng Y-H, Liu L, Mei J, et al. CD4+ Foxp3+ regulatory T cell differentiation mediated by endometrial stromal cell-derived TECK promotes the growth and invasion of endometriotic lesions. Cell Death & Disease. 2014;5(10):e1436-e.
31. Hou X-X, Wang X-Q, Zhou W-J, Li D-J. Regulatory T cells induce polarization of pro-repair macrophages by secreting sFGL2 into the endometriotic milieu. Communications Biology. 2021;4(1):499.
32. Chishima F, Hayakawa S, Hirata Y, Nagai N, Kanaeda T, Tsubata K, Satoh K. Peritoneal and peripheral B-1-cell populations in patients with endometriosis. Journal of Obstetrics and Gynaecology Research. 2000;26(2):141-9.

33. Greaves E, Temp J, Esnal-Zufiurre A, Mechsner S, Horne AW, Saunders PTK. Estradiol Is a Critical Mediator of Macrophage-Nerve Cross Talk in Peritoneal Endometriosis. The American Journal of Pathology. 2015;185(8):2286-97.
34. Shao J, Zhang B, Yu J-J, Wei C-Y, Zhou W-J, Chang K-K, et al. Macrophages promote the growth and invasion of endometrial stromal cells by downregulating IL-24 in endometriosis. Reproduction. 2016;152(6):673-82.
35. Gou Y, Wang H, Wang T, Wang H, Wang B, Jiao N, et al. Ectopic endometriotic stromal cells-derived lactate induces M2 macrophage polarization via Mettl3/Trib1/ERK/STAT3 signalling pathway in endometriosis. Immunology. 2023;168(3):389-402.
36. Ji J, Wang H, Yuan M, Li J, Song X, Lin K. Exosomes from ectopic endometrial stromal cells promote M2 macrophage polarization by delivering miR-146a-5p. International Immunopharmacology. 2024;128:111573.
37. Liu T, Liu M, Zheng C, Zhang D, Li M, Zhang L. Exosomal lncRNA CHL1-AS1 derived from peritoneal macrophages promotes the progression of endometriosis via the miR-610/MDM2 Axis. International journal of nanomedicine. 2021:5451-64.
38. Hogg C, Horne AW, Greaves E. Endometriosis-associated macrophages: origin, phenotype, and function. Frontiers in Endocrinology. 2020;11:7.
39. Budrys NM, Nair HB, Liu Y-G, Kirma NB, Binkley PA, Kumar S, et al. Increased expression of macrophage colony–stimulating factor and its receptor in patients with endometriosis. Fertility & Sterility. 2012;97(5):1129-35. e1.
40. Ueno T, Toi M, Saji H, Muta M, Bando H, Kuroi K, et al. Significance of macrophage chemoattractant protein-1 in macrophage recruitment, angiogenesis, and survival in human breast cancer. 2000;6(8):3282-9.
41. Gou Y, Li X, Li P, Zhang H, Xu T, Wang H, et al. Estrogen receptor β upregulates CCL2 via NF-κB signaling in endometriotic stromal cells and recruits macrophages to promote the pathogenesis of endometriosis. Human Reproduction. 2019;34(4):646-58.
42. Kitawaki J, Kado N, Ishihara H, Koshiba H, Kitaoka Y, Honjo HJTJosb, biology m. Endometriosis: the pathophysiology as an estrogen-dependent disease. 2002;83(1-5):149-55.
43. Liang Y, Xie H, Wu J, Liu D, Yao S. Villainous role of estrogen in macrophage-nerve interaction in endometriosis. Reproductive Biology and Endocrinology. 2018;16(1):122.
44. Ruiz-Alcaraz AJ, Carmona-Martínez V, Tristán-Manzano M, Machado-Linde F, Sánchez-Ferrer ML, García-Peñarrubia P, Martínez-Esparza M. Characterization of human peritoneal monocyte/macrophage subsets in homeostasis: phenotype, GATA6, phagocytic/oxidative activities and cytokines expression. Scientific Reports. 2018;8(1):1-14.
45. Irvine KM, Banh X, Gadd VL, Wojcik KK, Ariffin JK, Jose S, et al. CRIg-expressing peritoneal macrophages are associated with disease severity in patients with cirrhosis and ascites. JCI Insight. 2016;1(8).
46. Wynn TA, Chawla A, Pollard J. Macrophage biology in development, homeostasis and disease. Nature. 2013;496(7446):445-55.
47. Hudson QJ, Ashjaei K, Perricos A, Kuessel L, Husslein H, Wenzl R, Yotova I. Endometriosis Patients Show an Increased M2 Response in the Peritoneal CD14+low/CD68+low Macrophage Subpopulation Coupled with an Increase in the T-helper 2 and T-regulatory Cells. Reproductive Sciences. 2020;27(10):1920-31.

48. Tan Y, Flynn WF, Sivajothi S, Luo D, Bozal SB, Davé M, et al. Single-cell analysis of endometriosis reveals a coordinated transcriptional programme driving immunotolerance and angiogenesis across eutopic and ectopic tissues. Nature Cell Biology. 2022;24(8):1306-18.
49. Gomez Perdiguero E, Klapproth K, Schulz C, Busch K, Azzoni E, Crozet L, et al. Tissue-resident macrophages originate from yolk-sac-derived erythro-myeloid progenitors. Nature. 2015;518(7540):547-51.
50. Ghosn EEB, Cassado AA, Govoni GR, Fukuhara T, Yang Y, Monack DM, et al. Two physically, functionally, and developmentally distinct peritoneal macrophage subsets. Proceedings of the National Academy of Sciences. 2010;107(6):2568-73.
51. Bain CC, Hawley CA, Garner H, Scott CL, Schridde A, Steers NJ, et al. Long-lived self-renewing bone marrow-derived macrophages displace embryo-derived cells to inhabit adult serous cavities. Nature Communications. 2016;7(1):1-14.
52. Hogg C, Panir K, Dhami P, Rosser M, Mack M, Soong D, et al. Macrophages inhibit and enhance endometriosis depending on their origin. Proceedings of the National Academy of Sciences. 2021;118(6):e2013776118.
53. Wang Y, Fu Y, Xue S, Ai A, Chen H, Lyu Q, Kuang Y. The M2 polarization of macrophage induced by fractalkine in the endometriotic milieu enhances invasiveness of endometrial stromal cells. Int J Clin Exp Pathol. 2014;7(1):194-203.
54. Mei J, Chang KK, Sun HX. Immunosuppressive macrophages induced by IDO1 promote the growth of endometrial stromal cells in endometriosis. Molecular Medicine Reports. 2017;15(4):2255-60.
55. Johnson NP, Hummelshoj L, Adamson GD, Keckstein J, Taylor HS, Abrao MS, et al. World Endometriosis Society consensus on the classification of endometriosis. Human Reproduction. 2017;32(2):315-24.
56. Wang Y, Dragovic RA, Greaves E, Becker CM, Southcombe JH. Macrophages and small extracellular vesicle mediated-intracellular communication in the peritoneal microenvironment: Impact on endometriosis development. Front Reprod Health. 2023;5:1130849.
57. Welsh JA, Goberdhan DCI, O'Driscoll L, Buzas EI, Blenkiron C, Bussolati B, et al. Minimal information for studies of extracellular vesicles (MISEV2023): From basic to advanced approaches. J Extracell Vesicles. 2024;13(2):e12404.
58. Nazri HM, Imran M, Fischer R, Heilig R, Manek S, Dragovic RA, et al. Characterization of exosomes in peritoneal fluid of endometriosis patients. Fertil Steril. 2020;113(2):364-73.e2.
59. Van Niel G, d'Angelo G, Raposo G. Shedding light on the cell biology of extracellular vesicles. Nature Reviews Molecular Cell Biology. 2018;19(4):213-28.
60. Colombo M, Raposo G, Théry C. Biogenesis, secretion, and intercellular interactions of exosomes and other extracellular vesicles. Annual review of cell and developmental biology. 2014;30(1):255-89.
61. Baietti MF, Zhang Z, Mortier E, Melchior A, Degeest G, Geeraerts A, et al. Syndecan–syntenin–ALIX regulates the biogenesis of exosomes. Nature cell biology. 2012;14(7):677-85.
62. Trajkovic K, Hsu C, Chiantia S, Rajendran L, Wenzel D, Wieland F, et al. Ceramide triggers budding of exosome vesicles into multivesicular endosomes. Science. 2008;319(5867):1244-7.

63. Minciacchi VR, Freeman MR, Di Vizio D, editors. Extracellular vesicles in cancer: exosomes, microvesicles and the emerging role of large oncosomes. Seminars in Cell & Developmental Biology; 2015: Elsevier.
64. Fu S, Zhang Y, Li Y, Luo L, Zhao Y, Yao Y. Extracellular vesicles in cardiovascular diseases. Cell Death Discovery. 2020;6(1):1-9.
65. Iranifar E, Seresht BM, Momeni F, Fadaei E, Mehr MH, Ebrahimi Z, et al. Exosomes and microRNAs: new potential therapeutic candidates in Alzheimer disease therapy. Journal of Cellular Physiology. 2019;234(3):2296-305.
66. Tan L, Wu H, Liu Y, Zhao M, Li D, Lu Q. Recent advances of exosomes in immune modulation and autoimmune diseases. Autoimmunity. 2016;49(6):357-65.
67. Kalluri R. The biology and function of exosomes in cancer. The Journal of Clinical Investigation. 2016;126(4):1208-15.
68. Raposo G, Stahl PD. Extracellular vesicles: a new communication paradigm? Nature Reviews Molecular Cell Biology. 2019;20(9):509-10.
69. Möller A, Lobb R. The evolving translational potential of small extracellular vesicles in cancer. Nature Reviews Cancer. 2020;20(12):697-709.
70. Lee YJ, Shin KJ, Chae YC. Regulation of cargo selection in exosome biogenesis and its biomedical applications in cancer. Experimental & Molecular Medicine. 2024;56(4):877-89.
71. Taylor DD, Gercel-Taylor C. MicroRNA signatures of tumor-derived exosomes as diagnostic biomarkers of ovarian cancer. Gynecologic Oncology. 2008;110(1):13-21.
72. Huang X, Yuan T, Tschannen M, Sun Z, Jacob H, Du M, et al. Characterization of human plasma-derived exosomal RNAs by deep sequencing. BMC genomics. 2013;14:319.
73. Braza-Boïls A, Marí-Alexandre J, Gilabert J, Sanchez-Izquierdo D, Espana F, Estelles A, Gilabert-Estelles JJHr. MicroRNA expression profile in endometriosis: its relation to angiogenesis and fibrinolytic factors. 2014;29(5):978-88.
74. Gurung S, Perocheau D, Touramanidou L, Baruteau J. The exosome journey: from biogenesis to uptake and intracellular signalling. Cell Communication and Signaling. 2021;19(1):47.
75. Hoshino A, Costa-Silva B, Shen T-L, Rodrigues G, Hashimoto A, Tesic Mark M, et al. Tumour exosome integrins determine organotropic metastasis. 2015;527(7578):329-35.
76. Alvarez-Erviti L, Seow Y, Yin H, Betts C, Lakhal S, Wood MJA. Delivery of siRNA to the mouse brain by systemic injection of targeted exosomes. Nature Biotechnology. 2011;29(4):341-5.
77. Heusermann W, Hean J, Trojer D, Steib E, Von Bueren S, Graff-Meyer A, et al. Exosomes surf on filopodia to enter cells at endocytic hot spots, traffic within endosomes, and are targeted to the ER. Journal of Cell Biology. 2016;213(2):173-84.
78. Liam-Or R, Faruqu FN, Walters A, Han S, Xu L, Wang JT-W, et al. Cellular uptake and in vivo distribution of mesenchymal-stem-cell-derived extracellular vesicles are protein corona dependent. Nature Nanotechnology. 2024;19(6):846-55.
79. Moman RN, Gupta N, Varacallo M. Physiology, albumin. 2017.
80. Dietz L, Oberländer J, Mateos-Maroto A, Schunke J, Fichter M, Krämer-Albers EM, et al. Uptake of extracellular vesicles into immune cells is enhanced by the protein corona. J Extracell Vesicles. 2023;12(12):e12399.

81. Singh P, Szigyártó IC, Ricci M, Gaál A, Quemé-Peña MM, Kitka D, et al. Removal and identification of external protein corona members from RBC-derived extracellular vesicles by surface manipulating antimicrobial peptides. J Extracell Biol. 2023;2(3):e78.
82. Guan H, Peng R, Fang F, Mao L, Chen Z, Yang S, et al. Tumor-associated macrophages promote prostate cancer progression via exosome-mediated miR-95 transfer. Journal of Cellular Physiology. 2020;235(12):9729-42.
83. Zheng P, Luo Q, Wang W, Li J, Wang T, Wang P, et al. Tumor-associated macrophages-derived exosomes promote the migration of gastric cancer cells by transfer of functional Apolipoprotein E. Cell Death & Disease. 2018;9(4):434.
84. Li X, Chen Z, Ni Y, Bian C, Huang J, Chen L, et al. Tumor-associated macrophages secret exosomal miR-155 and miR-196a-5p to promote metastasis of non-small-cell lung cancer. Translational Lung Cancer Research. 2021;10(3):1338.
85. Zheng P, Chen L, Yuan X, Luo Q, Liu Y, Xie G, et al. Exosomal transfer of tumor-associated macrophage-derived miR-21 confers cisplatin resistance in gastric cancer cells. Journal of Experimental & Clinical Cancer Research. 2017;36(1):1-13.
86. Yang Y, Guo Z, Chen W, Wang X, Cao M, Han X, et al. M2 macrophage-derived exosomes promote angiogenesis and growth of pancreatic ductal adenocarcinoma by targeting E2F2. Molecular Therapy. 2021;29(3):1226-38.
87. Zhou J, Li X, Wu X, Zhang T, Zhu Q, Wang X, et al. Exosomes Released from Tumor-Associated Macrophages Transfer miRNAs That Induce a Treg/Th17 Cell Imbalance in Epithelial Ovarian Cancer. Cancer Immunology Research. 2018;6(12):1578-92.
88. Zhao S, Mi Y, Guan B, Zheng B, Wei P, Gu Y, et al. Tumor-derived exosomal miR-934 induces macrophage M2 polarization to promote liver metastasis of colorectal cancer. Journal of Hematology & Oncology. 2020;13(1):1-19.
89. Xiao M, Zhang J, Chen W, Chen W. M1-like tumor-associated macrophages activated by exosome-transferred THBS1 promote malignant migration in oral squamous cell carcinoma. Journal of Experimental & Clinical Cancer Research. 2018;37(1):143.
90. Benagiano G, Brosens I, Habiba M. Structural and molecular features of the endomyometrium in endometriosis and adenomyosis. Human Reproduction Update. 2013;20(3):386-402.
91. Juárez-Barber E, Segura-Benítez M, Carbajo-García MC, Bas-Rivas A, Faus A, Vidal C, et al. Extracellular vesicles secreted by adenomyosis endometrial organoids contain miRNAs involved in embryo implantation and pregnancy. Reprod Biomed Online. 2022.
92. Greening DW, Nguyen HPT, Elgass K, Simpson RJ, Salamonsen LA. Human Endometrial Exosomes Contain Hormone-Specific Cargo Modulating Trophoblast Adhesive Capacity: Insights into Endometrial-Embryo Interactions1. Biology of Reproduction. 2016;94(2).
93. Zhang L, Li H, Yuan M, Li D, Wang G. Exosomal miR-22-3p derived from peritoneal macrophages enhances proliferation, migration, and invasion of ectopic endometrial stromal cells through regulation of the SIRT1/NF-κB signaling pathway. Eur Rev Med Pharmacol Sci. 2020;24(2):571-80.
94. Liu T, Liu M, Zheng C, Zhang D, Li M, Zhang L. Exosomal lncRNA CHL1-AS1 Derived from Peritoneal Macrophages Promotes the Progression of Endometriosis via the miR-610/MDM2 Axis. Int J Nanomedicine. 2021;16:5451-64.

95. Senchenko VN, Krasnov GS, Dmitriev AA, Kudryavtseva AV, Anedchenko EA, Braga EA, et al. Differential expression of CHL1 gene during development of major human cancers. PloS One. 2011;6(3):e15612.
96. Zhang C, Wu W, Ye X, Ma R, Luo J, Zhu H, Chang X. Aberrant expression of CHL1 gene and long non-coding RNA CHL1-AS1, CHL1-AS2 in ovarian endometriosis. European Journal of Obstetrics & Gynecology and Reproductive Biology. 2019;236:177-82.
97. Li Q, Yuan M, Jiao X, Huang Y, Li J, Li D, et al. M1 Macrophage-Derived Nanovesicles Repolarize M2 Macrophages for Inhibiting the Development of Endometriosis. Front Immunol. 2021;12:707784.
98. Sun H, Li D, Yuan M, Li Q, Zhen Q, Li N, Wang G. Macrophages alternatively activated by endometriosis-exosomes contribute to the development of lesions in mice. Molecular Human Reproduction. 2018;25(1):5-16.
99. Sun SG, Guo JJ, Qu XY, Tang XY, Lin YY, Hua KQ, Qiu JJ. The extracellular vesicular pseudogene LGMNP1 induces M2-like macrophage polarization by upregulating LGMN and serves as a novel promising predictive biomarker for ovarian endometriosis recurrence. Human Reproduction. 2022;37(3):447-65.
100. Sun H, Li D, Yuan M, Li Q, li N, Wang G. Eutopic stromal cells of endometriosis promote neuroangiogenesis via exosome pathway. Biology of Reproduction. 2018;100(3):649-59.
101. Harp D, Driss A, Mehrabi S, Chowdhury I, Xu W, Liu D, et al. Exosomes derived from endometriotic stromal cells have enhanced angiogenic effects in vitro. Cell Tissue Research. 2016;365(1):187-96.
102. Qiu J-J, Lin X-J, Zheng T-T, Tang X-Y, Zhang Y, Hua K-Q. The exosomal long noncoding RNA aHIF is upregulated in serum from patients with endometriosis and promotes angiogenesis in endometriosis. Reproductive Sciences. 2019;26(12):1590-602.
103. Wu D, Lu P, Mi X, Miao J. Exosomal miR-214 from endometrial stromal cells inhibits endometriosis fibrosis. MHR: Basic Science of Reproductive Medicine. 2018;24(7):357-65.
104. Zhang Y, Chang X, Wu D, Deng M, Miao J, Jin Z. Down-regulation of exosomal miR-214-3p targeting CCN2 contributes to endometriosis fibrosis and the role of exosomes in the horizontal transfer of miR-214-3p. Reproductive Sciences. 2021;28(3):715-27.
105. Zhang M, Wang X, Xia X, Fang X, Zhang T, Huang F. Endometrial epithelial cells-derived exosomes deliver microRNA-30c to block the BCL9/Wnt/CD44 signaling and inhibit cell invasion and migration in ovarian endometriosis. Cell Death Discovery. 2022;8(1):151.
106. Cindrova-Davies T, Zhao X, Elder K, Jones CJP, Moffett A, Burton GJ, Turco MY. Menstrual flow as a non-invasive source of endometrial organoids. Communications Biology. 2021;4(1):651.
107. Boretto M, Maenhoudt N, Luo X, Hennes A, Boeckx B, Bui B, et al. Patient-derived organoids from endometrial disease capture clinical heterogeneity and are amenable to drug screening. Nature Cell Biology. 2019;21(8):1041-51.
108. Haney A. Identification of macrophages at the site of peritoneal injury: evidence supporting a direct role for peritoneal macrophages in healing injured peritoneum. Fertility and sterility. 2000;73(5):988-95.

109. Cassado AdA, D'Império Lima MR, Bortoluci KR. Revisiting mouse peritoneal macrophages: heterogeneity, development, and function. Frontiers in immunology. 2015;6:225.
110. Liu T, Liu F, Peng L-W, Chang L, Jiang Y-M. The peritoneal macrophages in inflammatory diseases and abdominal cancers. Oncology Research. 2018;26(5):817.
111. Honda M, Kadohisa M, Yoshii D, Komohara Y, Hibi T. Directly recruited GATA6 + peritoneal cavity macrophages contribute to the repair of intestinal serosal injury. Nature Communications. 2021;12(1):7294.
112. Hogg C, Horne AW, Greaves E. Endometriosis-associated macrophages: origin, phenotype, and function. Frontiers in endocrinology. 2020;11:507486.
113. Bacci M, Capobianco A, Monno A, Cottone L, Di Puppo F, Camisa B, et al. Macrophages are alternatively activated in patients with endometriosis and required for growth and vascularization of lesions in a mouse model of disease. Am J Pathol. 2009;175(2):547-56.
114. Murray PJ. Macrophage polarization. Annual review of physiology. 2017;79(1):541-66.
115. Miller JE, Ahn SH, Marks RM, Monsanto SP, Fazleabas AT, Koti M, Tayade C. IL-17A modulates peritoneal macrophage recruitment and M2 polarization in endometriosis. Frontiers in Immunology. 2020;11:108.
116. Duan J, Liu X, Wang H, Guo S-W. The M2a macrophage subset may be critically involved in the fibrogenesis of endometriosis in mice. Reproductive biomedicine online. 2018;37(3):254-68.
117. Laganà AS, Salmeri FM, Ban Frangež H, Ghezzi F, Vrtačnik-Bokal E, Granese R. Evaluation of M1 and M2 macrophages in ovarian endometriomas from women affected by endometriosis at different stages of the disease. Gynecological Endocrinology. 2020;36(5):441-4.
118. Guo M, Bafligil C, Tapmeier T, Hubbard C, Manek S, Shang C, et al. Mass cytometry analysis reveals a distinct immune environment in peritoneal fluid in endometriosis: a characterisation study. BMC medicine. 2020;18:1-16.
119. Nie M-F, Xie Q, Wu Y-H, He H, Zou L-J, She X-L, Wu X-Q. Serum and Ectopic Endometrium from Women with Endometriosis Modulate Macrophage M1/M2 Polarization via the Smad2/Smad3 Pathway. Journal of Immunology Research. 2018;2018(1):6285813.
120. Ghosn EEB, Cassado AA, Govoni GR, Fukuhara T, Yang Y, Monack DM, et al. Two physically, functionally, and developmentally distinct peritoneal macrophage subsets. Proceedings of the National Academy of Sciences. 2010;107(6):2568-73.
121. Ruiz-Alcaraz AJ, Carmona-Martínez V, Tristán-Manzano M, Machado-Linde F, Sánchez-Ferrer ML, García-Peñarrubia P, Martínez-Esparza M. Characterization of human peritoneal monocyte/macrophage subsets in homeostasis: Phenotype, GATA6, phagocytic/oxidative activities and cytokines expression. Sci Rep. 2018;8(1):12794.
122. Gibson DA, Collins F, De Leo B, Horne AW, Saunders PTK. Pelvic pain correlates with peritoneal macrophage abundance not endometriosis. Reprod Fertil. 2021;2(1):47-57.
123. Henlon Y, Panir K, McIntyre I, Hogg C, Dhami P, Cuff AO, et al. Single-cell analysis identifies distinct macrophage phenotypes associated with prodisease and proresolving functions in the endometriotic niche. Proceedings of the National Academy of Sciences. 2024;121(38):e2405474121.

124. Théry C, Zitvogel L, Amigorena S. Exosomes: composition, biogenesis and function. Nature reviews immunology. 2002;2(8):569-79.
125. Zhang L, Li H-H, Yuan M, Li D, Wang G-Y. Exosomal miR-22-3p derived from peritoneal macrophages enhances proliferation, migration, and invasion of ectopic endometrial stromal cells through regulation of the SIRT1/NF-κB signaling pathway. European Review for Medical & Pharmacological Sciences. 2020;24(2).
126. Morales-Kastresana A, Musich TA, Welsh JA, Telford W, Demberg T, Wood JC, et al. High-fidelity detection and sorting of nanoscale vesicles in viral disease and cancer. Journal of Extracellular Vesicles. 2019;8(1):1597603.
127. Welsh JA, Jones JC, Tang VA. Fluorescence and light scatter calibration allow comparisons of small particle data in standard units across different flow cytometry platforms and detector settings. Cytometry Part A. 2020;97(6):592-601.
128. Kolhe R, Owens V, Sharma A, Lee TJ, Zhi W, Ghilzai U, et al. Sex-specific differences in extracellular vesicle protein cargo in synovial fluid of patients with osteoarthritis. Life. 2020;10(12):337.
129. Wiklander OPB, Bostancioglu RB, Welsh JA, Zickler AM, Murke F, Corso G, et al. Systematic Methodological Evaluation of a Multiplex Bead-Based Flow Cytometry Assay for Detection of Extracellular Vesicle Surface Signatures. Front Immunol. 2018;9:1326.
130. Zhang H, Lyden D. Asymmetric-flow field-flow fractionation technology for exomere and small extracellular vesicle separation and characterization. Nature Protocols. 2019;14(4):1027-53.
131. Mateescu B, Kowal EJ, van Balkom BW, Bartel S, Bhattacharyya SN, Buzás EI, et al. Obstacles and opportunities in the functional analysis of extracellular vesicle RNA - an ISEV position paper. J Extracell Vesicles. 2017;6(1):1286095.
132. Vacchi E, Burrello J, Di Silvestre D, Burrello A, Bolis S, Mauri P, et al. Immune profiling of plasma-derived extracellular vesicles identifies Parkinson disease. Neurol Neuroimmunol Neuroinflamm. 2020;7(6).
133. Juratli MA, Pollmann NS, Oppermann E, Mohr A, Roy D, Schnitzbauer A, et al. Extracellular vesicles as potential biomarkers for diagnosis and recurrence detection of hepatocellular carcinoma. Scientific Reports. 2024;14(1):5322.
134. Villarroya-Beltri C, Baixauli F, Gutiérrez-Vázquez C, Sánchez-Madrid F, Mittelbrunn M. Sorting it out: regulation of exosome loading. Semin Cancer Biol. 2014;28:3-13.
135. Li L, Görgens A, Mussack V, Pepeldjiyska E, Hartz AS, Rank A, et al. Description and optimization of a multiplex bead-based flow cytometry method (MBFCM) to characterize extracellular vesicles in serum samples from patients with hematological malignancies. Cancer Gene Therapy. 2022;29(11):1600-15.
136. Becker CM, Laufer MR, Stratton P, Hummelshoj L, Missmer SA, Zondervan KT, et al. World endometriosis research foundation endometriosis phenome and biobanking harmonisation project: I. Surgical phenotype data collection in endometriosis research. Fertility and sterility. 2014;102(5):1213-22.
137. Fassbender A, Rahmioglu N, Vitonis AF, Viganò P, Giudice LC, D'Hooghe TM, et al. World endometriosis research foundation endometriosis phenome and biobanking harmonisation project: IV. Tissue collection, processing, and storage in endometriosis research. Fertility and sterility. 2014;102(5):1244-53.
138. Rahmioglu N, Fassbender A, Vitonis AF, Tworoger SS, Hummelshoj L, D'Hooghe TM, et al. World endometriosis research foundation endometriosis phenome and

biobanking harmonization project: III. Fluid biospecimen collection, processing, and storage in endometriosis research. Fertility and sterility. 2014;102(5):1233-43.
139. Vitonis AF, Vincent K, Rahmioglu N, Fassbender A, Louis GMB, Hummelshoj L, et al. World Endometriosis Research Foundation Endometriosis Phenome and biobanking harmonization project: II. Clinical and covariate phenotype data collection in endometriosis research. Fertility and sterility. 2014;102(5):1223-32.
140. Wu M-H, Sun HS, Lin C-C, Hsiao K-Y, Chuang P-C, Pan H-A, Tsai S-J. Distinct mechanisms regulate cyclooxygenase-1 and -2 in peritoneal macrophages of women with and without endometriosis. Molecular Human Reproduction. 2002;8(12):1103-10.
141. Njoroge JM, Mitchell LB, Centola M, Kastner D, Raffeld M, Miller JL. Characterization of viable autofluorescent macrophages among cultured peripheral blood mononuclear cells. Cytometry. 2001;44(1):38-44.
142. Hunt JV, Carpenter KLH, Bottoms MA, Carter NP, Marchant CE, Mitchinson MJ. Flow cytometric measurement of ceroid accumulation in macrophages. Atherosclerosis. 1993;98(2):229-39.
143. Welsh JA, Killingsworth B, Kepley J, Traynor T, Cook S, Savage J, et al. MPAPASS software enables stitched multiplex, multidimensional EV repertoire analysis and a standard framework for reporting bead-based assays. Cell Reports Methods. 2022;2(1).
144. Zhang Y, Zhou N, Yu X, Zhang X, Li S, Lei Z, et al. Tumacrophage: macrophages transformed into tumor stem-like cells by virulent genetic material from tumor cells. Oncotarget. 2017;8(47):82326-43.
145. Aubin JE. Autofluorescence of viable cultured mammalian cells. J Histochem Cytochem. 1979;27(1):36-43.
146. Kharraz Y, Lukesova V, Serrano AL, Davison A, Muñoz-Cánoves P. Full spectrum cytometry improves the resolution of highly autofluorescent biological samples: Identification of myeloid cells in regenerating skeletal muscles. Cytometry Part A. 2022;101(10):862-76.
147. Kong WT, Bied M, Ginhoux F. Spectral Flow Cytometry Analysis of Resident Tissue Macrophages. Tissue-Resident Macrophages: Methods and Protocols: Springer; 2023. p. 269-80.
148. Li MZ, Wu YH, Ali M, Wu XQ, Nie MF. Endometrial stromal cells treated by tumor necrosis factor-α stimulate macrophages polarized toward M2 via interleukin-6 and monocyte chemoattractant protein-1. Journal of Obstetrics and Gynaecology Research. 2020;46(2):293-301.
149. Huang Y, Zhu L, Li H, Ye J, Lin N, Chen M, et al. Endometriosis derived exosomal miR-301a-3p mediates macrophage polarization via regulating PTEN-PI3K axis. Biomedicine & Pharmacotherapy. 2022;147:112680.
150. Sun S, Guo J, Qu X, Tang X, Lin Y, Hua K, Qiu J. The extracellular vesicular pseudogene LGMNP1 induces M2-like macrophage polarization by upregulating LGMN and serves as a novel promising predictive biomarker for ovarian endometriosis recurrence. Human reproduction. 2022;37(3):447-65.
151. Jeppesen DK, Hvam ML, Primdahl-Bengtson B, Boysen AT, Whitehead B, Dyrskjøt L, et al. Comparative analysis of discrete exosome fractions obtained by differential centrifugation. Journal of extracellular vesicles. 2014;3(1):25011.
152. Théry C, Amigorena S, Raposo G, Clayton A. Isolation and characterization of exosomes from cell culture supernatants and biological fluids. Current protocols in cell biology. 2006;30(1):3.22. 1-3.. 9.

153. Szatanek R, Baran J, Siedlar M, Baj-Krzyworzeka M. Isolation of extracellular vesicles: Determining the correct approach. International journal of molecular medicine. 2015;36(1):11-7.
154. Lötvall J, Hill AF, Hochberg F, Buzás EI, Di Vizio D, Gardiner C, et al. Minimal experimental requirements for definition of extracellular vesicles and their functions: a position statement from the International Society for Extracellular Vesicles. Wiley Online Library; 2014. p. 26913.
155. Busatto S, Yang Y, Iannotta D, Davidovich I, Talmon Y, Wolfram J. Considerations for extracellular vesicle and lipoprotein interactions in cell culture assays. Journal of Extracellular Vesicles. 2022;11.
156. Lehrich BM, Liang Y, Khosravi P, Federoff HJ, Fiandaca MS. Fetal bovine serum-derived extracellular vesicles persist within vesicle-depleted culture media. International journal of molecular sciences. 2018;19(11):3538.
157. Lehrich BM, Liang Y, Fiandaca MS. Foetal bovine serum influence on in vitro extracellular vesicle analyses. J Extracell Vesicles. 2021;10(3):e12061.
158. Li P, Kaslan M, Lee SH, Yao J, Gao Z. Progress in exosome isolation techniques. Theranostics. 2017;7(3):789.
159. Wubbolts R, Leckie RS, Veenhuizen PT, Schwarzmann G, Mobius W, Hoernschemeyer J, et al. Proteomic and biochemical analyses of human B cell-derived exosomes: potential implications for their function and multivesicular body formation. Journal of Biological Chemistry. 2003;278(13):10963-72.
160. Yuana Y, Levels J, Grootemaat A, Sturk A, Nieuwland R. Co-isolation of extracellular vesicles and high-density lipoproteins using density gradient ultracentrifugation. Journal of extracellular vesicles. 2014;3(1):23262.
161. Böing AN, Van Der Pol E, Grootemaat AE, Coumans FA, Sturk A, Nieuwland R. Single-step isolation of extracellular vesicles by size-exclusion chromatography. Journal of extracellular vesicles. 2014;3(1):23430.
162. Zhang X, Borg EG, Liaci AM, Vos HR, Stoorvogel W. A novel three step protocol to isolate extracellular vesicles from plasma or cell culture medium with both high yield and purity. Journal of extracellular vesicles. 2020;9(1):1791450.
163. Nordin JZ, Lee Y, Vader P, Mäger I, Johansson HJ, Heusermann W, et al. Ultrafiltration with size-exclusion liquid chromatography for high yield isolation of extracellular vesicles preserving intact biophysical and functional properties. Nanomedicine: Nanotechnology, Biology and Medicine. 2015;11(4):879-83.
164. Welsh JA, Killingsworth B, Kepley J, Traynor T, Cook S, Savage J, et al. MPA_{PASS} software enables stitched multiplex, multidimensional EV repertoire analysis and a standard framework for reporting bead-based assays. Cell Reports Methods. 2022;2(1).
165. Ponta H, Sherman L, Herrlich PA. CD44: from adhesion molecules to signalling regulators. Nature reviews Molecular cell biology. 2003;4(1):33-45.
166. Kawana H, Karaki H, Higashi M, Miyazaki M, Hilberg F, Kitagawa M, Harigaya K. CD44 suppresses TLR-mediated inflammation. The Journal of Immunology. 2008;180(6):4235-45.
167. Wang J, Kubes P. A Reservoir of Mature Cavity Macrophages that Can Rapidly Invade Visceral Organs to Affect Tissue Repair. Cell. 2016;165(3):668-78.
168. Haynes BF, Telen MJ, Hale LP, Denning SM. CD44—a molecule involved in leukocyte adherence and T-cell activation. Immunology today. 1989;10(12):423-8.

169. Cho SH, Park YS, Kim HJ, Kim CH, Lim SW, Huh JW, et al. CD44 enhances the epithelial-mesenchymal transition in association with colon cancer invasion. International journal of oncology. 2012;41(1):211-8.
170. Gay D, Maddon P, Sekaly R, Talle MA, Godfrey M, Long E, et al. Functional interaction between human T-cell protein CD4 and the major histocompatibility complex HLA-DR antigen. Nature. 1987;328(6131):626-9.
171. Vassilopoulos A, Chisholm C, Lahusen T, Zheng H, Deng CX. A critical role of CD29 and CD49f in mediating metastasis for cancer-initiating cells isolated from a Brca1-associated mouse model of breast cancer. Oncogene. 2014;33(47):5477-82.
172. Nicolet BP, Guislain A, Wolkers MC. CD29 enriches for cytotoxic human CD4+ T cells. The Journal of Immunology. 2021;207(12):2966-75.
173. Ricklefs FL, Alayo Q, Krenzlin H, Mahmoud AB, Speranza MC, Nakashima H, et al. Immune evasion mediated by PD-L1 on glioblastoma-derived extracellular vesicles. Science advances. 2018;4(3):eaar2766.
174. Chan YK, Zhang H, Liu P, Tsao SW, Lung ML, Mak NK, et al. Proteomic analysis of exosomes from nasopharyngeal carcinoma cell identifies intercellular transfer of angiogenic proteins. International journal of cancer. 2015;137(8):1830-41.
175. Giovanazzi A, van Herwijnen MJC, Kleinjan M, van der Meulen GN, Wauben MHM. Surface protein profiling of milk and serum extracellular vesicles unveils body fluid-specific signatures. Scientific Reports. 2023;13(1):8758.
176. Colombo M, Raposo G, Théry C. Biogenesis, secretion, and intercellular interactions of exosomes and other extracellular vesicles. Annu Rev Cell Dev Biol. 2014;30:255-89.
177. Wollert T, Hurley JH. Molecular mechanism of multivesicular body biogenesis by ESCRT complexes. Nature. 2010;464(7290):864-9.
178. Villarroya-Beltri C, Baixauli F, Mittelbrunn M, Fernández-Delgado I, Torralba D, Moreno-Gonzalo O, et al. ISGylation controls exosome secretion by promoting lysosomal degradation of MVB proteins. Nat Commun. 2016;7:13588.
179. Faul F, Erdfelder E, Lang AG, Buchner A. G*Power 3: a flexible statistical power analysis program for the social, behavioral, and biomedical sciences. Behav Res Methods. 2007;39(2):175-91.
180. Vercellini P, Fedele L, Aimi G, Pietropaolo G, Consonni D, Crosignani PG. Association between endometriosis stage, lesion type, patient characteristics and severity of pelvic pain symptoms: a multivariate analysis of over 1000 patients. Hum Reprod. 2007;22(1):266-71.
181. Khalaji A, Yancheshmeh FB, Farham F, Khorram A, Sheshbolouki S, Zokaei M, et al. Don't eat me/eat me signals as a novel strategy in cancer immunotherapy. Heliyon. 2023;9(10).
182. Bourdely P, Petti L, Khou S, Meghraoui-Kheddar A, Elaldi R, Cazareth J, et al. Autofluorescence identifies highly phagocytic tissue-resident macrophages in mouse and human skin and cutaneous squamous cell carcinoma. Frontiers in Immunology. 2022;13:903069.
183. Kalu E, Sumar N, Giannopoulos T, Patel P, Croucher C, Sherriff E, Bansal A. Cytokine profiles in serum and peritoneal fluid from infertile women with and without endometriosis. Journal of Obstetrics and Gynaecology Research. 2007;33(4):490-5.

184. Pizzo A, Salmeri FM, Ardita FV, Sofo V, Tripepi M, Marsico S. Behaviour of cytokine levels in serum and peritoneal fluid of women with endometriosis. Gynecologic and obstetric investigation. 2003;54(2):82-7.
185. Khalaj K, Miller JE, Lingegowda H, Fazleabas AT, Young SL, Lessey BA, et al. Extracellular vesicles from endometriosis patients are characterized by a unique miRNA-lncRNA signature. JCI Insight. 2019;4(18).
186. O'Brien K, Breyne K, Ughetto S, Laurent LC, Breakefield XO. RNA delivery by extracellular vesicles in mammalian cells and its applications. Nature Reviews Molecular Cell Biology. 2020.
187. Wiklander OPB, Brennan M, Lötvall J, Breakefield XO, El Andaloussi S. Advances in therapeutic applications of extracellular vesicles. Sci Transl Med. 2019;11(492).
188. Hoshino A, Costa-Silva B, Shen T-L, Rodrigues G, Hashimoto A, Mark MT, et al. Tumour exosome integrins determine organotropic metastasis. Nature. 2015;527(7578):329-35.
189. Mallegol J, Van Niel G, Lebreton C, Lepelletier Y, Candalh C, Dugave C, et al. T84-intestinal epithelial exosomes bear MHC class II/peptide complexes potentiating antigen presentation by dendritic cells. Gastroenterology. 2007;132(5):1866-76.
190. Iversen T-G, Skotland T, Sandvig K. Endocytosis and intracellular transport of nanoparticles: Present knowledge and need for future studies. Nano today. 2011;6(2):176-85.
191. Yu Z-L, Liu J-Y, Chen G. Small extracellular vesicle PD-L1 in cancer: the knowns and unknowns. npj Precision Oncology. 2022;6(1):42.
192. Christianson HC, Svensson KJ, Van Kuppevelt TH, Li J-P, Belting M. Cancer cell exosomes depend on cell-surface heparan sulfate proteoglycans for their internalization and functional activity. Proceedings of the National Academy of Sciences. 2013;110(43):17380-5.
193. Costa-Silva B, Aiello NM, Ocean AJ, Singh S, Zhang H, Thakur BK, et al. Pancreatic cancer exosomes initiate pre-metastatic niche formation in the liver. Nature cell biology. 2015;17(6):816-26.
194. Becker CM, Bokor A, Heikinheimo O, Horne A, Jansen F, Kiesel L, et al. ESHRE guideline: endometriosis. Human reproduction open. 2022;2022(2):hoac009.
195. Coxon L, Evans E, Vincent K. Endometriosis – a painful disease. Current Opinion in Anesthesiology. 2023;36(5):595-601.
196. Becker K, Heinemann K, Imthurn B, Marions L, Moehner S, Gerlinger C, et al. Real world data on symptomology and diagnostic approaches of 27,840 women living with endometriosis. Scientific Reports. 2021;11(1):20404.
197. Ballard K, Seaman H, De Vries CS, Wright J. Can symptomatology help in the diagnosis of endometriosis? Findings from a national case–control study—part 1. BJOG: An International Journal of Obstetrics & Gynaecology. 2008;115(11):1382-91.
198. Cozzolino M, Coccia ME, Lazzeri G, Basile F, Troiano G. Variables Associated with Endometriosis-related Pain: A Pilot Study using a Visual Analogue Scale. Rev Bras Ginecol Obstet. 2019;41(3):170-5.
199. Vercellini P, Buggio L, Berlanda N, Barbara G, Somigliana E, Bosari S. Estrogen-progestins and progestins for the management of endometriosis. Fertility and Sterility. 2016;106(7):1552-71. e2.
200. Reis FM, Coutinho LM, Vannuccini S, Batteux F, Chapron C, Petraglia F. Progesterone receptor ligands for the treatment of endometriosis: the mechanisms

behind therapeutic success and failure. Human Reproduction Update. 2020;26(4):565-85.
201. Vercellini P, Eskenazi B, Consonni D, Somigliana E, Parazzini F, Abbiati A, Fedele L. Oral contraceptives and risk of endometriosis: a systematic review and meta-analysis. Human Reproduction Update. 2010;17(2):159-70.
202. Quaas AM, Weedin EA, Hansen KR. On-label and off-label drug use in the treatment of endometriosis. Fertility and sterility. 2015;103(3):612-25.
203. Taylor HS, Giudice LC, Lessey BA, Abrao MS, Kotarski J, Archer DF, et al. Treatment of endometriosis-associated pain with elagolix, an oral GnRH antagonist. New England Journal of Medicine. 2017;377(1):28-40.
204. Surrey ES, Hornstein MD, Group A-BS. Prolonged GnRH agonist and add-back therapy for symptomatic endometriosis: long-term follow-up. Obstetrics & Gynecology. 2002;99(5):709-19.
205. RAFIQUE S, DECHERNEY AH. Medical Management of Endometriosis. Clinical Obstetrics and Gynecology. 2017;60(3):485-96.
206. Vannuccini S, Clemenza S, Rossi M, Petraglia F. Hormonal treatments for endometriosis: The endocrine background. Reviews in Endocrine and Metabolic Disorders. 2022;23(3):333-55.
207. Bulun SE, Zeitoun KM, Takayama K, Sasano H. Molecular basis for treating endometriosis with aromatase inhibitors. Human Reproduction Update. 2000;6(5):413-8.
208. Pavone ME, Bulun SE. Aromatase inhibitors for the treatment of endometriosis. Fertility and sterility. 2012;98(6):1370-9.
209. Becker CM, Gattrell WT, Gude K, Singh SS. Reevaluating response and failure of medical treatment of endometriosis: a systematic review. Fertil Steril. 2017;108(1):125-36.
210. Flores VA, Vanhie A, Dang T, Taylor HS. Progesterone Receptor Status Predicts Response to Progestin Therapy in Endometriosis. The Journal of Clinical Endocrinology & Metabolism. 2018;103(12):4561-8.
211. Rome S, Tacconi S. High-fat diets: You are what you eat....your extracellular vesicles too! Journal of Extracellular Vesicles. 2024;13(1):12382.
212. Frühbeis C, Helmig S, Tug S, Simon P, Krämer-Albers E-M. Physical exercise induces rapid release of small extracellular vesicles into the circulation. Journal of extracellular vesicles. 2015;4(1):28239.
213. Blijdorp CJ, Hartjes TA, Wei KY, van Heugten MH, Bovée DM, Budde RP, et al. Nephron mass determines the excretion rate of urinary extracellular vesicles. Journal of Extracellular Vesicles. 2022;11(1):e12181.
214. Enjeti AK, Ariyarajah A, D'Crus A, Seldon M, Lincz LF. Circulating microvesicle number, function and small RNA content vary with age, gender, smoking status, lipid and hormone profiles. Thrombosis Research. 2017;156:65-72.
215. Toth B, Nikolajek K, Rank A, Nieuwland R, Lohse P, Pihusch V, et al. Gender-specific and menstrual cycle dependent differences in circulating microparticles. Platelets. 2007;18(7):515-21.
216. Rank A, Nieuwland R, Roesner S, Nikolajek K, Hiller E, Toth B. Climacteric Lowers Plasma Levels of Platelet-Derived Microparticles: A Pilot Study in Pre- versus Postmenopausal Women. Acta Haematologica. 2012;128(1):53-9.

217. Papadakis E, Sarigianni M, Tziomalos K, Mavromatidis G, Panidis D. Oral contraceptives increase platelet microparticle levels in normal-weight women with polycystic ovary syndrome. Hormones. 2020;19(4):565-71.
218. Carrillo Torres P, Martínez-Zamora MÁ, Tàssies D, Castillo H, Gracia M, Feixas G, et al. Impact of Continuous Estroprogestin Treatment on Circulating Microparticle Levels in Deep Endometriosis Patients. International Journal of Molecular Sciences. 2023;24(14):11802.
219. Trott M. Extracellular Vesicle Purity Enhanced by Gen 2 qEV Columns With Customised Resin [Available from: https://www.izon.com/news/gen-2-qev-columns-with-customised-proprietary-resin.
220. Wang J, Chen S, Zhang C, Stegeman S, Pfaff-Amesse T, Zhang Y, et al. Human endometrial stromal stem cells differentiate into megakaryocytes with the ability to produce functional platelets. 2012.
221. Schwab KE, Hutchinson P, Gargett CE. Identification of surface markers for prospective isolation of human endometrial stromal colony-forming cells. Human Reproduction. 2008;23(4):934-43.
222. Behzad F, Seif MW, Campbell S, Aplin JD. Expression of Two Isoforms of CD44 in Human Endometrium1. Biology of Reproduction. 1994;51(4):739-47.
223. Barkal AA, Brewer RE, Markovic M, Kowarsky M, Barkal SA, Zaro BW, et al. CD24 signalling through macrophage Siglec-10 is a target for cancer immunotherapy. Nature. 2019;572(7769):392-6.
224. Fang X, Zheng P, Tang J, Liu Y. CD24: from A to Z. Cellular & Molecular Immunology. 2010;7(2):100-3.
225. Yamamoto CM, Oakes ML, Murakami T, Muto MG, Berkowitz RS, Ng S-W. Comparison of benign peritoneal fluid-and ovarian cancer ascites-derived extracellular vesicle RNA biomarkers. Journal of ovarian research. 2018;11:1-9.
226. Quiralte M, Barquín A, Yagüe-Fernández M, Navarro P, Grazioso TP, Sevillano-Fernández E, et al. Proteomic profiles of peritoneal fluid-derived small extracellular vesicles correlate with patient outcome in ovarian cancer. The Journal of Clinical Investigation. 2024;134(10).
227. Muller L, Hong C-S, Stolz DB, Watkins SC, Whiteside TL. Isolation of biologically-active exosomes from human plasma. Journal of immunological methods. 2014;411:55-65.
228. Wu J-Y, Li Y-J, Hu X-B, Huang S, Xiang D-X. Preservation of small extracellular vesicles for functional analysis and therapeutic applications: a comparative evaluation of storage conditions. Drug Delivery. 2021;28(1):162-70.
229. Yang C, Han J, Liu H, He Y, Zhang Z, Liu X, et al. Storage of plasma-derived exosomes: evaluation of anticoagulant use and preserving temperatures. Platelets. 2024;35(1):2337255.
230. Self S, McMahan C, Mokalled S. Capturing the pool dilution effect in group testing regression: A Bayesian approach. Stat Med. 2022;41(23):4682-96.
231. Ding M, Wang C, Lu X, Zhang C, Zhou Z, Chen X, et al. Comparison of commercial exosome isolation kits for circulating exosomal microRNA profiling. Analytical and bioanalytical chemistry. 2018;410:3805-14.
232. Boriachek K, Islam MN, Möller A, Salomon C, Nguyen NT, Hossain MSA, et al. Biological functions and current advances in isolation and detection strategies for exosome nanovesicles. Small. 2018;14(6):1702153.

233. Bachurski D, Schuldner M, Nguyen P-H, Malz A, Reiners KS, Grenzi PC, et al. Extracellular vesicle measurements with nanoparticle tracking analysis–An accuracy and repeatability comparison between NanoSight NS300 and ZetaView. Journal of extracellular vesicles. 2019;8(1):1596016.
234. Vestad B, Llorente A, Neurauter A, Phuyal S, Kierulf B, Kierulf P, et al. Size and concentration analyses of extracellular vesicles by nanoparticle tracking analysis: a variation study. Journal of extracellular vesicles. 2017;6(1):1344087.
235. Hong C-S, Funk S, Muller L, Boyiadzis M, Whiteside TL. Isolation of biologically active and morphologically intact exosomes from plasma of patients with cancer. Journal of extracellular vesicles. 2016;5(1):29289.
236. Gardiner C, Ferreira YJ, Dragovic RA, Redman CWG, Sargent IL. Extracellular vesicle sizing and enumeration by nanoparticle tracking analysis. Journal of Extracellular Vesicles. 2013;2(1):19671.
237. Gardiner C, Ferreira YJ, Dragovic RA, Redman CW, Sargent IL. Extracellular vesicle sizing and enumeration by nanoparticle tracking analysis. Journal of extracellular vesicles. 2013;2(1):19671.
238. Bottazzo G, Hanafusa T, Pujol-Borrell R, Feldmann M. ROLE OF ABERRANT HLA-DR EXPRESSION AND ANTIGEN PRESENTATION IN INDUCTION OF ENDOCRINE AUTOIMMUNITY. The Lancet. 1983;322(8359):1115-9.
239. Panagiotou E, Syrigos NK, Charpidou A, Kotteas E, Vathiotis IA. CD24: A Novel Target for Cancer Immunotherapy. J Pers Med. 2022;12(8).
240. Barkal AA, Brewer RE, Markovic M, Kowarsky M, Barkal SA, Zaro BW, et al. CD24 signalling through macrophage Siglec-10 is a target for cancer immunotherapy. Nature. 2019;572(7769):392-6.
241. Chen G-Y, Tang J, Zheng P, Liu Y. CD24 and Siglec-10 selectively repress tissue damage–induced immune responses. Science. 2009;323(5922):1722-5.
242. Zhang P, Lu X, Tao K, Shi L, Li W, Wang G, Wu K. Siglec-10 is associated with survival and natural killer cell dysfunction in hepatocellular carcinoma. journal of surgical research. 2015;194(1):107-13.
243. Cho S, Ahn YS, Choi YS, Seo SK, Nam A, Kim HY, et al. Endometrial osteopontin mRNA expression and plasma osteopontin levels are increased in patients with endometriosis. American journal of reproductive immunology. 2009;61(4):286-93.
244. Huang H-F, Hong L-H, Tan Y, Sheng J-Z. Matrix metalloproteinase 2 is associated with changes in steroid hormones in the sera and peritoneal fluid of patients with endometriosis. Fertility and sterility. 2004;81(5):1235-9.
245. Collette T, Bellehumeur C, Kats R, Maheux R, Mailloux J, Villeneuve M, Akoum A. Evidence for an increased release of proteolytic activity by the eutopic endometrial tissue in women with endometriosis and for involvement of matrix metalloproteinase-9. Human Reproduction. 2004;19(6):1257-64.
246. Chung HW, Lee JY, Moon H-S, Hur SE, Park MH, Wen Y, Polan ML. Matrix metalloproteinase-2, membranous type 1 matrix metalloproteinase, and tissue inhibitor of metalloproteinase-2 expression in ectopic and eutopic endometrium. Fertility and sterility. 2002;78(4):787-95.
247. Tosti C, Biscione A, Morgante G, Bifulco G, Luisi S, Petraglia F. Hormonal therapy for endometriosis: from molecular research to bedside. European Journal of Obstetrics & Gynecology and Reproductive Biology. 2017;209:61-6.

248. Kaipparettu BA, Malik S, Konduri SD, Liu W, Rokavec M, van der Kuip H, et al. Estrogen-mediated downregulation of CD24 in breast cancer cells. International journal of cancer. 2008;123(1):66-72.
249. Kim KH, Choi JS, Kim JM, Choi YL, Shin YK, Lee HC, et al. Enhanced CD24 expression in endometrial carcinoma and its expression pattern in normal and hyperplastic endometrium. Histol Histopathol. 2009;24(3):309-16.
250. Mirantes C, Espinosa I, Ferrer I, Dolcet X, Prat J, Matias-Guiu X. Epithelial-to-mesenchymal transition and stem cells in endometrial cancer. Human Pathology. 2013;44(10):1973-81.
251. Chanput W, Mes JJ, Wichers HJ. THP-1 cell line: an in vitro cell model for immune modulation approach. International immunopharmacology. 2014;23(1):37-45.
252. Harris P, Ralph P. Human leukemic models of myelomonocytic development: a review of the HL-60 and U937 cell lines. Journal of leukocyte biology. 1985;37(4):407-22.
253. Maeß MB, Wittig B, Cignarella A, Lorkowski S. Reduced PMA enhances the responsiveness of transfected THP-1 macrophages to polarizing stimuli. Journal of Immunological Methods. 2014;402(1):76-81.
254. Hornung D, Waite LL, Ricke EA, Bentzien F, Wallwiener D, Taylor RN. Nuclear peroxisome proliferator-activated receptors α and γ have opposing effects on monocyte chemotaxis in endometriosis. The Journal of Clinical Endocrinology & Metabolism. 2001;86(7):3108-14.
255. Sidell N, Han SW, Parthasarathy S. Regulation and modulation of abnormal immune responses in endometriosis. Annals of the New York Academy of Sciences. 2002;955(1):159-73.
256. Genin M, Clement F, Fattaccioli A, Raes M, Michiels C. M1 and M2 macrophages derived from THP-1 cells differentially modulate the response of cancer cells to etoposide. BMC Cancer. 2015;15(1):577.
257. Park EK, Jung HS, Yang HI, Yoo MC, Kim C, Kim KS. Optimized THP-1 differentiation is required for the detection of responses to weak stimuli. Inflamm Res. 2007;56(1):45-50.
258. Lund ME, To J, O'Brien BA, Donnelly S. The choice of phorbol 12-myristate 13-acetate differentiation protocol influences the response of THP-1 macrophages to a pro-inflammatory stimulus. Journal of Immunological Methods. 2016;430:64-70.
259. Aderem A, Underhill DM. Mechanisms of phagocytosis in macrophages. Annual review of immunology. 1999;17(1):593-623.
260. Gordon S. Phagocytosis: An Immunobiologic Process. Immunity. 2016;44(3):463-75.
261. Uribe-Querol E, Rosales C. Phagocytosis: Our Current Understanding of a Universal Biological Process. Front Immunol. 2020;11:1066.
262. Chuang PC, Wu MH, Shoji Y, Tsai SJ. Downregulation of CD36 results in reduced phagocytic ability of peritoneal macrophages of women with endometriosis. The Journal of Pathology: A Journal of the Pathological Society of Great Britain and Ireland. 2009;219(2):232-41.
263. Steinberg BE, Grinstein S. Analysis of Macrophage Phagocytosis: Quantitative Assays of Phagosome Formation and Maturation Using High-Throughput Fluorescence Microscopy. In: Reiner NE, editor. Macrophages and Dendritic Cells: Methods and Protocols. Totowa, NJ: Humana Press; 2009. p. 45-56.

264. Liang Z, Zhang Q, Thomas CMR, Chana KK, Gibeon D, Barnes PJ, et al. Impaired macrophage phagocytosis of bacteria in severe asthma. Respiratory Research. 2014;15(1):72.
265. Taylor A, Finney-Hayward T, Quint J, Thomas C, Tudhope S, Wedzicha J, et al. Defective macrophage phagocytosis of bacteria in COPD. European Respiratory Journal. 2010;35(5):1039-47.
266. Gordon P, Okai B, Hoare JI, Erwig LP, Wilson HM. SOCS3 is a modulator of human macrophage phagocytosis. Journal of Leucocyte Biology. 2016;100(4):771-80.
267. Lindner B, Burkard T, Schuler M. Phagocytosis assays with different pH-sensitive fluorescent particles and various readouts. Biotechniques. 2020;68(5):245-50.
268. Neaga A, Lefor J, Lich KE, Liparoto SF, Xiao YQ. Development and validation of a flow cytometric method to evaluate phagocytosis of pHrodo™ BioParticles® by granulocytes in multiple species. Journal of immunological methods. 2013;390(1-2):9-17.
269. Kapellos TS, Taylor L, Lee H, Cowley SA, James WS, Iqbal AJ, Greaves DR. A novel real time imaging platform to quantify macrophage phagocytosis. Biochem Pharmacol. 2016;116:107-19.
270. Cao M, Wang Z, Lan W, Xiang B, Liao W, Zhou J, et al. The roles of tissue resident macrophages in health and cancer. Experimental Hematology & Oncology. 2024;13(1):3.
271. Fujioka Y, Matozaki T, Noguchi T, Iwamatsu A, Yamao T, Takahashi N, et al. A novel membrane glycoprotein, SHPS-1, that binds the SH2-domain-containing protein tyrosine phosphatase SHP-2 in response to mitogens and cell adhesion. Molecular and cellular biology. 1996.
272. Neel BG, Gu H, Pao L. The 'Shp'ing news: SH2 domain-containing tyrosine phosphatases in cell signaling. Trends Biochem Sci. 2003;28(6):284-93.
273. Kharitonenkov A, Chen Z, Sures I, Wang H, Schilling J, Ullrich A. A family of proteins that inhibit signalling through tyrosine kinase receptors. Nature. 1997;386(6621):181-6.
274. Lindberg FP, Gresham HD, Schwarz E, Brown EJ. Molecular cloning of integrin-associated protein: an immunoglobulin family member with multiple membrane-spanning domains implicated in alpha v beta 3-dependent ligand binding. The Journal of cell biology. 1993;123(2):485-96.
275. Adams S, van der Laan LJW, Vernon-Wilson E, Renardel de Lavalette C, Döpp EA, Dijkstra CD, et al. Signal-Regulatory Protein Is Selectively Expressed by Myeloid and Neuronal Cells. The Journal of Immunology. 1998;161(4):1853-9.
276. Kim D, Wang J, Willingham Sa, Martin R, Wernig G, Weissman I. Anti-CD47 antibodies promote phagocytosis and inhibit the growth of human myeloma cells. Leukemia. 2012;26(12):2538-45.
277. Willingham SB, Volkmer J-P, Gentles AJ, Sahoo D, Dalerba P, Mitra SS, et al. The CD47-signal regulatory protein alpha (SIRPa) interaction is a therapeutic target for human solid tumors. Proceedings of the National Academy of Sciences. 2012;109(17):6662-7.
278. Zhang W, Huang Q, Xiao W, Zhao Y, Pi J, Xu H, et al. Advances in anti-tumor treatments targeting the CD47/SIRPα axis. Frontiers in immunology. 2020;11:18.

279. Li Y, Wu Y, Federzoni EA, Wang X, Dharmawan A, Hu X, et al. CD47 cross-dressing by extracellular vesicles expressing CD47 inhibits phagocytosis without transmitting cell death signals. Elife. 2022;11:e73677.
280. Kaur S, Elkahloun AG, Singh SP, Arakelyan A, Roberts DD. A function-blocking CD47 antibody modulates extracellular vesicle-mediated intercellular signaling between breast carcinoma cells and endothelial cells. Journal of cell communication and signaling. 2018;12:157-70.
281. Xie F, Xu M, Lu J, Mao L, Wang S. The role of exosomal PD-L1 in tumor progression and immunotherapy. Molecular cancer. 2019;18:1-10.
282. Kamerkar S, LeBleu VS, Sugimoto H, Yang S, Ruivo CF, Melo SA, et al. Exosomes facilitate therapeutic targeting of oncogenic KRAS in pancreatic cancer. Nature. 2017;546(7659):498-503.
283. Li J, Yan S, Li Q, Huang Y, Ji M, Jiao X, et al. Macrophage-associated immune checkpoint CD47 blocking ameliorates endometriosis. Molecular Human Reproduction. 2022;28(5):gaac010.
284. Hu L, Zhang J, Lu Y, Fu B, Hu W. Estrogen receptor beta promotes endometriosis progression by upregulating CD47 expression in ectopic endometrial stromal cells. Journal of Reproductive Immunology. 2022;151:103513.
285. Xie Q, He H, Wu Y-H, Zou L-J, She X-L, Xia X-M, Wu X-Q. Eutopic endometrium from patients with endometriosis modulates the expression of CD36 and SIRP-α in peritoneal macrophages. Journal of Obstetrics and Gynaecology Research. 2019;45(5):1045-57.
286. Zhang W, Ou M, Yang P, Ning M. The role of extracellular vesicle immune checkpoints in cancer. Clinical and Experimental Immunology. 2024;216(3):230-9.
287. Himes BT, Peterson TE, de Mooij T, Garcia LMC, Jung M-Y, Uhm S, et al. The role of extracellular vesicles and PD-L1 in glioblastoma-mediated immunosuppressive monocyte induction. Neuro-oncology. 2020;22(7):967-78.
288. Wu L, Lv C, Su Y, Li C, Zhang H, Zhao X, Li M. Expression of programmed death-1 (PD-1) and its ligand PD-L1 is upregulated in endometriosis and promoted by 17beta-estradiol. Gynecological Endocrinology. 2019;35(3):251-6.
289. Wu MY, Ho HN. The role of cytokines in endometriosis. American Journal of Reproductive Immunology. 2003;49(5):285-96.
290. Reis FM, Petraglia F, Taylor RN. Endometriosis: hormone regulation and clinical consequences of chemotaxis and apoptosis. Human reproduction update. 2013;19(4):406-18.
291. Görgens A, Wiklander O, Bostancıoğlu RB, Zickler A, Murke F, Heider U, et al. A robust and semi-quantitative method for analyzing exosomes by flow cytometry2021.
292. Aldo PB, Craveiro V, Guller S, Mor G. Effect of culture conditions on the phenotype of THP-1 monocyte cell line. Am J Reprod Immunol. 2013;70(1):80-6.
293. Forrester MA, Wassall HJ, Hall LS, Cao H, Wilson HM, Barker RN, Vickers MA. Similarities and differences in surface receptor expression by THP-1 monocytes and differentiated macrophages polarized using seven different conditioning regimens. Cell Immunol. 2018;332:58-76.
294. Triantafilou M, Triantafilou K. Lipopolysaccharide recognition: CD14, TLRs and the LPS-activation cluster. Trends in immunology. 2002;23(6):301-4.

295. Poussin C, Foti M, Carpentier J-L, Pugin J. CD14-dependent Endotoxin Internalization via a Macropinocytic Pathway*. Journal of Biological Chemistry. 1998;273(32):20285-91.
296. Bazil V, Strominger JL. Shedding as a mechanism of down-modulation of CD14 on stimulated human monocytes. J Immunol. 1991;147(5):1567-74.
297. Baxter EW, Graham AE, Re NA, Carr IM, Robinson JI, Mackie SL, Morgan AW. Standardized protocols for differentiation of THP-1 cells to macrophages with distinct M(IFNγ+LPS), M(IL-4) and M(IL-10) phenotypes. Journal of Immunological Methods. 2020;478:112721.
298. Lurier EB, Dalton D, Dampier W, Raman P, Nassiri S, Ferraro NM, et al. Transcriptome analysis of IL-10-stimulated (M2c) macrophages by next-generation sequencing. Immunobiology. 2017;222(7):847-56.
299. Feng X, Deng T, Zhang Y, Su S, Wei C, Han D. Lipopolysaccharide inhibits macrophage phagocytosis of apoptotic neutrophils by regulating the production of tumour necrosis factor α and growth arrest-specific gene 6. Immunology. 2011;132(2):287-95.
300. Poli-Neto OB, Meola J, Rosa-e-Silva JC, Tiezzi D. Transcriptome meta-analysis reveals differences of immune profile between eutopic endometrium from stage I-II and III-IV endometriosis independently of hormonal milieu. Scientific Reports. 2020;10(1):313.
301. Lagana AS, Salmeri FM, Ban Frangež H, Ghezzi F, Vrtačnik-Bokal E, Granese R. Evaluation of M1 and M2 macrophages in ovarian endometriomas from women affected by endometriosis at different stages of the disease. Gynecological Endocrinology. 2020;36(5):441-4.
302. Fan Y-Y, Chen H-Y, Chen W, Liu Y-N, Fu Y, Wang L-N. Expression of inflammatory cytokines in serum and peritoneal fluid from patients with different stages of endometriosis. Gynecological Endocrinology. 2018;34(6):507-12.
303. Iyer SS, Cheng G. Role of interleukin 10 transcriptional regulation in inflammation and autoimmune disease. Crit Rev Immunol. 2012;32(1):23-63.
304. Martinez FO, Sica A, Mantovani A, Locati M. Macrophage activation and polarization. Front biosci. 2008;13(13):453-61.
305. Unuvar Purcu D, Korkmaz A, Gunalp S, Helvaci DG, Erdal Y, Dogan Y, et al. Effect of stimulation time on the expression of human macrophage polarization markers. PloS one. 2022;17(3):e0265196.
306. Sun H, Li D, Yuan M, Li Q, Zhen Q, Li N, Wang G. Macrophages alternatively activated by endometriosis-exosomes contribute to the development of lesions in mice. MHR: Basic science of reproductive medicine. 2019;25(1):5-16.
307. Gnecco JS, Brown A, Buttrey K, Ives C, Goods BA, Baugh L, et al. Organoid co-culture model of the human endometrium in a fully synthetic extracellular matrix enables the study of epithelial-stromal crosstalk. Med. 2023;4(8):554-79.e9.
308. Yang Y, Li C-W, Chan L-C, Wei Y, Hsu J-M, Xia W, et al. Exosomal PD-L1 harbors active defense function to suppress T cell killing of breast cancer cells and promote tumor growth. Cell research. 2018;28(8):862-4.
309. Liu H, Lang JH. Is abnormal eutopic endometrium the cause of endometriosis? The role of eutopic endometrium in pathogenesis of endometriosis. Medical science monitor: international medical journal of experimental and clinical research. 2011;17(4):RA92.

310. Lv H, Zhao G, Jiang P, Wang H, Wang Z, Yao S, et al. Deciphering the endometrial niche of human thin endometrium at single-cell resolution. Proceedings of the National Academy of Sciences. 2022;119(8):e2115912119.
311. Spencer TE, Hayashi K, Hu J, Carpenter KD. Comparative developmental biology of the mammalian uterus. Current topics in developmental biology. 2005;68:85-122.
312. Fitzgerald HC, Dhakal P, Behura SK, Schust DJ, Spencer TE. Self-renewing endometrial epithelial organoids of the human uterus. Proceedings of the National Academy of Sciences. 2019;116(46):23132-42.
313. Buckley CE, St Johnston D. Apical–basal polarity and the control of epithelial form and function. Nature Reviews Molecular Cell Biology. 2022;23(8):559-77.
314. Fanning AS, Little BP, Rahner C, Utepbergenov D, Walther Z, Anderson JM. The unique-5 and-6 motifs of ZO-1 regulate tight junction strand localization and scaffolding properties. Molecular biology of the cell. 2007;18(3):721-31.
315. Diedrich K, Fauser BCJM, Devroey P, Griesinger G, Group obotEARW. The role of the endometrium and embryo in human implantation. Human Reproduction Update. 2007;13(4):365-77.
316. Klein G, Langegger M, Timpl R, Ekblom P. Role of laminin a chain in the development of epithelial cell polarity. Cell. 1988;55(2):331-41.
317. Critchley HO, Maybin JA, Armstrong GM, Williams AR. Physiology of the endometrium and regulation of menstruation. Physiological reviews. 2020.
318. Gargett CE, Chan RW, Schwab KE. Hormone and growth factor signaling in endometrial renewal: role of stem/progenitor cells. Molecular and cellular endocrinology. 2008;288(1-2):22-9.
319. Hawkins SM, Matzuk MM. The menstrual cycle: basic biology. Annals of the New York Academy of Sciences. 2008;1135(1):10-8.
320. Mihm M, Gangooly S, Muttukrishna S. The normal menstrual cycle in women. Animal reproduction science. 2011;124(3-4):229-36.
321. Sampson JA. Metastatic or embolic endometriosis, due to the menstrual dissemination of endometrial tissue into the venous circulation. The American journal of pathology. 1927;3(2):93.
322. Nisolle M, Donnez J. Peritoneal endometriosis, ovarian endometriosis, and adenomyotic nodules of the rectovaginal septum are three different entities. Fertility and sterility. 1997;68(4):585-96.
323. Gołąbek-Grenda A, Olejnik A. In vitro modeling of endometriosis and endometriotic microenvironment – Challenges and recent advances. Cellular Signalling. 2022;97:110375.
324. Clement PB. The pathology of endometriosis: a survey of the many faces of a common disease emphasizing diagnostic pitfalls and unusual and newly appreciated aspects. Advances in anatomic pathology. 2007;14(4):241-60.
325. Fonseca MA, Wright KN, Lin X, Abbasi F, Haro M, Sun J, et al. A cellular and molecular portrait of endometriosis subtypes. bioRxiv. 2021:2021.05. 20.445037.
326. Gurung S, Greening DW, Rai A, Poh QH, Evans J, Salamonsen LA. The proteomes of endometrial stromal cell-derived extracellular vesicles following a decidualizing stimulus define the cells' potential for decidualization success. Molecular human reproduction. 2021;27(10):gaab057.

327. Suda K, Nakaoka H, Yoshihara K, Ishiguro T, Adachi S, Kase H, et al. Different mutation profiles between epithelium and stroma in endometriosis and normal endometrium. Human Reproduction. 2019;34(10):1899-905.
328. Burns GW, Fu Z, Vegter EL, Madaj ZB, Greaves E, Flores I, Fazleabas AT. Spatial Transcriptomic Analysis Identifies Epithelium-Macrophage Crosstalk in Endometriotic Lesions. bioRxiv. 2024:2024.03.23.586434.
329. Fitzgerald HC, Schust DJ, Spencer TE. In vitro models of the human endometrium: evolution and application for women's health. Biology of reproduction. 2021;104(2):282-93.
330. Turco MY, Gardner L, Hughes J, Cindrova-Davies T, Gomez MJ, Farrell L, et al. Long-term, hormone-responsive organoid cultures of human endometrium in a chemically defined medium. Nature Cell Biology. 2017;19(5):568-77.
331. Boretto M, Cox B, Noben M, Hendriks N, Fassbender A, Roose H, et al. Development of organoids from mouse and human endometrium showing endometrial epithelium physiology and long-term expandability. Development. 2017;144(10):1775-86.
332. Simintiras CA, Dhakal P, Ranjit C, Fitzgerald HC, Balboula AZ, Spencer TE. Capture and metabolomic analysis of the human endometrial epithelial organoid secretome. Proceedings of the National Academy of Sciences. 2021;118(15):e2026804118.
333. Esfandiari F, Favaedi R, Heidari-Khoei H, Chitsazian F, Yari S, Piryaei A, et al. Insight into epigenetics of human endometriosis organoids: DNA methylation analysis of HOX genes and their cofactors. Fertility and Sterility. 2021;115(1):125-37.
334. Luddi A, Pavone V, Semplici B, Governini L, Criscuoli M, Paccagnini E, et al. Organoids of human endometrium: a powerful in vitro model for the endometrium-embryo cross-talk at the implantation site. Cells. 2020;9(5):1121.
335. Juárez-Barber E, Segura-Benítez M, Carbajo-García MC, Bas-Rivas A, Faus A, Vidal C, et al. Extracellular vesicles secreted by adenomyosis endometrial organoids contain miRNAs involved in embryo implantation and pregnancy. Reproductive BioMedicine Online. 2023;46(3):470-81.
336. Ahmad V, Yeddula SGR, Telugu BP, Spencer TE, Kelleher AM. Development of polarity-reversed endometrial epithelial organoids. Reproduction. 2024;167(3).
337. Canis M, Donnez JG, Guzick DS, Halme JK, Rock JA, Schenken RS, Vernon MW. Revised american society for reproductive medicine classification of endometriosis: 1996. Fertility and sterility. 1997;67(5):817-21.
338. Vissers G, Giacomozzi M, Verdurmen W, Peek R, Nap A. The role of fibrosis in endometriosis: a systematic review. Human Reproduction Update. 2024.
339. Meresman GF, Auge L, Baranao RI, Lombardi E, Tesone M, Sueldo C. Oral contraceptives suppress cell proliferation and enhance apoptosis of eutopic endometrial tissue from patients with endometriosis. Fertility and sterility. 2002;77(6):1141-7.
340. Carneiro FP, Muniz-Junqueira MI, De Vasconcelos Carneiro M, De Araújo Oliveira Í, Soares AC, De Vargas Haar N, et al. Anti-EpCAM antibodies for detection of metastatic carcinoma in effusions and peritoneal wash. Oncol Lett. 2019;18(2):2019-24.
341. Bortot B, Di Florio R, Merighi S, Peacock B, Lees R, Valle F, et al. Platelets as key cells in endometriosis patients: insights from small extracellular vesicles in peritoneal fluid and endometriotic lesions analysis. bioRxiv. 2024:2024.08.21.607595.

342. de Lau W, Peng WC, Gros P, Clevers H. The R-spondin/Lgr5/Rnf43 module: regulator of Wnt signal strength. Genes & development. 2014;28(4):305-16.
343. Kim K-A, Kakitani M, Zhao J, Oshima T, Tang T, Binnerts M, et al. Mitogenic influence of human R-spondin1 on the intestinal epithelium. Science. 2005;309(5738):1256-9.
344. Matsuzaki S, Darcha C. Involvement of the Wnt/β-catenin signaling pathway in the cellular and molecular mechanisms of fibrosis in endometriosis. PloS one. 2013;8(10):e76808.
345. Pazhohan A, Amidi F, Akbari-Asbagh F, Seyedrezazadeh E, Farzadi L, Khodarahmin M, et al. The Wnt/β-catenin signaling in endometriosis, the expression of total and active forms of β-catenin, total and inactive forms of glycogen synthase kinase-3β, WNT7a and DICKKOPF-1. European Journal of Obstetrics & Gynecology and Reproductive Biology. 2018;220:1-5.
346. Harnack C, Berger H, Antanaviciute A, Vidal R, Sauer S, Simmons A, et al. R-spondin 3 promotes stem cell recovery and epithelial regeneration in the colon. Nature Communications. 2019;10(1):4368.
347. Sigal M, Logan CY, Kapalczynska M, Mollenkopf H-J, Berger H, Wiedenmann B, et al. Stromal R-spondin orchestrates gastric epithelial stem cells and gland homeostasis. Nature. 2017;548(7668):451-5.
348. Thomas H. R-spondin 3 is a critical regulator of gastric antral stem cell homeostasis. Nature Reviews Gastroenterology & Hepatology. 2017;14(10):565-.
349. Guare LA, Das J, Caruth L, Rajagopalan A, Akerele AT, Brumpton BM, et al. Expanding the genetic landscape of endometriosis: Integrative -omics analyses uncover key pathways from a multi-ancestry study of over 900,000 women. medRxiv. 2024:2024.11.26.24316723.
350. NIKAS G, MAKRIGIANNAKIS A. Endometrial Pinopodes and Uterine Receptivity. Annals of the New York Academy of Sciences. 2003;997(1):120-3.
351. Enders AC, Nelson DM. Pinocytotic activity of the uterus of the rat. American Journal of Anatomy. 1973;138(3):277-99.
352. Kabir-Salmani M, Nikzad H, Shiokawa S, Akimoto Y, Iwashita M. Secretory role for human uterodomes (pinopods): secretion of LIF. Molecular human reproduction. 2005;11(8):553-9.
353. Quinn CE, Casper RF. Pinopodes: a questionable role in endometrial receptivity. Human Reproduction Update. 2008;15(2):229-36.
354. Apodaca G, Gallo LI, Bryant DM. Role of membrane traffic in the generation of epithelial cell asymmetry. Nature cell biology. 2012;14(12):1235-43.
355. Rodriguez-Boulan E, Macara IG. Organization and execution of the epithelial polarity programme. Nature reviews Molecular cell biology. 2014;15(4):225-42.
356. Fields IC, Shteyn E, Pypaert M, Proux-Gillardeaux V, Kang RS, Galli T, Fölsch H. v-SNARE cellubrevin is required for basolateral sorting of AP-1B–dependent cargo in polarized epithelial cells. The Journal of cell biology. 2007;177(3):477-88.
357. Sharma N, Low SH, Misra S, Pallavi B, Weimbs T. Apical targeting of syntaxin 3 is essential for epithelial cell polarity. The Journal of cell biology. 2006;173(6):937-48.
358. Beest MBt, Chapin SJ, Avrahami D, Mostov KE. The role of syntaxins in the specificity of vesicle targeting in polarized epithelial cells. Molecular biology of the cell. 2005;16(12):5784-92.

359. Liu C, Liu D, Wang S, Gan L, Yang X, Ma C. Identification of the SNARE complex that mediates the fusion of multivesicular bodies with the plasma membrane in exosome secretion. J Extracell Vesicles. 2023;12(9):e12356.
360. Lessan K, Aguiar DJ, Oegema T, Siebenson L, Skubitz AP. CD44 and β1 integrin mediate ovarian carcinoma cell adhesion to peritoneal mesothelial cells. The American journal of pathology. 1999;154(5):1525-37.
361. Nishimura S, Chung YS, Yashiro M, Inoue T, Sowa M. CD44H plays an important role in peritoneal dissemination of scirrhous gastric cancer cells. Japanese journal of cancer research. 1996;87(12):1235-44.
362. Dechaud H, Witz CA, Montoya-Rodriguez IA, Degraffenreid LA, Schenken RS. Mesothelial cell–associated hyaluronic acid promotes adhesion of endometrial cells to mesothelium. Fertility and sterility. 2001;76(5):1012-8.
363. Knudtson JF, Tekmal RR, Santos MT, Binkley PA, Krishnegowda N, Valente P, Schenken RS. Impaired Development of Early Endometriotic Lesions in CD44 Knockout Mice. Reproductive Sciences. 2015;23(1):87-91.
364. Hasegawa A, Yoshino O, Osuga Y, Hirata T, Yano T, Taketani Y. High soluble CD44 concentration in peritoneal fluid in endometriosis. Fertility and sterility. 2008;89(5):1267-8.
365. Mashayekhi F, Aryaee H, Mirzajani E, Yasin AA, Fathi A. Soluble CD44 concentration in the serum and peritoneal fluid samples of patients with different stages of endometriosis. Archives of gynecology and obstetrics. 2015;292:641-5.
366. Fransvea E, Mazzocca A, Antonaci S, Giannelli G. Targeting transforming growth factor (TGF)-βRI inhibits activation of β1 integrin and blocks vascular invasion in hepatocellular carcinoma. Hepatology. 2009;49(3):839-50.
367. Geng S, Guo Y, Wang Q, Li L, Wang J. Cancer stem-like cells enriched with CD29 and CD44 markers exhibit molecular characteristics with epithelial–mesenchymal transition in squamous cell carcinoma. Archives of Dermatological Research. 2013;305:35-47.
368. Brown E, Martínez-Aguilar R, Maybin JA, Gibson DA. Endometrial macrophages in health and disease. Int Rev Cell Mol Biol. 2022;367:183-208.
369. Scholz T, Temmler U, Krause S, Heptinstall S, Lösche W. Transfer of tissue factor from platelets to monocytes: role of platelet-derived microvesicles and CD62P. Thrombosis and haemostasis. 2002;88(12):1033-8.
370. Moody DB, Ulrichs T, Mühlecker W, Young DC, Gurcha SS, Grant E, et al. CD1c-mediated T-cell recognition of isoprenoid glycolipids in Mycobacterium tuberculosis infection. Nature. 2000;404(6780):884-8.
371. Tedder TF, Engel P. CD20: a regulator of cell-cycle progression of B lymphocytes. Immunology today. 1994;15(9):450-4.
372. Jiang S, Sun L. Tongue Sole CD209: A Pattern-Recognition Receptor that Binds a Broad Range of Microbes and Promotes Phagocytosis. Int J Mol Sci. 2017;18(9).
373. Konrad L, Kortum J, Nabham R, Gronbach J, Dietze R, Oehmke F, et al. Composition of the stroma in the human endometrium and endometriosis. Reproductive Sciences. 2018;25(7):1106-15.
374. Vachon E, Martin R, Plumb J, Kwok V, Vandivier RW, Glogauer M, et al. CD44 is a phagocytic receptor. Blood. 2006;107(10):4149-58.

375. Gebel HM, Rana N, Braun DP, Dmowski WP. Differential expression of VLAβ1 (CD29) on monocytes from patients with endometriosis. American Journal of Reproductive Immunology. 1995;34(5):317-22.
376. Luo Y, Duan H, Qian Y, Feng L, Wu Z, Wang F, et al. Macrophagic CD146 promotes foam cell formation and retention during atherosclerosis. Cell research. 2017;27(3):352-72.
377. Sumathi VP, McCluggage W. CD10 is useful in demonstrating endometrial stroma at ectopic sites and in confirming a diagnosis of endometriosis. Journal of clinical pathology. 2002;55(5):391-2.
378. McCluggage W, Sumathi V, Maxwell P. CD10 is a sensitive and diagnostically useful immunohistochemical marker of normal endometrial stroma and of endometrial stromal neoplasms. Histopathology. 2001;39(3):273-8.
379. Kobayashi H, Shiba T, Yoshida T, Bolidong D, Kato K, Sato Y, et al. Precise analysis of single small extracellular vesicles using flow cytometry. Scientific Reports. 2024;14(1):7465.
380. Shen W, Guo K, Adkins GB, Jiang Q, Liu Y, Sedano S, et al. A single extracellular vesicle (EV) flow cytometry approach to reveal EV heterogeneity. Angewandte Chemie International Edition. 2018;57(48):15675-80.
381. Yan J, Zhou L, Liu M, Zhu H, Zhang X, Cai E, et al. Single-cell analysis reveals insights into epithelial abnormalities in ovarian endometriosis. Cell Rep. 2024;43(3):113716.